NTNU – Trondheim
Norwegian University of
Science and Technology

Validation of Wet Gas Surge Phenomena

Lars Andreas Øvrum Sørvik

Master of Energy and Environmental Engineering
Submission date: June 2012
Supervisor: Lars Erik Bakken, EPT
Co-supervisor: Trond Gruner, EPT
Øyvind Hundseid, EPT

Norwegian University of Science and Technology
Department of Energy and Process Engineering

NTNU
Norges teknisk-naturvitenskapelige universitet

Institutt for energi- og prosessteknikk

EPT-M-2012-83

MASTEROPPGAVE

for

Stud.techn. Lars A Sørvik

Våren 2012

Validering av våtgass surgefenomener

Validation of Wet Gas Surge Phenomena

Bakgrunn
De fleste store felt i Nordsjøen er utbygd med tradisjonell teknologi. Fokus har i de senere år skiftet mot mindre og mer fjerntliggende felt med begrenset infrastruktur. Utvikling og drift av slike felt krever ny kostnadseffektiv teknologi. Et helt sentralt element her er havbunnsbasert brønnkompresjon for å frakte brønnstrømmen direkte til land, eller mer fjerntliggende prosesseringsanlegg offshore.
Teknologien kan i enkelte tilfelle eliminere behovet for offshore prosessanlegg, noe som kan gi en formidabel kostnadsreduksjon. De fleste leverandører av turbomaskiner satser derfor på utvikling av havbunnsbaserte våtgasskompressorer. Noen få prototype konsepter eksisterer og det foregår i dag utstrakt testing og validering av teknologien.
Ved NTNU er det bygd opp en rigg for å teste våtgass kompressorer og analysere de grunnleggende mekanismene relatert til våtgass kompresjon. Riggen er unik og sentral i blant annet analyser av ustabilitet i våtgass strømning.

Mål
Basert på litteratur og eksperimentelt arbeid i våtgass kompresjonsrigg er det et mål å visualisere og dokumentere fenomener relatert til våtgass surge. Spesielt vektlegges bruk av pitotmålinger for å validere strømningsbildet og ustabilitet.

Oppgaven bearbeides ut fra følgende punkter:

1. Dokumentere relevant litteratur med hensyn til bruk av pitotmålinger for å detektere strømningsbildet og ustabilitet.
2. Validere strømningsbildet ved utløpet av løpehjulet ved hjelp av pitotmålinger i eksisterende rigg.
3. Identifisering av våtgass surge ved hjelp av våtgass pitotprober

" - "

Senest 14 dager etter utlevering av oppgaven skal kandidaten levere/sende instituttet en detaljert fremdrift- og eventuelt forsøksplan for oppgaven til evaluering og eventuelt diskusjon med faglig ansvarlig/veiledere. Detaljer ved eventuell utførelse av dataprogrammer skal avtales nærmere i samråd med faglig ansvarlig.

Besvarelsen redigeres mest mulig som en forskningsrapport med et sammendrag både på norsk og engelsk, konklusjon, litteraturliste, innholdsfortegnelse etc. Ved utarbeidelsen av teksten skal kandidaten legge vekt på å gjøre teksten oversiktlig og velskrevet. Med henblikk på lesning av besvarelsen er det viktig at de nødvendige henvisninger for korresponderende steder i tekst, tabeller og figurer anføres på begge steder. Ved bedømmelsen legges det stor vekt på at resultatene er grundig bearbeidet, at de oppstilles tabellarisk og/eller grafisk på en oversiktlig måte, og at de er diskutert utførlig.

Alle benyttede kilder, også muntlige opplysninger, skal oppgis på fullstendig måte. For tidsskrifter og bøker oppgis forfatter, tittel, årgang, sidetall og eventuelt figurnummer.

Det forutsettes at kandidaten tar initiativ til og holder nødvendig kontakt med faglærer og veileder(e). Kandidaten skal rette seg etter de reglementer og retningslinjer som gjelder ved alle (andre) fagmiljøer som kandidaten har kontakt med gjennom sin utførelse av oppgaven, samt etter eventuelle pålegg fra Institutt for energi- og prosessteknikk.

Risikovurdering av kandidatens arbeid skal gjennomføres i henhold til instituttets prosedyrer. Risikovurderingen skal dokumenteres og inngå som del av besvarelsen. Hendelser relatert til kandidatens arbeid med uheldig innvirkning på helse, miljø eller sikkerhet, skal dokumenteres og inngå som en del av besvarelsen.

I henhold til "Utfyllende regler til studieforskriften for teknologistudiet/sivilingeniørstudiet" ved NTNU § 20, forbeholder instituttet seg retten til å benytte alle resultater og data til undervisnings- og forskningsformål, samt til fremtidige publikasjoner.

Besvarelsen leveres digitalt i DAIM. Et faglig sammendrag med oppgavens tittel, kandidatens navn, veileders navn, årstall, instituttnavn, og NTNUs logo og navn, leveres til instituttet som en separat pdf-fil. Etter avtale leveres besvarelse og evt. annet materiale til veileder i digitalt format.

NTNU, Institutt for energi- og prosessteknikk, 16. januar 2012

Olav Bolland
Instituttleder

Lars E Bakken
Faglig ansvarlig/veileder

Medveileder(e)
T Gruner, NTNU
Ø Hundseid, NTNU

Preface and Acknowledgments

This master's thesis concludes my NTNU Master of Science degree program at the department of energy and process engineering.

I would like to thank my supervisor Lars Erik Bakken for all the help in connection with my master thesis with excellent guidance and for a very interesting year. I would also like to thank my fellow students at the office 501 for social cohesion and technical discussions that have stimulated to a good learning environment. PhD Øyvind Hundseid for guidance and Lars Konrad for the implementation of the measuring devices in the test rig. Last but not least, I want to thank PhD and researcher Trond Gammelsæter Grüner who has been of invaluable help during the project work. You have all been of great importance for me and my master's thesis.

Lars Andreas Øvrum Sørvik

Trondheim, June 13, 2012

Abstract

In order to utilize the fossil resources on the Norwegian continental shelf, technology and expertise have proven to be of great importance and hence, essential for further exploration and development of new resources. A key element in this matter is the subsea wet gas compression technology which enables the transport of well stream directly to a land based treatment system, or more remote processing facilities offshore. Compression of gas at the seabed is a significant technology advance no one has previously made. The technology of subsea gas compression is one of the most important measures to deliver increased volumes from existing gas fields as well as developing resources in more remote and vulnerable areas.

Due to the need of expertise and development of subsea installations, in order to meet the demand for fossil fuels and be competitive in a constantly increasing market, the Norwegian University of Science and Technology (NTNU) has built an experimental rig to test a wet gas compressor. The rig is unique and important to analyze the basic mechanisms and occurrence of instabilities related to wet gas compression. Both the literature review and the experimental work presented here are performed in order to visualize and document instabilities related to the phenomena surge and stall. Experimental data in this master thesis are obtained from a one- stage wet gas centrifugal compressor with an axial direct inlet. The stage involves a shrouded impeller, a vaneless diffuser and a volute. The compressor is a part of an open loop facility that is located at NTNU in Trondheim. The test rig is designed to operate with different amounts of liquid in the gas with gas volume fractions (GVF) and gas mass fractions (GMF) down to correspondingly 0.95 and 0.5. Applications in LabView were made and designed to analyze the raw data from the pressure sensors and pitot tubes in order to post-process and represent the data in a graphical manner. Log files from a total of seven scientific experiments with dry- and wet gas were documented and analyzed to identify the impeller outlet angle and achieving a more precise identification of wet gas surge initiation and instability precursor.

The steady state flow angle experiments revealed a stringent increase in flow angle with decreasing volume flow, for both the dry gas test of 10000 and 9000 rpm, with maximum corresponding flow angles of 81.5 and 86 degrees. A sudden rise in flow angle gradient was found to occur at a volume flow of 0.95 m^3/s and 0.8 m^3/s for 10000 rpm and 9000 rpm, respectively, due to the volute causing a shift change from deceleration to acceleration performance, at the respective volume flows. Flow angle measurements of dry gas were further validated and compared with Matlab and CFD simulation revealing coincident trends. The performed wet gas tests were associated with a greater uncertainty than dry gas, due to the influence of liquid. However, the wet gas curves showed distinct trends with lower discharge angles across the spectrum compared to the case for dry gas measurements.

The transient surge identification test was conducted on 7500 rpm with alternating GMF in the range from 0.6 to 0.42. The pressure characteristic revealed the first sign of intermittent behavior at a volume flow of 0.26 m^3/s prevailing sudden stringent static pressure fluctuations. The corresponding frequency spectrum for dynamic pressure sensors shows that the critical disturbance occurs, and is enhanced at low frequencies causing the initiation of surge at a volume flow of 0.27 m^3/s. A pitot tube set-up for identification of surge onset was evaluated and compared to the measurements conducted by a static pressure-, a differential pressure- and a high responsive dynamic pressure sensor. The detection tube indicated a possible precursor to surge by prevailing change and high fluctuations in the stagnation pressure.

Abstract

Observation through the impeller inlet showed that an annular backflow ring was formed with decreasing volume flow. The first observation of the ring shape was done for a volume flow of 0.3 m^3/s, followed by larger developments and a chaotic flow path with complete backflow for volume flow lower than 0.25 m^3/s.

Sammendrag

For å utnytte fossile ressursene på norsk kontinentalsokkel, har teknologi og kompetanse vist seg å være av stor betydning og viktig for videre utforskning samt utvikling av nye ressurser. Et sentralt element i dette er havbunns våtgass kompresjon teknologi som muliggjør transport av brønnstrøm direkte til et landbasert prosess anlegg, eller mer fjerntliggende prosessanlegg til havs. Kompresjon av gass på havbunnen er en viktig teknologi ingen tidligere har gjort. Teknologien ved undervanns gasskompresjon er en av de viktigste tiltakene for å levere økt volum fra eksisterende gassfelt, samt utvikle ressurser i mer fjerntliggende og sårbare områder.

På grunn av behovet for kompetanse og utvikling av havbunns installasjoner, for å møte etterspørselen etter fossilt brennstoff og være konkurransedyktig i et stadig økende marked; har NTNU bygget en eksperimentell rigg for å teste en våt gass kompressor. Riggen er unik og et viktig verktøy for å analysere de grunnleggende mekanismer og forekomst av ustabilitet knyttet til våtgass kompresjon. Både litteratur og eksperimentelt arbeid presenteres her og er utført for å visualisere og dokumentere ustabiliteter knyttet til fenomener «surge» og «stall». Eksperimentelle data i denne masteroppgaven er hentet fra en ett-trinns våtgass sentrifugal kompressor med en aksial direkte inntak. Kompressor trinnet består av en shrouded impeller, en vaneless diffusor og en volute. Kompressoren er konstruert for å operere med ulike mengder væske i gassen med gass volum fraksjoner (GVF) og gass masse fraksjoner (GMF) ned til korresponderende 0,95 og 0,5. LabView programmer ble benyttet og designet for å analysere rådata fra trykksensorer og pitot-rør for å kunne behandle og representere dataene på en grafisk måte. Loggfiler fra sju vitenskapelige eksperimenter med tørr- og våtgass ble dokumentert og analysert for å identifisere impeller utløps vinkel og oppnå en mer presis identifisering av våtgass «surge» initiering og forløper til denne ustabiliteten.

Steady state strømningsvinkel eksperimenter viste en stringent økning i strømningsvinkel med avtagende volum strøm, for tørrgass testen med 10000 og 9000 rpm, med maksimale korresponderende strømningsvinkler på 81,5 og 86 grader. En plutselig økning i strømningsvinkel gradient ble funnet å skje ved en volumstrøm på 0,95 m3 / s og 0,8 m3 / s for henholdsvis10000- og 9000 rpm, på grunn av at voluten forårsaker en endring fra nedbremsing til akselerasjon ytelse, ved de respektive volum strømmene. Strømningsvinkel målinger av tørr gass ble ytterligere validert og sammenlignet med Matlab og CFD simulering som viste sammenfallende trender. De utførte våtgass tester var assosiert med en større usikkerhet enn tørr gass, på grunn av innflytelsen av væske. Imidlertid viste våtgass kurvene tydelige trender med lavere vinkler over hele spekteret i forhold til tørrgass målinger.

En transient surge test ble utført på 7500 rpm med vekslende GMF i området fra 0,6 til 0,42. Trykk karakteristikken avslørte det første tegnet på ujevn atferd på en volumstrøm på 0,26 m^3/s med plutselige statiske trykksvingninger. Det tilsvarende frekvensspekteret for dynamiske trykksensorer viste at kritiske forstyrrelse oppstår, og forsterkes ved lave frekvenser som forårsaker initiering av surge ved en volumstrøm på 0,27 m^3 / s. Et pitotrør for identifisering av surge ble evaluert og sammenlignet med målingene utført av en statisk trykk-, en differansetrykk-og en høy responsiv dynamisk trykksensor. Påvisning fra pitot røret indikerte en mulig forløper til surge med gjeldende endring og høye svingninger i stagnasjon trykket. Observasjon gjennom impeller innløpet viste at en ringformet tilbakestrøm ble dannet med avtagende volum flyt. Den første observasjonen av ring formen ble gjort for en

volumstrøm på 0,3 m^3 / s, etterfulgt av større ringdannelser og komplett tilbakestrøm for volumstrøm lavere enn 0,25 m^3 / s.

Table of Contents

Table of Contents

Table of Contents

List of Figures

Table of Contents

List of Tables

Table of Contents

Nomenclature

Abbreviations and acronyms

CFD	Computional Fluid Dynamics
ETH	Eidgenössische Technische Hochschule
FA	Film Anemometry
FFT	Fast Fourier Transform
GE	General Electric
GMF	Gas Mass Fraction
GVF	Gas Volume Fraction
HV	High Voltage
HWA	Hot-Wire Anemometry
LDV	Laser Doppler Velocimetry
MAE	Mean Absolute Error
MHP	Multi-Hole probe
FRAP	Fast Responsive Aerodynamic Probe
L2F	Laser two-focused Velocimetry
MHP	Multi Hole Probe
NTNU	Norwegian University of Science and Technology
PCB	PicoCoulomB
PIV	Particle Image Velocimetry
PSP	Pressure Sensitive Paint
PXI	PCI Extensions for Instrumentation
RPM	Rotations Per Minute
UPS	Uninterruptible Power Supply
VDC	Volts of Direct Current

Greek letters

α	Flow angle	[degree]
α'	Measured flow angle	[degree]
β	Flow angle	[degree]
β'	Angle between center radius to pitot position	[degree]
ΔP_{tp}	The total dynamic head (droplet)	[]
ΔP_{TP}	The total dynamic head	[]
ΔP_{TPM}	The total homogenous dynamic head	[]
ρ	Density	[kg/m^3]
δ^*	Density ratio	[-]
μ	Slip factor	[-]
τ	Shear stress	[kg/ms^2]

Table of Contents

Roman letters and expression

a	Speed of sound	[m/s]
B	Greitzer parameter	[-]
b	Width	[mm]
C	Actual flow velocity	[m/s]
$C*$	Calibration constant	[-]
$C_{\theta 2}$	Tangential absolute velocity with finite number of blades	[m/s]
$C_{\theta 2\infty}$	Tangential component with infinite number of blades	[m/s]
H	Hold-up	[-]
L	Length	[mm]
N	Number of blades	[-]
$\dot{m}$	Mass flow	[kg/s]
Ma	Mach number	[-]
Q	Volume flow	[m^3/s]
r	Radius	[mm]
$\vec{R}$	Length between impeller center and pitot tube center	[mm]
Re	Reynolds number	[-]
$\vec{r}$	Length of pitot “foot”	[mm]
U	Impeller tip velocity	[m/s]
v	Volume	[m^2]
V_{SG}	Superficial gas velocity	[m/s]
V_{SL}	Superficial liquid velocity	[m/s]
x	Distance	[mm]
X	Laminar turbulent transition point	[-]

Subscripts

1	Impeller inlet
2	Impeller outlet/diffuser inlet
3	Diffuser outlet
C	Compressor
c	Critical
CR	Cross- section
d	Droplet
DP	Dynamic pressure
L	logarithmic
l	Liquid
F	Film
g	Gas
h	Consistent density
H	Hub
HR	Helmholtz resonator
S	Shroud
p	Plenum
t	Throttle

r	Ratio
m	Mixture
w	Wall

Table of Contents

1 Introduction

1.1 Background

Norway is the seventh largest oil exporter in the world and the second largest exporter of natural gas to Europe. Despite the fact that oil production has declined since its peak in 2001 the total production is still high due to increased gas production. Historically new production capacity has come from the development of large oil/gas fields. Over the last five years a significant portion of new production capacity has come from few large projects. In the future a change towards more but smaller fields is expected. However, the recent Skrugaard/Havis discovery in the Barents Sea and the Johan Sverdrup discovery in the North Sea represent significant new opportunities. Together with the potential for improved recovery from existing fields the new discoveries are important for the long term perspective with substantial production on the Norwegian continental shelf [1].

In order to utilize the fossil resources on the Norwegian continental shelf, technology and expertise have proven to be of great importance and hence, essential for further exploration and development of new resources. A continued focus on research, development and implementation of new technology are therefore regarded critical to future value creation. Recent attention has shifted towards smaller and more remote fields with limited infrastructure. As a consequence development and operation of such fields requires new cost effective technology [1].

A key element in this matter is the subsea wet gas compression technology which enables the transport of well stream directly to a land based treatment system, or more remote processing facilities offshore. The technology may in some cases eliminate the need for offshore processing facilities, which can contribute to a remarkable cost reduction. Most suppliers of turbo machinery are thereby investing in the development of sea-floor-based wet gas compressors. Subsea compression is a ground-breaking technology representing a paradigm shift for the oil and gas industry [1].

Statoils ultimate vision is a complete subsea factory on the sea floor within 2020 which could be a potential game changer in future arctic field development under ice far from shore. In that context subsea compression is extremely important. The slogan " longer, deeper and colder " is used by Statoil to emphasize on longer from shore, deeper waters and colder environment [2].

Due to the need of expertise and development of subsea installations, in order to meet the demand of fossil fuels and be competitive in a constantly increasing market, NTNU has built an experimental rig to test a wet gas compressor. The rig is unique and important to analyze the basic mechanisms and occurrence of instabilities related to wet gas compression. This is what the master thesis is about.

1.2 Multiphase compression concepts

Compression of gas at the seabed is a significant technology advance no one has previously developed. The technology of subsea gas compression is one of the most important measures to deliver increased volumes from existing gas fields as well as developing resources in more remote and vulnerable areas. When the pressure in the reservoirs declines the flow become unstable and the drive mechanisms i.e. well pressure becomes too weak to transport the gas. The closer the compressor is to the wellhead the higher the efficiency, production rates and total recovery become.

On the Norwegian Continental shelf there are currently 4 subsea gas compression projects going on with different maturity. Åsgard subsea gas compression, Gullfaks subsea wet gas compression, the Ormen Lange compression pilot and Snøhvit phase 2.

The Åsgard wet gas compression is under execution and the subsea module are 71 m long, 40 m wide and 20 m high and includes pumps , gas scrubbers ,coolers and 2 x 10 MW MAN compressors. It will be installed at the seabed and tied to the templates for Mikkel and Midgard reservoirs and the pipeline system to the Åsgard B platform 40 km away. Åsgard subsea compression increases recovery from 60% to 86 % on Mikkel and from 60 % to 69 % on Midgard. The well stream from the reservoirs contains some condensate which is separated before the gas stream enters the gas compressor. Initially two compressor trains will be operated in parallel but change to a series configuration at the end of the fields' lifetime. Åsgard wet gas compression will start operation in 2015 [2].

The Gullfaks wet gas compression project is an increased gas recovery project for the Gullfaks South Brent reservoirs, and comprises the installation of a subsea compressor solution in the vicinity of existing templates in order to prolong the gas production plateau at the Gullfaks C platform; and increase the recoverable reserves from the Gullfaks South Brent reservoir. The subsea solution includes a subsea station with 2 x 5 MW FRAMO compressors with power supply from Gullfaks C. The Gullfaks wet gas compressors have a higher tolerance for liquid and are not dependent on a scrubber like on Åsgard. The project is expected to start up late 2015 [2].

Ormen lange subsea gas compression system is currently considered for further developing of the Ormen lange field as an alternative to a floater. This will be a major leap for subsea processing systems as both the required step-out distance for power is about 120 km and the total installed power will probably be around 50 MW. The installation will include four compression trains each with a capacity of 12.5 MW, variable speed drive (VSD), 11000 rpm compressor, one 400 kW VSD pump, UPS and High voltage (HV) switchgear. The Compression Pilot which consists of one complete train, is now installed in a pit on Nyhavna for full integration testing prior to a possible sanction of the project in late 2012/2013 [2].

Snøhvit phase 2 is in the concept selection phase. Whether Snøhvit phase two will comprise a gas pipe line or a LNG export solution, most probably two subsea stations will be located offshore on sea floor.

1.3 Project scope

Based on literature written by some of the most experienced people within the field and experimental work conducted by the author himself and previous students in the wet gas compression rig located at NTNU it is a goal to visualize and document phenomena related to wet gas surge. Especially emphasize the use of pitot measurements in order to validate the flow pattern and instability.

In order to best possible achieve the main goals of this thesis it is chosen to proceed, and hence keep the main focus on the following tasks:

1) Document the relevant literature regarding the use of pitot measurements to detect the flow pattern and instability.

2) Validate the flow pattern at the end of the impeller by using pitot measurements in existing rig.

3) Identification of wet gas surge using wet gas pitot probes.

1.4 Report structure

The pre project "Aerodynamic instabilities in a centrifugal compressor" conducted by the same author, was written as a preparation to this master's thesis. For the reader's convenience the most important findings will be listed here, however, for the full investigation the reader is encouraged to fully review the pre project. The listing below gives a brief overview of the content in the chapters present in this work.

Chapter 2 serve as an introductory review of the NTNU rig test facility

Chapter 3 describes the multiphase flow fundamentals with wet gas compression

Chapter 4 presents an introduction of the flow pattern principles of the centrifugal compressor

Chapter 5 gives an insight into the theory behind the aerodynamic instabilities that can occur for a centrifugal compressor exposed to dry gas.

Chapter 6 provides a comprehensive literature review related to stability of a centrifugal compressor based on recent research on the subject of wet gas.

Chapter 7 presents the theory behind the analysis techniques applied to the experimental testing, together with a review of comparable visualization methods.

Chapter 8 documents the experimental set-up of the rig.

Chapter 9 presents the results from the two main experimental investigations.

Chapter 10 concludes the work that has been presented

Chapter 11 provides a discussion related to the recommendation for further work

2 Test rig facility

Experimental testing presented in this master thesis is conducted from a one-stage wet gas centrifugal compressor with an axial direct inlet and a radial discharge. The experimental facility for wet gas compression was initiated and installed in 2008 at the Norwegian University of Science and Technology (NTNU) in Trondheim. Since then different configurations of impeller geometries and liquid injection modules have been tested and in June 2012 an inducer, in terms of an axial extension for the existing impeller, was inserted. In addition, based on Computional Fluid Dynamics (CFD) of existing diffuser and volute interactions, a new volute design with larger flow area is scheduled to be installed later in 2012. A picture of the test facility is given below in Figure 2-1.

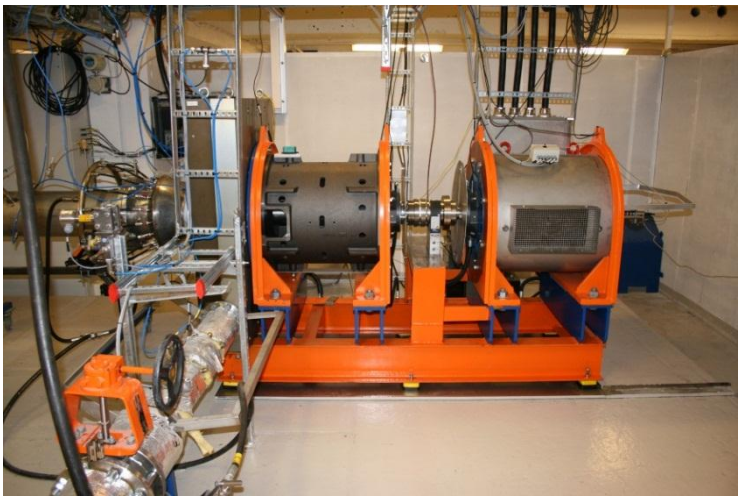

Figure 2-1: Compressor test rig facility

2.1 Main facility data

In its current state the compressor stage includes a shrouded 3D backswept impeller, a vaneless parallel-walled diffuser and a symmetric-circular volute section. The compressor is driven by an electrical motor with a maximum power of 450kW at 11000 rpms regulated by a frequency converter. Regulation of volume flow is done by manually closing and opening a discharge throttle valve. The test rig is designed to operate with a gas mass fraction (GMF) in the range of 0.5 to 1. To ensure the injection of liquid provides an equal distribution, 16 nozzles are distributed uniformly over the circumference of the tube positioned 400 mm upstream to the inlet of the impeller. The water is supplied at maximum 16 bar. For visual flow observations at the impeller inlet and in the diffuser, a transparent section and a Plexiglas are installed, respectively. The injection module together with the see through parts is shown in Figure 2-2.

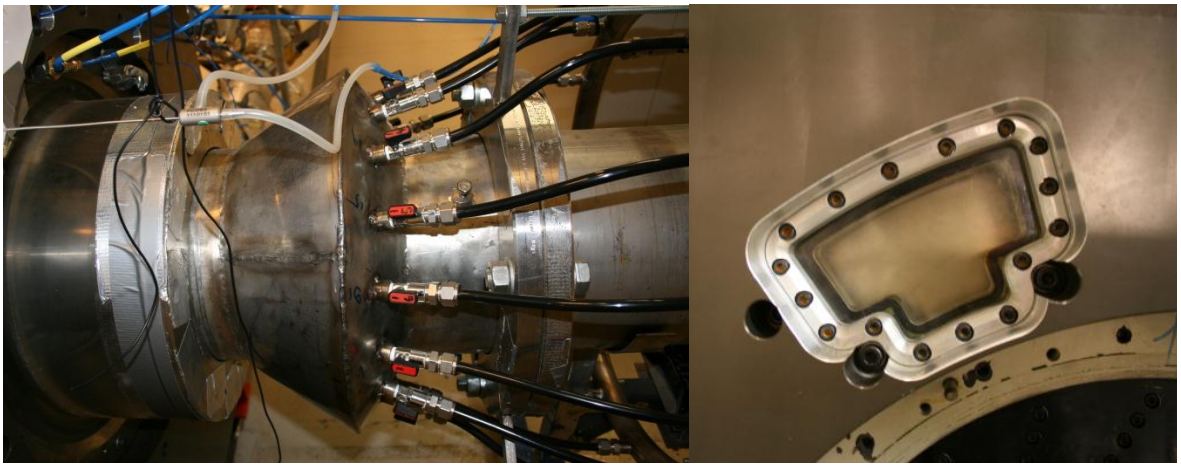

Figure 2-2: Liquid injection module with transparent inlet section and diffuser plexiglas.

2.2 Compressor data

The impeller diameter and width are 0.455 m and 0.014 m, respectively, which gives an inlet width ratio of 0.0615. This particular medium diffusion ratio, indicates a good tolerance regarding flow stability in the diffuser. Moreover, the main parameters describing the test rig are listed in Table 2-1.

Table 2-1: Compressor parameters.

Impeller		
Outlet diameter	D_2	455 mm
Hub diameter	D_H	176-180 mm
Shroud diameter	D_S	251.7 mm
Outlet width	b_2	14 mm
Number of blades	N	18
Exit blade angle	β_2	50˚
Diffuser		
Diffusion ratio	D_3/D_2	1.7
With	b_3	14 mm
Inlet with ratio	b_2/r_2	0.0615

2.3 Instrumentation

The instrumentation includes strategically placed measuring devices throughout the compressor as seen in Figure 2-3. In order to ensure compliance with the standardization i.e. ASME PTC10, a dual instrumentation, with an additional computer monitors the logging. PXI instrumentation has a sampling rate of 20 kHz and 24-bit dynamic signal acquisition modules to ensure synchronous data acquisition. The calibrations of the instrumentation are conducted with GE Sensing P3023-6-P. Moreover a differential- and a static pressure transmitter are used to measure the compression ratio, while an orifice plate is used for mass flow metering. The volume flow is consistently calculated from the density given by the temperature and pressure measurements at the inlet of the compressor. Two sets of three dynamic pressure sensors A, B, C with natural frequencies of 350 kHz are mounted in the circumference of the diffuser as seen in Figure 2-4. To ensure the correct wet gas composition an accurate water injection system, accompanied with inductive flow meters is used. The maximum uncertainties parameters are according to co- super advisor Trond Grüner given in Table 2-2 and a more in depth description of the different meters are given in the data sheets in Appendix C. A comprehensive Risk Assessment report of the NTNU impeller rig facility performed by the the author among others is attached in Appendix D.

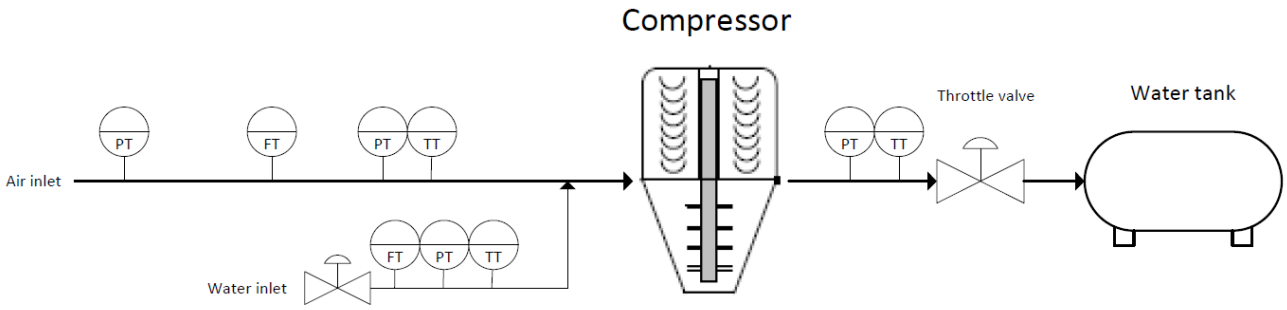

Figure 2-3: Basic schematic of the impeller rig

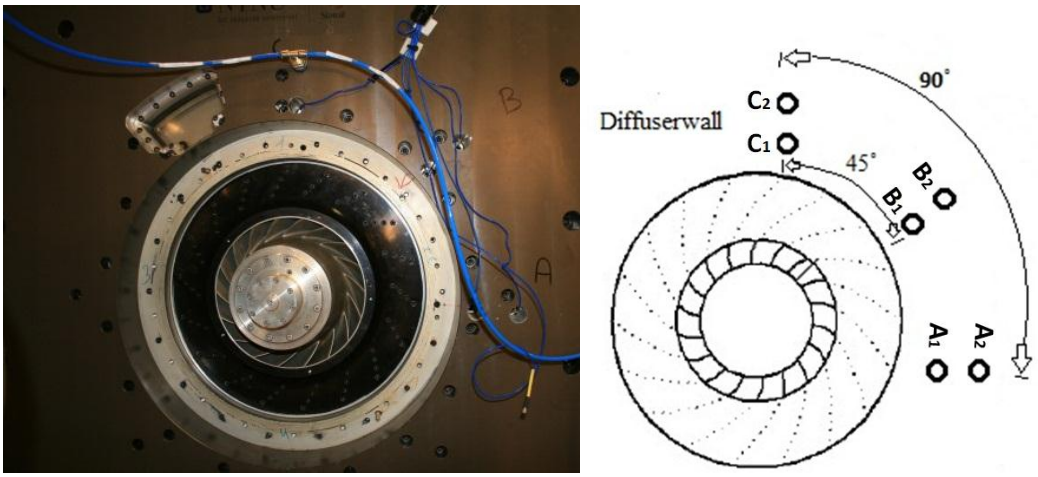

Figure 2-4: Positioning of PCB sensors.

Table 2-2: Maximum uncertainty.

Instrumentation	Uncertainty
Static pressure ratio	0.4 %
Volume flow Q	0.6 %
Rotational speed	1 %
GMF	0.7 %

2.4 Chapter summary and conclusion

Experimental testing presented in this master thesis is conducted from a one-stage wet gas centrifugal compressor with an axial direct inlet and a radial discharge. In its current state the compressor stage includes a shrouded 3D backswept impeller, a vaneless parallel-walled diffuser and a symmetric-circular volute section. The instrumentation includes strategically placed measuring devices throughout the compressor

The impeller test rig is developed, built and modified during the last years, based on the most leading theory available and experimental results. From this it can be concluded that the facility is reliable and will give satisfying results for the purpose of this master's thesis.

3 Multiphase flow

Explanations and equations in this chapter have different relevancy to the master thesis, but will give a more thorough fundament for understanding the multiphase effects on the flow.

3.1 Multiphase fundamentals

Multiphase flow for wet gas compression is defined from an industrial point of view as a gas containing maximum 5% liquid on volume basis, i.e. gas volume fraction (GVF) between 0.95 and 1. However, the gas mass fraction (GMF) can at the same time be less than 0.5 for low pressure ratios verified by Grüner and Bakken [3] among others through experiments. Unfortunately most available work is based on gas containing less than 0.95 on a gas volume fraction (GVF), which makes it somewhat difficult to compare previous work with this master thesis. However, in lack of better experiments, they will, to some extent, be used for comparison. Equations for GVF and GMF are:

$$GVF = \frac{\dot{Q}_g}{\dot{Q}_g + \dot{Q}_l} \qquad \textbf{Equation 3-1}$$

$$GMF = \frac{\dot{m}_g}{\dot{m}_g + \dot{m}_l} \qquad \textbf{Equation 3-2}$$

Normally the GVF parameter is the most preferred one for wet gas fluid mechanics comparison because its properties reflecting geometrics of the fluid mechanic conditions. Nonetheless, the GMF parameter is preferred in application in thermo-analysis as it has proven to be the best parameter in terms of wet gas at low pressure conditions.

The ability of liquid droplets to respond to the gas flow i.e. indicates the possibilities for phase separation depends on the ratio given by Equation 3-3.

$$\delta^* = \frac{\rho_g}{\rho l} \qquad \textbf{Equation 3-3}$$

This simplifies the complex multiphase model into single phase behavior with a consistent density given by:

$$\rho_h = \rho_g + (1-\alpha)\rho_l \qquad \textbf{Equation 3-4}$$

Furthermore, the velocity regarding the multiphase components are denoted V_{SG} and V_{SL} i.e. superficial velocity meaning the single- phase velocity based on mass flow and channel cross-section area. The superficial velocities given in Equation 3-5 and Equation 3-6 are particularly important parameters in order to determine in which flow regime a current flow is categorized as.

$$V_{SG} = \frac{\dot{m}_g}{\rho_g A_{CR}} \qquad \textbf{Equation 3-5}$$

$$V_{SL} = \frac{\dot{m}_l}{\rho_l A_{CR}}$$ **Equation 3-6**

With that in hand a new expression for GMF is obtained, showing how the gas mass fraction term incorporates the phase density difference by the use of Equation 3-2 and Equation 3-6.

$$GMF = \frac{V_{SG}\delta^*}{V_{SG}\delta^* + V_{SL}}$$ **Equation 3-7**

which can also be written

$$GVF = \frac{\dot{Q}_g}{\dot{Q}_g + \dot{Q}_l / \delta^*}$$ **Equation 3-8**

As the gas composition changes the same yields for the performance correction parameters [4]. The increased water content leads to lower Mach number; this is illustrated in Figure 3-1 for wet gas flow at 1 bar. The figure displays the enormous impact increased liquid affects the flow speed and hence compressibility effects that for dry gas were ignored can for wet gas no longer be neglected. The compressibility plays a major role in particular for circulation of the diffuser performance which will be discussed in more detail in Section 4.3.

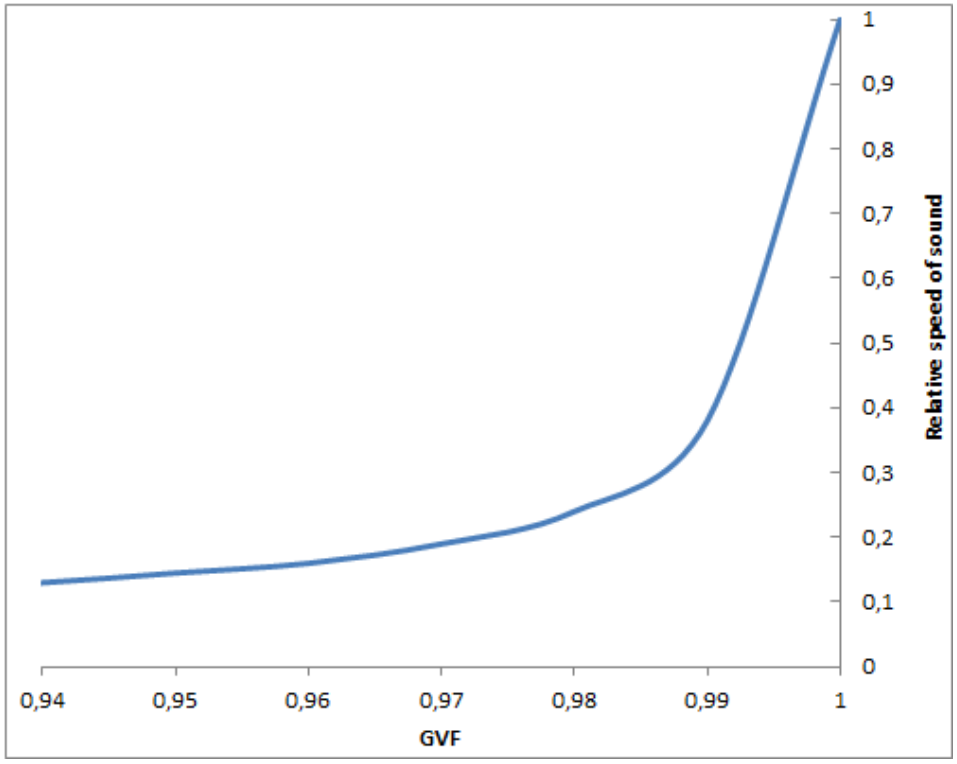

Figure 3-1: Multiphase relative speed of sound in air-water at 1 bar (Wood's model) [5].

The presence of a liquid phase has a substantial impact on the compressor aerodynamics and the thermodynamic behavior of the compressed fluid; accordingly the wet gas is described as

annular flow due to its low liquid content and high gas velocity as reflected in the blue circular area in Figure 3-2.

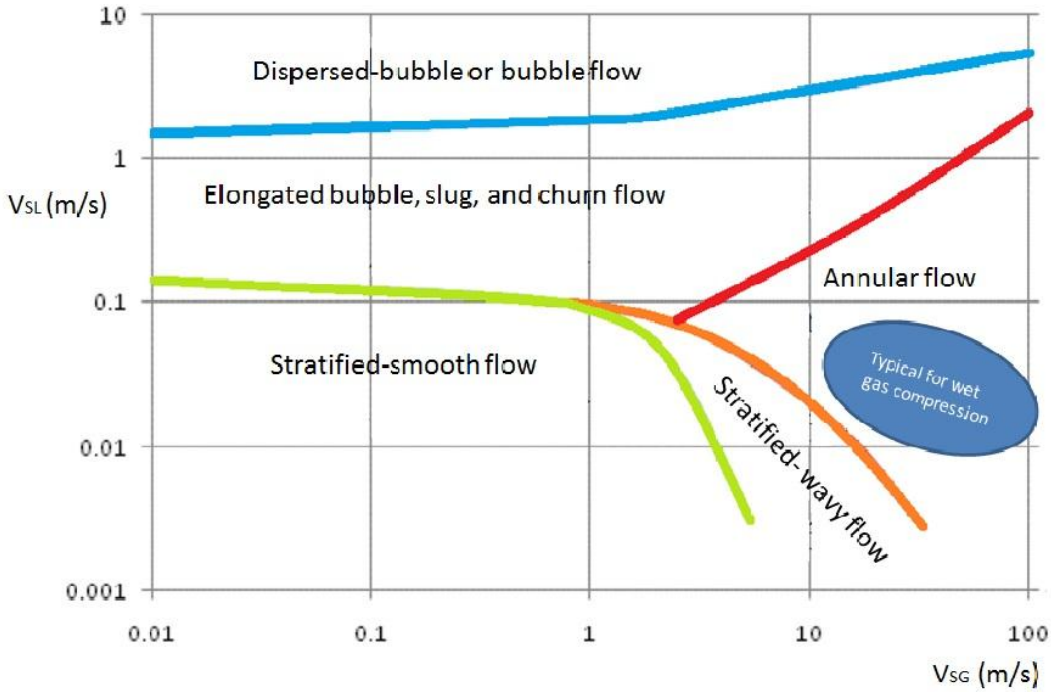

Figure 3-2: Flow regimes for different gas and liquid velocities [6].

The cross- sectional area ratio between the liquid phase and the total channel, i.e. the liquid area fraction known as the liquid holdup H_l, are given in Equation 3-9.

$$H_l = \frac{A_l}{A}$$ **Equation 3-9**

Equalizing Equation 3-9, the droplet hold-up H_d and the film hold-up H_F, respectively can be written:

$$H_d = \frac{A_d}{A_{CR}}$$ **Equation 3-10**

$$H_F = \frac{A_F}{A_{CR}}$$ **Equation 3-11**

The cross section of the flow shows the presence of a thin liquid film on the walls and entrained liquid droplets in the gas core as seen in Figure 3-3. Entrainment describes the mass-fraction of dispersed droplets related to the entire liquid phase given by Equation 3-12.

$$E = \frac{\dot{m}_d}{\dot{m}_d + \dot{m}_F}$$ **Equation 3-12**

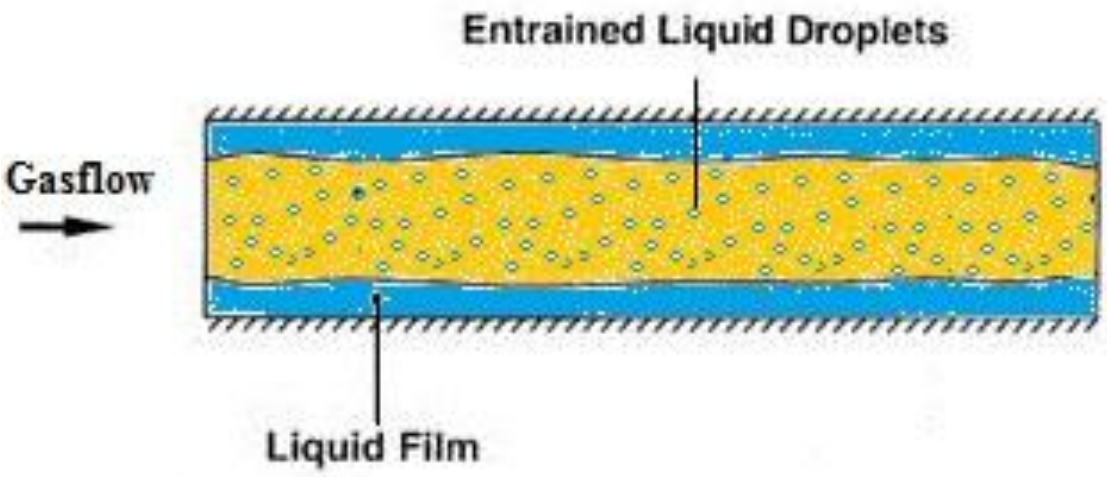

Figure 3-3: Sketch of annular flow.

Regarding gas compression, wet gas that passes the impeller inlet is characterized by dispersed droplets in the core and as dense droplet spray in the core that furthermore prevails through the impeller and the diffuser. The interaction between the phases contributes to multiphase effects not present in single phase flow and it is therefore of high value to identify the liquid distribution in the flow. The interfacial effects between the two phases results in energy, mass and momentum transfer which alter the flow characteristics significantly from single phase flow. Consequently wet gas flow have complicated characteristics given by the interactions and relative movement between the phases[4].

The liquid film in an annular flow will not be symmetrical. Due to gravity the liquid film will always be in the lower part of a tube channel to be thicker than the upper section. The average film thickness around the pipe can be expressed as[7]:

$$\delta = \frac{\delta_{top} + 2\delta_{side} + \delta_{bottom}}{4} \qquad \textbf{Equation 3-13}$$

Hence, an approximation to a film thickness correlation is given as:

$$\delta = 12,5D\,\mathrm{Re}_{gas}^{-\frac{3}{4}} \qquad \textbf{Equation 3-14}$$

where the liquid flow is completely ignored, regardless it gives an good accuracy according to Schubring [7] within a Mean Absolute Error (MAE) of 11%. The MAE relation is given in Equation 3-15.

$$MAE = \frac{1}{n}\sum_{i=1}^{n}\left|\frac{x_{corr,i} - x_{\exp,i}}{x_{\exp,i}}\right| 100\% \qquad \textbf{Equation 3-15}$$

Furthermore Schubring findings suggest that the base film thickness is inversely related to gas flow and increases with increasing liquid flow, due to increased shear stress. At high gas flow rates, the dependence of liquid flow becomes small. Asymmetry shows similar gross trends as

average base film thickness, with an dominant inverse gas flow rate effect and small liquid flow rate effect that is most significant both increase with increasing diameter, but the dependencies are less than linear [7].

3.2 Multiphase effects on the boundary layer

This section gives a brief introduction to the development of boundary layer and the multiphase effects. The latter are important in order to, among other things, explain the occurrence of compressor instabilities that is caused by boundary layer separation. However, aerodynamic instabilities and boundary layer separation are treated in more detail in Chapter5.

In order to explain boundary layer development an airfoil is the most relevant geometric shape to look at because it describes the additional pressure forces that is not evident for instance on a flat plate analogy. Figure 3-4 is an illustration of a typical airfoil shape, whereas the dimension in the traverse direction is enlarged greatly for reason of clarity. A laminar boundary layer begins to develop at the nose of the airfoil. Further along the contour of the airfoil the boundary layer experiences a transition between the laminar and a turbulent flow at a certain point denoted x_{crit} [8].

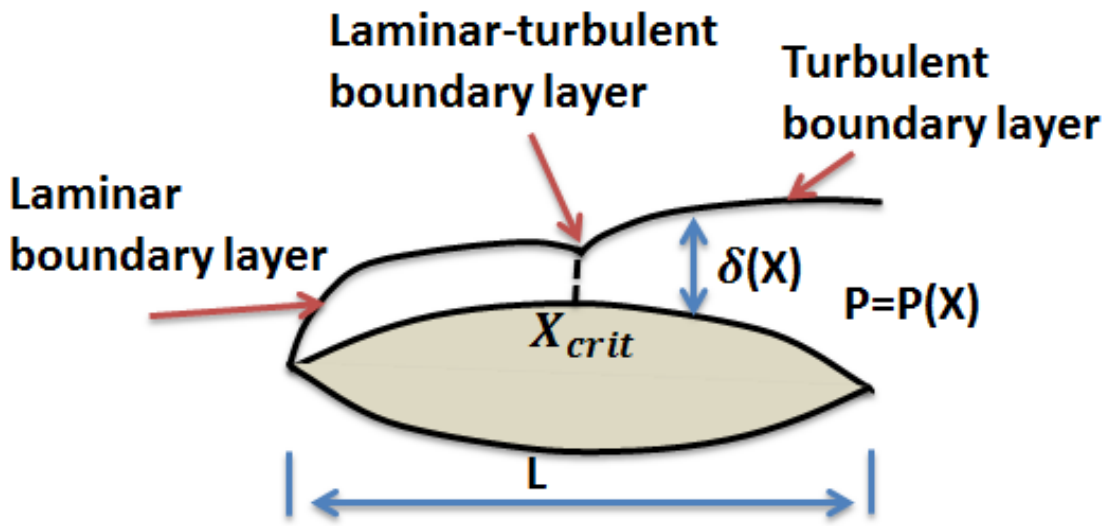

Figure 3-4: Boundary development of an airfoil

The geometry of an airfoil causes a pressure increase in the inviscid outer flow, and hence, the pressure distribution of the boundary layer. Applying a control volume, equalizing the pressure in the boundary layer perpendicular to the airfoil, the pressure on the outer edge of the boundary layer equals the pressure distribution on the airfoil. It is the pressure distribution imposed by the outer flow which is of importance as it determines the positioning in which the laminar-turbulent transition occurs. This means that a great pressure increase in the flow direction can cause a separation of the boundary layer form the wall. However, separation of boundary layer together with aerodynamic instabilities will be outlined in upcoming chapters.

3.3 Chapter summary and conclusion

Multiphase flow for wet gas compression contains maximum 5% liquid on volume basis, i.e. gas volume fraction (GVF) between 0.95 and 1. However, the gas mass fraction (GMF) can be less than 0.5.The presence of a liquid phase has a substantial impact on the compressor aerodynamics and the thermodynamic behavior of the compressed fluid; accordingly the wet gas is described as annular flow due to its low liquid content and high gas velocity. Wet gas that passes the impeller inlet is characterized by dispersed droplets in the core and as dense droplet spray in the core that furthermore prevails through the impeller and the diffuser.

4 Aerodynamic in centrifugal compressor

This Chapter addresses aerodynamics in the main components of a centrifugal compressor in particular with respect to the flow pattern and the interactions between the components. The knowledge of aerodynamic forms the basis of the understanding of instabilities that occur for centrifugal compressors. A cross section sketch showing the main components of the centrifugal compressor at the impeller rig including impeller, diffuser and volute are given in Figure 4-1.

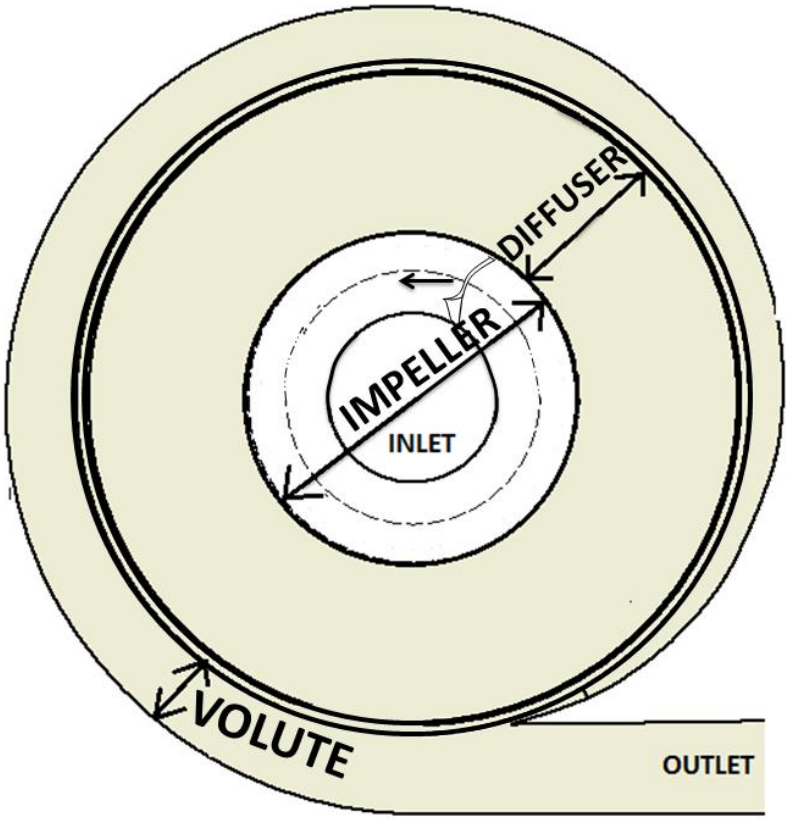

Figure 4-1: Centrifugal compressor (NTNU Impeller test rig).

4.1 Shrouded impeller

The impeller is one of the key components of a centrifugal compressor as it determines the angle of attack, and hence efficiency of the system. Aerodynamic and structure designs of the impeller are critical to the success of the entire compressor stage.

In a centrifugal compressor flow enters axially into the impeller eye before it is whirled around in high velocity in the radial direction and out from the vanes of the impeller disc [9].

The static pressure of the air increases from the eye to the tip of the impeller, in order to accelerate the flow to obtain the necessary pressure head.

The anterior portion of the impeller is designed in order to allow the flow entering the channels evenly and turn the flow in a radial direction with minimal loss. Most of the energy transfer takes place in the radial part of the impeller. The inlet blades are usually given an angle, β, curve, being forward, backward or straight in order to match the relative speed. The optimum flow angle, α_2, is defined by the operational conditions of the compressor. For a multi-step impeller machine it can be convenient to have a configuration of different curved blades setups for best optimization. Backward curved blades stabilize the flow of the impeller and decrease the absolute velocity in the diffuser to help with pressure recovery in the diffuser. The backward bending impeller blades lower the power transfer to the fluid since the radial velocity component of flow is lower, but the efficiency of power transfer increases. The impeller blades at the end are usually quite straight or given an angle to the radial direction. [10]. For the theory about other types of impeller blading the reader is encourage to review the authors pre project [11] on the subject.

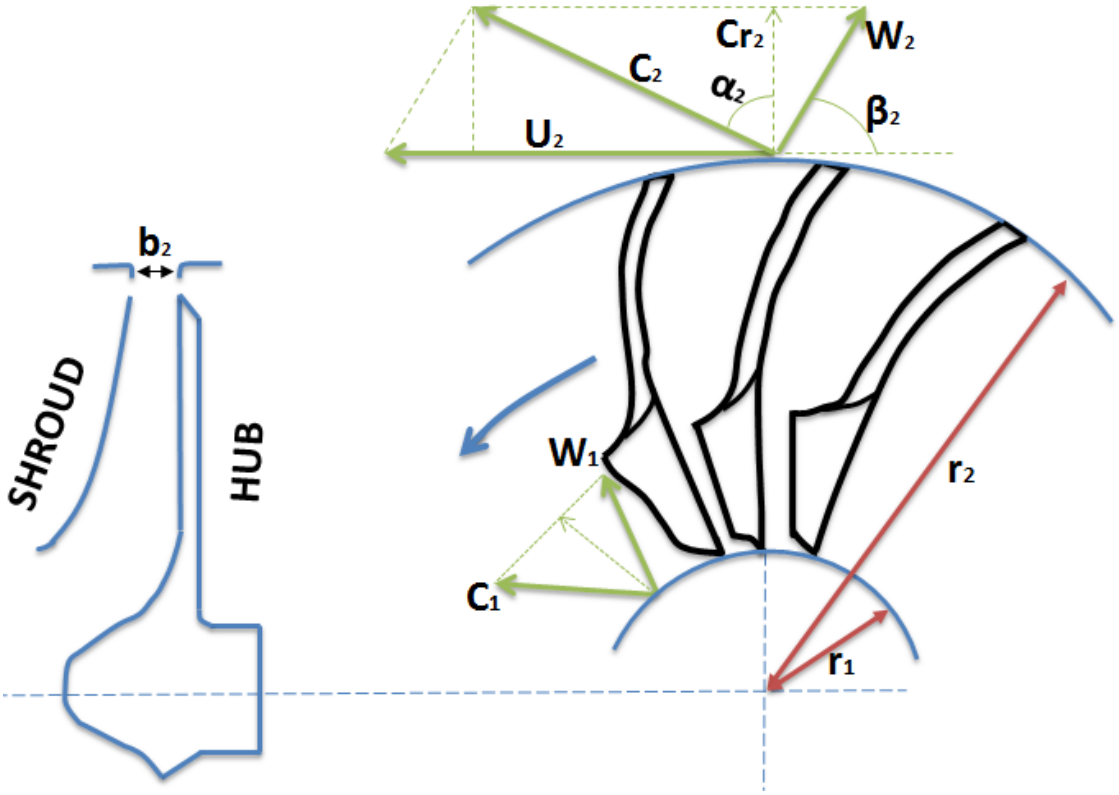

Figure 4-2: Impeller with backswept vanes.

Although the tip speed of the impeller is extremely high, the relative velocities in the impeller channel are generally low. Due to uneven velocity distribution sonic velocities can be obtained at the impeller tip, but not in the impeller channel for dry gas compression [12]. However, the flow pattern differs regarding gas with presence of liquid, which is given a more detailed explanation in the next Section 4.4.

As described above, flow deceleration is essential in order to obtain the necessary pressure caused by centrifugal forces in the impeller. The channels have low hydraulic diameter in

relation to axial compressors and are therefore subject to greater friction at the channel walls. An uneven velocity distribution along the impellers causes an uneven pressure distribution and, consequently a temporal variation in both pressure and velocity of the flow entering the diffuser [12].

4.1.1 Impeller flow patterns

Experimental studies of the flow within the impeller passages have shown that the distribution of velocities on the blade surfaces deviates from the correlations available in theory. Nevertheless, it is most likely that the discrepancies between theoretical and experimental results are due to secondary flows from pressure losses and boundary- layer separation in the blade passages. The complicated flow distribution is shown from a perpendicular- and a meridional (hub to shroud) reference in Figure 4-3 and Figure 4-4, respectively. As seen from Figure 4-3 the stream lines does not cross each other, but are nonetheless actually in different planes observed near the shroud. From the meridional surface in Figure 4-4 it is evident that separation regions occur at the inducer section and at the outlet. From a manufacturing point of view the impeller should be designed in such a way that large decelerations or accelerations of the flow in the impeller that lead to high losses and separation of the flow should, be avoided. In the impeller the viscous shearing forces create a boundary layer with reduced kinetic energy. If the kinetic energy is reduced below a certain limit, the flow in the boundary layer becomes stagnant, then it reverses, which for obvious reasons are undesirable[13].

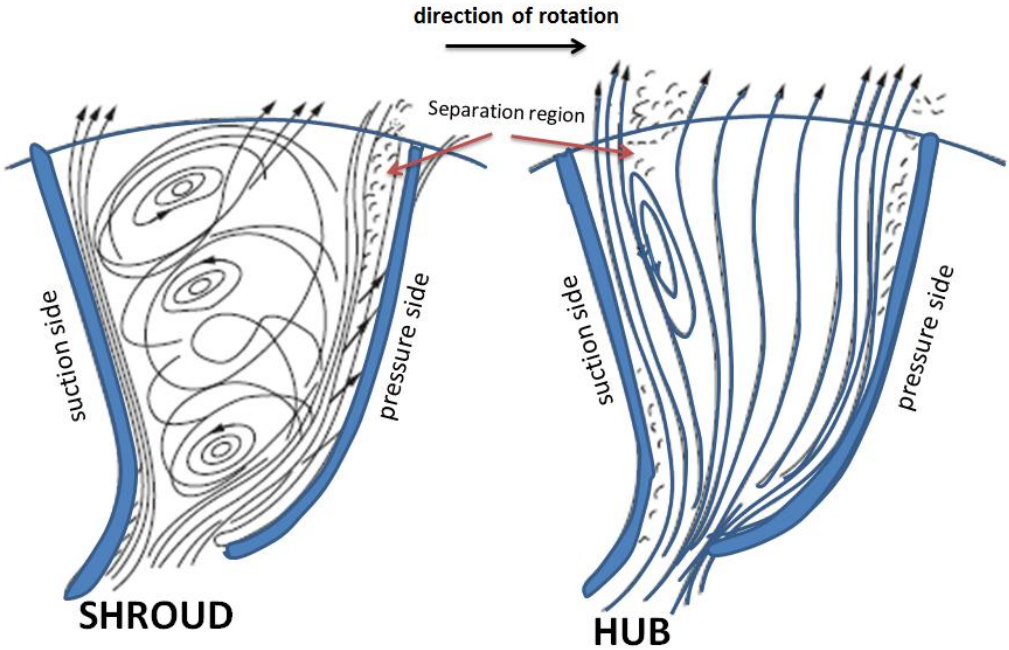

Figure 4-3: Flow map of impeller plane (blade to blade) [13].

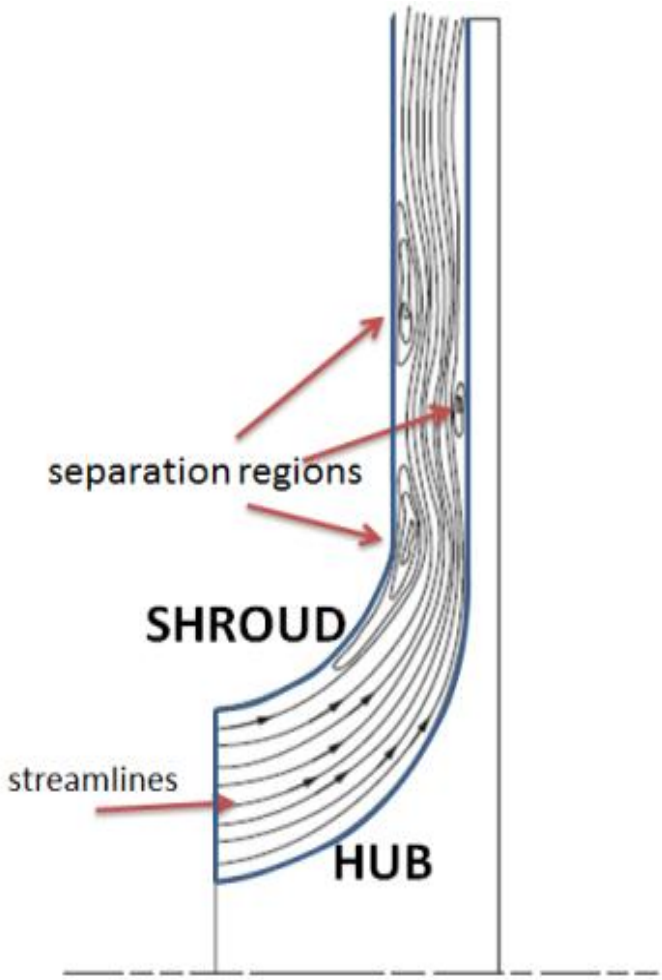

Figure 4-4: Flow map as seen in meridional plene(hub to shroud) [13]

In 1976 D.Eckardt [14] investigated the flow within a high speed centrifugal compressor impeller in order to deepen the insight into the complicated internal flow structure of the impellers. The studies included measurements of velocities, directions, and fluctuation intensities in the internal flow field of a radial discharge impeller. Moreover the relative flow distributions were presented in five different measurements areas from inducer inlet to impeller discharge. The flow pattern increasingly reverses with flow separation from the blades on the suction side, hence developing a rapidly increased wake in the radial impeller. The findings coincide largely with potential-theory calculations in the axial inducer. Furthermore, indications of a beginning flow separation in the shroud/ suction- side corner of the flow channel leading to flow distortions appeared with increased energy. The dominating factor for this is turbulence stabilization of the shroud/suction- side boundary layer, due to streamline curvature and system rotation effects. After onset of separation a rapid growth of the wake area in the shroud /suction side corner of the flow channel appears.

4.2 Impeller and diffuser interactions

The flow on the outlet of the impeller is not completely guided by the blades. This section will outline the theory describing factors affecting the outlet flow of the impeller as it is not solely guided by the blades. In the case of an impeller with backswept blades the effective fluid outlet angle does not equal the blade outlet angle. For this deviation the slip factor given in Equation 4-1 is used.

$$\mu = \frac{C_{\theta 2}}{C_{\theta 2\infty}}$$ **Equation 4-1**

Where $C_{\Theta 2}$ is the tangential component of the absolute exit velocity with a finite number of blades and and $C_{\Theta 2\infty}$ is the tangential component of the absolute exit velocity given infinite number of blades.

A definite cause of the slip phenomena that occurs within an impeller is not known, nevertheless the coriolis circulation, the theory with boundary layer development among other factors contributes to underline the explanation of why the flow is changed. The combined forces from pressure gradient between the walls of two adjacent blades, the Coriolis forces, the centrifugal forces, and the fluid causes a fluid movement from one wall to the other and vice versa. Consequently this movement sets up circulation within the passage resulting with a net change in the exit angle at the impeller exit.

The flowing fluid experiences a smaller exit area due to the development of boundary layer within the impeller passage as illustrated in Figure 4-5. The figure is equipped with radial blades, notwithstanding the same effect of smaller exit area yield whether it is radial or backswept blades. The speed of the flowing fluid must increase to overcome the smaller area. The increase gives a higher relative exit velocity which must be accompanied with a decrease in absolute velocity since the meridional velocity remains constant.

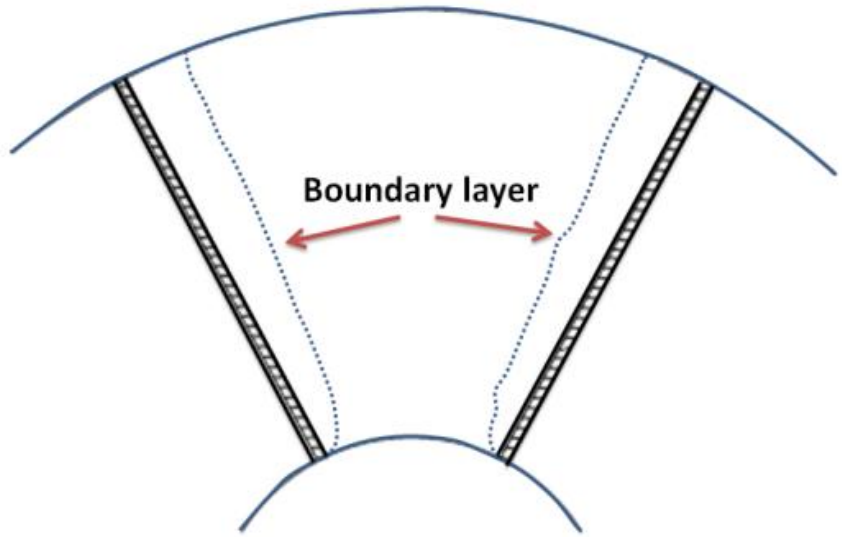

Figure 4-5: Boundary-layer development

Another contributor to reduce the energy transfer from impeller to fluid and decreases the exit velocity angle is leakage of fluid from one side to the other side of the blade.

When fluid exits the impeller, the vanes no longer contain the flow, and the velocity is immediately slowed. As a result of the decreased meridional velocity both the relative and absolute velocities decrease, changing the exit angle of the fluid. The exit velocity triangles for some of the aforementioned factors with the different slip phenomena are illustrated in Figure 4-6 for a backward- swept impeller [13].

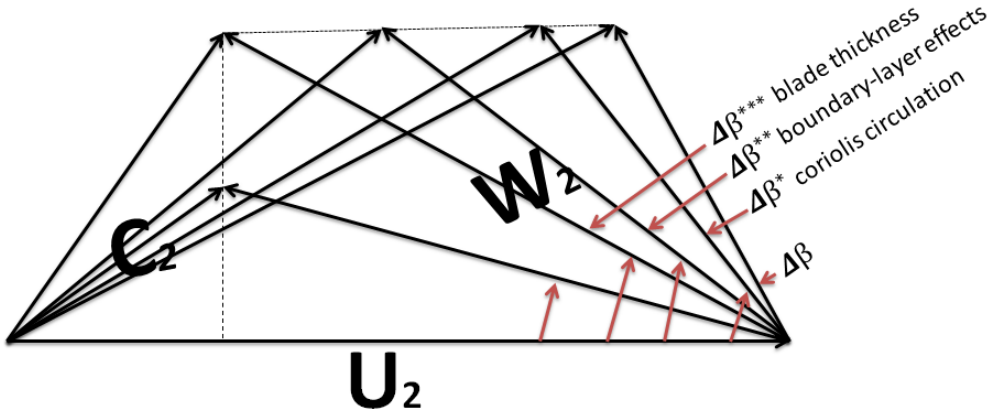

Figure 4-6: Effects on velocity triangles by various parameters[13].

As previous outlined the flow pattern within the impeller is not uniform, meaning that it is a temporal variation in both pressure and velocity of the flow that enters the diffuser. Due to both the non-uniform flow pattern and the fact that the flow path changes from a rotating system into a stationary one, the flow between the impeller and the diffuser is complex and a jet wake will appear and affects the flow. Dean and Senoo [15] introduced through their work a model for rotating wake behavior in a vaneless diffuser. Their theory regarding the model predicted a significant reversible work transfer between the primary (jet) and the secondary (wake) flow leaving the impeller and entering the diffuser. The boundary layer between the primary and secondary zones is poorly defined because of turbulent mixing of the flow. Figure 4-7 displays an idealized jet wake model showing a square wake/jet approximation of the flow.

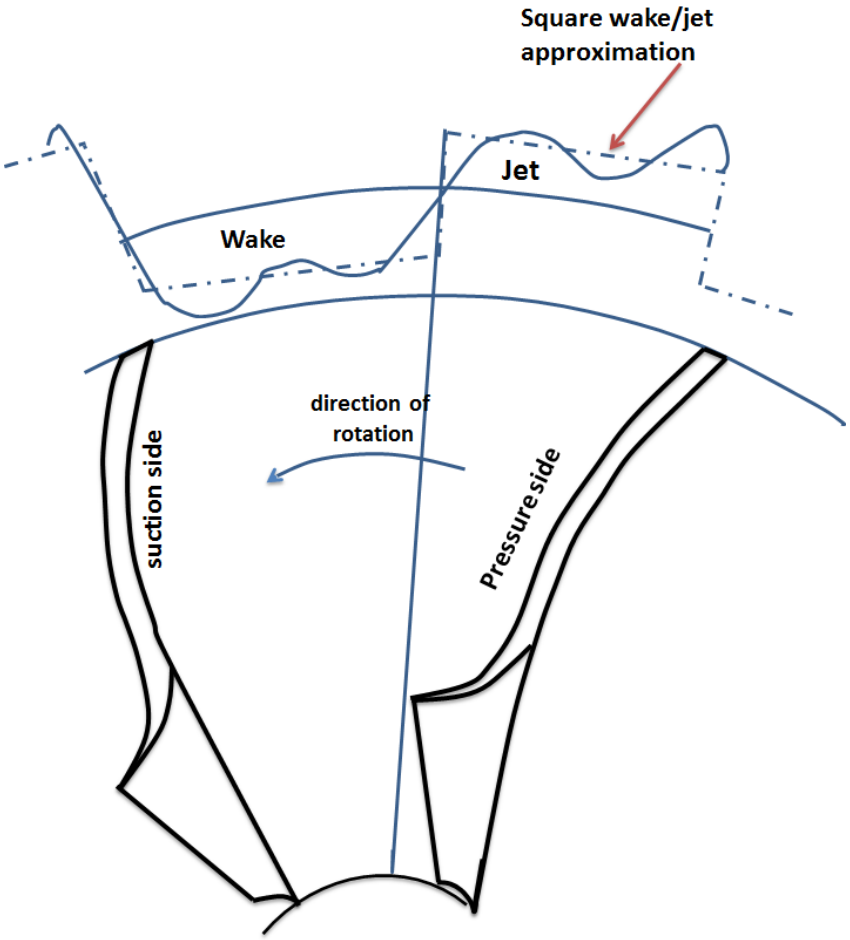

Figure 4-7: Jet-wake distribution from an impeller [13]

4.3 Vaneless diffuser

The diffuser is one of the simplest components of any turbo machinery and yet the most critical and vital component of the compressor. The diffusers purpose is to decelerate the flow from the impeller in order to increase the pressure as efficiently as possible; namely to convert the velocity energy into to static pressure. Outside the diffuser there is a volute which collects the flow and decelerates it further.

Two types of diffusers for a centrifugal compressor exist, i.e. the vaneless diffuser and the vaned diffuser. It is well known that a well-designed vaned diffuser operates at a higher efficiency than vaneless diffusers. However, they are less flexible as they have a narrow operation area compared to vaneless diffusers. As oil and gas applications experiences large differences in flow rates, the natural choice is a system with a vaneless diffuser configuration [16].

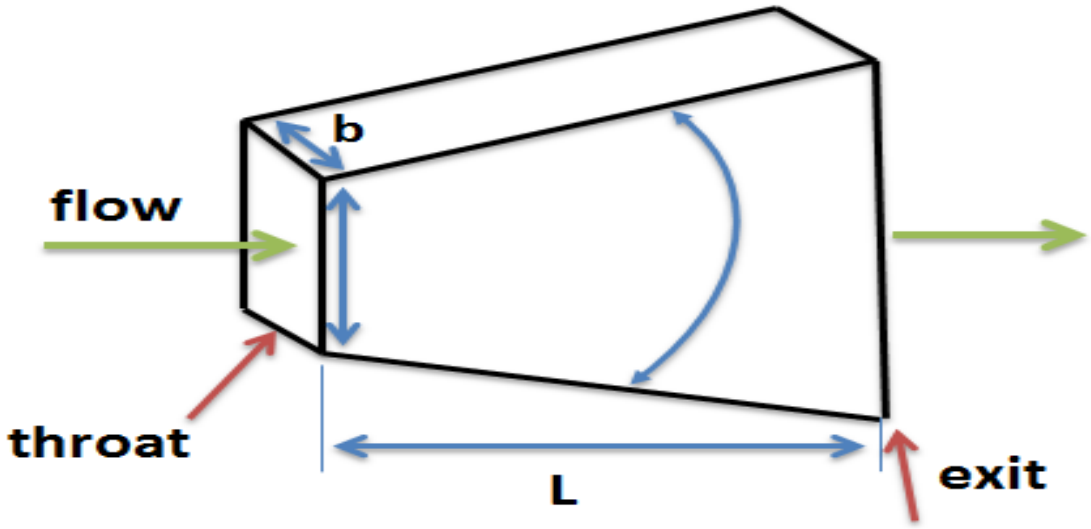

4.3.1 Diffuser flow patterns

The main geometrical variables that affect the performance in the vaneless diffuser is the diameter ratio from the inlet to outlet d_3 and d_4, the ratio of the axial width to the inlet diameter b_3/D_3 and the angle between the diffuser walls. Aerodynamic flow variables are the inlet flow angle α_3 and the inlet Mach number,Ma_3 [12]. In order to develop a basic analysis for the flow in the vaneless diffuser, a summary of the main equations describing the flow pattern are needed.
The continuity
Equation 4-2 , the radial Equation 4-3
and angular momentum Equation 4-4 for axisymmetric incompressible frictionless flow in a radial parallel wall diffuser are:

$$\frac{1}{r}\frac{\partial}{\partial r}(p_0 r v_r) = 0$$ **Equation 4-2**

$$v_r \frac{\partial v_r}{\partial r} - \frac{v_\theta^2}{r} = -\frac{1}{\rho_0}\frac{\partial p}{\partial r}$$ **Equation 4-3**

$$v_r \frac{\partial v_\theta}{\partial r} + \frac{v_r v_\theta}{r} = 0$$ **Equation 4-4**

Hence the flow is assumed to be steady for the simplified analysis and the tangential pressure gradient is assumed to be zero. An integration of the continuity and the angular momentum equation gives Equation 4-5 and Equation 4-6.

$$r v_r = r_3 v_{r3}$$ **Equation 4-5**

$$r v_\theta = r_3 v_{\theta 3}$$ **Equation 4-6**

by combining Equation 4-4, Equation 4-5 and Equation 4-6 the equation becomes:

$$\frac{p - p_1}{\frac{1}{2}\rho_0 v_3^2} = (1 - (\frac{r_3}{r})^2)$$ **Equation 4-7**

$$v_3^2 = v_{\theta 3}^2 + v_{r3}^2$$

In an incompressible flow, both the radial and the tangential velocity components decrease with increased radius. Thus from continuity and conservation of angular momentum, both velocity components are reduced in the vaneless diffuser due to the increase in the radius. A streamline for an incompressible flow is given by Equation 4-8

$$\frac{1}{r}\frac{dr}{d\theta} = \frac{v_r}{v_\theta}$$ **Equation 4-8**

Assumed steady, frictionless, axisymmetric flow i.e. by using Equation 4-4 and Equation 4-5, the equation becomes:

$$\frac{1}{r}\frac{dr}{d\theta} = \frac{v_{r3}}{v_{\theta 3}}$$ **Equation 4-9**

Moreover, by integrating Equation 4-8 from the diffuser inlet yields:

$$\ln\frac{r}{r_3} = \frac{(\theta - \theta_3)}{\tan(\alpha_L)}$$ **Equation 4-10**

$$\alpha_L = \tan^{-1}(\frac{v_{\theta 3}}{v_{r3}})$$

which is an equation of a logarithmic spiral, which forms an angle, α_L ,with any radial line, where, α_L, is termed the logarithmic spiral angle. Thus, the incompressible flow in a parallel wall radial diffuser follows logarithmic spiral streamlines [17].

Regardless of the simple design of a vaneless diffuser the flow theory is rather complicated which is due to the non-uniform flow discharged from the impeller. In addition to non-uniform flow, the logarithmic flow lines, that is long flow paths through the diffuser, prevails viscous shear forces between the fluid and the walls resulting in several secondary flows. In order to decrease the tangential deflection, and hence the flow path through the diffuser, the diffuser width can be reduced with increasing radius. This will cause a small decrease in radial velocity compared to parallel walls, while the tangential velocity will decrease with decreased diffuser width. A decrease in the axial diffuser width, will decrease the radial velocity due to continuity, however, this will have little effect on the tangential speed [18].

Compressibility plays a major role in the calculation of the diffuser performance. Since the retarded fluid through the diffuser increases the pressure and density. This increase in density helps to slow the radial velocity further by increasing the radius. The tangential velocity is not affected by this effect and thus has the real flow a greater tendency to bend in the tangential direction than the radial [18]. The Figure 4-8 show a good flow path in the diffuser with the radial, R and the tangential, T, component drawn in.

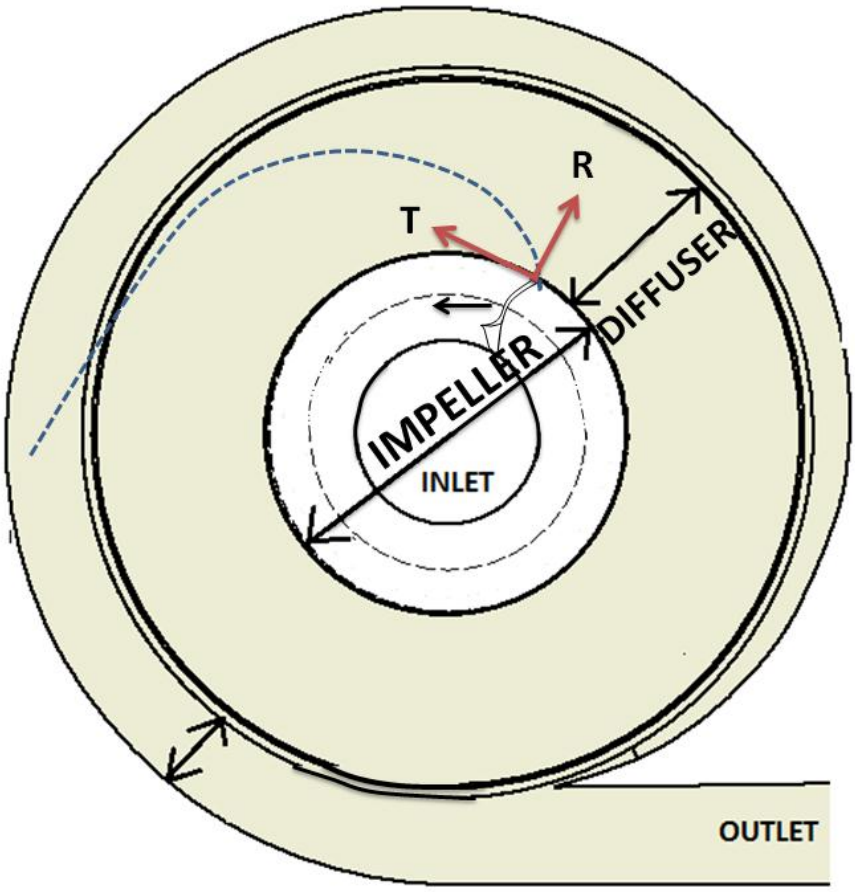

Figure 4-8: Tangential and radial direction in diffuser flow

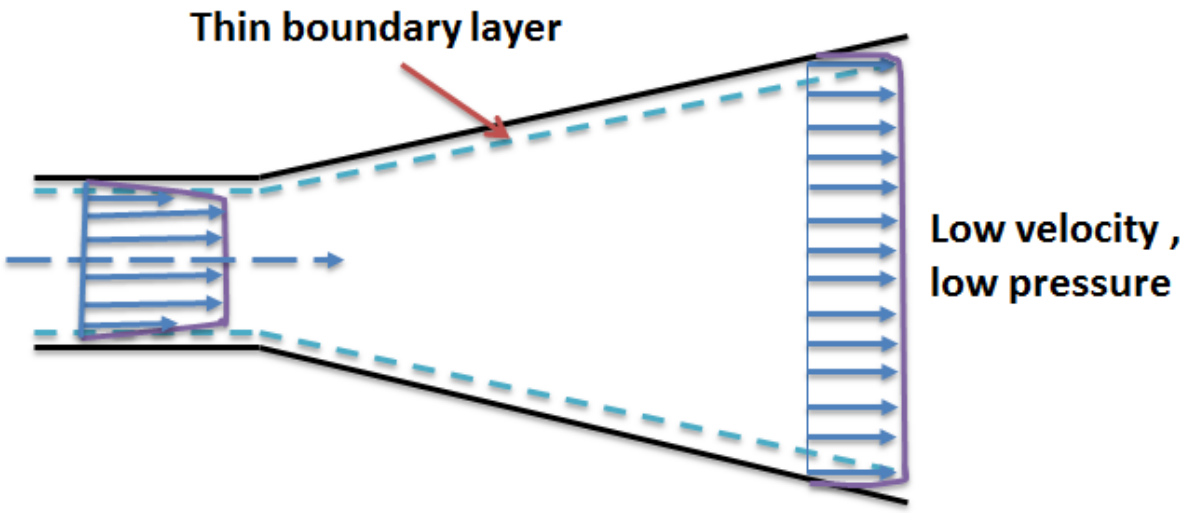

Figure 4-9: Diffuser performance with good performance.

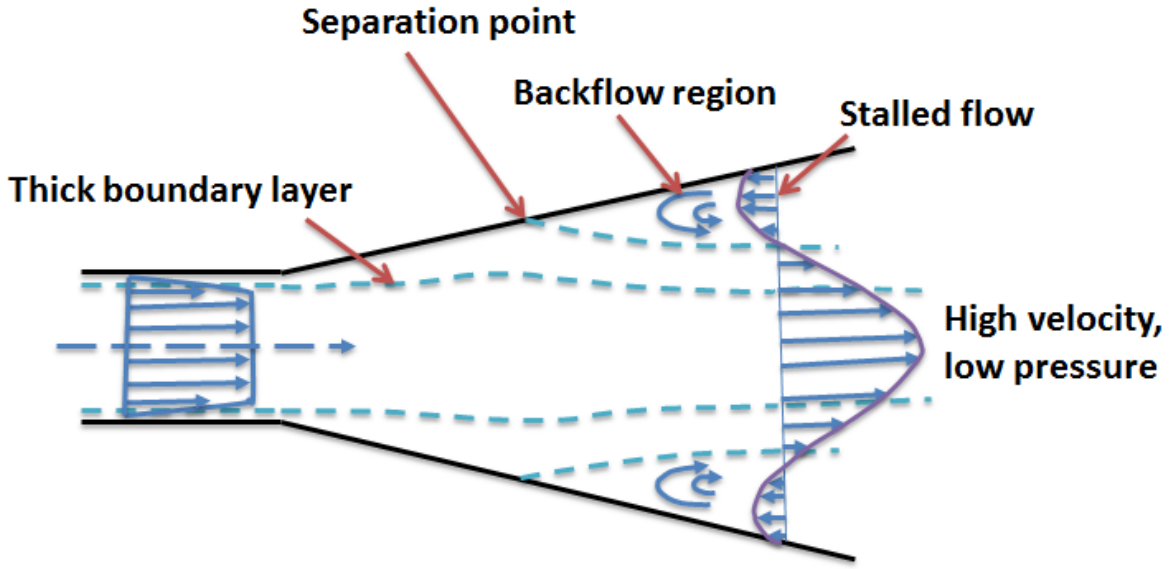

Figure 4-10 : Actual measured boundary layer separation and poor performance.

A comprehensive Computional Fluid Dynamic (CFD) simulation of the components in the NTNU compressor rig test facility i.e. impeller, diffuser and volute are performed by S. Irgens and T.Viseth (2012) [19, 20]. Some of the findings that reflect the diffuser flow regime are pointed out here. Figure 4-11 shows a cross section view of the diffuser and the circled volute with a dry gas volume flow of 0,85m^3 at 9000 rpms. In addition an enlargement of the diffuser inlet is shown in the figure in order to give a closer look at the stream lines. A strong indication of separation appears at the point marked with an arrow at the hub side of the diffuser inlet whereas the flow is stagnated or slightly negative. The backflow in this region does not follow the wall but instead the top of the back flow, thereby reducing the flow effective area. Reduced flow area causes the speed to increase so that the flow will be constant. In order to compensate for reduced flow area the flow velocity increases resulting in less pressure recovery. Viseth [19] findings for optimization of the diffuser and the volute suggests that by introducing a narrowing diffuser where the separation occurs the backflow is reduced because the flow is forced to follow the wall rather then follow the top of the back flow.

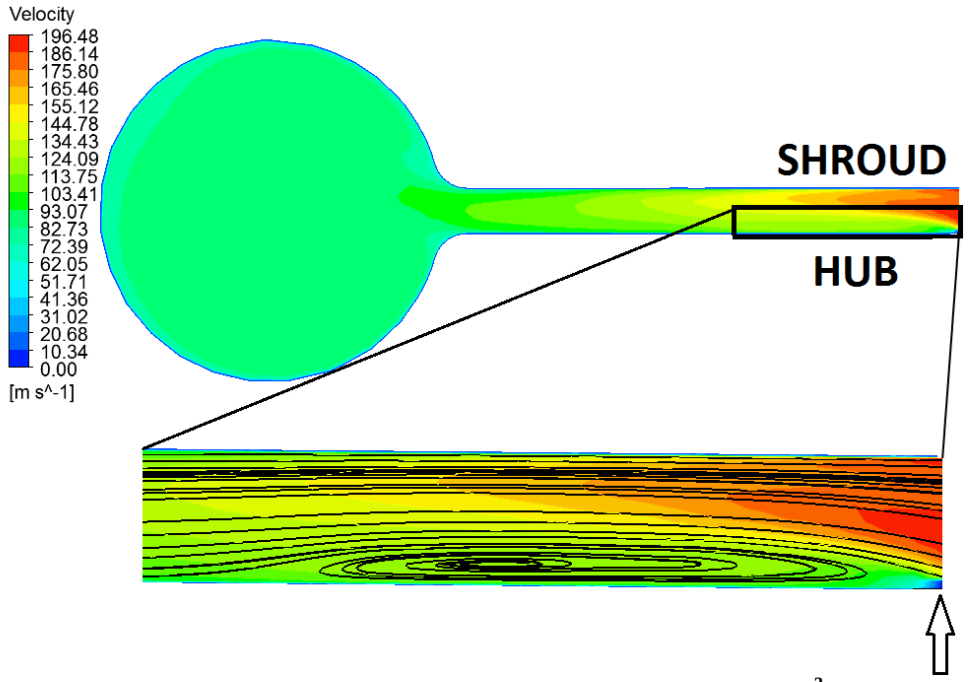

Figure 4-11:Cross section view of the diffuser and volute for 0.85m^3/s at 9000 rpm [19]

From Figure 4-12 the flow velocity drops dramatically coincident with an increase in the pressure field from the impeller outlet i.e. radially outwards the circumference of the diffuser and into the volute from approximately 160 m/s to 90m/s. A formation can be seen of a whirlwind of the stream velocity field in the volute area. According to Viseth [19] the vortex flow comes as a consequence of the spiral head is unable to maintain the stroke that comes from the meridian velocity at the end. The speed is a swirl component of spiraling house and will spread downstream in a spiral housing. Figure 4-13 shows the corresponding cross sectional velocity field where the streamlines marks the direction of the flow.

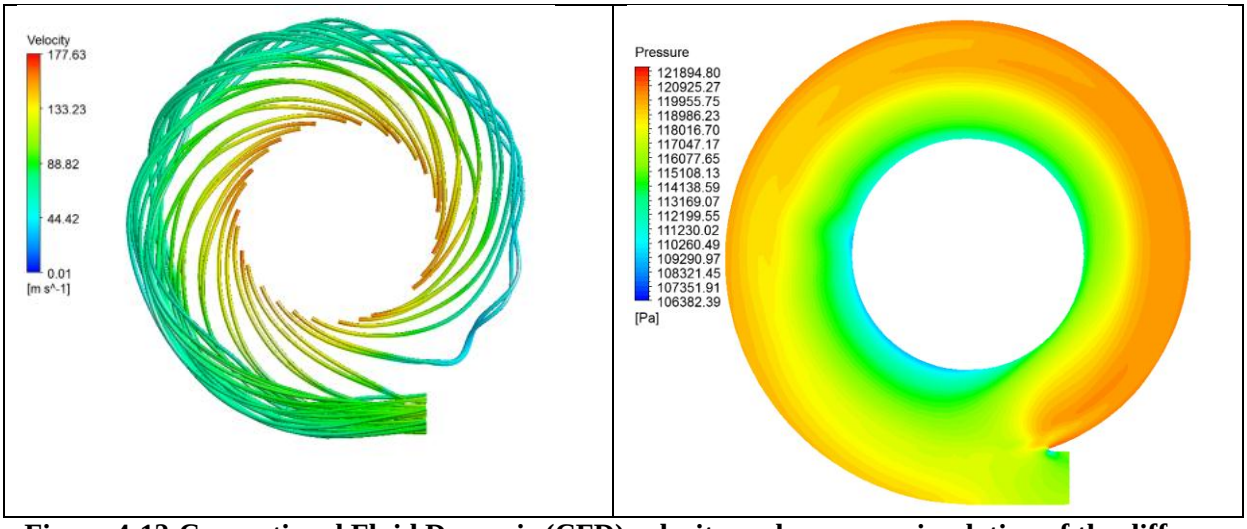

Figure 4-12:Computional Fluid Dynamic (CFD) velocity and pressure simulation of the diffuser and volute[19].

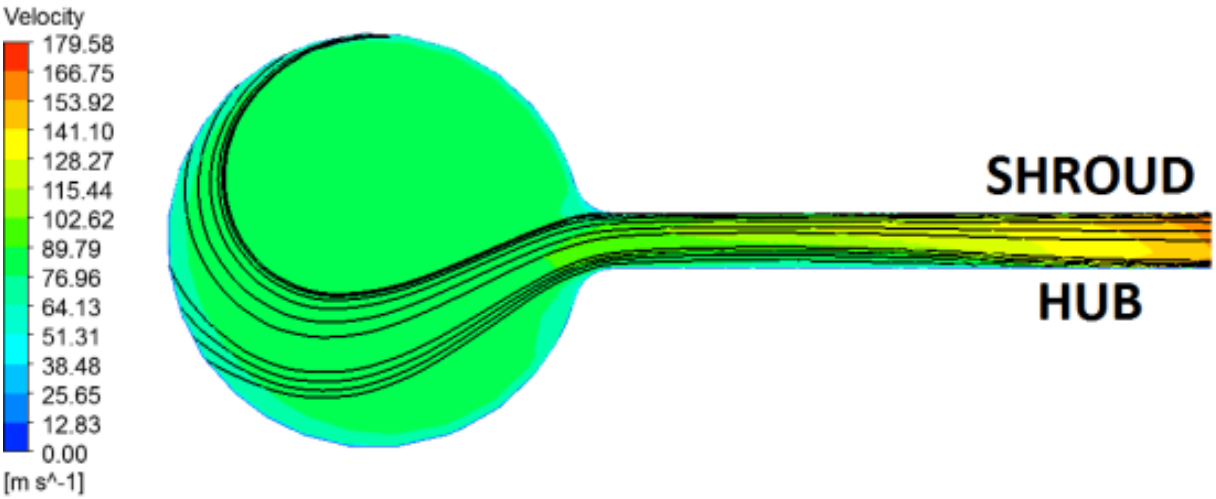

Figure 4-13: Computional Fluid Dynamic (CFD) velocity simulation of the diffuser [5].

4.4 Wet gas implementation

The flow pattern in the diffuser is considerably more complex regarding supply of wet gas in the flow. Moreover, droplet deposition and the interfacial mechanisms are evident. Droplet deposition leads to liquid formation on the diffuser wall and the shear stresses induced by the outer gas- droplet mixture causes the liquid fragments to become released from the film surface. Consequently the liquid acceleration along the pipe centerline depends on the flow pattern development and the droplet size distribution [21].

Brenne (2004) performed an experimental investigation of a straight walled diffuser including injection of two-phase annular flow. The experimental work concluded with several important findings regarding the diffuser flow pattern exposed to wet gas. A short point wise summary of the concluding remarks are given below [21]:

- The way of thinking behind single phase flow is not directly united when approaching the two-phase diffuser flow. With that in hand the flow regimes for single-phase flow cannot be adopted and is accordingly not valid for an annular two-phase flow whereas the velocity profile is highly distorted.
- Accumulation of liquid occurs in the low energy region, which is where the boundary layer thickness distribution along the wall perimeter is at its peak value. Moreover, it is identified at the corner in a rectangular cross- section where initiation of separation is most likely to occur.
- Due to insufficient deceleration of the interia- liquid phase the diffuser performance decreases when liquid droplets are entrained into a continuous gas.
- Unlike the case for single phase flow the diffuser experiences a significant pressure recovery at the outlet section which is explained by the increased flow area attended with backflow regions within the diffuser [21].

Figure 4 shows the relative velocity pattern of a CFD simulation with a small amount of liquid particles in the gas conducted by Irgens og Viseth [19, 20] on the NTNU impeller rig for a volume flow of 0.96 m^3/s at 9000 rpm. It shall be mentioned liquid film and phase interactions between the particles is not governed by the model. However, the flow pattern reveals that the particles are disposed tangentially through the diffuser. This is

according to Irgens and Viseth [19, 20] explained by the fact that the inertia of the particles overcomes the frictional force acting decelerating and inflecting. The particles have a low forward speed reduction through the diffuser.

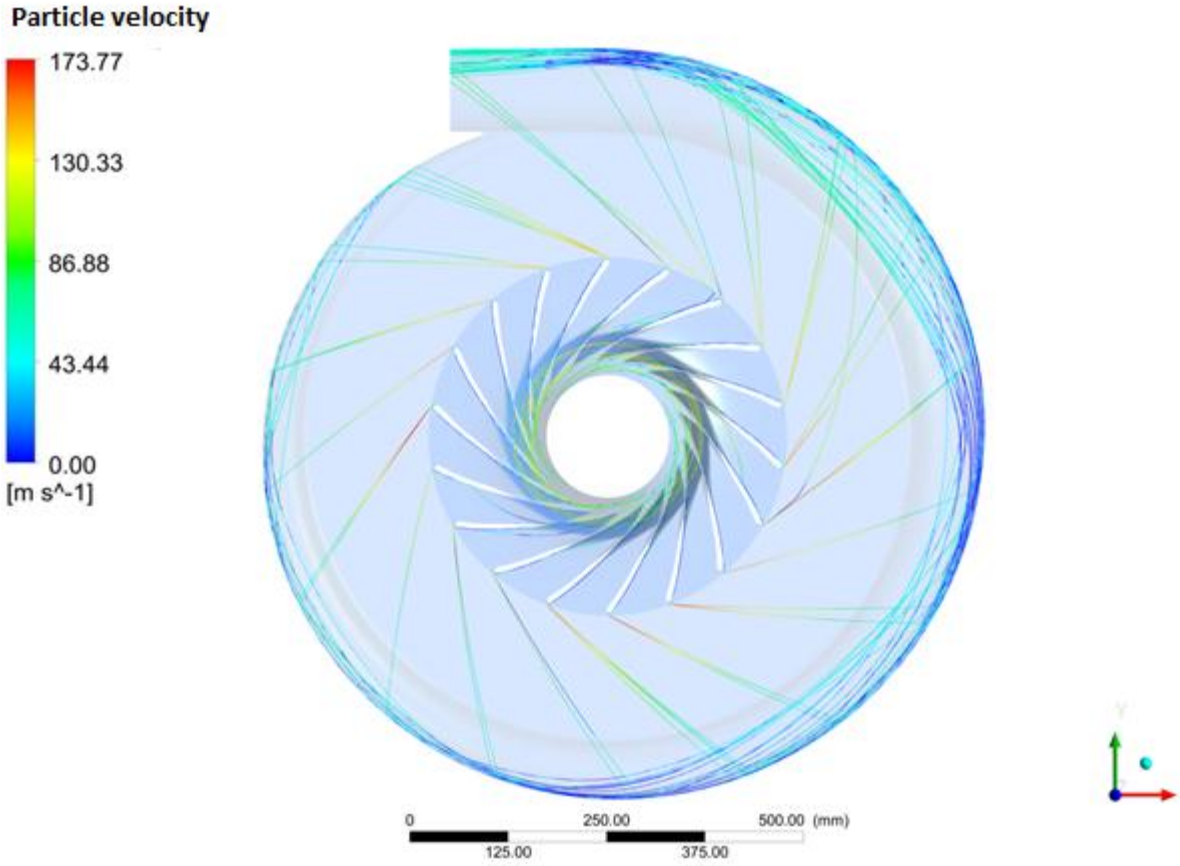

Figure 4-14: Particle simulation on the impeller rig for 0.96 m^3/s at 9000 rpm[19, 20].

5 Aerodynamic instabilities for dry gas

Much of the text in this chapter are extracted and reproduced from the pre-project work by the author [11] for practical considerations.

In compression systems, several types of instabilities can be present. Some of these are combustion-, aero elastic -, and aerodynamic instabilities. The scope of this master thesis is however limited to aerodynamic instabilities, with the respect of the surge phenomena for dry and wet gas. As the theory of dry gas compression is well investigated and understood it is chosen to limit the theory of aerodynamic instabilities in this chapter to dry gas. However, in order to make it relevant for the investigation in this master thesis, it will be related to compression of wet gas in Section 6.2. The section will also go into and discuss implementation of wet gas in relation to dry gas.

5.1 Compressor instability for dry gas

According to Pampreen [22] the aerodynamic stability is in brief the compressors response to disturbance that changes the operation point of the compressor. If the disturbance is temporary which leads to a recurring operation point, the system is stable and otherwise it is unstable. In other words, stability is the system's ability to maintain or increase the outlet pressure to a downstream reservoir, when decreasing the operation point of the compressor by lowering the flow rate.

The performance of centrifugal compressors is highly influenced by aerodynamic instabilities and it is important to distinguish between the different reasons to aerodynamic instabilities. There are in general two types of instabilities that can be encountered in a compressor, known as surge and stall. Surge and stall restricts the compressor performance (pressure rise) and efficiency and can in outmost consequence cause great damage and possibly degradation of the compressor. Surge and stall are therefore important instabilities to understand, whereas the compressors performance is highly influenced by these mechanisms. While compressor surging is in generally easy to understand, the concept of stall is more difficult to explain and understand. Regardless of its complexity stall is an operation mode in which parts of the compressor does not have an efficient energy transfer between the machine and fluid, although the global compressor flow rate is mostly unaffected.

Instabilities are illustrated in Figure 5-1 which examines the case of a system consisting of a compressor and a throttling valve downstream of the compressor. The figure can be used as a tool to illustrate the unstable operating mode of a centrifugal compressor. The starting point is at point A, which reflects the normal operation for the compressor. If the throttle valve is closed, the volume flow through the compressor drops and the operating point moves from A to B. The energy consumption will typically increase and losses are reduced resulting in a higher pressure conditions. Somewhere between A and B the compressor will have a maximum efficiency. The pressure ratio will still increase toward C by further choking because power consumption increases more than the losses. Ultimately, power consumption and losses will match and pressure ratio will reach its maximum. However, by closing the valve further losses will exceed the power consumption and pressure ratio is reduced. In other words, if you are at the operating point that yields the highest pressure conditions and throttle the flow, the outlet pressure drop. The compressor will deliver a lower pressure compare to the pressure which was delivered to the downstream reservoir at the previous operating point. High pressure in the reservoir will lead to delays in the compressor; this is reflected in

instabilities of surge and rotating stall. Although ,inverse flow due to surge to the compressor causes the pressure in the reservoir to decrease to an executable compressor modus; great fluctuations will continue oscillate in and out of the compressor [22].

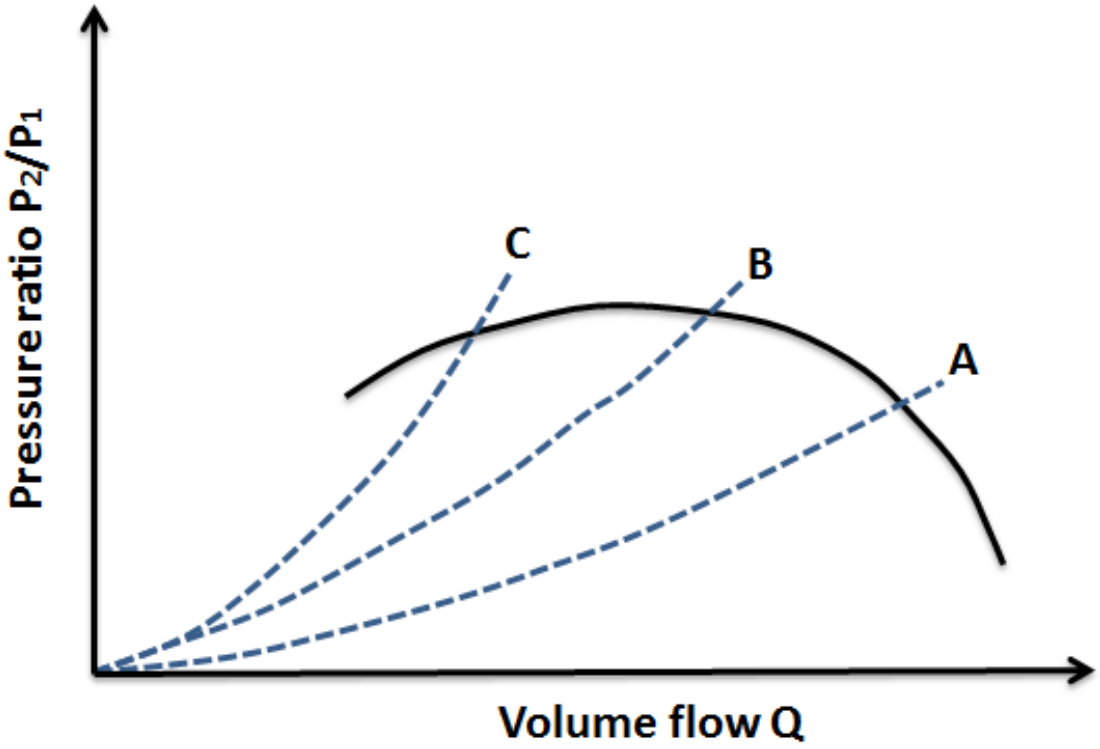

Figure 5-1: Progressiv throttling on a compressor test rig [22].

In the book “Compressor surge and rotating stall: modeling and control" Gravdahl [23] investigate the stability of compression systems. Gravdahl reflects Dean's (1974) way to illustrate stability based on a basic component compression system, existing of a centrifugal compressor, a plenum and a throttle valve. As mentioned above the zero-slope point of Figure 5-1 is the surge point, however, in order to develop the characteristic curve it was necessary to determine the surge point with different rotating speeds. It was found that, as a rule of thumb, the instabilities whether it is rotating stall or surge, occur at operating points with a mass flow rate and pressure ratio, where the compressor reaches high efficiency values. Equation 5-1below illustrates the flow stability and is stable if the left hand side of Equation 5-1 is less or equal to zero:

$$\frac{\partial PR}{\partial \dot{m}} \leq 0 \qquad \textbf{Equation 5-1}$$

where $\dot{m}$ is the mass flow rate and PR is the overall compressor ratio. Hence, as illustrated in Equation 5-2 the pressure ratio is the summarized pressure product of n components i.e. the impeller, diffuser, volute etc.

$$PR = \prod_{i=1}^{n} PR_i \qquad \textbf{Equation 5-2}$$

With this in hand, the stability criterion can be written as

$$\frac{\partial PR}{\partial \dot{m}} = PR\sum_{i=1}^{n}\frac{1}{PR_i}\frac{\partial PR_i}{\partial \dot{m}} \triangleq PR\sum_{i=1}^{n} SP_i \leq 0$$ **Equation 5-3**

Dean investigated the effect of the different components on SP and found that if the components in which SP_i is positive or negative are destabilizing and stabilizing respectively. Whether a particular component in the compression system is more important than another in the case of determine instability is widely debated in the literature, however most literature states that the diffuser channel play an inherently and destabilizing role while the impeller and the diffuser inlet are typically stabilizing. From the above review conclusion can be made that there is great uncertainties regarding instabilities and that an increased understanding of the mechanisms behind instabilities will result in permission of lower safety margins which will contribute to provide an increased area of operation. In order to cope with the occurrence of instabilities it is therefore common practice to operate with a surge margin to prevent the compressor to operate in this area. With a better understanding it will be possible to develop compressors with a lower tendency to go into stall and surge and consequently achieving higher efficiency of the machinery. The Figure 5-2 shows the typical operation point for the compressor i.e. to the right of the surge line with the associated control line. For the full review of surge control an anti-surge systems the reader is advised to review the pre project thesis [11].

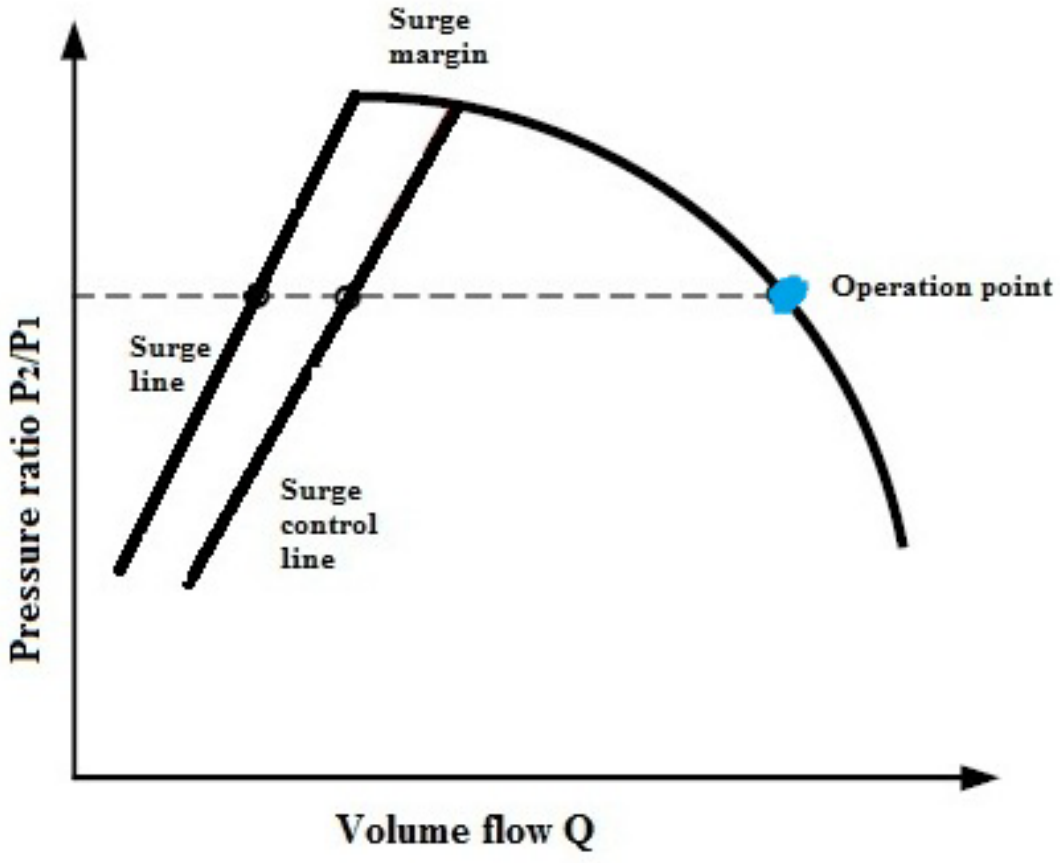

Figure 5-2: Centrifugal compressor characteristic.

5.2 Rotating stall

There are two types of stall reported for dry gas in a centrifugal compressor namely impeller stall and stall in diffuser for both vaned and vaneless diffusers.

For centrifugal compressors the stall instability is created by areas of stalled passages identified as stall cells occupying volume in the compressor. This affects the flow around stall cells and leads to a phenomenon known as rotating stall. Rotating stall cells have been detected in both the impeller and diffuser. In rotating stall cells rotates in the same direction as the impeller, but at lower speeds. Stall cells are categorized as sub-synchronous vibrations, at 0.6-0.95 of rotational frequency. However, the classification of rotating stall may be various depending on different factors, among them being size, location of separation, compressor component and the compressor curve [24].

The operation mode of stall is associated with the separation of the boundary layer in flow through the compressor. According to Ferrara [25] separation is due to high positive attack angles of the blades in the impeller and in the diffuser vanes, while in the vaneless diffusers the stall cells has been described as a 3D separation of boundary layers at the diffuser walls. Boundary layer mechanisms are therefore highly important in relation to understanding the phenomenon behind stall. A more detailed review about boundary layer separation is given in Section 5.3.

5.3 Boundary Layer development and separation

In order to explain stall, and hence, the boundary layer separation, a simplification considering a circular cylinder, is used. As illustrated in Figure 5-3 the cylinder is immersed in inviscid symmetric flow whereupon an accelerated flow with pressure drop from point D to E is presented, as a consequence of friction along the cylinder. The pressure drop is due to the energy transfer from potential to kinetic energy. However, the pressure will increase yet again as the flow will perceive a retardation moving from E to F. At the same time a particle moving in the outer flow from D to E, pressure is transformed into kinetic energy, and moving from E to F, kinetic energy is transformed into pressure. The same pressure distribution yields for the boundary layer as for the particle since it is imposed to the outer flow. The particle will lose a lot of kinetic energy due to the large gravitational forces that dominates in the boundary layer. This loss of energy causes the particles to no longer flow towards the pressure gradient from E to F. Consequently the particle stops and is pressed back against the original speed. There is always a danger of separation in region S as shown in Figure 5-3and Figure 5-4, where the pressure increases because of positive pressure gradient alongside the flow direction [8].

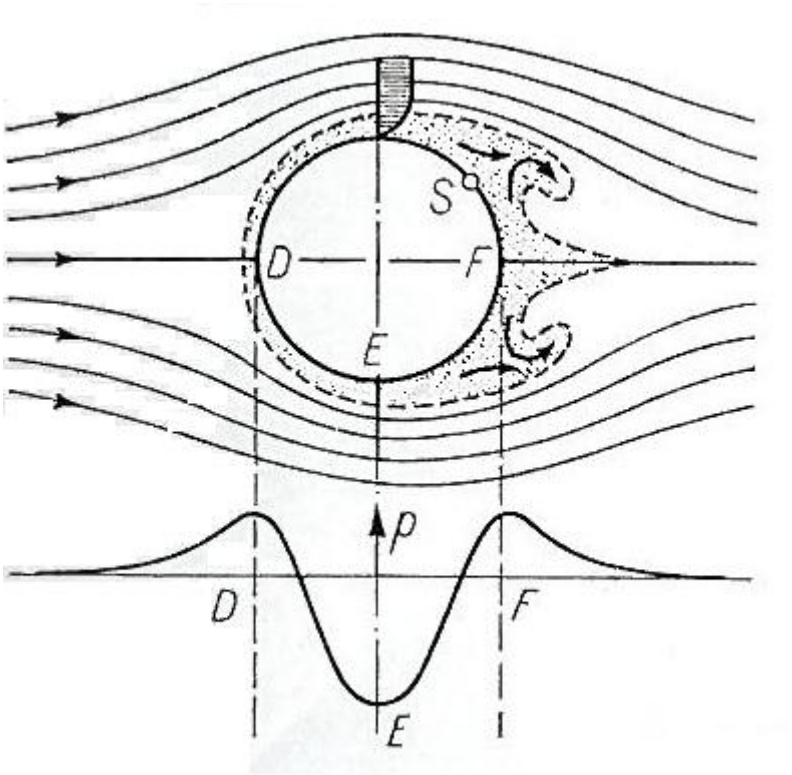

Figure 5-3: Separation of the boundary layer and vortex formation at a circular cylinder[8]

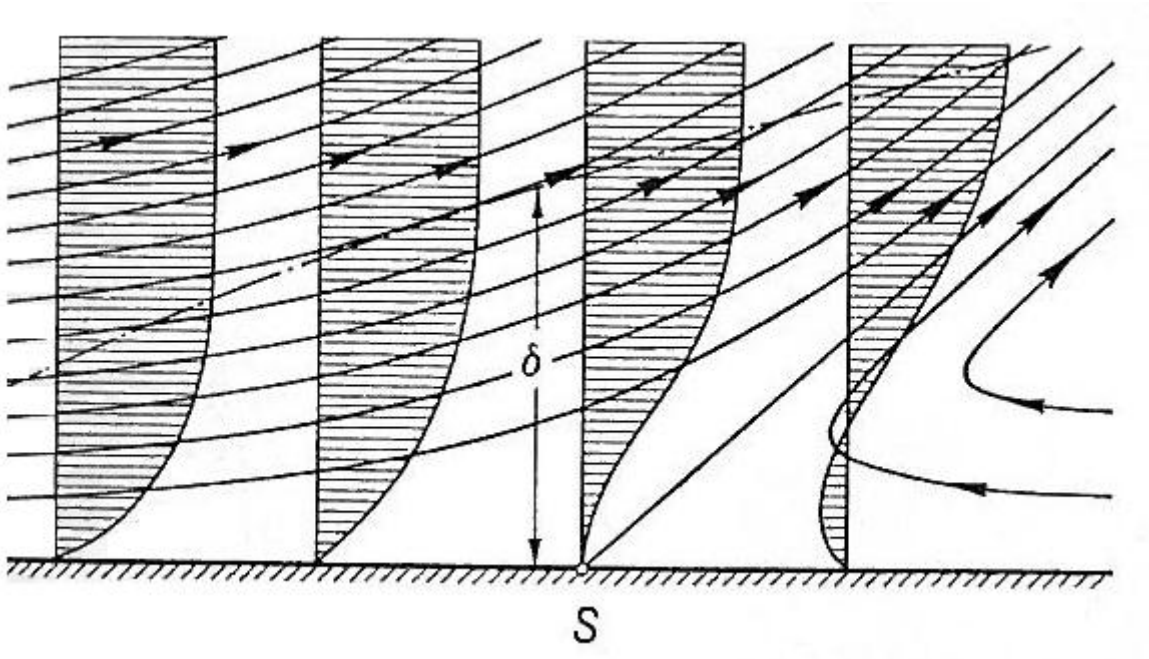

Figure 5-4: Boundary layer flow close to the separation point S [8]

Figure 5-4 illustrates that the originally flow in the boundary layer will deflect, and flow away from the wall due to back-flowing particles. As a result of the backflow, a strong thickening of the boundary takes place and consequently the boundary layer mass is transported away into the outer flow. Separation is given where the velocity gradient perpendicular to the wall is zero, marked S in Figure 5-4. Consequently the shear stresses τ_w are zero as given by Equation 5-4.

$$\tau_w = \mu(\frac{\partial u}{\partial y})_w = 0$$ **Equation 5-4**

This reasoning is directed transferable to the flow inside the diffuser illustrated in Figure 5-5 and Figure 5-6. The effect of separation is prevails causing high velocity and low pressure recovery as seen in Figure 5-6.

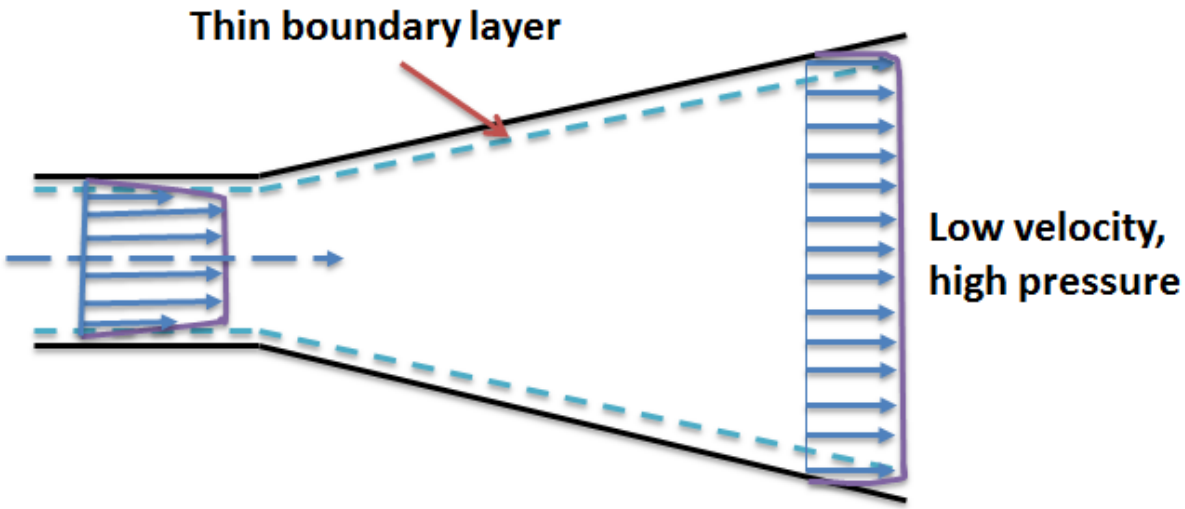

Figure 5-5: Diffuser flow with good performance.

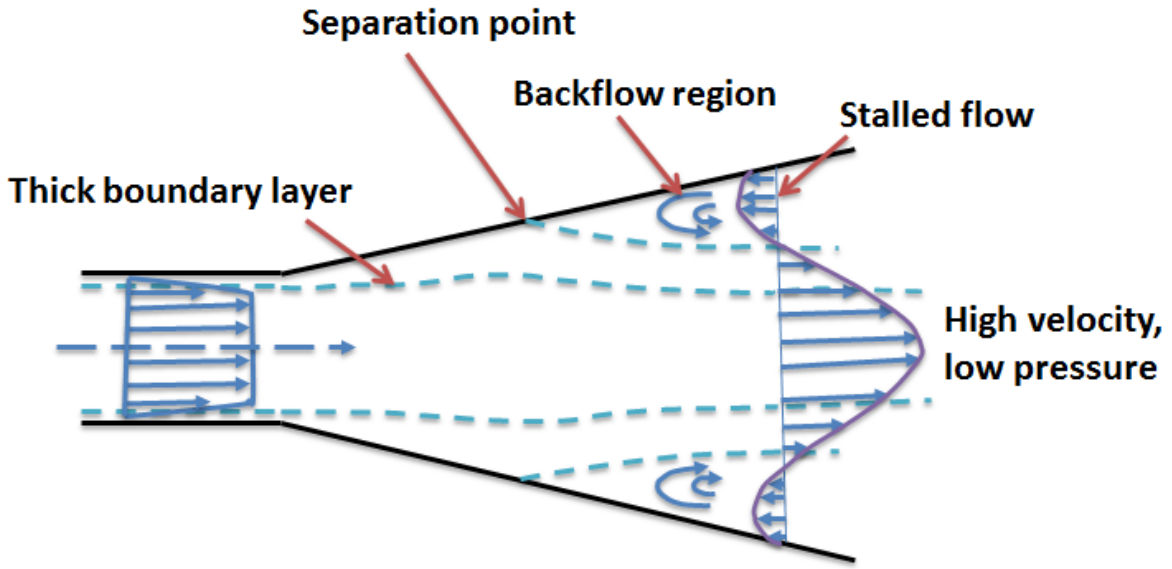

Figure 5-6 : Actual measured boundary layer separation with poor performance.

The same theory of boundary layer separation can be applied for airfoils and blading inside compressors. Furthermore, on the basis of expansion on the upper side of the blade a positive pressure gradient is formed along the streamline.

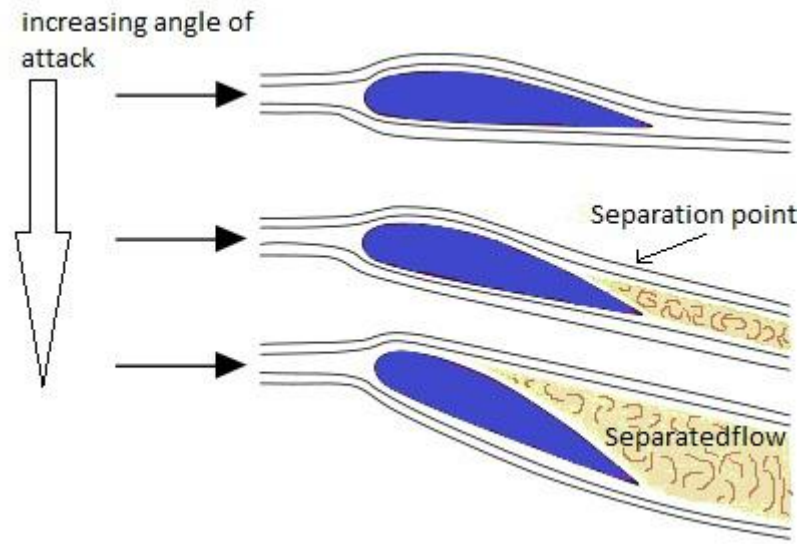

Figure 5-7: Separation over a wing profile with increasing attack angles [8].

Figure 5-7 displays how the separation develops over an airfoil with increased angle of attack. At small attack angles, the kinetic energy of the boundary layer is large enough to overcome the pressure gradient. As the angle of attack increases above a certain point, the stall point, the lift force on the airfoil is at its maximum. Further increase results in decreased lift as the separation region on the top of the wing increases in size. This can be explained by at higher attack angles the expansion and the pressure increase is so great that the boundary layer does not have enough energy to follow the wing profile. Large vortexes are formed occupying a large area obstructing the remaining stream to flow through [8].

An important finding from boundary layer separation is that the point of separation is postponed at the turbulent boundary layer relative to the laminar boundary layer as illustrated in Figure 5-8. This is because the turbulence provides the boundary layer with much greater energy in comparison with the case of laminar flow [8].

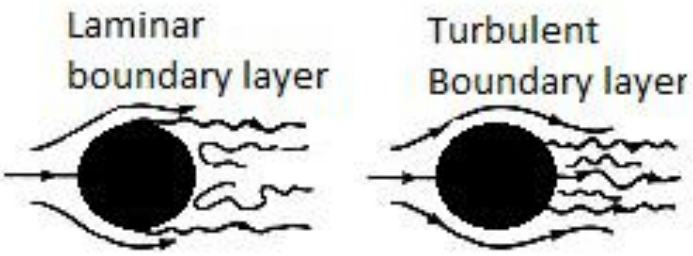

Figure 5-8: Laminar versus turbulent boundary layer [8].

5.4 Impeller rotating stall

In order for rotating impeller stall to occur the angle of attack must be sufficient large, and beyond a certain point, allowing separation of the boundary layer to emerge while the flow stream passes around the impeller blades. The angle of attack increases with decreasing volume flow as the axial velocity component, which is facing into the impeller, becomes reduced. Consequently the reduced flow increases the angle of the flow at a neighboring blade, affecting the nearby blade to stall. Thus the stalled cell moves from blade to blade rotating in the opposite direction of impeller rotation as seen from a rotating reference that follows the impeller. In general the rotating impeller rotating stall is recognized in the range of 50-80 % of the rotational speed [3].

A number of impeller blades commonly stalls at the same time in accordance to multiply stalls that rotate around the impeller result in the occurrence to be quite close to the surge point on a compressor characteristic curve. Once an impeller begins to stall, only a small decrease in flow will stall the impeller completely and cause the compressor to surge. Flow separation behind a stalled blade reduces the volume of the flow in the passage behind the blade, which will cause some of the flow to reverse itself and flow back out of the passage [26].

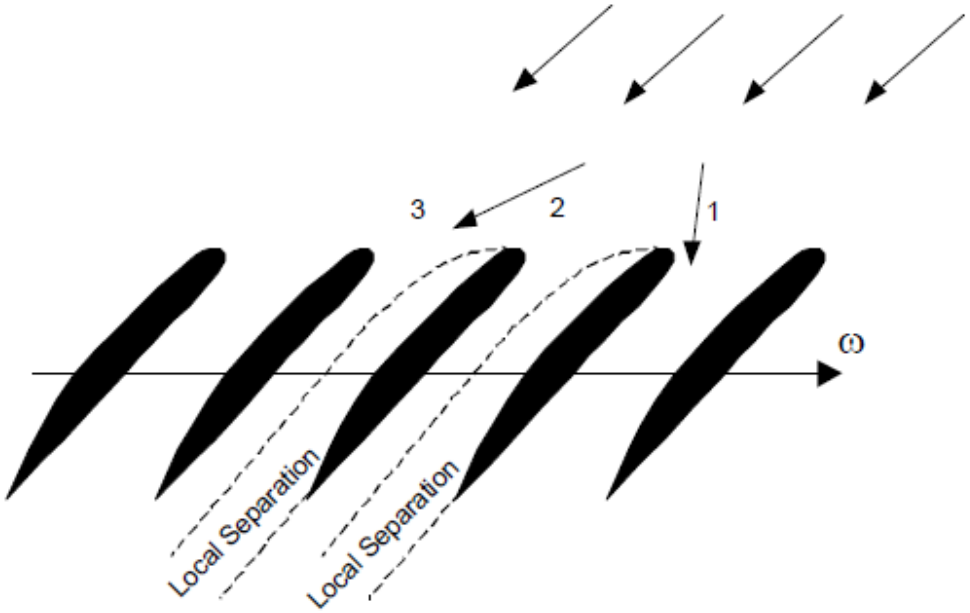

Figure 5-9: Stall affects adjacent blades[12].

5.5 Vaneless diffuser rotating stall

The vaneless diffuser is simple and relatively cheap as it provides a simple design without vanes that can cause traditionally airfoil stall. however, stall can occur as a result of among others, change in volume flow and pressure change, if the vaneless diffuser is not cautiously design [24]. In contrast to impeller- and vaned diffuser rotating stall, vaneless diffuser rotating stall can start to evolve at a quite considerable distance away from the surge point. The stall cells are basically types of recirculated swirls that appear in the flow. When a swirl or a stall cell starts to develop the changed flow on the other side of the swirl causes the swirl to move in an oblique direction. Gradually, additional stalled cells start to emerge and rotate around the circumference of the diffuser. Consequently if the flow is further reduced the stall cells becomes larger and finally causing the compressor to surge [26]. For the diffuser, the stall recognition is in the range of 6-33 % of the rotational speed [3].

A great number of documentations based on experiments and theoretical investigations of the fundamental mechanisms behind rotating stall in a vaneless diffuser are documented and available. Jansen [27] investigated rotating pressure fluctuations and found that separation of the three dimensional boundary layer triggers rotational stall. His calculations showed that even a potential flow in the diffuser can become unstable causing rotating pressure perturbations. The assumptions for the calculations were consistence with a symmetric flow distribution in the diffuser depth from shroud to hub.

Contradicting experimental studies to the assumption of symmetric flow was conducted by Senoo and Kinoshita [28] whom proved that local reverse flow occurs firstly in the hub-side wall in the diffuser inlet region, before it transfers to the shroud side. The studies claimed that that the inlet conditions account for the distortions of radial and tangential velocity over the diffuser width, meaning that for an inlet flow angle α_2 above a certain value α_{2crit}, reverse flow commences in the diffuser. It was shown that the diffuser width ratio b_2/d_2, the inlet Mach number Ma_2 and the distortion of the inlet velocity profile have a significant influence on the critical flow angle. Figure 5-10 shows how the critical flow angle reduces with increasing inlet Mach number for a given diffuser geometry [29]. The blue dotted line represents the geometry for the NTNU impeller rig i.e. with inlet width geometric ratio, b_2/r_2, of 0.0615. With a corresponding Mach number of about 0.8 this gives a critical diffuser flow angle, $\alpha_{2crit,}$ of about 78 degrees.

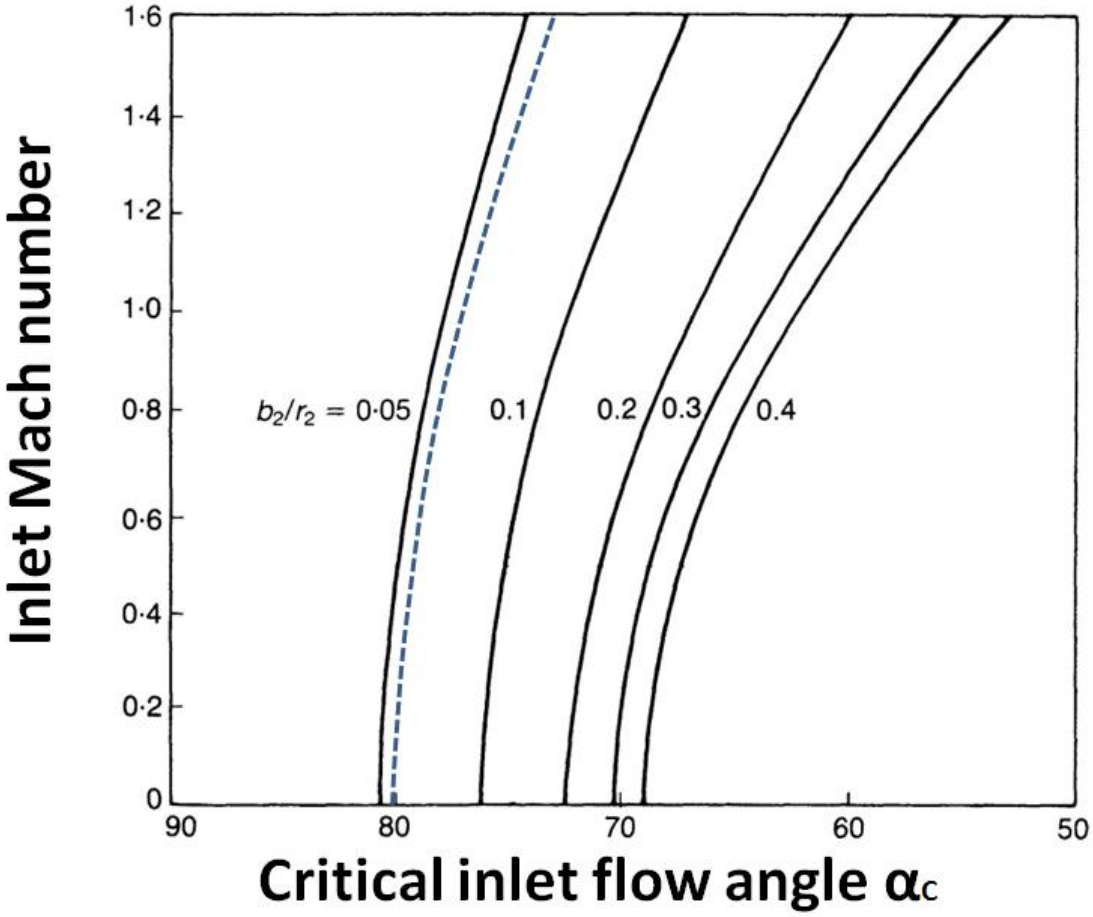

Figure 5-10: Effect of inlet Mach number on critical flow angle [28].

A conservative estimate for moderate Mach numbers is illustrated in Figure 5-11 showing the critical diffuser flow angle α_c at which the onset of rotating stall can be expected as predicted by Senoo and Kinoshita [30] The blue dotted line represents the impeller rig which in this case gives a slightly higher , $\alpha_{2crit,}$ of 80 degrees.

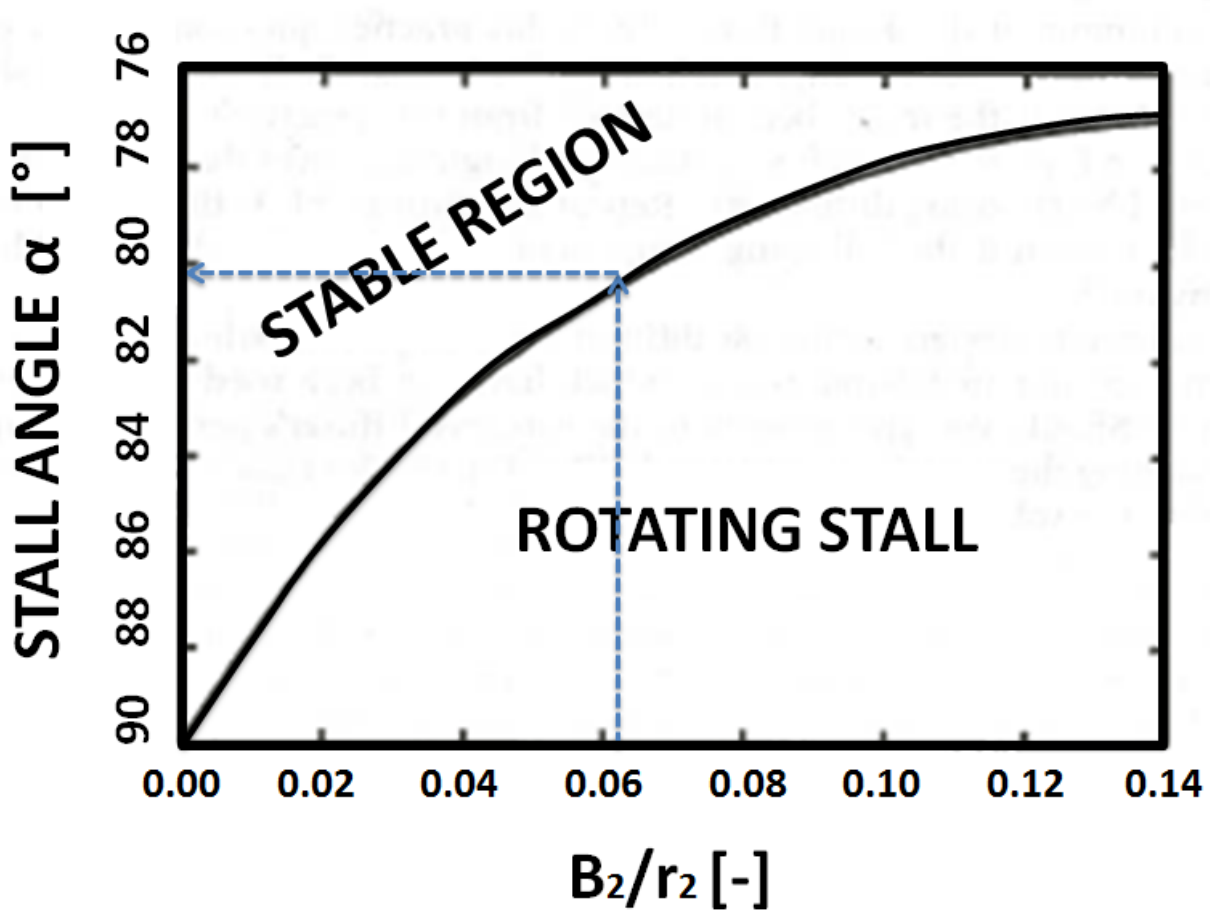

Figure 5-11: Vaneless diffuser stability [30].

Abdelhamid [31] on the other hand presented flow calculations proving that the flow in the diffuser can become unstable if the radial velocity at the diffuser inlet rapidly drops at a critical value. The velocity predictions of Abdelhamid was later verified by Frigne et al. [32] whom described the occurrence of high and low frequency rotating stall in a vaneless diffuser.

5.6 Surge

Surge is considered as a major instability that affects the entire compression system. In the course of surge, the average mass flow is unsteady but circumferentially uniform leading to severe changes of inlet and outlet conditions. Unlike rotating stall, where the mass flow rate remains approximately constant, surge results in large amplitude fluctuations of the pressure and the systems flow rate. The phenomena of surge together with inverse flow, is illustrated in Figure 5-12.Backflow into the impeller occurs because of some kind of aerodynamic instability within the system.

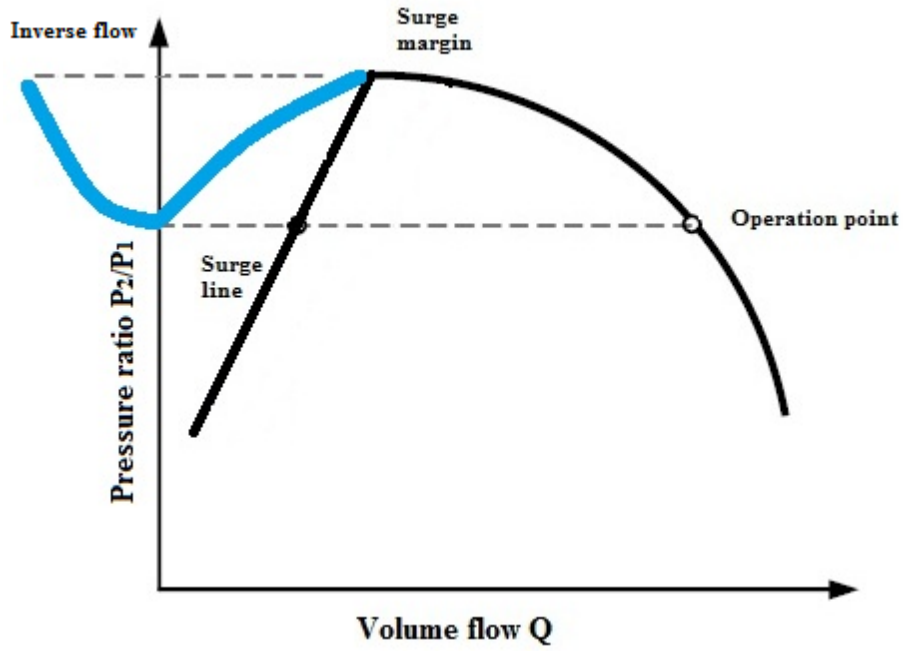

Figure 5-12: Surge cycle

However, in spite the fact that aerodynamic instabilities usually are a consequence of compressor design it is also possible that the system arrangement, and hence design, could be capable of enhancing this instability. Furthermore, surge is often symptomized with vibration and an audible sound although there have been reported cases were the audible sound were absent. Nonetheless, it is quite evident that the underlying cause of surge is aerodynamic stall which occurs in either the impeller or the diffuser.

As opposed to the axial compressor, the centrifugal compressor is not dependent on rotational stall behavior before going into surge mode. Whether surge is caused by a decrease in flow velocity or an increase in rotational speeds, either the impeller or the vaneless diffuser can stall. Which stalls first is difficult to determine, but considerable testing has shown that for a low-pressure-ratio compressor, the surge initiates in the diffuser section. For units with single-stage pressure ratios above 3:1, surge is probably initiated in the impeller [24].

For cases in which there are strong indications that the impeller seems to be the cause of surge, a flow separation begins in the inducer part of the impeller. Thus, either a decrease in the mass flow rate, an increase in the rotational speed of the impeller or occurrence of both can cause the compressor to surge. Surge can also be initiated in the diffuser by flow

separation occurring at the diffuser entrance. However, when the diffuser stalls, the flow will not enter the volute. A separation occurs, causing the flow to finally reverse and subsequently surge the compressor. Stalling of the vaneless diffuser can be accomplished by either increasing the impeller speed or decreasing the flow rate. Reduced volume flow in the impeller will consequently cause a decrease in the relative velocity leaving the impeller. Subsequently the flow angle, $\alpha_{2,}$ decreases resulting in an increase in the length of the flow path spiral. Moreover, if the length of the flow path spiral increases to a certain value the flow momentum at the diffuser walls is excessively dissipated by friction and stall. With this increase in friction, and hence, greater loss, the diffuser becomes less efficient and converts a proportionately smaller part of the velocity head to pressure. As this condition progresses, the stage will eventually stall and lead to surge if the circumstance endures. This effect is illustrated in Figure 5-13 with blue and red dotted lines representing the flow trajectory in the diffuser at normal and at near surge condition. At normal condition i.e. the blue line, the flow path is relatively short providing optimal flow angle and minimum frictional loss. The near surge line is characterized by a long flow path due to high flow angle α_2 causing high frictional loss. In the latter, there is a possibility of the flow re-entering the impeller, which is a high indication of surge [13].

Retardation of the fluid through the diffuser increases the pressure and density and compressibility plays a major role in (the calculation of the) diffuser performance. This increase in density helps to slow the radial velocity further by increasing the radius. The tangential velocity is not affected by this effect and thus has the actual flow a greater tendency to bend in the tangential direction than the radial [13].

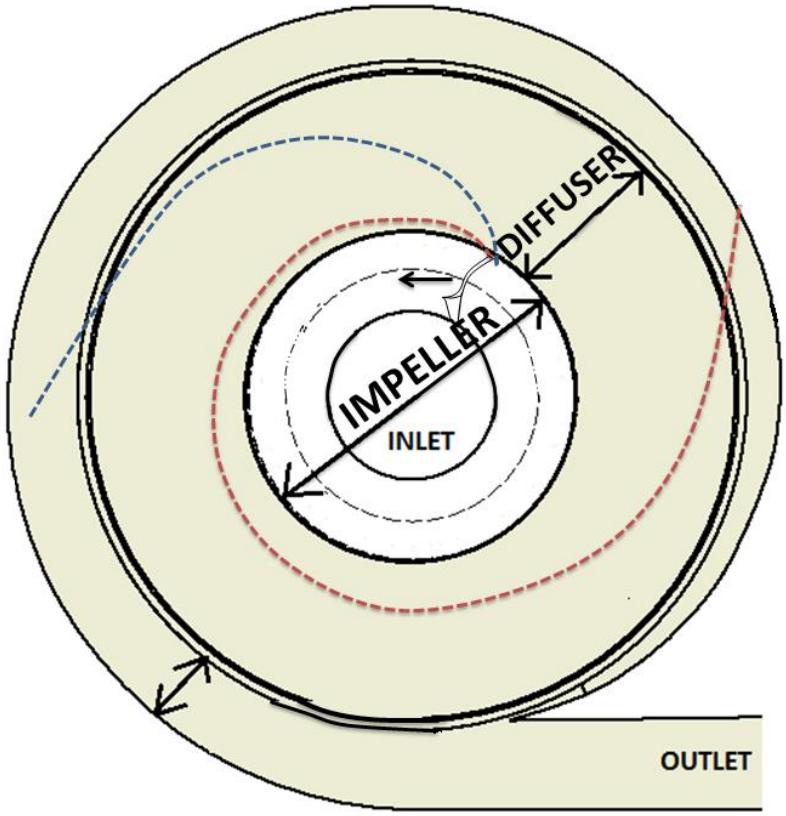

Figure 5-13: Flow trajectory in the diffuser.

According to Jager et al. [33] there are at least four different categories of surge for centrifugal compressors namely mild-, classic- , modified- and deep surge. The distinction between the different types is with respect to the amplitude and the frequency of the oscillations of the mass flow rate and the pressure ratio. However, a review of an important compression model that simplifies the frequency mindset is appropriate before entering a more in depth description of the surge categories.

Geitzer et al. [34] developed a theory of compressor surge that considers a compressor discharging into a plenum, simulating a simple model of a gas turbine as illustrated in Figure 5-14. The theory on the model is based on the introduction of a so called B- parameter with the purpose of describing the large amplitude pulsations encountered during a surge cycle in order to determining which instability the compressor would enter.

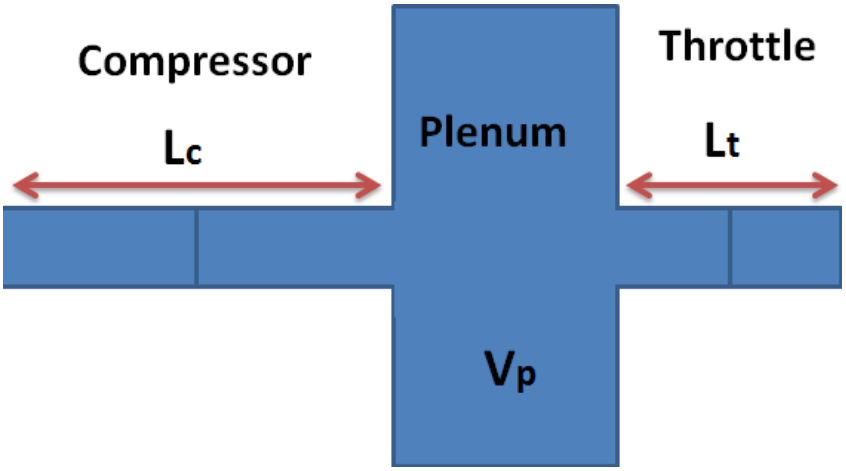

Figure 5-14: Basic compression system[23].

Greitzer B- parameter given in Equation 5-5 with the intention of estimating the dynamics in which the instabilities the compressor suffers at reduced volume flow. The B-parameter is furthermore used as a correlation factor to account for the instabilities caused by reduced volume flow and the deep frequency.

$$B = \frac{U}{2\omega_{HR} L_c} = \frac{U}{2a}\sqrt{\frac{v_p}{A_c L_c}} \qquad \textbf{Equation 5-5}$$

Where U is the rotor velocity, ω_{HR} is the Helmholtz resonator frequency, L_C is the compressor effective duct length, V_P is the plenum volume and A_C is the volume flow-through area. Helmholtz resonator frequency ω_{HR} is given in Equation 5-6.

$$\omega_{HR} = \frac{a}{2\pi}\sqrt{\frac{A_T}{v_p L_T}} \qquad \textbf{Equation 5-6}$$

where a is the speed of sound, A_T and L_T is the volume flow true area and length of the exit duct. Helmholtz frequencies are unique for a compression system and are a result of the inertia of the gas to be balanced by compression downstream of the compressor. A surge

occurrence with the absence of mass flow inversion, small pressure fluctuations together with a periodicity governed by the Helmholtz resonance frequency is regarded as a **mild surge**.

The second version of surge is the **classic surge** which is on the other hand categorized with higher amplitude and lower frequency than the mild surge. Nonetheless as with the mild surge, the occurrence of backflow is not present in the classic surge.

In the **modified surge** the entire annulus fluctuates in the axial direction forcing the flow to be unsteady and non-axisymmetric allowing a mix of classic surge and rotational stall to take place.

Deep surge is the last and generally the most severe form of surge which is associated with low frequent, large amplitude oscillation and the presence of backflow within the flow, i.e. inverse flow as seen in Figure 5-12.The deep frequency is considerable lower than the Helmholtz frequency so in order to determine the effect the Greitzer B-parameter is used to estimate the dynamic in which the instabilities the compressor suffer at reduced volume flow. The B-parameter is used as a correlation factor to account for the instabilities caused by reduced volume flow and the deep frequency [35].

5.7 Chapter summary and conclusion

The aerodynamic stability is in brief the compressors response to disturbance that changes the operation point of the compressor. The performance of centrifugal compressors is highly influenced by aerodynamic instabilities and it is important to distinguish between the different reasons to the aerodynamic instabilities, stall and surge. There are two types of stall reported for dry gas in a centrifugal compressor namely impeller stall and stall in diffuser. For centrifugal compressors the stall is created by areas of stalled passages identified as stall cells occupying volume in the compressor. The operation mode of stall is associated with the separation of the boundary layer in flow through the compressor. In order for rotating impeller stall to occur, the angle of attack must be sufficient large, and beyond a certain point, allowing separation of the boundary layer to emerge while the flow stream passes around the impeller blades. In general the impeller rotating stall is recognized in the range of 50-80 % of the rotational speed whereas the range is 6-33 % for the diffuser. Surge is considered as a major instability that affects the entire compression system. In the course of surge, the average mass flow is unsteady but circumferentially uniform leading to severe changes of inlet and outlet conditions. Unlike rotating stall, where the mass flow rate remains approximately constant, surge results in large amplitude fluctuations of the pressure and the systems flow rate.

6 The influence of wet gas for compressor stability

Surge and stall are two extremely difficult phenomena's to understand in particular with the presence of liquid in the flow. Theory and experiments based on injection of water into a dry gas system in order to investigate instabilities exists, nonetheless especially for axial compressors. Most of the experiments are brought out on inlet or inter-stage fogging and heavy rain ingestion which will be outlined in Section 6.1 followed by a literature review associated of stability issues of recently research on centrifugal compressor subjected to wet gas.

6.1 Fogging and heavy rain ingestion for axial compressors

Water injection in the axial compressor was initially intended for increasing the gas turbine outlet power when the ambient temperature increases. Fogging and overspray has successfully been applied in gas turbines worldwide due to its potential to maintain the operation stability of the compressor, however the technology has not been fully understood.

A research on the influence of fogging on an axial compressor was conducted by Härtel and Pfeiffer [36] ,it includes a broad coverage of the influence of droplet diameter, relative humidity and gas volume fraction has on the compressor performance. The findings suggested that influence of polytrophic efficiency on the gains of high fogging is addressed; meaning also that operation stability of the machine was retained, hence more effective for compressors of low efficiency. A Moore Greitzer based model for wet gas compression was developed by Wang et al [37] simulating different steady state inlet conditions for a S1A-02 gas turbine. The simulations revealed that the pressure- ratio increased and the surge line moved –up left relative to the dry gas surge line in the compressor map in Figure 5-12. In other words, wet gas compression can, to a certain extent, eliminate stall and surge and hence extend the range of stable operation. Similar experiments based on heavy rain ingestion in terms of large droplets in a axial flow compressor was accompanied by Day et al. [38] showing contradictory results in comparison to the work regarding inter- stage fogging. A decrease in both the compressor efficiency and the stability was imminent. The explanation lies in the fact that after the droplets collide with the first row blades and centrifuged towards the casing where the normal air flow patterns in the vicinity of the rotor tips are disrupted causing endwall blocking of the flow channel.

Some concluding remarks are appropriate due to the fact to the existence of consistency related to centrifugal compression. When the compressor operates near stall, the suited particle diameter for liquid injection has proven to increase the inlet flow rate and pressure ratio and extend the stable operation. However, injection of water has also proven adverse effects that decrease the inlet flow rate and pressure ratio runs at design point when the liquid extend a particular size.

6.2 Wet gas centrifugal compressor stability

For wet gas compression in centrifugal compressors it is only during recent years that a satisfactory amount of research has been accomplished. However, despite the numerous recent works on this topic, the fundamental understanding of wet gas compression processes remains challenging. Two of the reasons for this are undefined standards for testing and performance, and lack of understanding of the basic physical phenomena. Some of the contributions that have dealt with the wet gas injection in centrifugal compressors related to instabilities will be discussed here.
Abdelwahab [39] performed calculations for wet gas compression by injection of water in an industrial centrifugal compressor. The findings revealed that wet gas compression can be used for centrifugal compression if the droplet size diameter is kept below 5µm. This is due to a fact that small droplet diameters led to a much faster evaporation time compared to the fluid particle travel time. The higher the injection rate, the higher the total pressure ratio the stage could develop. This was due to colder compression temperatures allowing the work transferred from the impeller to the flow and then converted into higher total pressures.

Brenne et al [40] performed an initial testing to verify multiphase boosting capabilities of a centrifugal compressor. The testing consisted of performing dynamic pressure measurements injecting liquid into the compressor. The tests showed that the compressor pressure ratio increased with increasing gas volume fraction due to rising density of the flowing fluid i.e. relative to the case of dry gas. Moreover data from the pressure transducers gave strong indications that the pressure fluctuations within the flow were reduced by the presence of liquid in the gas stream. In the case of high liquid in the flow the findings indicated that a reduced blade -pass frequency amplitude emerged with subsequent acoustic reduction triggering instabilities in the rotor. In experiments brought out by Hundseid et al. [4] a wet gas compressor test with hydrocarbons were performed at high pressure i.e. ranging from 30-70 bar. The findings suggested that dry gas parameters are not directly applicable for wet gas performance analysis, nonetheless, Wood's two phase speed of sound correction model were used in order to compensate for the different tests. The pressure ratio increased relative to dry conditions when GVF was decreased. Furthermore, when liquid was present the degradation linked to performance was noticeable.

Grüner et al. [41] performed experimental analysis on a single airfoil immersed in wet gas flow and revealed an expanding premature boundary layer separation with reducing gas volume fractions. At the point of separation a local film thickening followed by increased liquid film fluctuations was observed. A continuity wave was initiated by deposited and secondary droplets surrounding the airfoil as a U shape of increased liquid concentration. On the basis of this it was concluded that the operation characteristics of a compressor changes as a consequence of the premature separation of the boundary layer caused by liquid impact. Increased blockage caused by wake formation reduces the effective flow area and increases the losses whereas the continuity wave causes substantial changes to the inlet flow.

In the work conducted by Fabbrizzi et al. [42] a single stage compressor was used to investigate the effects of wet gas compression based on variation in the gas mass fraction GMF (1-0.5) the impeller speed, droplet size and the injection pattern of the liquid. The results clearly demonstrate that wet gas strongly influences compressor performance, considering adsorbed power, efficiency and compressor characteristics. The results also show that, although the impeller design did not account for heavily wet streams, the overall compression characteristics remain good and the machine was able to process the two-phase mixture without failures, in some cases with improved pumping. In fact, the compression ratio

initially increased for small amounts of injected liquid relative to dry gas and decreased when the GMF was further decreased. Grüner and Bakken [3] demonstrated through experiments involving aerodynamic instability investigation of an centrifugal compressor exposed to wet gas that the compressor encountered a delayed instability inception due to the presence of the liquid. The findings suggested that the liquid altered the frequency spectrum consisting of low- frequent throughout the entire compressor characteristic. In addition the compressor characteristic revealed increased pressure ratio rise to surge with decreasing GMF.

A two- stage wet gas compression campaign was conducted by Ransom et al. [43] in 2011 which focused on characterizing the mechanical performance of the compressor. The compressor was tested with a various mixture of air and water within a range of GVF varying from 95% to 100 % for different speed lines while the suction pressure was held at 19 and 20 bara. The pressure ratio increased during the injection of water suggesting that it is directly related to the increasing Mach number at the stage discharge.

Experimental testing with respect to aerodynamic instabilities for wet gas within a centrifugal compressor was conducted by the author of this master thesis [11] with guidance from Trond Grüner. The findings revealed a delayed development of instabilities for wet gas relative to tests on dry gas. The frequency spectrum analysis performed did not conceal any stall frequencies which is typical for dry gas before entering surge, suggesting that the compressor did not attend rotating stall prior to surge. The visual observation from the experiments showed backflow at the impeller inlet and a deviating liquid flow path for the diffuser with reduced GMF. However, the observed water backflow in the inlet of the impeller occurs without pressure fluctuations recorded at the outlet, which may indicate an impeller stall with zones of reversal flow near the inlet. In the latest work of Grüner and Bakken [44] formation of an extending annulus ring of liquid was identified at the impeller inlet with reducing volume flow prior to surge. Droplet entrainment from the ring was revealed with a disordered flow reversal. Visual observations of the flow inside the diffuser showed a tangential liquid film flow path suggesting that liquid may be forced to deposit on the pressure side of the impeller blades due to inertia forces. The high energy in the fluid will affect the gas phase so that the flow path through the diffuser is shortened with less friction.
Consequently the absolute core angle out of the impeller will be less tangential than the liquid film flow.

7 Flow visualization techniques

A comprehensive evaluation of different visualization techniques related to characterizing stall and surge for turbo machinery was performed by Dahl [45]. The main purpose was to determine whether the visualizations techniques could be adopted for the detection of stall and surge in multiphase flow in the NTNU Impeller rig. The survey consisted of optical and non-optical visualization measurement techniques. The optical methods includes Laser Doppler Velocimetry (LDV), Particle Image Velocimetry (PIV), Laser two-focused Velocimetry (L2F), Doppler Global Velocimetry (DGV) and Pressure Sensitive Paint (PSP). Common for all of them is the ability to not cause any disturbance within the flow field when implementing in rotating impeller or diffuser channels because the method uses particles that follow the flow without the influence of buoyancy effects. The concept of LDV was tested by Dahl [45] for dry gas purposes on the NTNU impeller rig facility where the measurement was conducted through the diffuser plexiglas. The system was unfortunately not capable of detecting the velocities due to glare and reflections from the plexiglas. It was obvious that the problem would enhance in the case of wet gas implementing due to difficulties in detecting the particles as they would be hidden because of liquid film development on the diffuser walls. It was concluded that other optical measurements techniques also would have suffer from the same problems when implementing wet gas [45].

The non-optical visualization techniques on the other hand, includes Hot-Wire Anemometry (HWA), Film Anemometry (FA), Pitot static probes, High frequent dynamic- and Static-pressure sensors. These methods are characterized by high complexity in the shape of the actual measuring device regarding size and practicability. In addition, complex methods for data analysis are needed in order to detect the instabilities that occur.

Some of these, non-optical measurement techniques namely high frequent dynamic and static pressure sensors has showed good results in multiphase analysis of instabilities in the NTNU impeller rig [45, 46]. High-response dynamic pressure sensors i.e. piezoelectric sensors (PCB) flush mounted in the diffuser was implemented by Grüner [47] and used for instability investigations for wet gas in the impeller rig. When wet gas was injected to the compressor, the PCB sensors detected amplified low frequencies compared to the case of dry gas, suggesting that dynamic film and droplet impact on the sensing element together with interference between the phases leading to pressure fluctuations that will be identified in the frequency analysis. In addition Grüner and Bakken[46] performed an attempt using a pitot tube for wet gas surge detection for comparison with the PCB sensor arrangement. The pitot probe was positioned in the opposite direction upstream from the injection module and the impeller inlet, i.e. not in direct contact with the liquid. The findings from the pitot probe and the PCB measurements gave synchronously surge indications.

Based on the findings from Grüner regarding pitot probe it was decided to conduct a more in depth review of pitot probe based measurement devices as a method for wet gas measurements of instabilities. A literature review of pitot –tube and pitot based measurement techniques are given in Section 7.1

7.1 Pitot probe investigation

This section are intended for a literature review of the use of pitot tube for compressor dry and wet gas measurements.

7.1.1 Pitot tube fundamentals and measurement principles

A pitot static tube is essentially a simple device that measures the flow stream velocity. Pitot tubes are reliable, inexpensive and suited for a variety of environmental conditions, including extremely high temperatures and a wide range of pressures. A calibrated, clean and properly inserted pitot tube can provide ±1% of full scale flow accuracy over a low range of 3:1; and, with some loss of accuracy, it can even measure over a range of 4:1, however a decrease in the accuracy (up to 5%) is found if not carefully installed. Pitot tubes are generally used for flow measurements of secondary importance where cost is a major concern, due to additional limitations including errors from velocity profile changes or from plugging of the pressure ports [48].

There are generally two types of pitot probe concepts i.e. the pitot static -probe and the simple pitot probe. For the pitot static probes both the static- and the total impact- pressure are measured by a small diameter open L-shaped tube facing in opposite and parallel direction of the stream, illustrated in Figure 7-1. As seen from the figure it is generally two channels in the tube, i.e. one port for static pressure opening oriented parallel to the flow and one port for the total impact pressure oriented directed perpendicular to the flow. The static pressure, P_{static} is the operating pressure upstream to the pitot tube and the total impact pressure P_{tot} , is the sum of the static pressure and the total kinetic pressure for one phase measurements are given by Equation 7-1 [49].

$$P_{tot} = P_{static} + \frac{1}{2} P V_2^2 \qquad \textbf{Equation 7-1}$$

the fluid velocity, V_2 are given from the Bernoulli Equation 7-2:

$$\frac{V_1^2}{2} + \frac{P_1}{\rho} + gZ_1 = \frac{V_2^2}{2} + \frac{P_2}{\rho} + gZ_2 \qquad \textbf{Equation 7-2}$$

given the fact that the fluid velocity V1 is at rest at port 1 i.e. equal to 0 and Z is negligible for gases, V_2 becomes:

$$V_2 = C*$$ **Equation 7-3**

From equation 8-2 and 8-3 the pressure difference can be expressed as given by Equation 7-4 below

$$\Delta P = P_{tot} - P_{static} \qquad \textbf{Equation 7-4}$$

C* is a dimensional calibration constant that takes into account the fact that the velocity at port 2 is higher than it would have been if the tube had not displaced a volume. The calibration constant is generally either given by calibration or obtained from the manufactures.

The simple pitot probe on the other hand works almost the same way and is basically govern by the same equations as the static pitot probe; however the static and the total pressure are measured at different locations as illustrated in Figure 7-2. As seen from the figure the static pressure is measured in the wall that surrounds the flow while the total pressure is measured by the probe [49].

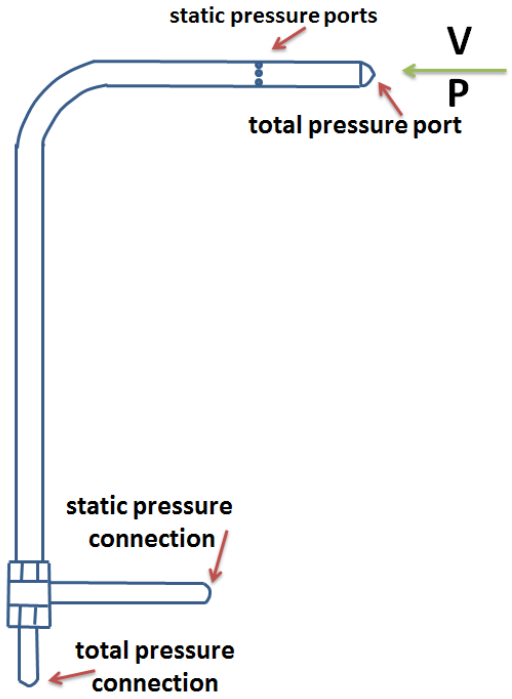

Figure 7-1: Pitot static probe.

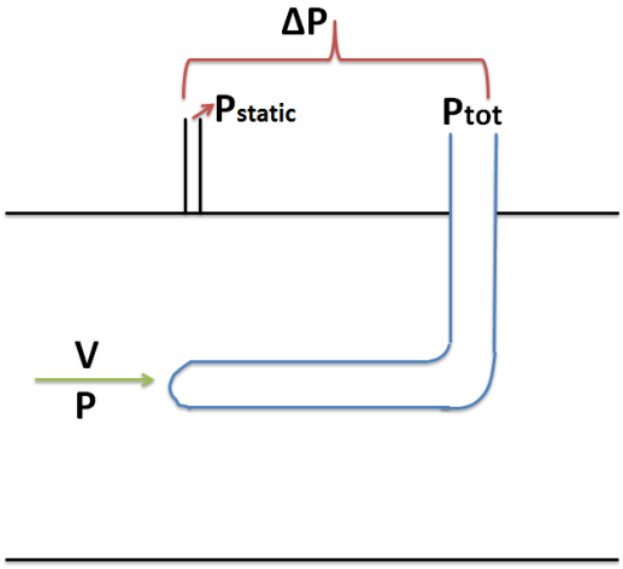

Figure 7-2: Pitot tube

Pitot tubes have been used for many years in the measurement of velocity in single- phase flow, particularly in the aircraft industry. As a research tool they are often sophisticated instruments with multiple heads containing orifices inclined at various angles in order to obtain the velocity vectors required for flow mapping. When used to measure total pipe flow they are either employed in a traversing mode or mounted in rakes in order to give multiple velocity readings which can be integrated spatially as illustrated in Figure 7-3 [49].

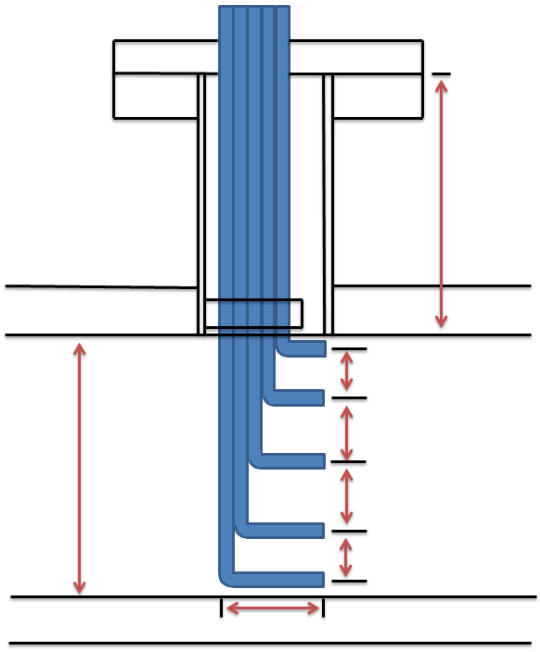

Figure 7-3: Pitot tube rake geometry [49].

The Averaging Pitot Tube is A different type of pitot solution which is designed to overcome the challenge of finding the average velocity point. The averaging pitot tube is similar to the pitot tube, however it is equipped with several openings in order to provide a better overall accuracy for pipe flows applications. Figure 7-4 shows the averaging pitot tube with its multiple impact and static ports on both upstream and downstream sides. The different pressure ports are combined and the square root of their difference is measured as an indication of the average flow in the pipe [48]. However, the flow area in the diffuser can by no means be characterized as a pipe flow, and further investigation of the averaging pitot tube is not relevant for this master thesis.

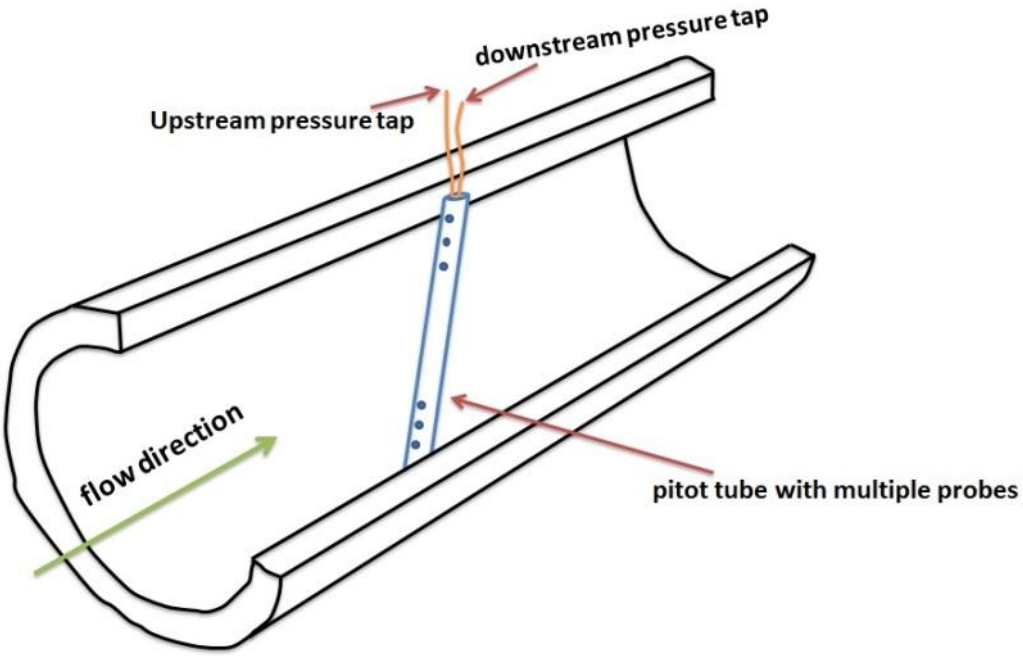

Figure 7-4: Averaging Pitot tube [49].

7.1.2 Pitot tube for turbo machinery applications

Ziegler et al. [50, 51] investigated the interaction between the diffuser and the impeller, by means of pitot probes, among other measurement techniques. Due to the narrow flow channel in the centrifugal compressor the pitot probes were customized for the investigation, i.e. aiming to achieve as small dimensions as possible. The pitot probes were inserted into the sensitive transonic flow field at the impeller exit at four different circumferential positions. Due to the lack in flow angle information, the pitot probes were adjusted to the flow direction manually based on the flow angle calculated from the mass flow measured in the nozzle. The findings from this particular test, reveals that the jet-wake structure in the diffuser becomes more pronounced, by increasing the speed of the machine.

Many attempts have been made to use pitot tubes to measure velocity in multi- phase flow. The experiments have shown that the pitot tube is affected by the influence of multiple fluid phases which in turn makes the measurement analysis considerably more difficult. Thus, for instance when a pitot tube is applied in highly turbulent two-phase flow conditions a somewhat large uncertainty is unavoidable. There is no universal probe capable of providing accurate measurements in all two- phase flow regimes without calibrations as each pitot probe is designed to match a specific research requirement and usually calibrated in situ.

For two- phase flow Equation 7-1differ due to the different density of the two phases. More precisely, the pitot tube is impacted sequentially by liquid of density ρ_l, moving at velocity V_l, and by gas of density ρ_g moving at velocity Vg. The total dynamic head ΔP_{TP} is therefore:

$$\Delta P_{TP} \approx (1-\varepsilon)\rho_l \frac{V_l^2}{2} + \varepsilon\rho_g \frac{V_g^2}{2} \qquad \textbf{Equation 7-5}$$

where ε is the void fraction. For homogenous flow $V_l = V_g = V$. Hence

$$\Delta P_{TPM} \approx (1-\varepsilon)\rho_l + \varepsilon\rho_g \frac{V_g^2}{2} \approx \frac{\rho_m V}{2}$$ **Equation 7-6**

where ρ_m is the mixture density, provides the following Equation 7-7 for two-phase homogenous flow:

$$V = C * \sqrt{\frac{2\Delta P_{TPM}}{\rho_m}}$$ **Equation 7-7**

The pitot tube can therefore be used to measure velocity given the mixture density ρ_m is known. This simplification is widely used in order to determine the mass flow rate of e.g. steam and water mixtures in pipes. However, for some flow regimes, the homogenous model is not suitable. A study by Gill et al [52] concludes that a more generalized expression than the homogeneous Equation 7-5 must be applied for applications with e.g. droplets in the gas stream.

$$\Delta P_{tp} \approx \sigma(1-\varepsilon)\rho_l V_l^2 + \frac{1}{2}\rho_g V_g^2$$ **Equation 7-8**

In Equation 7-8 σ is 0.5 if the droplets follow the streamlines and if they impact the pitot tube. However, in practice σ has an intermediate value in which may be dependent on relatively phase velocities[49].

Despite the theoretical and practical interest in how the multiphase flow will affect the measurements from the pitot tube, the existing literature on the subject is virtually non-existent. However, some theory regarding interpreting of pitot pressure measurements in multiphase flow has been performed on the aerodynamics of wet steam in large steam turbines. Crane and Moore [45] presented calculations for the flow of wet stream around purged and unpurged pitot tubes, by means of determining the vapor velocity field around the tubes using incompressible, potential flow theory assuming that the same velocities field applies for droplets as well. From momentum loss equations and droplet calculations the contribution of the droplets to the total pressure rise could be found. Notwithstanding the important calculations, they did not take into account the likely effect regarding mass transfer between the liquid droplets and the vapor phase. White et al. [53] on the other hand based the experimental testing of pitot tube for wet gas flow on the supposition that the flow structure in a partly disperged shock wave is not very unlike the flow structure between a frozen shock wave and the pitot head. Frozen meaning that the pitot tube records the pressure as if the vapor phase alone was brought to rest from the same velocity, assuming that all interface transfer process remains essentially stationary due to large droplets. The findings showed good correspondence between total pressure measured downstream of a wet gas steam cascade operating with condensation shocks, and that predicted by a two-dimensional scheme for this particular case.

As long as the multiphase flow is thoroughly mixed, the use of pitot tube as measurement device could be used in conjunction with other devices to measure total mass flow. However, visualization and measurement of multiphase flow requires a probe that is robust against liquid droplets, possess high frequency response and cause low impact on the actual flow.

Falcone [49] points out several factors that militate against using pitot tubes in subsea applications. The book points out factors that include:

- The need for a rake and suitable integration procedures
- Pipe penetrations and possible probe damage
- Intrusiveness: pitot tubes would prevent cleaning
- Sensitivity to erosion, corrosion and blockage
- The need for multiple connecting lines between the probes and the sensing instruments.

7.1.3 Pitot probes for wet gas measurements in the NTNU impeller rig.

This sub section discusses the pitot as a measuring device at the NTNU impeller rig. Small Pitot tube placed inside the diffuser can provide good measurements of the dry gas flow without affecting the flow to a large extent. A pitot tube will also bypass the problem of liquid film on the inside of diffusor walls. Equally important is the measurement of the diffuser inlet angle i.e. an extremely important key parameter for determination of the occurrence of instabilities in a vaneless diffuser.

Notwithstanding the bypass of the liquid film; the pitot probes are also sensitive to contaminants in the flow, as these can clog the small holes in the probe. Regarding wet gas flow, the water will in worst case either clog or penetrate the holes and potentially fill them. Airplanes operate often in wet environments and uses Pitot tubes to calculate speed. They solve this problem by heating the Pitot tube so that water and other contaminants vaporize, or burn up. Similarly, the same method can be used in the diffuser, allowing the surrounding flow to be heated, resulting in expanded flow and subsequently increased speed.

Instead, a flush system that periodically blow channels in the pitot tube clean will conceivably work. Since the droplets in the flow are spread, it will take some time for the droplets to hit the holes in the Pitot tube. In this time interval with dry pitot tubes, it is possible that the velocities can be measured.

7.2 Pitot- based measuring devices

This Section discusses two other pitot based measuring techniques. A better understanding of the unsteady flow phenomena such as secondary flow or rotor- stator interactions is a key to further improvements in turbo machinery. In addition to complex CFD methods modern measurements techniques with time resolving capabilities are necessary to determine the instantaneous flow quantities.

7.2.1 Fast- Response Aerodynamic Probe measurement system

The Fast- Response Aerodynamic Probe measurement system (FRAP) are developed at the Turbo machinery Lab of the Institute of Energy Technology (ETH) in Zurich. FRAP probes are a promising alternative to other time resolved measurement techniques, such as hot-wire anemometry or laser techniques that was mentioned at the beginning of Chapter 0). In

addition to the flow angles, Mach number, and velocity, FRAP can additionally measure both time-resolved total and static pressures. All these flow quantities are determined from the pressure levels and fluctuations at different points of the probe tip measured with miniature piezoresistive pressure sensor chips. The FRAP probes provides a high-performance system primarily dedicated to turbo machinery applications. The one sensor probe, operating as pseudo-three sensor probes, have shown a high potential because it combines the simple application and evaluation methods with detailed information about the time-resolved flow patterns [54]. The current improvement of selected components make the FRAP system suited for more complex applications, such as detailed-two- dimensional flow field measurements or even three- dimensional with four sensor probes. The system has been successfully used for measurement campaigns in different turbo machines at the ETH and in industrial test facilities[54]. The FRAP probes are able to measure high frequency rotor- governed systematic fluctuations (like blade to blade phenomena) alone or in combination with flow-governed low- frequency fluctuations as rotating stall and mild surge. However, three sensor probes would be needed to measure stochastic (turbulence-related) or other aperiodic velocity transients [55].

As a consequence of increasing demand of customized probe measuring devices several research groups worldwide have developed their own probes custom made to their applications. Hence the FRAP probes has experienced regular improvements, particularly in terms of diameter reduction since it was invented. Roduner et al. [55] measured time-resolved flow quantities in a centrifugal compressor using a cylinder shape 3- sensor probe of a diameter of 1.8 mm. A further reduction of the probe head to 0.84 mm was achieved by Schlienenger et al. [56] in order to perform measurements of the cavity flow in labyrinth seals of an axial compressor. In the recent work of Porecco et al. [57] a newly designed 2- sensor FRAP probe was used in a virtual 4- sensor mode to yield measurements of non- isotropic turbulence in a multi-stage axial turbine. Moreover a novel high temperature fast response aerodynamic probe has been developed, built and tested which is based on the virtual 4-sensor probe. The probe can be applied in flows with temperatures up to 533 K (806 °C) and can measure three dimensional and unsteady flows up to the cut-off frequency of 25 kHz, covering flow angles of ±24° in yaw and ±20° in pitch direction. Furthermore, the probe is able to measure the steady flow temperature [58].

Roduner et al. [55] investigated the impeller exit and the vaned diffuser of a single- stage high- subsonic centrifugal compressor by the use of FRAP probes in order to detect rotating stall and surge at stable and unstable running conditions. The probes were mounted in eleven different positions I to XI at the front wall of the diffuser as seen from Figure 7-5 and Figure 7-6. The position I is highlighted in Figure 7-7. Further the investigation concluded that even the one sensor FRAP probe was a valuable tool for investigating time- dependent systematic flow phenomena occurring in turbo machines. A highly detailed insight into blade passing, mild surge and rotating stall can be achieved not only qualitatively but quantitatively with high accuracy and resolution.

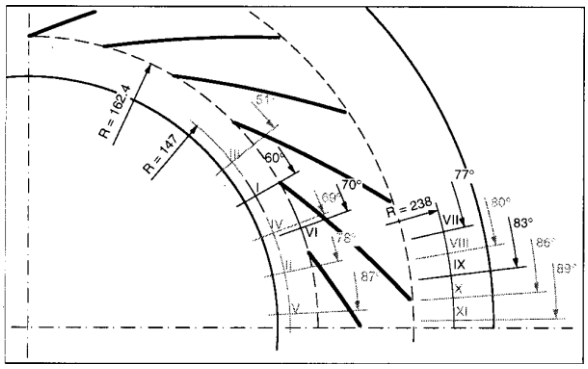

Figure 7-5: FRAP probe configurations

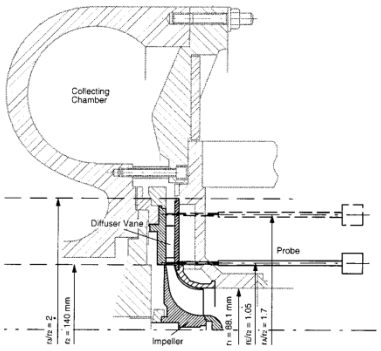

Figure 7-6: FRAP probe configurations

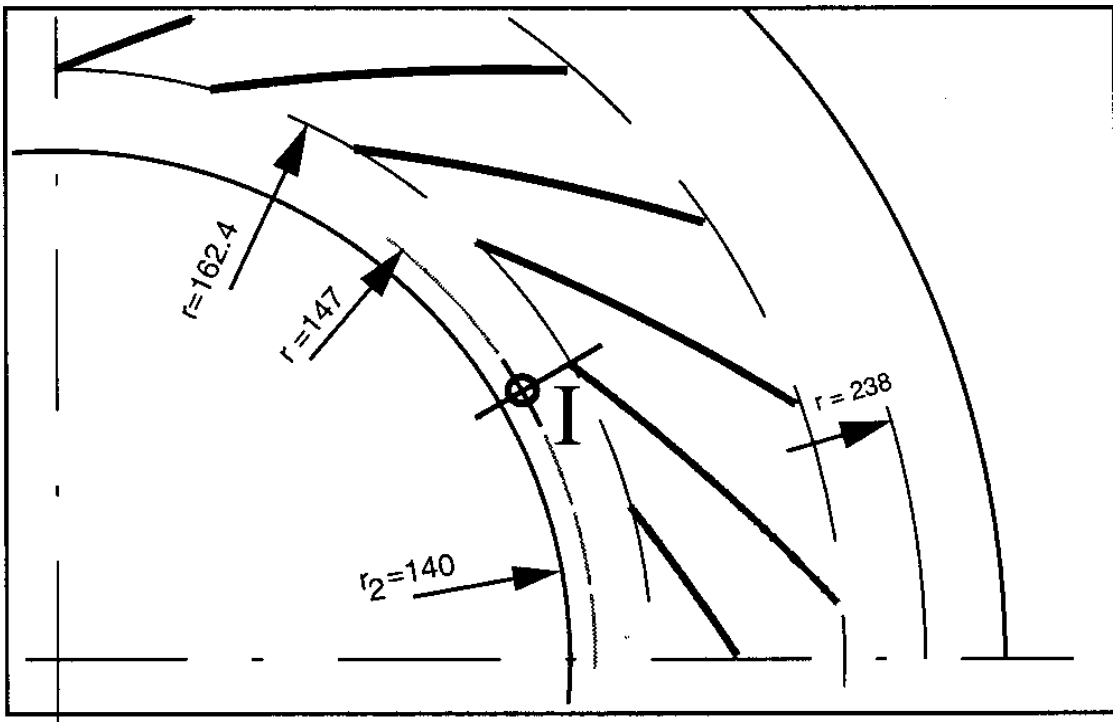

Figure 7-7: Position I

Schleer et al. [59] on the other hand, investigated the unsteady flow field within the diffuser, close to the impeller exit, of an inversely designed centrifugal compressor with two different impeller configurations. All the probe traverses were performed with a single- sensor FRAP probe operated in pseudo three sensor mode. The FRAP measurements were compared to detailed CFD simulations [59, 60]. The variations in the diffuser inlet flow pattern with the flow coefficient were investigated, using the 2-sensor FRAP technique for a scaled-up turbo compressor with a vaneless diffuser by Hazby et al.[61]. The probe traverses provide time resolved static and total pressures as well as the flow angle and Mach number.

7.2.2 Multi hole probe technology

Multi-hole probes (MHP) are designed based upon the principle of operation of pitot- static probes fluid flow instruments that measure pressure along pressure ports arranged on their tips. Whereas pitot- static probes are extensively used in situations where the direction of the flow is known, MHP technology is proven and mature to resolve the 3-dimensional velocity vectors in flow fields notwithstanding the direction of the flow. In particular MHP are based

on the fact that the static pressure varies over a solid surface immersed in the flow, i.e. the maximum flow which yields the stagnation pressure and the pressure distributions around the wake of the body. By measuring the pressure at distinct points over the body the probe provides all the information necessary on the velocity components that is needed to generalize the flow. Another important feature of the MHP is its ability to measure the flow over bodies that often separates, without influence of the separation. This alters the local pressure distribution and introduces adverse pressure gradients in regions where the slopes of the surface of the body is decreasing, but not yet zero. In other words, MHP provides correct measurements in cases where separation occurs in a certain position from the point of stagnation rather than where the tangent to the surface is parallel to the free-stream velocity. Figure 7-8 illustrates a very simple three-hole probe with pressure taps 1, 2 and 3 along the meridional angles of 0, -45 and 45 degrees respectively. The incoming flow field in the figure inclines with respect to the probe's axis by an angle α , i.e. the incidence angle, then pressure measurements from the different pressure taps can determine the free stream velocity magnitude, the incidence angle, together with both the static and dynamic pressure.

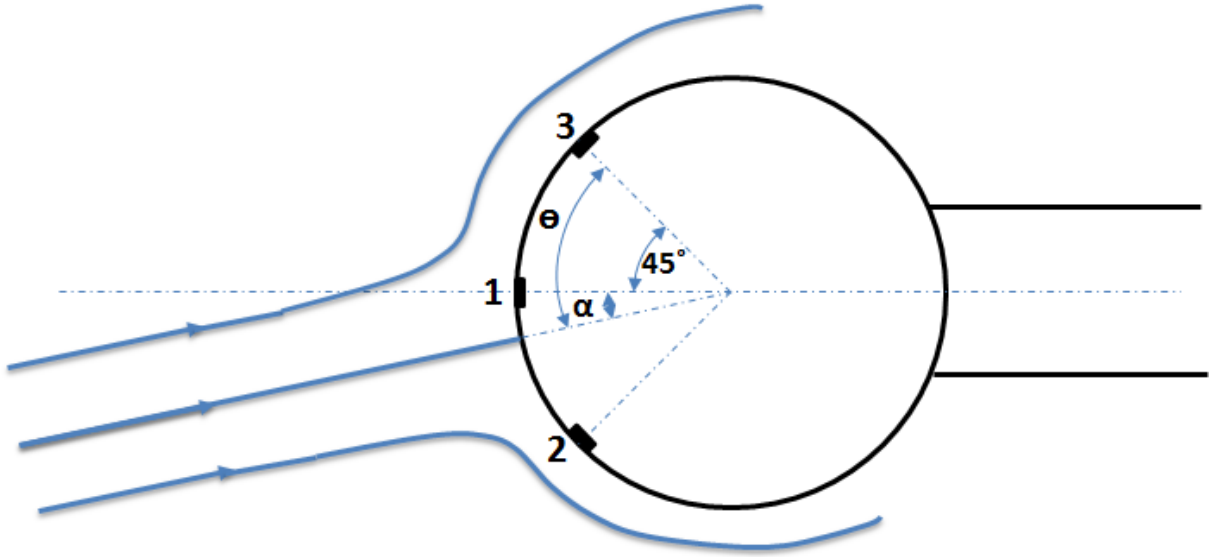

Figure 7-8: Three- hole probe in a incoming flow field

For incompressible flow the pressure, P, and velocity, V, at a point are related to the pressure and velocity far from the body, P_∞ , V_∞ , respectively This is governed by the Bernoulli equation in Equation 7-9, which is similar to Equation 7-2.

$$\frac{V_\infty^2}{2}+\frac{P_\infty}{\rho}=\frac{V^2}{2}+\frac{P}{\rho}$$ **Equation 7-9**

For a circular cylinder, the potential flow solution gives the velocity on the cylinder as

$$V(\theta)=2V\sin\theta$$ **Equation 7-10**

Hence, by insert and arrange for the three pressure taps into Equation 7-9 and Equation 7-10 the equations becomes as illustrated in Equation 7-11 to Equation 7-13 respectively. Moreover, the unknowns i.e. P_∞ , V_∞ and α can be found by substitute from Equation 7-11 to Equation 7-13.

$$\frac{V_\infty^2}{2}+\frac{P_\infty}{\rho}=\frac{P(45°-\alpha)}{\rho}+2V_\infty^2\sin^2(45°-\alpha)$$ **Equation 7-11**

$$\frac{V_\infty^2}{2}+\frac{P_\infty}{\rho}=\frac{P\alpha}{\rho}+2V_\infty^2\sin^2\alpha$$ **Equation 7-12**

$$\frac{V_\infty^2}{2}+\frac{P_\infty}{\rho}=\frac{P(45°+\alpha)}{\rho}+2V_\infty^2\sin^2(45°+\alpha)$$ **Equation 7-13**

7.3 Chapter summary and conclusion

Pitot tubes are reliable, inexpensive and suited for a variety of environmental conditions, including extremely high temperatures and a wide range of pressures. Pitot tubes are generally used for flow measurements of secondary importance where cost is a major concern
Many attempts have been made to use pitot tubes to measure velocity in multi- phase flow. The experiments have shown that the pitot tube is affected by the influence of multiple fluid phases which in turn makes the measurement analysis considerably more difficult.
There is no universal probe capable of providing accurate measurements in all two- phase flow regimes without calibrations because each pitot probe is designed to match a specific research requirement and usually calibrated in situ. As long as the multiphase flow is thoroughly mixed, the use of pitot tube as measurement device could be used in conjunction with other devices to measure total mass flow. However, visualization and measurement of multiphase flow requires a probe that is robust against liquid droplets, possess high frequency response and cause low impact on the actual flow. Small Pitot tubes placed inside the diffuser can provide good measurements of the dry gas flow without affecting the flow to a large extent. A pitot tube will also bypass the problem of liquid film on the inside of diffusor walls. Equally important is the measurement of the diffuser inlet angle i.e. an extremely important key parameter for determination of the occurrence of instabilities in a vaneless diffuser.
A flush system that periodically blow channels in the pitot tube clean will conceivably work. Since the droplets in the flow are spread, it will take some time for the droplets to hit the holes in the Pitot tube. In this time interval with dry pitot tubes, it is possible that the velocities can be measured.

In addition to complex CFD, methods modern measurements techniques with time resolving capabilities ,are necessary to determine the instantaneous flow quantities.
FRAP probes are a promising alternative to other time resolved measurement techniques. Besides the flow angles, Mach number, and velocity, FRAP can additionally measure both time-resolved total and static pressures. The FRAP probes provides a high-performance system primarily dedicated to turbo machinery applications. The current improvement of selected components make the FRAP system suited for more complex applications, such as detailed-two- dimensional flow field measurements or even three- dimensional with four sensor probes.

Multi-hole probes (MHP) are designed based upon the principle of operation of pitot- static probes fluid flow instruments that measure pressure along pressure ports arranged on their tips. Whereas pitot- static probes are extensively used in situations where the direction of the

flow is known, MHP technology is proven and mature to resolve the 3-dimensional velocity vectors in flow fields notwithstanding the direction of the flow.

8 Description of experimental setup and procedure

This chapter presents the specifications and the changes conducted in the impeller rig exclusively for this master thesis. The first section is reserved a conclusive summary of the findings that form the basis for the focus of this master thesis that is given in Section 8.2. A description of the arrangement of the measuring devices is included in Section 8.3 and 8.4.

8.1 Summary previous work

This Section is intended as a point wise representation of the key findings and observations made from the pre project of this master thesis [11] regarding instabilities for dry and wet gas compression. The experimental tests performed in the project thesis confirmed depiction of recently research concerning instabilities. Other important findings was:

- The frequency spectrum concealed a **stall propagation that approached the impeller frequency at reduced flow rate for dry gas**, overlapped by the development of sub-sequent stall frequency propagation.
- The phase-lag analysis **detected altered tendencies in the phase shift for dry gas**, i.e. deviation in the stall propagation around the circumference of the diffuser.
- The compressor characteristic revealed **increased pressure ratio rise prior to surge for wet gas with decreasing gas mass fractions**.
- Tests showed a **tendency of delayed development of instabilities for wet gas** compared to the case of dry gas.
- **The frequency spectrum for wet gas did not reveal any stall frequencies which is typical for dry gas before entering surge**. However, it gave an indication of the impact of the reduced GMF had on the surge formation.
- Visual observation showed **backflow at the impeller inlet for wet gas** and a **deviating liquid flow path in the diffuser** [11].

8.2 Focus of experiment

Based on the findings described in Section 8.1, together with important findings by Grüner and Bakken [46], there was an essential necessity to further document the phenomena related to wet gas surge, especially regarding validation of flow pattern and instability. It was chosen to conduct experiments on the identification of the impeller outlet angle in order to describe the diffuser flow pattern. In addition it was chosen to perform experiments on achieving a more precise identification of the wet gas surge initiation and instability precursors. The main bullet points were thus to:

- Validate the flow pattern at the outlet of the impeller by using pitot measurements.
- Identify wet gas surge using wet gas pitot probes.

8.3 Installation of Pitot –static probe in diffuser wall

In order to best possible identify the flow angle it was decided to implement a 2.1 mm L-shaped pitot tube for angle identification. The positioning of the device turned out to be easiest through the existing diffuser plexiglas, due to the accessibility of the plexiglas in the diffuser wall. The mounting of the pitot- static tube is shown in Figure 8-1, However, for a more comprehensive appearance, the reader is encouraged to take a look at the technical drawing in Appendix B1.

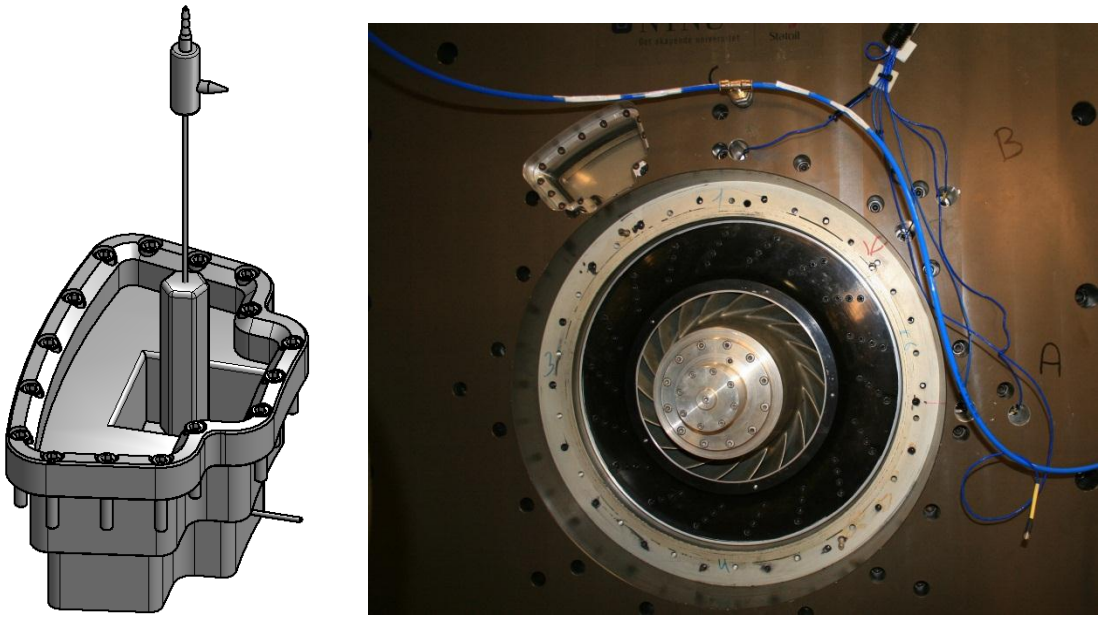

Figure 8-1: Mounting and localization of the pitot tube.

The position of the pitot tube setup with velocity triangles and geometry relations are illustrated in Figure 8-2. The vector $\vec{R}$ gives the distance from the center of the impeller to the center of the pitot static tube denoted S_1 and S_2, respectively. The distance from S_2 to the point S_3 marks the length $\vec{r}$ of the pitot "foot". Hence the measured angle α' is the angle between $\vec{R}$ and $\vec{r}$ while the actual flow angle, α, is the angle between $\vec{r}$ and the extension of the line through point S_3. The correlation between the measured and the actual flow angle are given in Equation 8-1.

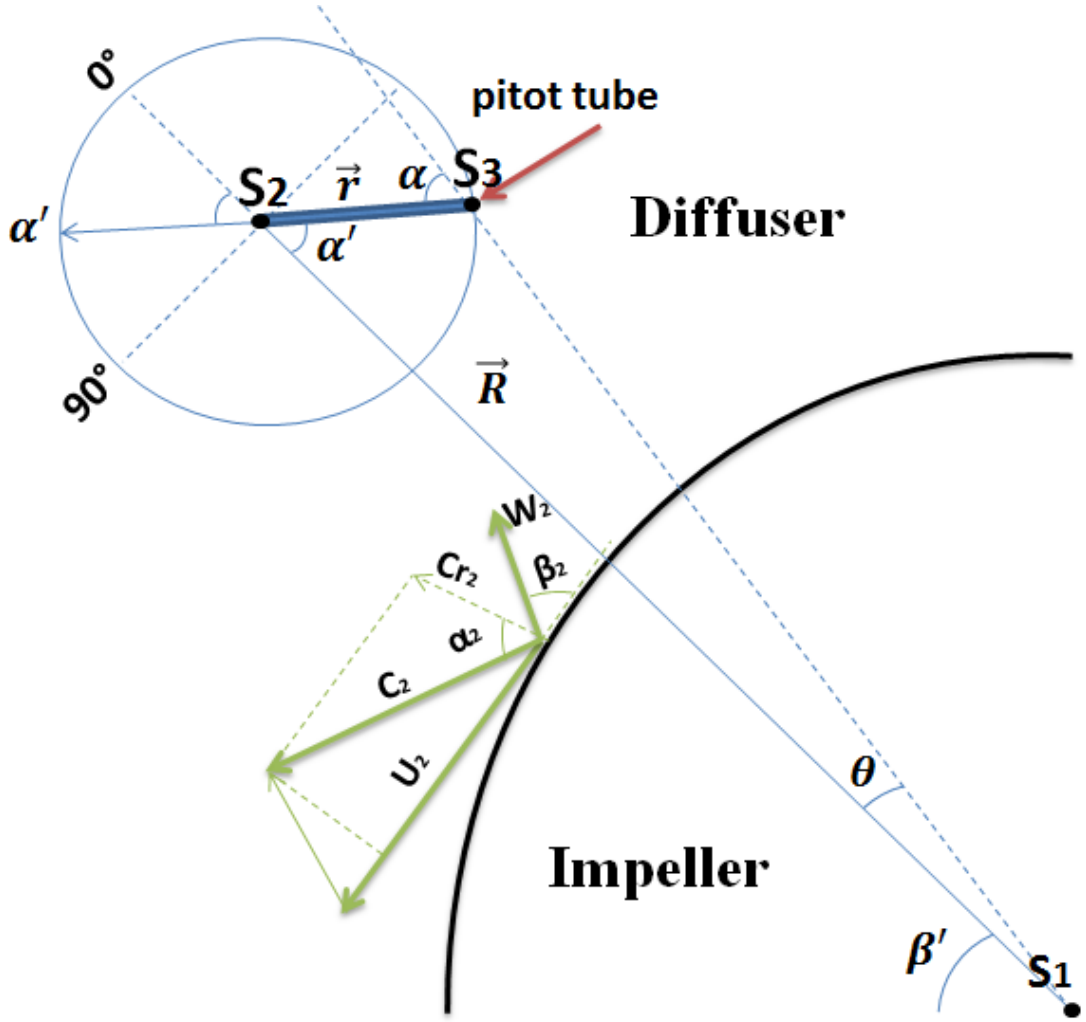

Figure 8-2: Sketch of the pitot- probe positioning

$$\alpha = (\alpha' - \beta') + \tan^{-1}\left(\frac{|\vec{R}|\sin(\beta') + |\vec{r}|\cos(\alpha' - \beta')}{|\vec{R}|\cos(\beta') - |\vec{r}|\cos(\alpha' - \beta')}\right)$$ **Equation 8-1**

A picture of the complete pitot probe setup is shown in Figure 8-3. The probe was connected to a UNIK 5000 GE sensing transmitter element covering a differential pressure range from -500 mbar to 500 mbar. The data sheet for the transmitter is attached in Appendix C. The measuring of the diffuser flow angle, α' was done manually by continuous change the position of the pitot probe by using a magnetic arrow for reading the angle, and a 5-Volts signal generator signaling a change in the angle position. Actual flow angle is given when the impact frequency is greatest, where the flow is parallel to the inlet of the Pitot probe. The point where the flow angle is measured will then move around its own axis i.e. the blue circle in Figure 8-2, positioned in the middle of the diffuser width between the shroud and the reference hub, at 50% width.

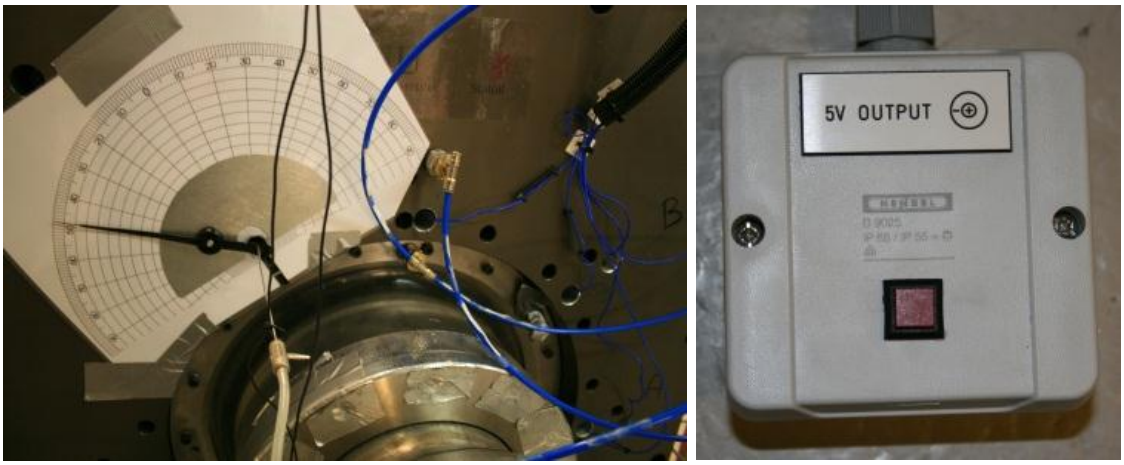

Figure 8-3: Protractor set-up and signal generator

8.4 Installation of the surge detection tube

The surge detection setup involves a 1.6 mm diameter tube that was installed in the reverse flow direction facing 1 mm upstream from the impeller blade inlet. The tube was connected to a Kulite 5 VDC pressure transducer attached in Appendix C. Additionally the 5 -Volts signal generator was used to signal the logging by visual confirmation of the observation of an annular ring of backflow. A section of the technical drawing of the tube positioning is shown in Figure 8-4.

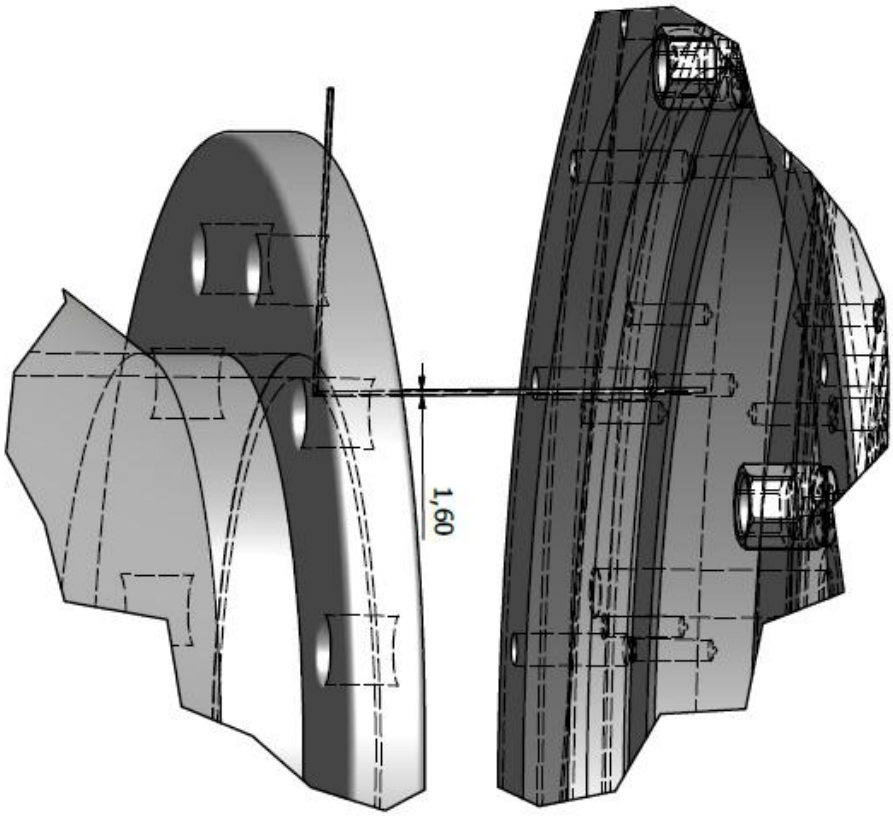

Figure 8-4: Section of a CAD drawing given from Appendix B2.

8.5 Chapter summary and conclusion

It was chosen to conduct experiments on the identification of the impeller outlet angle in order to describe the diffuser flow pattern. In addition it was chosen to perform experiments on achieving a more precise identification of the wet gas surge initiation and instability precursors. The main bullet points were thus to:

- Validate the flow pattern at the outlet of the impeller by using pitot measurements.
- Identify wet gas surge using wet gas pitot probes.

9 Experimental results and discussion

For the purpose of measurements conducted in this master thesis LabVIEW 2010, from National Instruments, was used to analyze the raw data from the pressure sensors in order to post-process and represent the data in a graphical manner. Log files from a total of seven experiments with dry and wet gas were documented and analyzed to verify the flow pattern in the diffuser and identify and characterize surge instability signatures.

LabVIEW applications, together with modules for spectral Fast Fourier Transform (FFT) analysis, are used to best possible visualize the results. An insight in frequency analysis and FFT for experimental testing is presented in the pre project of this master's thesis [11]. The experimental tests are mainly divided into two areas of investigation i.e. verifying the flow pattern in the diffuser and identification of surge instability for wet gas.

9.1 Diffuser pattern investigation

One of the two primary experimental goals of this master thesis was to identify the flow angle for dry and wet gas and the results from the investigation are given in the following subsections.

9.1.1 Dry gas flow angle

Flow angle experiments for dry gas were performed at 10000 and 9000 rpm steady state, at approximately the same volume flow in each point, in order to maintain good repeatability for comparison. Table 9-1 contains the key data for the tests.

Table 9-1: Test matrix steady state dry gas

Test	Volume flow Q [m^3/s]	Rotational speed [rpm]	Date
1	0.82-1.13	10000	10.April
2	0.80-1.18	10000	25.April
3	0.80-1.14	10000	26.April
4	0.70-1.10	9000	25.April

Figure 9-1 shows the measured flow angles at 10000 rpm for different volume flow points. As can be seen the flow angle increases with decreasing volume flow. The maximum flow angle for test 2 and 3 are 81.5 and 78.5, respectively, giving a global maximum deviation of less than 3 %. The figure reveals a sudden rise in flow angle gradient that occurs between volume flows close to 1 and 0.90 m^3/s. This particular gradient increase may be related to findings conducted by Reitan [62] on the diffuser and impeller characteristics at the NTNU impeller rig. Figure 9-2 shows the impeller and diffuser characteristics for 9000 and 10000 rpm. For 10000 rpm the impeller characteristic was, according to Reitan, found to make a sudden drop and hence, a similar reverse rise in the diffuser characteristic that was initiated at the same

volume flow of 0.95 m^3/s. The pressure drop in the impeller was to some extent dominating the pressure rise in the diffuser, resulting in a minor global drop for the compressor. Grüner and Bakken [46] detected the same abrupt changes for the impeller and diffuser characteristic, suggesting that the phenomena may be attributed to the volute performance. The volute performance causes a shift from deceleration to acceleration of the flow at the instance were the volute pressure ratio is 1 as seen from the impeller/diffuser characteristics in Figure 9-2.

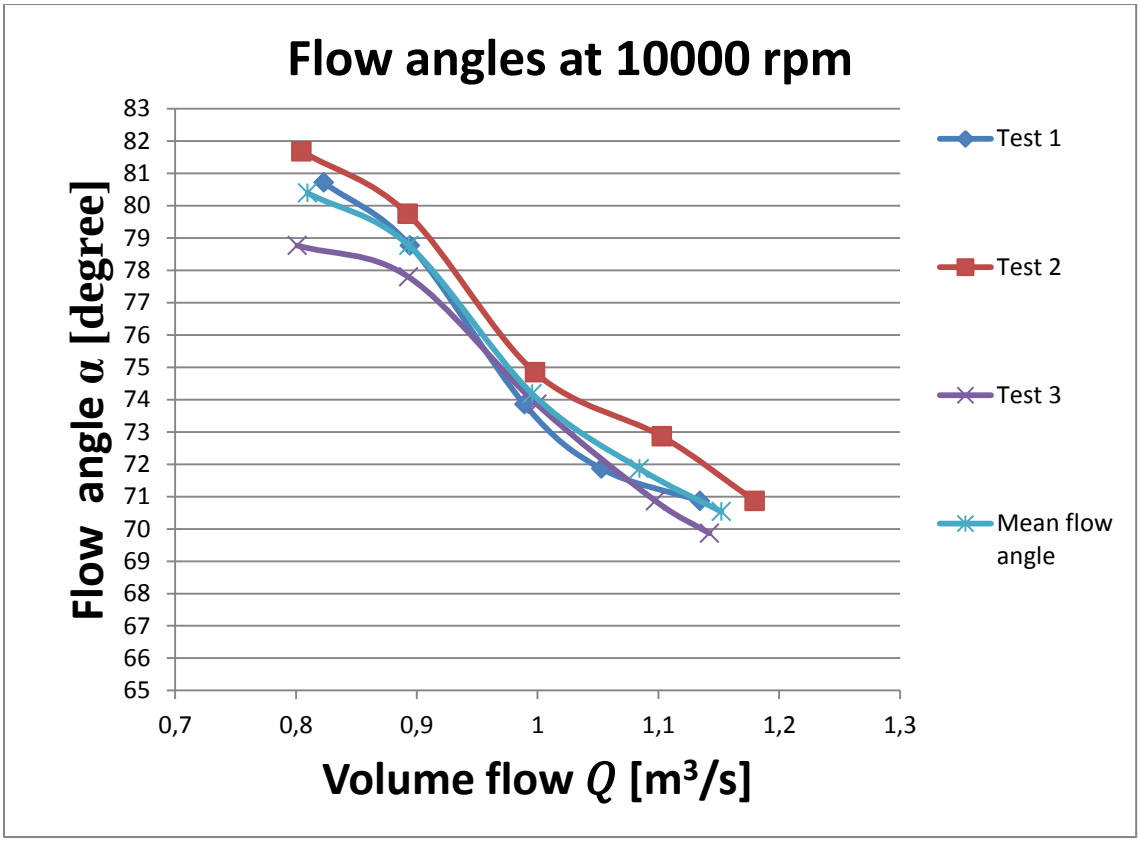

Figure 9-1: Flow angles at 10000 rpm dry gas

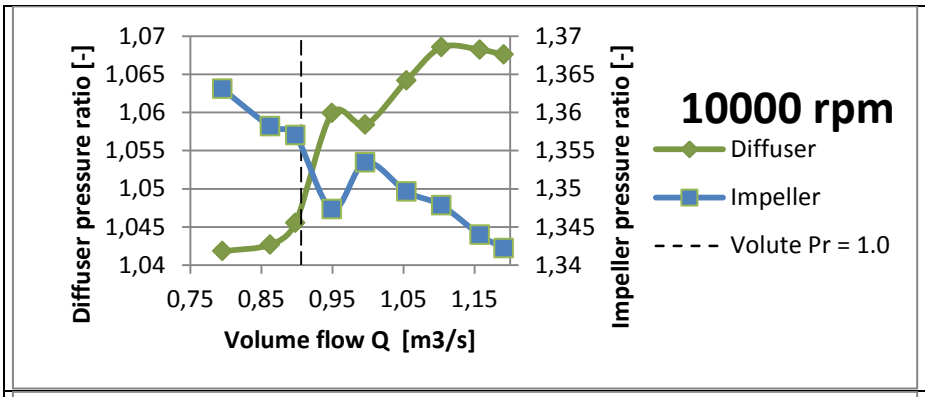

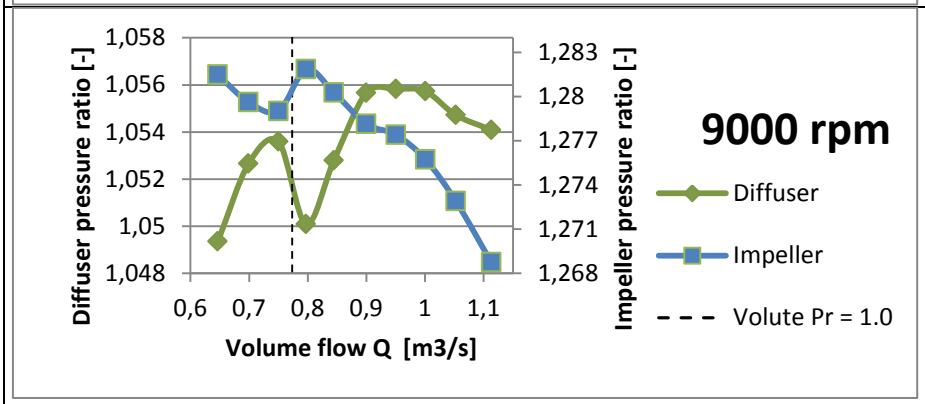

Figure 9-2: Impeller and diffuser characteristic for 10000 and 9000 rpm [62]

Figure 9-3 shows the measured flow angles at 9000 rpm showing the same trend as for the case with 10000 rpm i.e. flow angle increases with decreasing volume flow. The 9000 rpm curve experiences a gradient rise, with decreasing volume flow, at 0.8 m^3/s. This implies that the same impact, related to the impeller and diffuser characteristics, yields for both 9000 rpm and 10000 rpm.

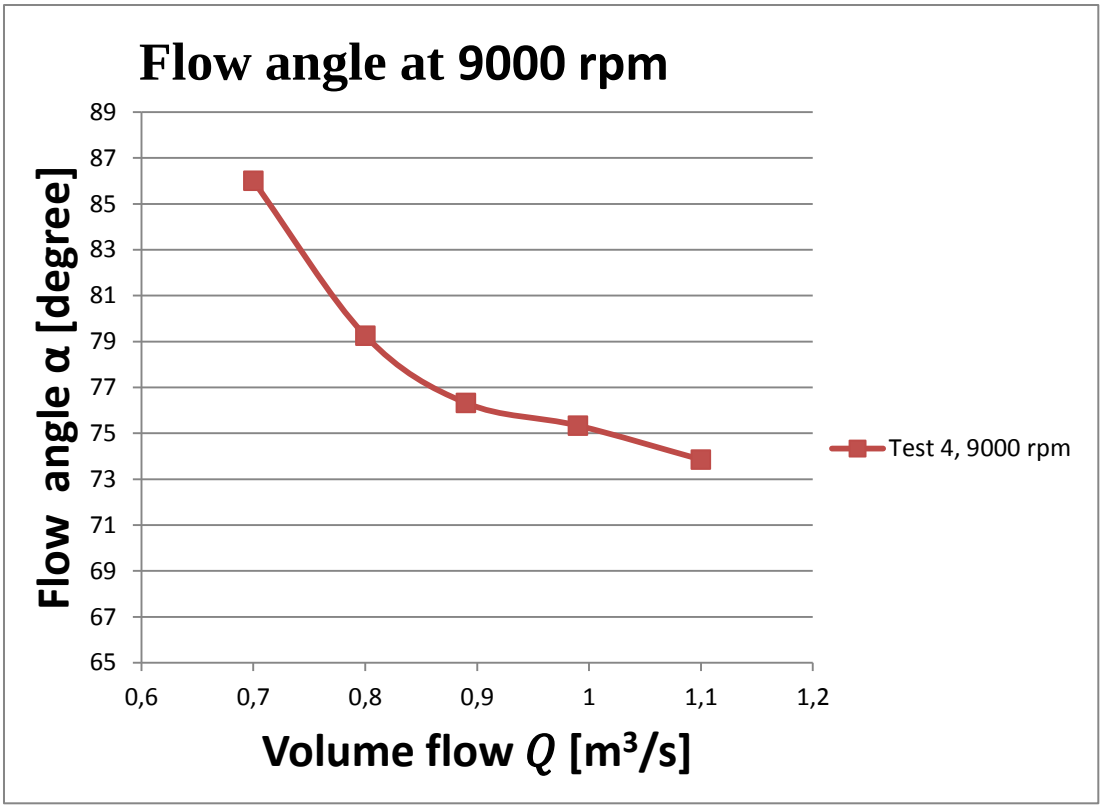

Figure 9-3: Flow angles at 9000 rpm dry gas

A comparison of the evolution of impeller outlet flow angles are given in Figure 9-4. The curves intersect after the point in which the volume flow is 1 m^3 /s. From the figure the two plots operate in a slightly different volume range. The maximum flow angle for the 9000 and 10000 curves are 86 and 80 degrees, respectively. From the trends of the figure it seems like another intersection will occur at a volume flow of about 0.8 m^3/s, however, more experiments will be necessary in order to justify this theory.

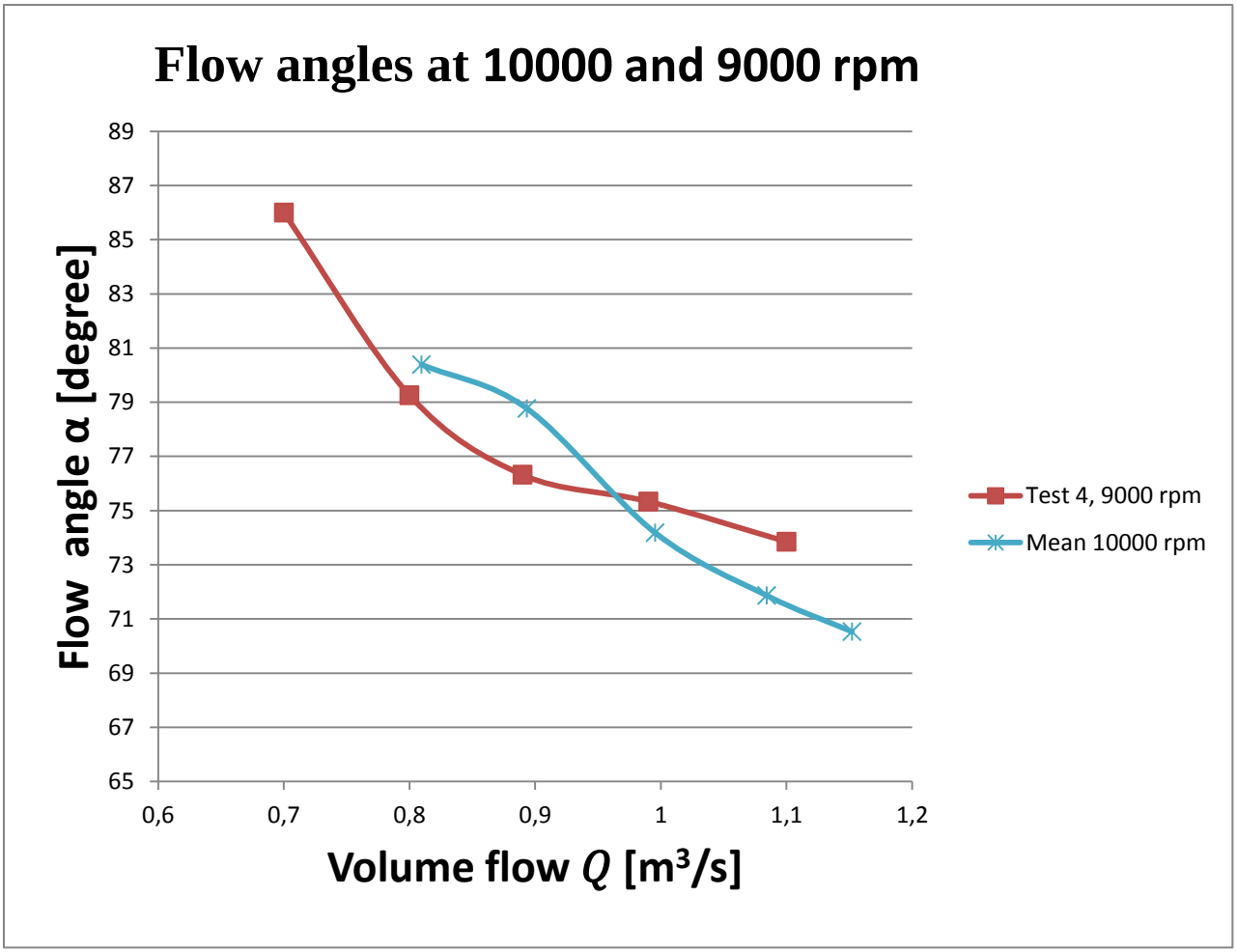

Figure 9-4: Flow angles for 10000 and 9000 rpm

9.1.2 Comparison between Laboratory measurements and Matlab simulations

Simulations of the discharge flow angle has been carried out by Mele [63] using a numerical Matlab model made for the NTNU impeller rig. The comparison between the Matlab simulation and the measured flow angle are shown in Figure 9-5. The Matlab curve reveals a approval coincident trends with the measured curve with maximum deviation of less than 5%.

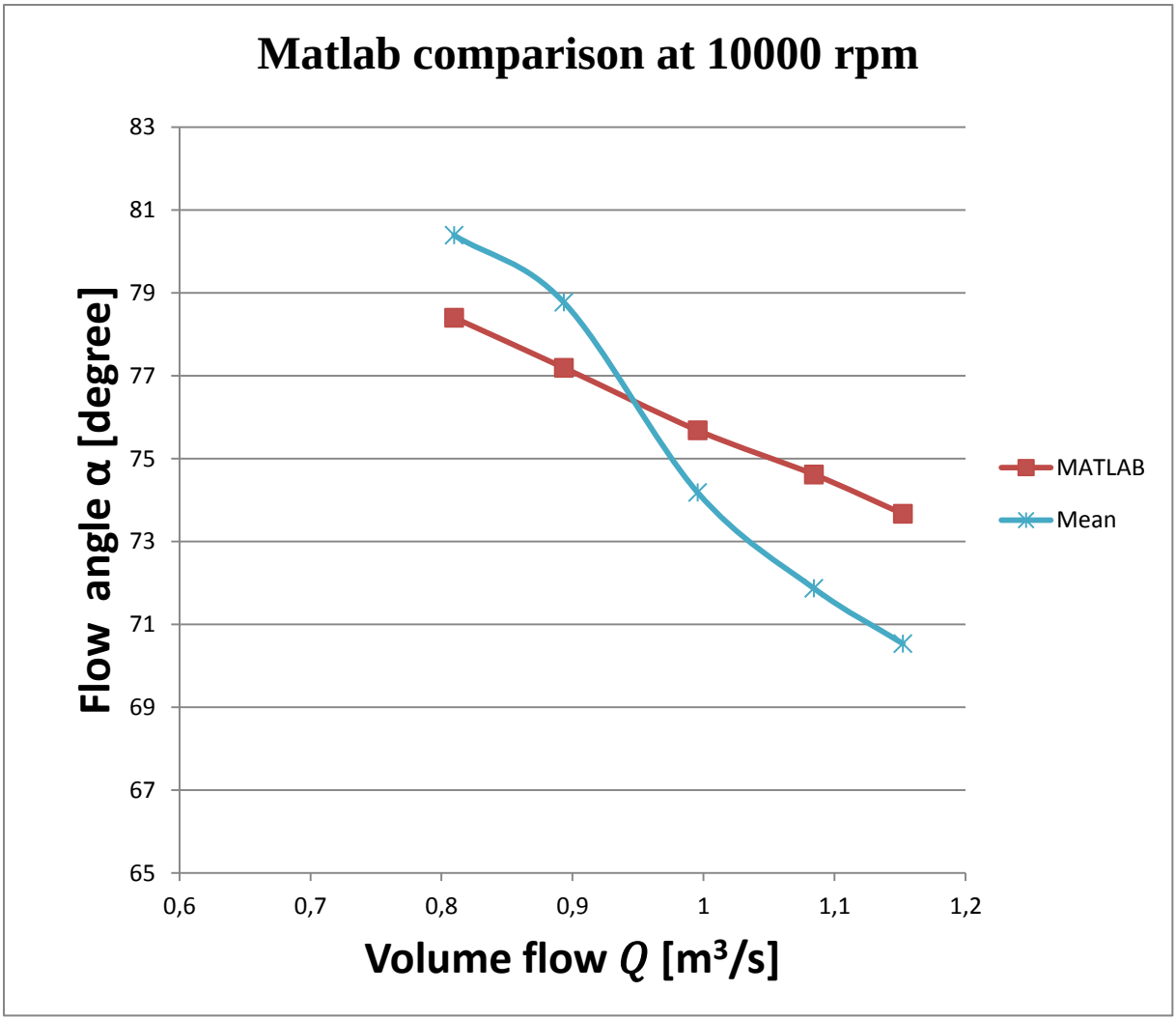

Figure 9-5: Matlab and lab flow angle comparison at 10000 rpm.

9.1.3 Comparison between Laboratory measurements and CFD simulations

As previously mentioned CFD measurements of the diffuser angle was performed by Irgens [20] for comparison with the experimental findings. The CFD simulation was carried out for three different widths in the diffuser with accordance to shroud and hub side as illustrated in Figure 9-6. Figure 9-7 and Figure 9-8 shows the plot for 10000 and 9000 rpm, respectively. The values from the simulations are averaged over a line on the impeller outlet at three different widths, i.e. 20%, 50% and 80% corresponding to 2.8 mm, 7 mm and 11.2 mm away from the reference hub side of the diffuser.

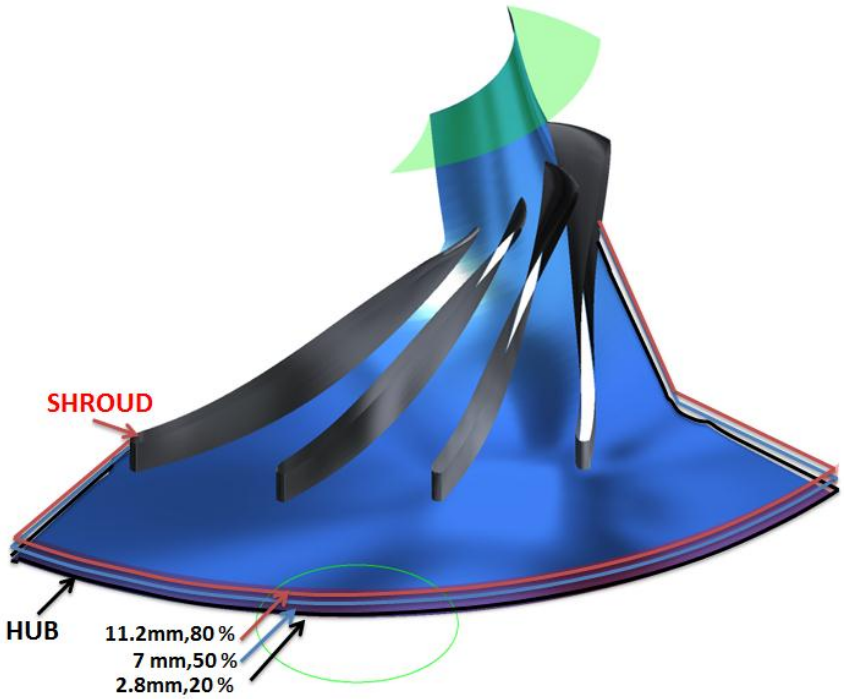

Figure 9-6: Simulation domain where the pitot measurements are conducted [20]

The plots in Figure 9-7 and Figure 9-8 show that the flow angle varies a lot in accordance to the width. The curve that represents the pitot measured values should correspond to the 7 mm curve because the positioning of the tube was centered in the middle of the diffuser. Notwithstanding, in Figure 9-7 the measured curve and the 7 mm curve shows a nonconforming correlation at 9000 rpm, although they meet and crosses at low volume flow. The curve near the shroud side, on the other hand, shows an enhanced trend line correspondence with the measured curve for 9000 rpm. The congruent trend between the measured curve and the 7 mm simulated curve appears even clearer for the case of 10000 rpm in Figure 9-8. The maximum deviation discrepancies between CFD and Laboratory experiments based on 7 mm simulations are 6.7 % and 11.7 % for 9000 and 10000 rpm, respectively, hence the case for simulation based on 11.2 mm width the maximum deviations are 4 % and 5 %, correspondingly. This finding suggests that the actual position of the pitot tube is installed closer to the shroud than first anticipated. The deviation between the measured flow angle values and the simulated values are given in Table 9-2.

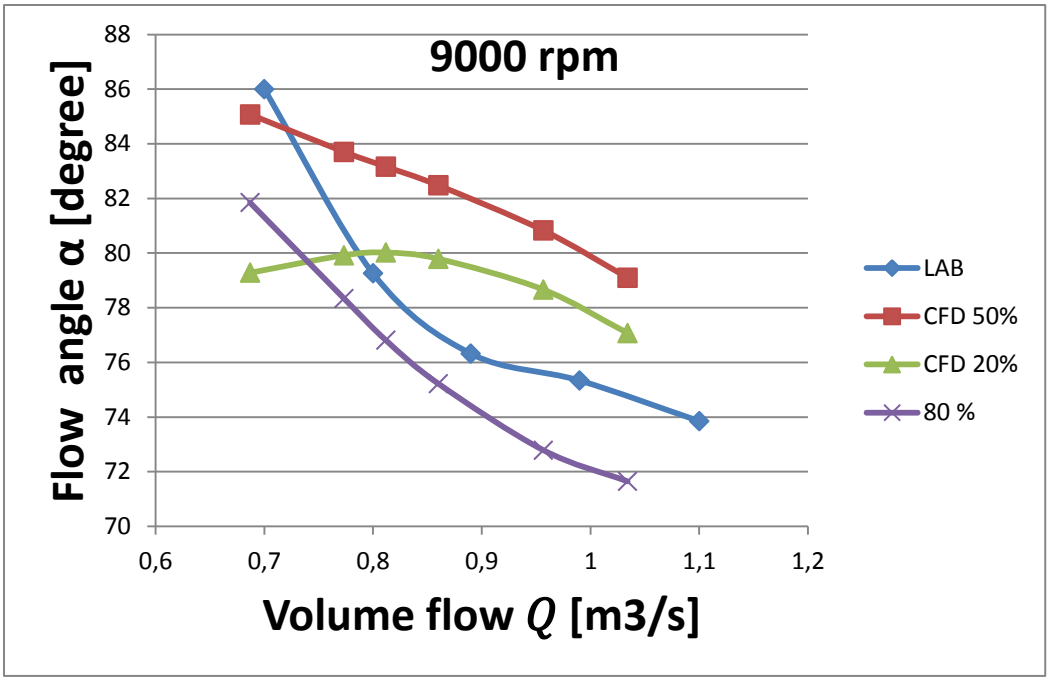

Figure 9-7: CFD and Lab flow angle comparison at 9000 rpm

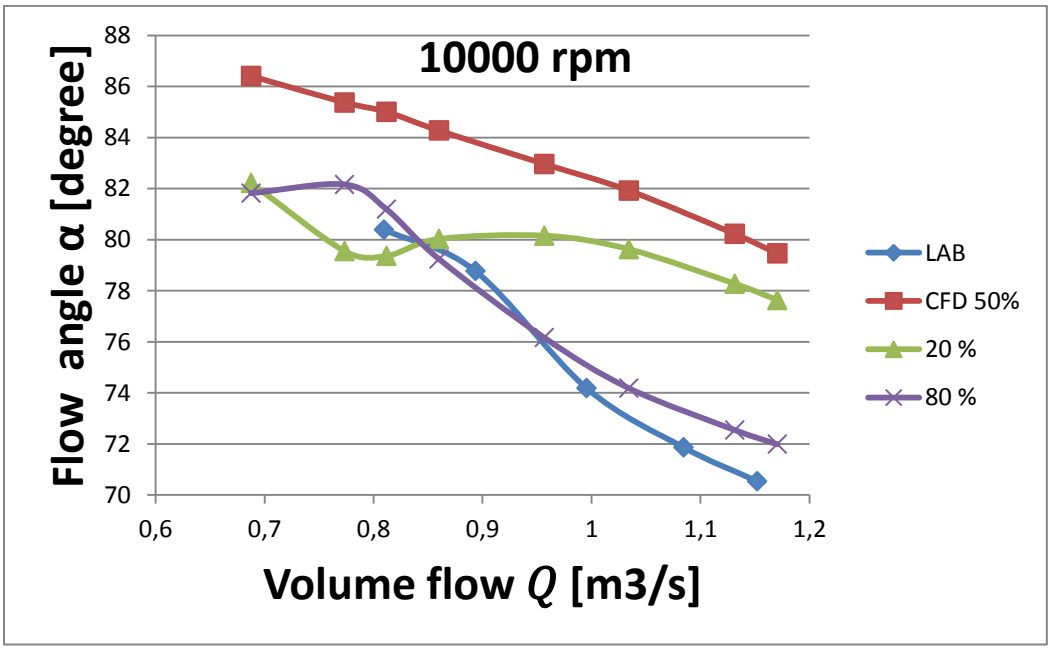

Figure 9-8: CFD and Lab flow angle comparison at 10000 rpm

Table 9-2: Flow angle devation between CFD and laboratory measurements

		9000 rpm	10000 rpm
CFD 80 % 2.8 mm	Average	3.3 %	1.5 %
	High	4.0 %	3.0 %
CFD 50 % 7 mm	Average	4.8 %	9.0 %
	High	6.7 %	11.7 %
CFD 20 % 11.2 mm	Average	2.6 %	5.8 %
	High	4.1 %	9.4 %

9.1.4 Wet gas flow angle

Laboratory experiments for core flow angle measurements on wet gas was attempted by means of high liquid injection i.e. low GMF. Unfortunately, with low GMF the variation in measured flow angles was abundant due to the impact from the droplets and the liquid film on the pitot tube. An attempt was made turning the pitot tube 180 degrees in order to measure the angles corresponding with the lowest impact on the probe, regardless without success. It was nonetheless performed experiments on wet gas at high GMF in which the probes seemed to be close to unaffected by the liquid. The test matrix for two experimental wet gas tests with constant and variable GMF are given in Table 9-3.

Table 9-3: Test matrix steady state wet gas

Test	Volume flow Q [m^3/s]	Rotational speed [rpm]	GMF [-]	Date
5	0.79-1.17	10000	0.9	25.April
6	0.89-1.14	10000	0.81-.93	09.May

Figure 9-9 shows the measured flow angles at 10000 rpm. As is evident from the figure, measurement of wet gas is associated with a greater uncertainty than dry gas, due to the influence of liquid. However the same trend with increasing angles at reduced volume flow is imminent for both alternating and constant GMF. The maximum flow angle for test 5 and 6 are 67.5 and 63 degrees, respectively. By comparison, the critical angle, α_c, which provide a tentative transition between the stable operation area and rotating stall is 78 °.

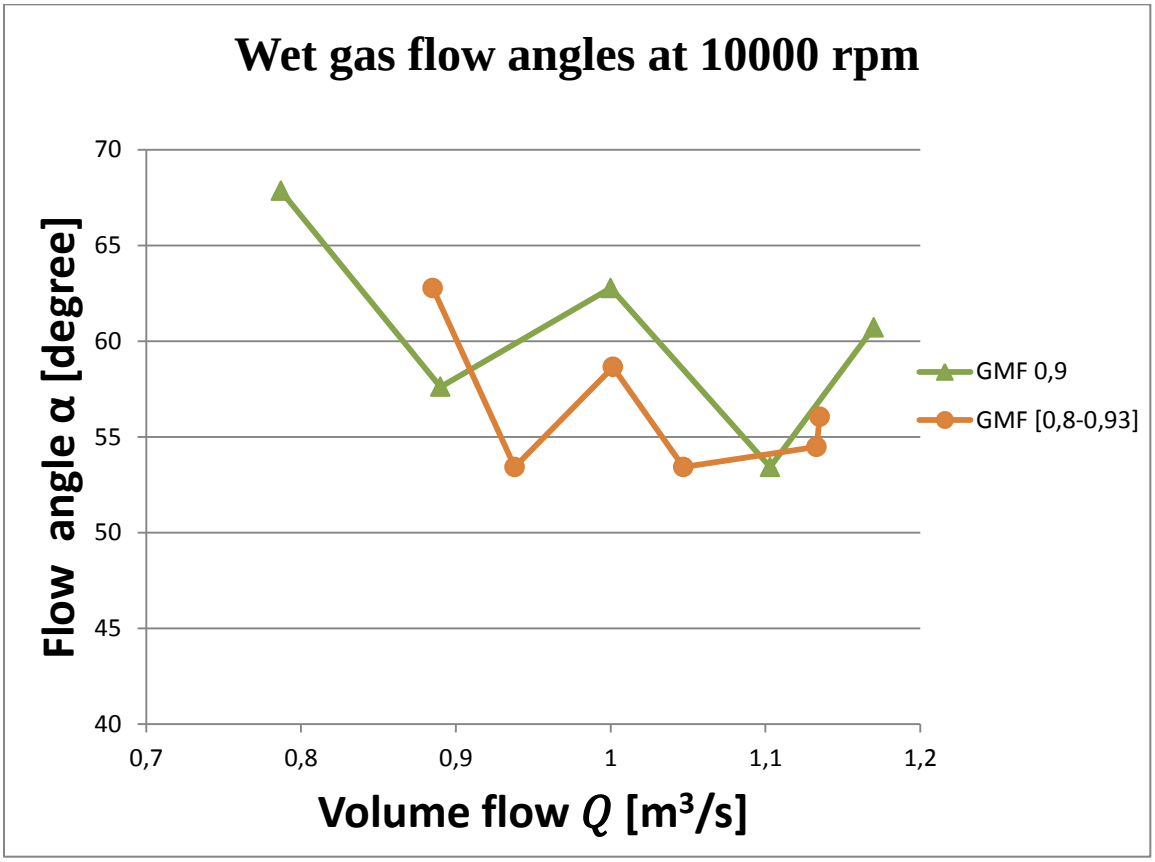

Figure 9-9: Wet gas flow angle measurements

9.1.5 Comparison between wet and dry gas

The comparison between the flow angle measurements for dry and wet gas are displayed in Figure 9-10. Despite the difficulties of measuring wet gas, the wet gas curves shows distinct trends with lower discharge angles across the spectrum compared to the case for dry gas measurements. This may support the findings of Grüner and Bakken [46] suggesting that the global core flow path through the diffuser becomes shorter and hence better with the presence of liquid, with reduced frictional losses.

The fact that the measured flow angels for wet gas are far below the critical flow angle, α_c, for the system, may support the finding that it was not revealed any sub synchronous stall frequencies prior to surge on wet gas tests by Grüner [8] and the author himself [11] which is typical for dry gas before entering surge.

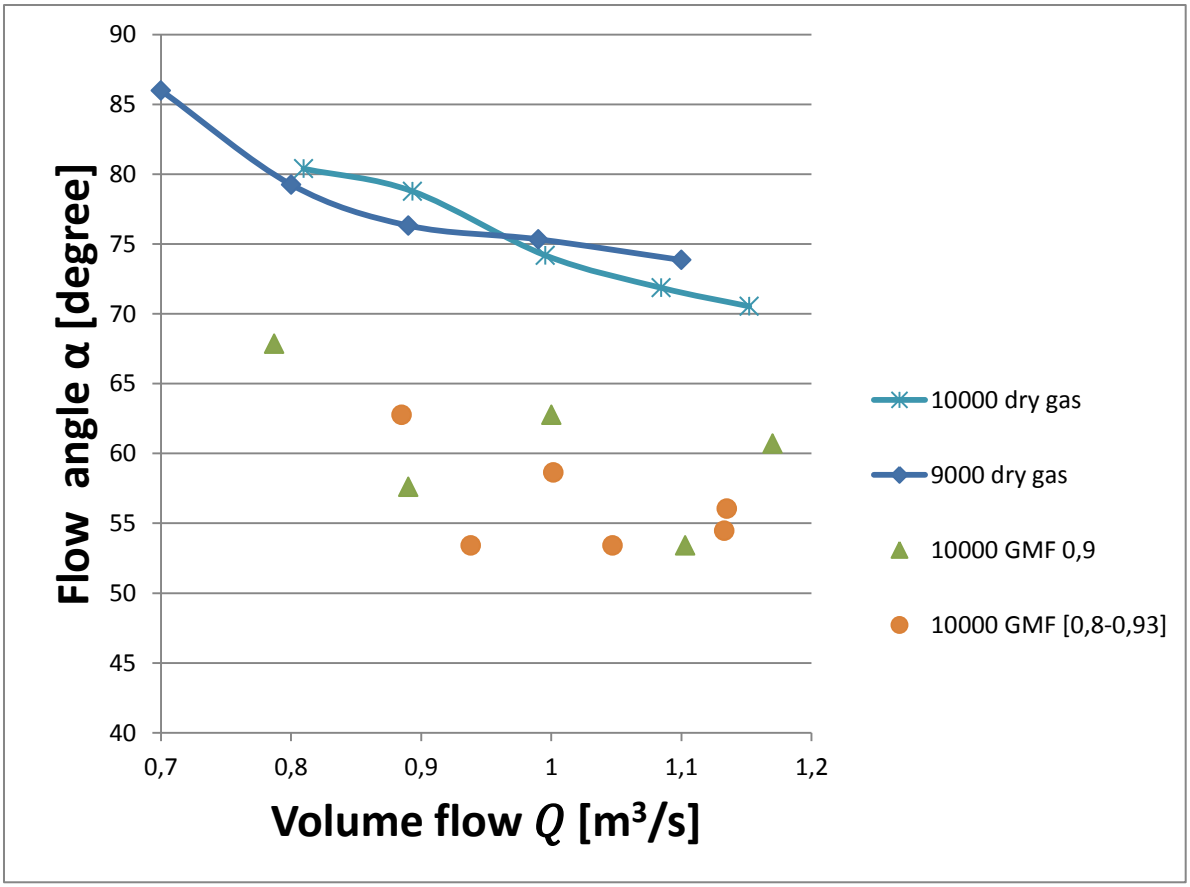

Figure 9-10: Flow angle comparison between Dry and wet gas

9.2 Impeller surge detection

Identification of wet gas surge and possible precursors of surge for a transient test on 7500 rpm are documented in the following subsections. The different measuring channels used for the investigation are given in Appendix C with the corresponding data sheets attached.

9.2.1 Transient wet gas performance characteristic

The wet gas surge detection test was carried out for the compressor while operating at 7500 rpm. The test matrix for the investigation is given in Table 9-4. Steady state points were logged for three volume flows before conducting a transient operation bringing the compressor into surge by supplying a constant liquid flow rate and manually gradually throttling the valve.

Table 9-4: Test matrix for transient wet gas

Run	Volume flow Q [m^3/s]	Rotational speed ω [°/min]	Pressure ratio PR [-]	GMF [-]	Logging time [s]	Date
1	0.14-0.4	7500	1.21-1.24	0.6-0.42	42	24. April

The pressure characteristic for the experiment is displayed in Figure 9-11 whereas the corresponding volume flow alteration is presented in Figure 9-12. The first sign of intermittent behavior seen from Figure 9-11 occurs after about 30 seconds into the transient segment at a volume flow of about 0.26 m^3/s prevailing sudden stringent static pressure fluctuations. The volume flow, and hence GMF, were subsequently reduced from 0.6 to 0.42 due to throttling of the valve into surge. The transient time span of GMF is provided in Figure 9-13**.** At lower flow rates the effect of GMF is imminent.

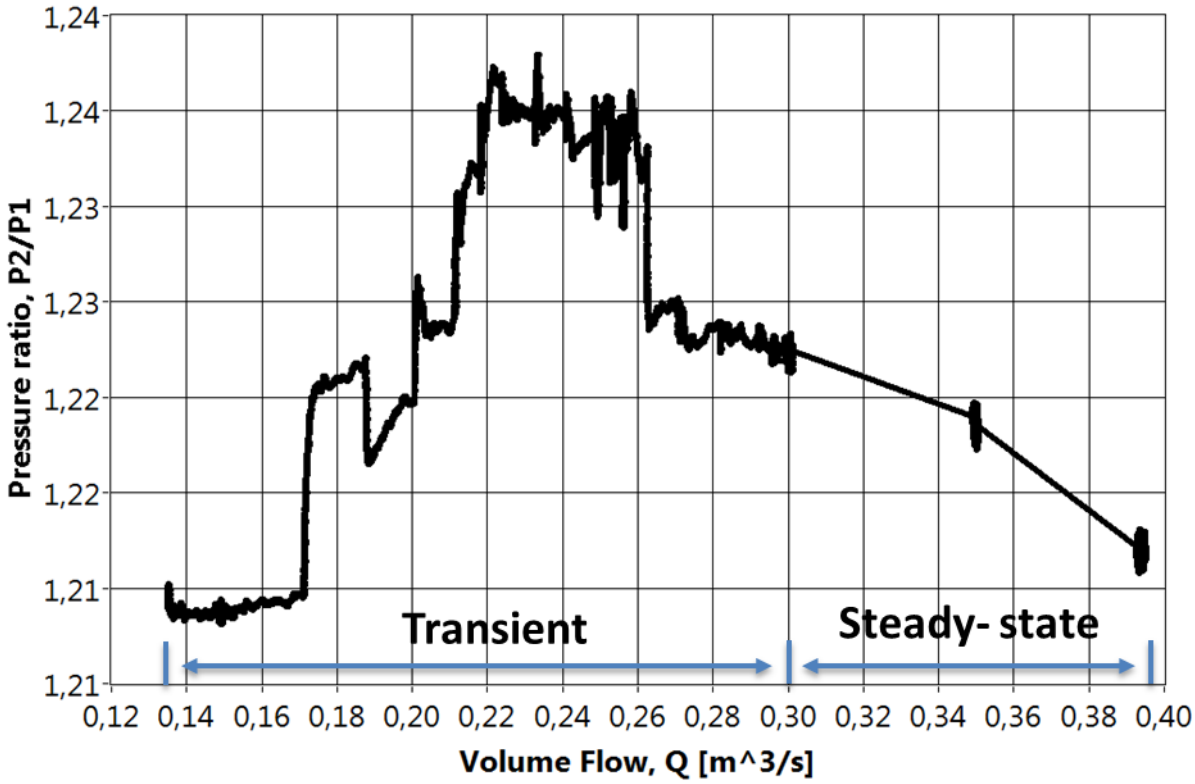

Figure 9-11: Pressure characteristic for wet gas at 7500 rpm

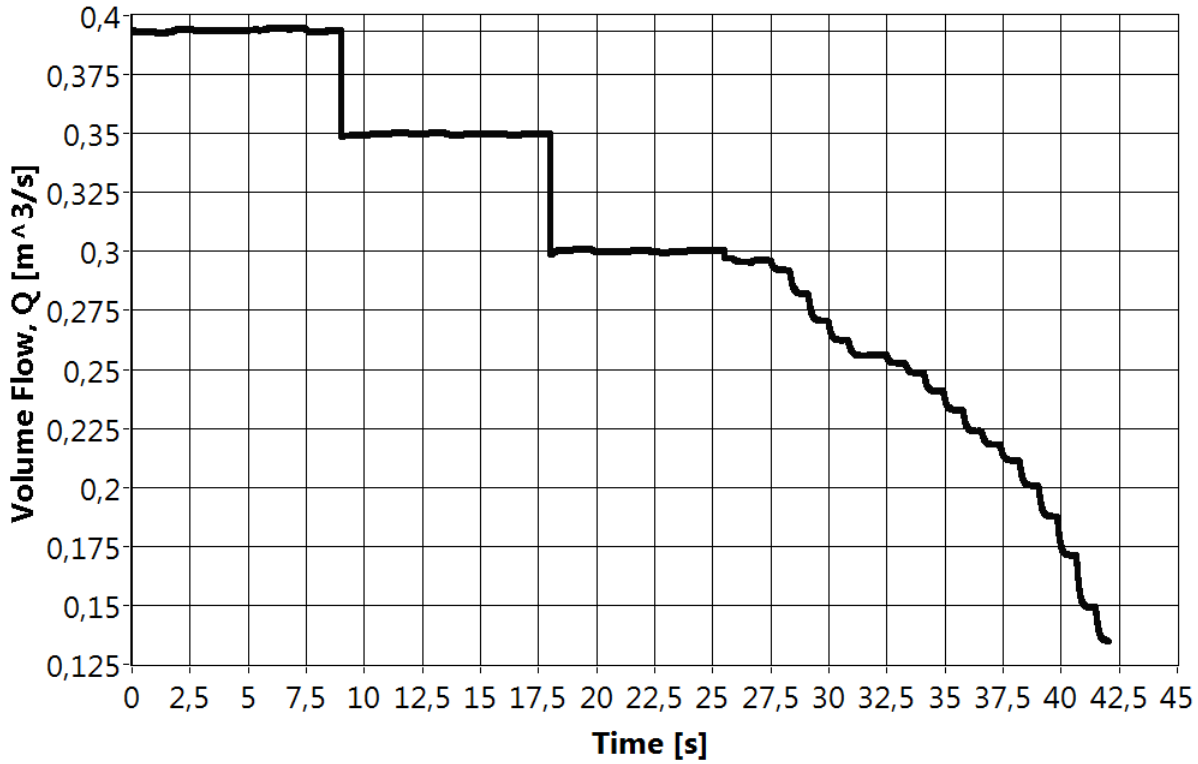

Figure 9-12: Volume flow characteristic for wet gas at 7500 rpm

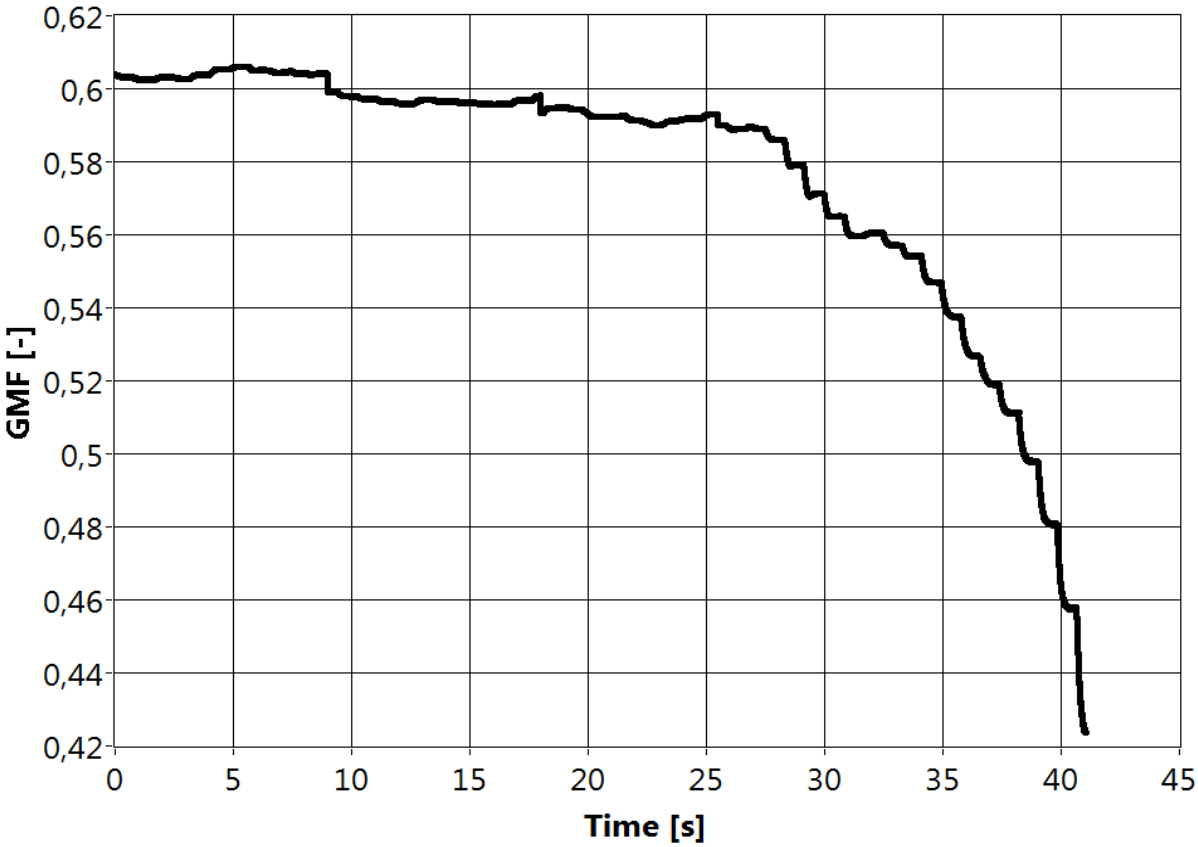

Figure 9-13: Transient GMF change for wet gas at 7500 rpm

Figure 9-14 displays the corresponding frequency spectrum for the transient test in a waterfall plot for the dynamic pressure sensor PCB C1. The plot shows a segment of the total time span starting from 20 seconds into the log file, meaning that one second into the plot corresponds to 21 seconds into the log file. A small peak at 125 kHz is seen as equivalent to the rotating speed of the impeller. The plot shows that the critical disturbance occurs and is enhanced at low frequencies causing the initiation of surge. Figure 9-15 shows the equivalent transient segment into surge for the sensor of channel 22 i.e. the diffuser dp2.

By comparing the transient characteristic curve with the waterfall plots, the surge formation is most likely to be initiated after approximately 29 seconds i.e. at a volume flow of 0.27 m^3/s and a corresponding GMF of 0.57. At a volume flow around 0.19 m^3/s, the compressor is in a severe condition suffering from deep surge.

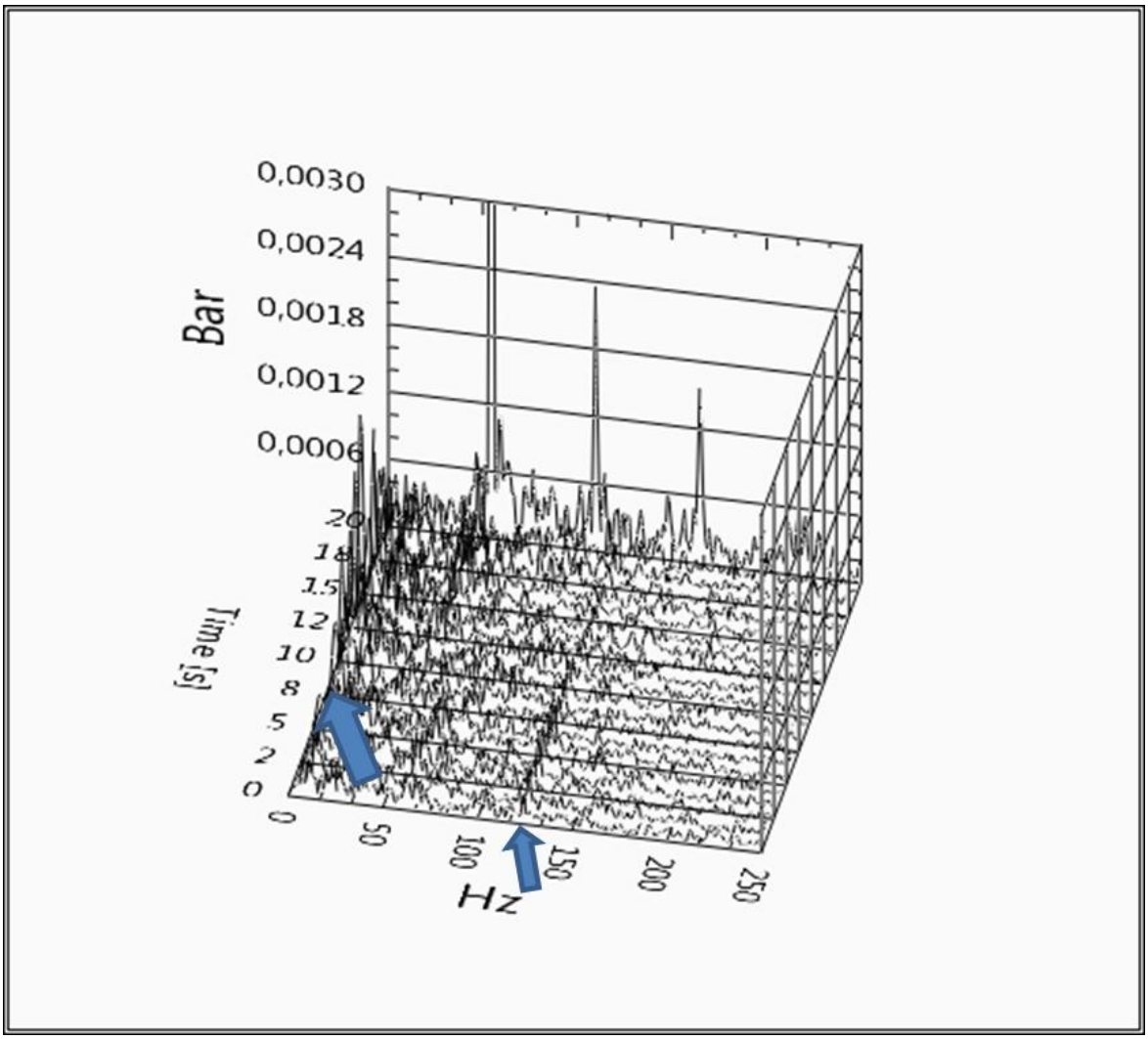

Figure 9-14: Frequency spectrum for wet gas at 7500 rpm for sensor channel 20

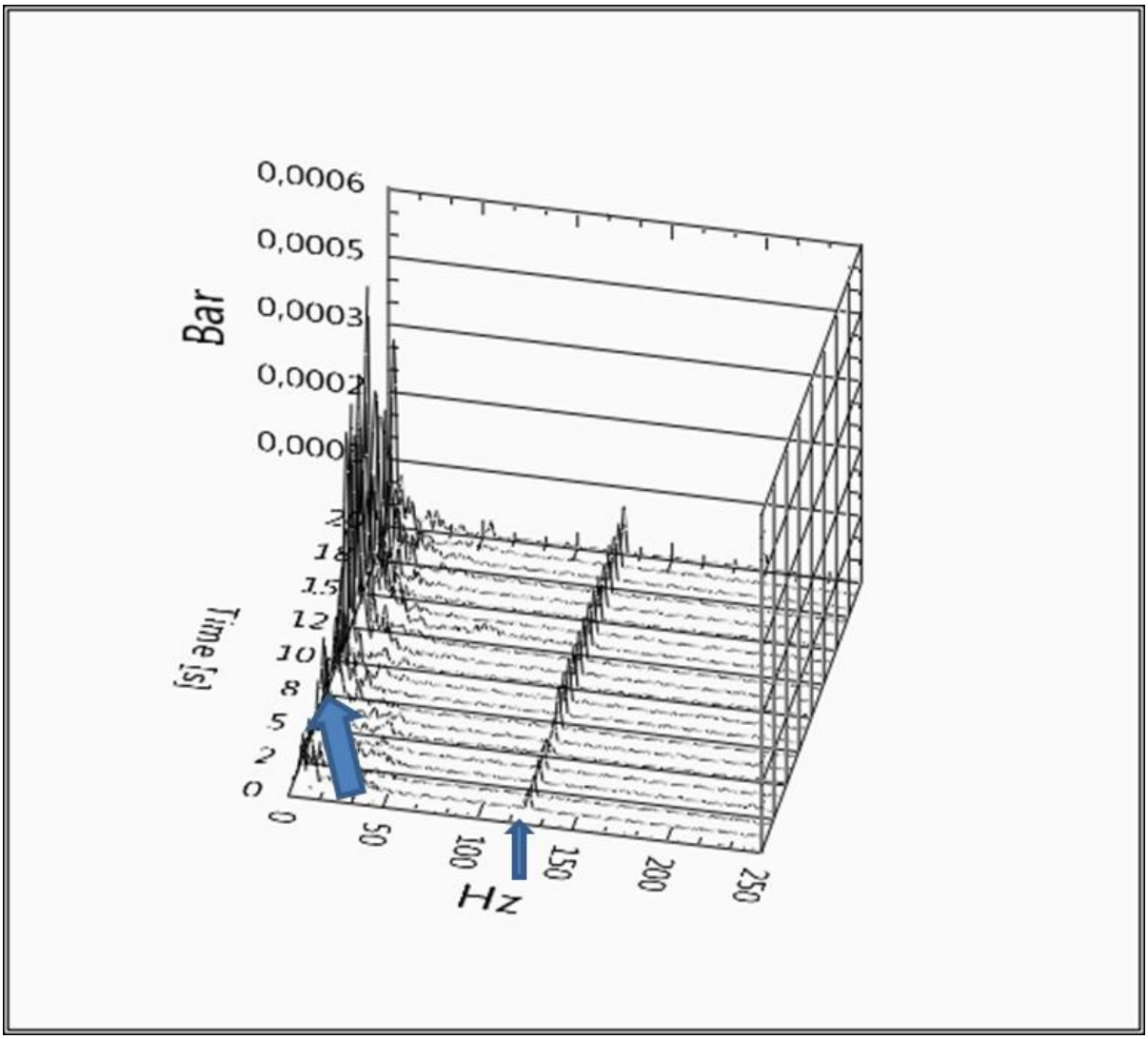

Figure 9-15: Frequency spectrum for wet gas at 7500 rpm for sensor channel 22

9.2.2 Pressure surge detection and identification measurements

The detection tube set-up was used to identify surge initiation by changes in the stagnation pressure for the wet gas at the 7500 rpm test. Figure 9-16 shows the stagnation pressure development into surge. The blue parallel lines mark the first initial increase starting after 26 seconds i.e. volume flow of 0.29 m^3/s, that may indicate an initiation or a possible precursor to surge by the change in pressure amplitude. High fluctuations after 28 seconds into the log file provide a strong indication of surge and a stringent liquid flow reversal. The pipe had a tendency to slightly vibrate concurrently with the return flow, whether this affected the amplitude measurements are however unknown.

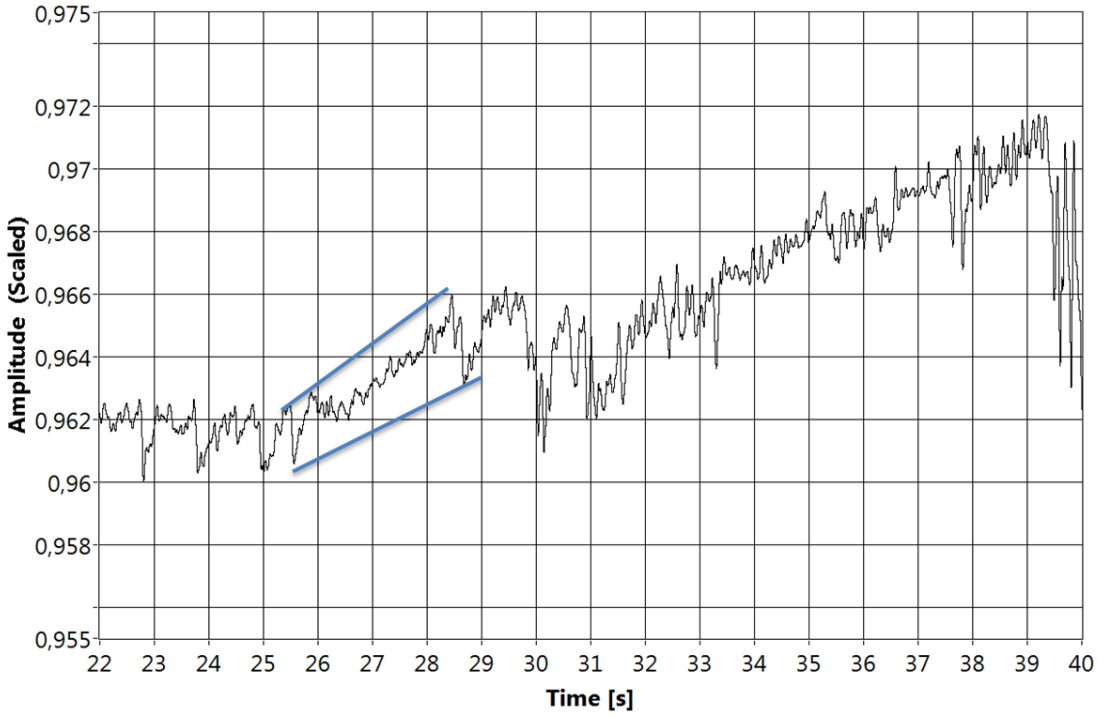

Figure 9-16: Pressure characteristic into surge, channel 27

The method of using a tube to detect the surge onset was compared to the measurements conducted by a static pressure sensor, a differential pressure sensor and a high responsive dynamic pressure sensor i.e. channel 17, 21, 19 respectively. The scaled pressure development into surge from the different sensors is shown in Figure 9-17. The black lines in the figure is where alternations in pressure fluctuations start to emerge for the different sensors.

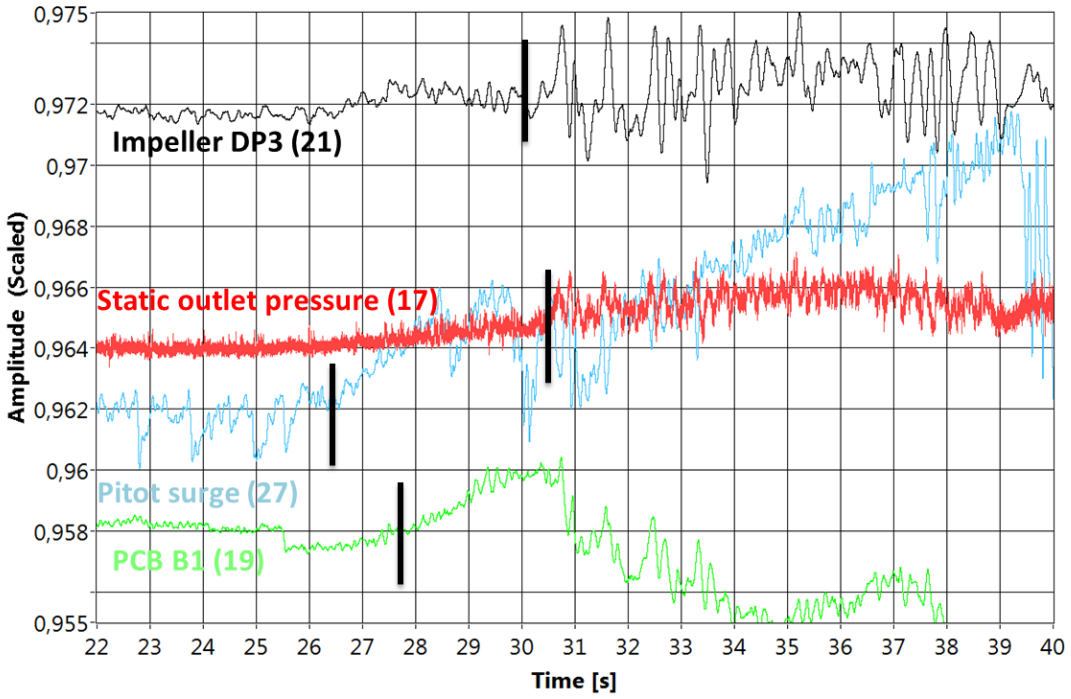

Figure 9-17: Comparison of pressure characteristics into surge for various channels

9.2.3 Visual observation of surge

Visual observation was performed by basically touch the 5 volt signal generator button each time a sign of back flow was observed. It was evident that an annular backflow ring was formed and emerged. Figure 9-18 shows the volume flow changes in a time segment, whereupon the red curve shows the amplitude fluctuations for the signal generator when touched. The blue arrows indicate when it has been carried out observations. The first observation of an emerging annular growing liquid ring shape was done after only 21 seconds, while sub synchronous larger rings was continuous after 23 seconds giving a chaotic flow path with complete back-flow at 31 seconds i.e. at 0.26 m^3/s. The first occurrence of visual verification is much earlier than the meters are able to detect any alternate frequencies.

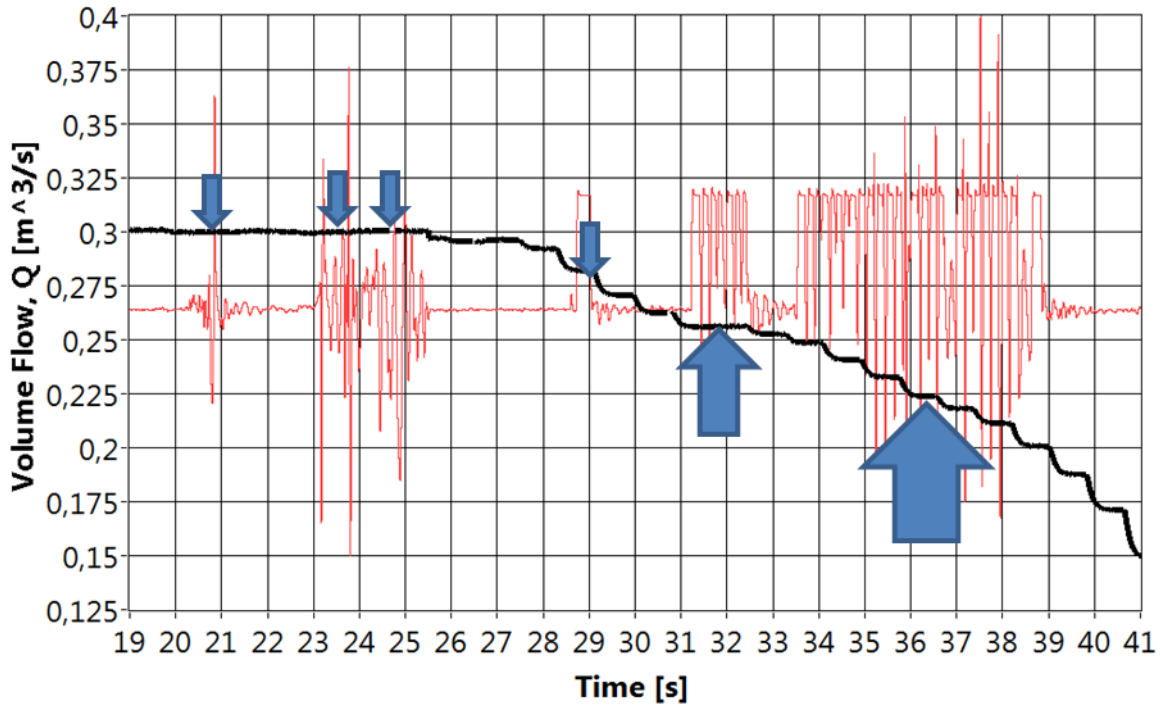

Figure 9-18: Visual observation of annulus ring of reversed flow

10 Discussion

This chapter will serve as a discussion and conclusion for the results of the two main experimental investigations performed in this master thesis.

Flow angle investigation

Flow angle experiments for dry gas were performed at 10000 and 9000 rpm steady state. The flow angle increases with decreasing volume flow. The maximum flow angle conducted for dry gas on 10000 rpm was 81.5 degrees. A sudden rise in flow angle gradient was found to occur between volume flows close to 1 and 0.90 m3/s. As for 10000 rpm, the 9000 rpm curve experiences a gradient rise, with decreasing volume flow, from 0.8 m3/s. This implies that the same impact, related to the impeller and diffuser characteristics, yields for both 9000 rpm and 10000 rpm. Maximum flow angle 9000 rpm was found to be 86 degrees. The available correlations used in the Matlab simulation gives a fairly accurate result with a deviation of less than 5 %. Deviation between CFD and laboratory experiments based on 7 mm simulations are 6.7 % and 11.7 % for 9000 and 10000 rpm, respectively, hence the case for simulation based on 11.2 mm width the maximum deviations are 4 % and 5 %, correspondingly.

This finding suggests that the actual position of the pitot tube is installed closer to the shroud than first anticipated. Measurement of wet gas is associated with a greater uncertainty than dry gas, due to the influence of liquid. However, the same trend with increasing angles at reduced volume flow is imminent for both alternating and constant GMF. The maximum flow angle for test 5 and 6 are 67.5 and 63 degrees, respectively. Despite the difficulties of measuring wet gas, the wet gas curves shows distinct trends with lower discharge angles across the spectrum compared to the case for dry gas measurements. This may support the suggesting that the global core flow path through the diffuser becomes shorter and hence better with the presence of liquid with reduced frictional losses.

Wet gas surge detection

The wet gas surge detection test was carried out for the compressor while operating at 7500 rpm. The first sign of intermittent behavior occurs after about 30 seconds into the transient segment at a volume flow of about 0.26 m^3/s prevailing sudden stringent static pressure fluctuations. At lower flow rates the effect of GMF is imminent. By comparing the transient characteristic curve with the waterfall plots the surge formation is most likely to be initiated after approximately 29 seconds i.e. at a volume flow of 0.27 m3/s and a corresponding GMF of 0.57. At a volume flow of roughly 0.19 m3/s, the compressor is in a severe condition suffering from deep surge. A change in the stagnation pressure after 26 seconds might be a possible indication of surge. The pipe had a tendency to slightly vibrate concurrently with the return flow, whether this affected the amplitude measurements are however unknown. The first observation of an emerging liquid ring shape was done after only 21 seconds, while sub synchronous larger rings was continuous after 23 seconds giving a chaotic flow path with complete back-flow at 31 seconds i.e. at 0.26 m^3/s.

11 Recommendations for further work

This chapter will present advices for further work for the results of the two main experimental investigations performed in this master thesis.

Flow angle investigation

The liquid may impact the flow velocity and direction by means of providing the flow with momentum, and thereby change the global core flow path through the diffuser to a shorter and hence better flow path with reduced frictional losses. Exact measuring of the wet gas flow velocity angle is thereby of high importance providing higher insight into stability considerations due to the presence of liquid.

The tests on dry gas flow angle measurements revealed higher angles with decreasing flow rate with uncertainty based on the manual measurement method. More precise measurements can be achieved by use of a configuration of multi-hole probes that provides a larger operation area meaning that the tube does not need to be turned around in the measurement domain.

Flow test for wet gas turned out to be very uneven due to interference and blockage at especially high GMF. By introduce a blow-out function or heating of the pitot tube one can circumvent the problem of blocking. In addition other types of measurement methods should be considered and examined. The development of sensors for wet gas flow may be required. Identification of the liquid film flow will also be a major discovery for comparison. For both the wet and dry gas tests is should be tested for a larger volume-flow range, preferably into the very unstable area for different rpms. In addition since the the flow distribution is highly uneven across the width of the diffuser, it is important to perform several measurements across the full width to validate against for instance CFD simulation.

Wet gas surge detection

In the case of detection of surge it should be performed more repeatable tests at different speeds and validate against the visually confirmation of back flow. Unfortunately the pipe that was used for surge identification was not necessarily sufficient rigid. In addition the length of the coupling tubing between the tube and the transmitter could have been shorter favor earlier detection of the surge. It was conducted machining of two additional pipes with greater diameter of 3mm and 6mm respectively. However, these were not tried out due to downtime on the impeller rig because of inducer implementation on the impeller. The author recommends that these tubes should be tested together with alternative methods to ensure exact identification of instability inception. The author believes that the FRAP system with built in detectors should be validated and tested for the purpose of identification of possibel surge precursors.

1
Recommendations for further work

References

1. Oljedirektoratet, *PETROLEUMSRESSURSENE PÅ NORSK KONTINENTALSOKKEL.* **2011**.
2. STATOIL, **2011**.
3. Bakken, T.G.G.a.L.E., *AERODYNAMIC INSTABILITY INVESTIGATION OF A CENTRIFUGAL COMPRESSOR EXPOSED TO WET GAS.* Department of Energy and Process Engineering, Norwegian University of Science and Technology (NTNU), **2010**: p. 12.
4. Hundseid, O., et al., *Wet Gas Performance of a Single Stage Centrifugal Compressor.* ASME Conference Proceedings, **2008**(43178): p. 661-670.
5. Wood, A.B., *A Textbook of Sound*, ed. G.B.a.S. Ltd **1944**, London.
6. Taitel Y., D.A.E., *A Model For Predicting Flow Regime Transitions in Horizontal and Near-Horizontal Gas-Liquid Flow.* AIChE Journal, **1976**. 22(1): p. 47-55.
7. Schubring, D. and T.A. Shedd, *Critical friction factor modeling of horizontal annular base film thickness.* International Journal of Multiphase Flow, **2009**. 35(4): p. 389-397.
8. Schlichting, H. and K. Gersten, *Boundary-layer theory*. 8th rev. and enl. ed **2000**, Berlin ; New York: Springer. xxiii, 799 p.
9. C.Xu., R.S.A., *The development of centrifugal compressor impeller.* Proceedings of ASME Turbo Expo **2008**:,.
10. Saravanamuttoo, H.I.H., *Gas turbine theory*. 6th ed**2009**, Harlow, England ; New York: Pearson Prentice Hall. xvi, 590 p.
11. Sørvik, L.A.Ø., *Aerodynamic instabilities in a centrifugal compressor*, in *Department of Energy and Process Engineering***2011**, NTNU: Trondheim, Norway.
12. Cumpsty, N.A., *Compressor aerodynamics***1989**, Harlow, Essex, England New York: Longman Scientific & Technical ; J. Wiley. 509 p.
13. Boyce, M.P., *Gas turbine engineering handbook*. 3rd ed**2006**, Boston: Gulf Professional Pub. xviii, 936 p.
14. Eckardt, D., *Detailed Flow Investigations Within a High-Speed Centrifugal Compressor Impeller.* Journal of Fluids Engineering, **1976**. 98(3): p. 390-399.
15. Robert C. Dean, J. and Y. Senoo, *Rotating Wakes in Vaneless Diffusers.* Journal of Basic Engineering, **1960**. 82(3): p. 563-570.
16. AhmadR.Ganji, A.J.W., *Introduction to Engineering Experiments*. Third Edition ed**2010**: Pearson.
17. Bryan, W.B., *An investigation of unsteady impeller-diffuser interactions in a centrifugal compressor*, in *Mechanical engineering* **1991**, Purdue University: United States Indiana. p. 192.
18. Cumpsty, N.A., *Compressor aerodynamics*. 2nd ed **2004**, Harlow, Essex, England New York: Krieger Pub Co.
19. O.Viseth, T., *Optimalisering av våtgass diffusor og spiralhus*, in *Institutt for Energi- og Prosessteknikk* **2012**, NTNU: Trondheim, Norway.
20. J.Irgens, S., *Optimailisering av løpehjul for våtgass*, in *Institutt for Energi- og Prosessteknikk* **2012**, NTNU: Trondheim, Norway.
21. Brenne, L., *Straight -Walled Diffuser Performance: An experimental investigaion of the diffuser pressure recovery with single- phase airflow and two phase air- water annular flow*, in *Department of Energy and Prosess Engineering***2004**, The Norwegian University of Technology
22. C.Pampreen, R., *Compressor Surge and Stall* **1993**.

23. Gravdahl, J.T. and O. Egeland, *Compressor surge and rotating stall : modelling and control*. Advances in industrial control **1999**, London ; New York: Springer. xix, 225 p.
24. Engeda, A., *The unsteady performance of a centrifugal compressor with different diffusers.* Proceedings of the Institution of Mechanical Engineers, Part A: Journal of Power and Energy, **2001**. 215(5): p. 585-599.
25. G Ferrara , L.a.L.B., *Rotating Stall in Centrifugal Compressor Vaneless Diffuser: Experimental Analysis of Geometrical Parameters Influence on Phenomenon Evolution.* International Journal of Rotating Machinery, **2004**. 10(6): p. 433–442.
26. Brillhart, J., *Rotating stall in centrifugal compressors.* **2009**.
27. Jansen, W., *Rotating stall in a radial vaneless diffuser.* ASME, **1964**.
28. Senoo, Y. and Y. Kinoshita, *Influence of Inlet Flow Conditions and Geometries of Centrifugal Vaneless Diffusers on Critical Flow Angle for Reverse Flow.* Journal of Fluids Engineering, 1977. **99**(1): p. 98-102.
29. Baines, A.W.a.N.C., *Design of Radial Turbomachines*, ed. P. Education**1990**, New York: Pearson Education Longman Scientific & Technical. 414.
30. Yasutoshi Senoo, Y.K., *Limits in rotating stall and stall in vaneless diffusers of centrifugal compressors*, in *ASME paper 78-GT- 19***1978**.
31. Abdelhamid, A.N., *Analysis of rotating stall in vaneless diffusers of centrifugal compressors.* ASME paper 80-GT- 184, **1980**.
32. Frigne, P., Van Den Braembusche,R, *Distinction between different types of impeller and diffuser rotating stall in a centrifugal compressor with vaneless diffuser.* ASME paper 83-GT-61, **1983**.
33. Jager, B.d., *Rotating stall and surge control: A survey.* Proceedings of the 34th Conference on Decision & Control, **1995**.
34. Greitzer, E.M., *Surge and Rotating Stall in Axial Flow Compressors---Part I: Theoretical Compression System Model.* Journal of Engineering for Power, **1976**. 98(2): p. 190-198.
35. Fink, D.A., N.A. Cumpsty, and E.M. Greitzer, *Surge Dynamics in a Free-Spool Centrifugal Compressor System.* Journal of Turbomachinery, **1992**. 114(2): p. 321-332.
36. Hartel, C. and P. Pfeiffer, *Model Analysis of High-Fogging Effects on the Work of Compression.* ASME Conference Proceedings,. **2003**(36851): p. 689-698.
37. Wang, Y., et al., *Analysis of Effects on Wet Compression on Surge Margin of a Small Gas Turbine.* ASME Conference Proceedings,. **2002**(36177): p. 247-252.
38. Day, I., J. Williams, and C. Freeman, *Rain Ingestion in Axial Flow Compressors at Part Speed.* ASME Conference Proceedings,. **2005**(47306): p. 223-235.
39. Abdelwahab, A., *An Investigation of the Use of Wet Compression in Industrial Centrifugal Compressors.* ASME Conference Proceedings,. **2006**(42398): p. 741-750.
40. L. Brenne, T.B., Josè l.Gilarranz, Jay M. Koch and Harry Miller, *Performance evaluation of a centrifugal compressor operating under wet gas conditions*, in *In Proceedings of the Thirty-Fourth Turbomachinery Symposium***2005**: Houston, Texas, USA. p. 10.
41. Gruner, T.G., et al., *An Experimental Investigation of Airfoil Performance in Wet Gas Flow.* ASME Conference Proceedings, 2008. **2008**(43178): p. 575-584.
42. Fabbrizzi, M., et al., *An Experimental Investigation of a Single Stage Wet Gas Centrifugal Compressor.* ASME Conference Proceedings,. **2009**(48869): p. 443-453.
43. Bigi, D.R.L.P.M.W.M.B.a.M., *Mechanical Performance of a Two Stage Centrifugal Compressor under Wet Gas Conditions.* Proceedings of the Fortieth Turbomachinery Symposium September 12-15, 2011, Houston, Texas, 2011.

44. Bakken, T.G.G.a.L.E. *INSTABILITY CHARACTERISTIC OF A SINGLE-STAGE CENTRIFFUGAL COMPRESSOR EXPOSED TO DRY AND WET GAS*. in *Proceedings of ASME Turbo Expo **2012**: Power Land, Sea and Air June 11-15* 2012. Copenhagen , Denmark.
45. Crane, R.I.M., M. J, *Interpretation of pitot pressure in compressible two-phase flow.* J. Mech. Engng Sci., **1972**. 14: p. 128-133.
46. Grüner.T., a.B., L.E.,, *Instability Characteristic of a Single-Stage Centrifugal Compressor Exposed to Dry and Wet gas.* ASME Turbo Expo **2012**: Power for Land, Sea And Air June 11-15 Copenhagen, Denmark, 2012(GT2012-69473).
47. Grüner, T.G., *Wet Gas Compression: Experimental investigation of the aerodynamics within a centrifugal compressor exposed for wet gas*, in *Faculty of Engineering Science and Process Engineering Department of Energy and Process Engineering***2012**, NTNU Norwegian University of Science and Technology: Trondheim
48. C. Bertani, M.D.S., M. Malandrone, G. Monni and B. Panella, *State-of-Art and selection of techniques in multiphase flow measurement*, l.E.e.l.S.E.S. Agenzia Nazionale per le Nuove Tecnologie, Editor, POLITECNICO' DI TORINO DIPARTIMENTO DI ENERGETICA: Torino, Luglio **2010**.
49. Falcone, G.H., G.F and Alimonti, C, *Multiphase flow metering :principles and applications*. Developments in Petroleum science, ed. Elsevier. Vol. 54. **2010**, Great Britain: Elsevier. 329.
50. Ziegler, K.U., H.E. Gallus, and R. Niehuis, *A Study on Impeller-Diffuser Interaction--- Part I: Influence on the Performance.* Journal of Turbomachinery, **2003**. 125(1): p. 173-182.
51. Ziegler, K.U., H.E. Gallus, and R. Niehuis, *A Study on Impeller-Diffuser Interaction--- Part II: Detailed Flow Analysis.* Journal of Turbomachinery, 2003. 125(1): p. 183-192.
52. Gill, L.E., *Sampling probe studies of the gas core in annular two-phase flow.* Chem. Eng. Sci, **1963**. 18(8): p. 525–535.
53. White, A.J., Young, J. B. & Walters, *Experimental validation of condensing flow theory for a stationary cascade of steam turbine blades.* Phil. Trans. R. Soc. Lond, **1996**. **A** 354: p. 354.
54. Kupferschmied, P., et al., *On the Development and Application of the Fast-Response Aerodynamic Probe System in Turbomachines---Part 1: The Measurement System.* Journal of Turbomachinery, **2000**. 122(3): p. 505-516.
55. Roduner, C., et al., *On the Development and Application of the Fast-Response Aerodynamic Probe System in Turbomachines---Part 2: Flow, Surge, and Stall in a Centrifugal Compressor.* Journal of Turbomachinery, **2000**. 122(3): p. 517-526.
56. Schlienger, J., et al., *Effects of Labyrinth Seal Variation on Multistage Axial Turbine Flow.* ASME Conference Proceedings,. **2003**(36894): p. 173-185.
57. Porreca, L., Hollenstein, M., Kalfas, A. I., and Abhari R. S.,, *Turbulence Measurements and Analysis in a Multistage Axial Turbine.* Journal of Propulsion and Power, 2007. **23**(1): p. 227-234.
58. Christian, L., *High Temperature Fast Response Aerodynamic Probe*, **2010**, ETH ZURICH: Zurich.
59. Schleer, M., et al., *Investigation of an Inversely Designed Centrifugal Compressor Stage---Part II: Experimental Investigations.* Journal of Turbomachinery, **2004**. 126(1): p. 82-90.

60. Zangeneh, M., et al., *Investigation of an Inversely Designed Centrifugal Compressor Stage---Part I: Design and Numerical Verification.* Journal of Turbomachinery, **2004**. 126(1): p. 73-81.
61. Hazby, H.R., L. Xu, and M. Schleer, *Study of the Flow in a Vaneless Diffuser at Part Speed Operating Conditions.* ASME Conference Proceedings,. **2010**(44021): p. 1913-1923.
62. Reitan, D.R., *Validation of Wet Gas Performance*, in *Department of Energy and Process Engineering***2012**, NTNU: Trondheim, Norway.
63. Mele, E., *Wet Gas Compressor Performance*, in *Department of Energy and Process Engineering***2012**, NTNU: Trondheim, Norway.

Appendix A: Supplementary experimental graphs and figures

Appendix A.1 Frequency spectrums at 7500 rpm for wet gas

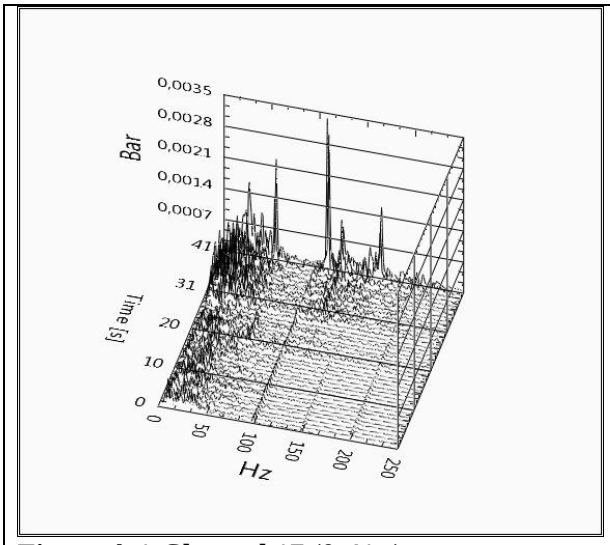

Figure A 1:Channel 17 (0-41 s)

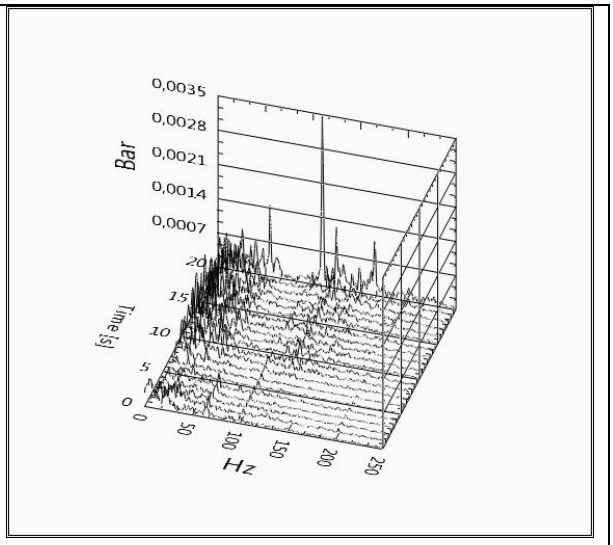

Figure A 2: Channel 17 (20-40 s)

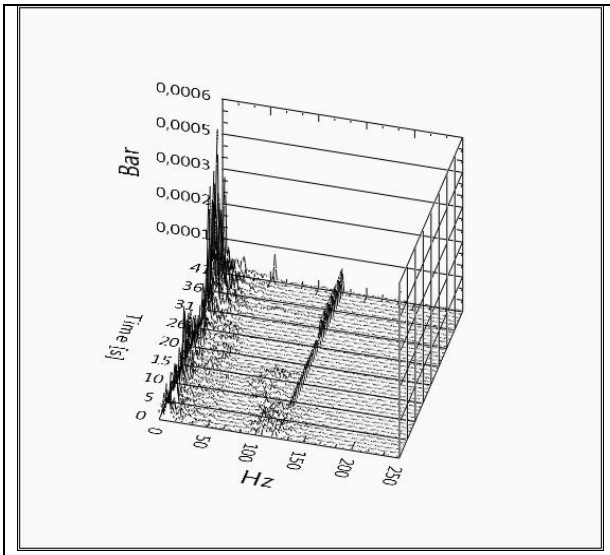

Figure A 3: Channel 22 (0-41 s)

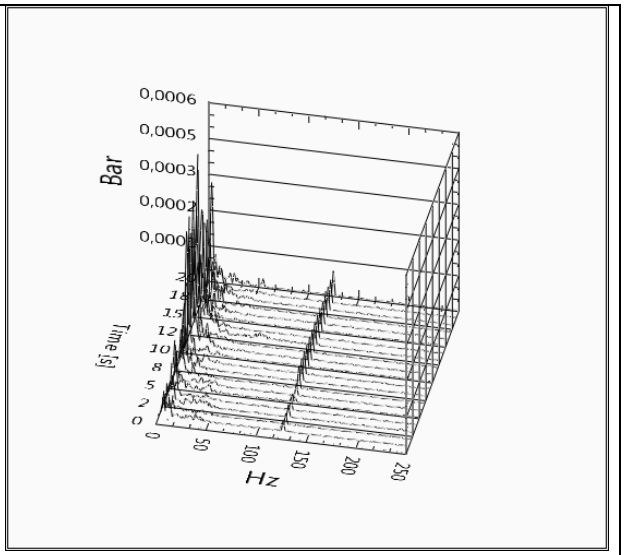

Figure A 4: Channel 22 (20-41 s)

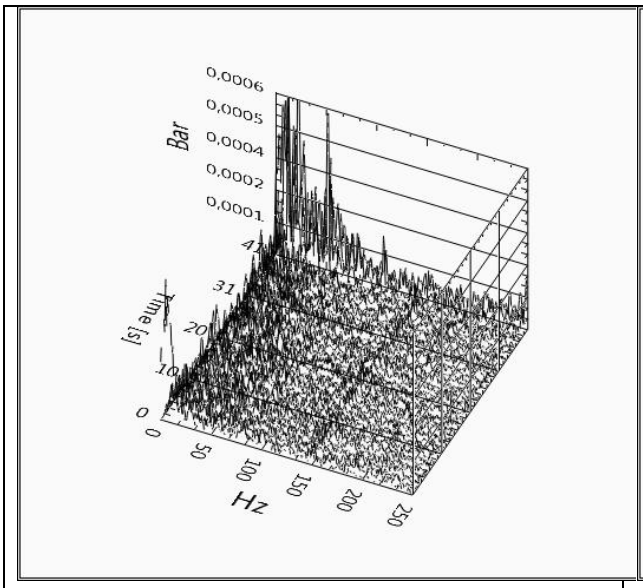

Figure A 5: Channel 27 (0-41 s)

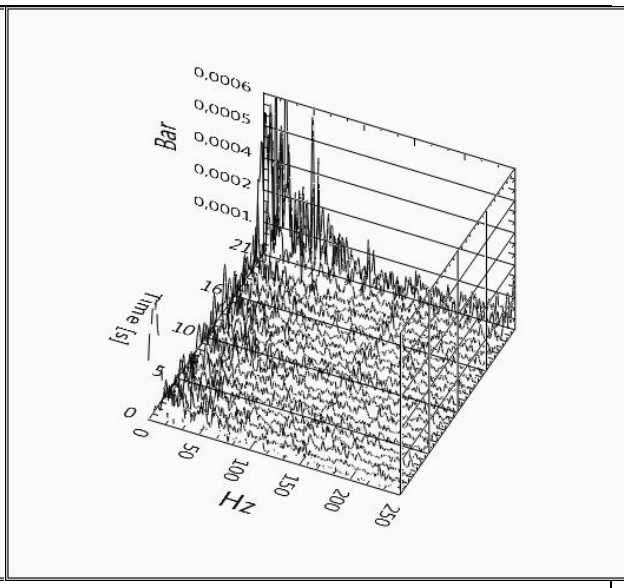

Figure A 6 Channel 27 (20-41 s)

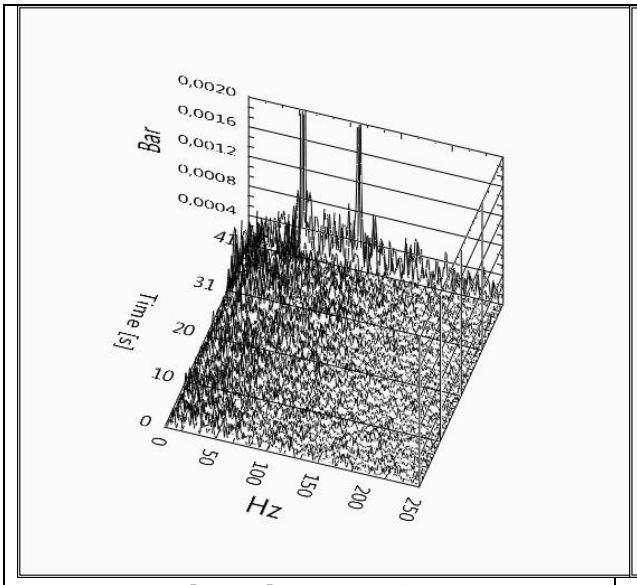

Figure A 7: Channel 20 (0-41 s)

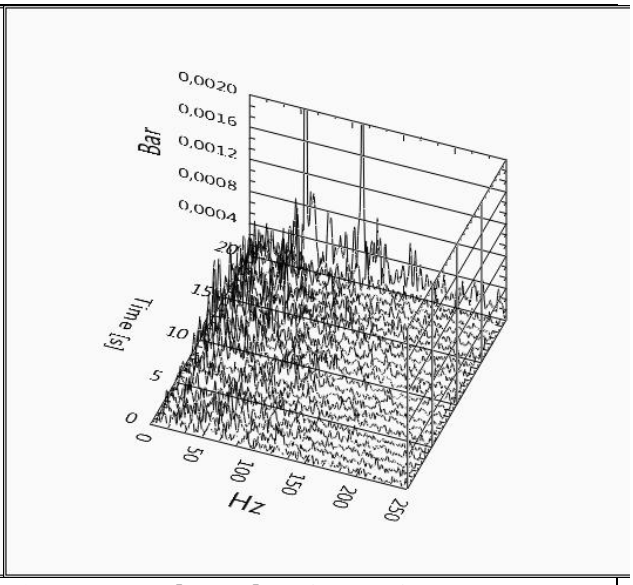

Figure A 8: Channel 20 (20-41 s)

Appendix A.2 Identification of Surge

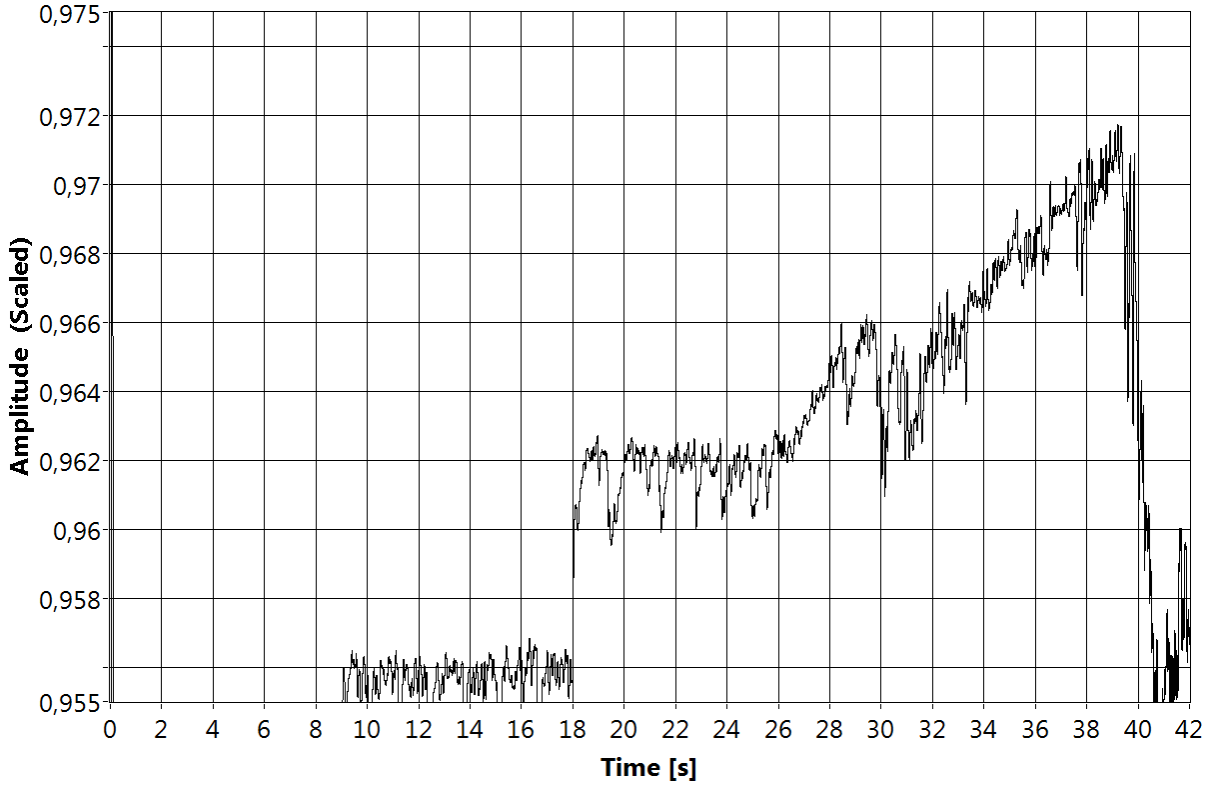

Figure A 9

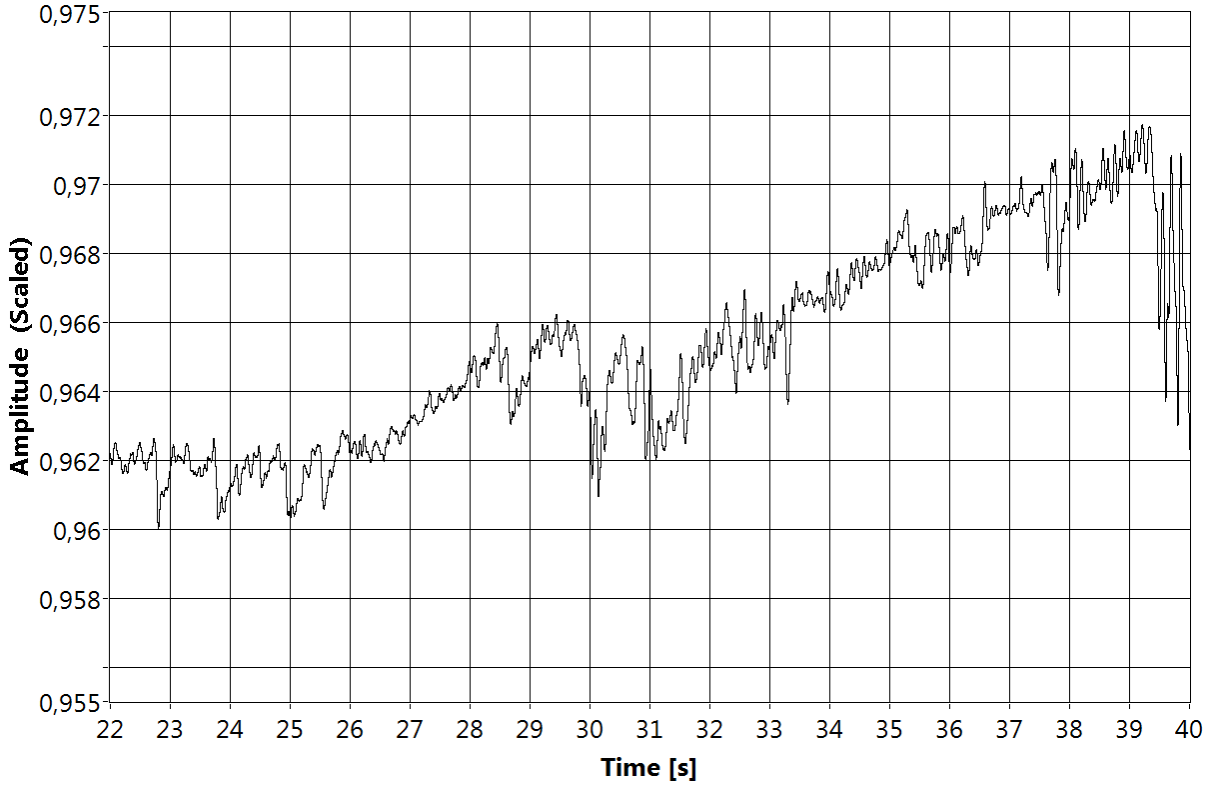

Figure A 10

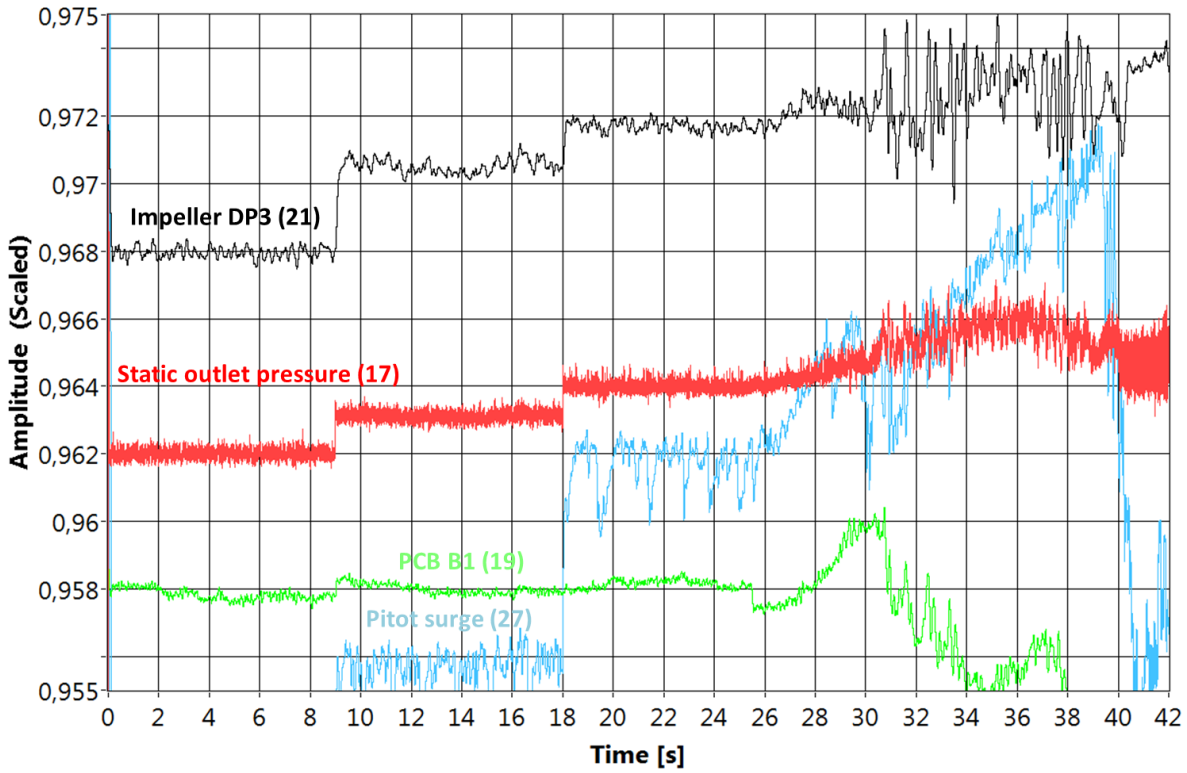

Figure A 11:

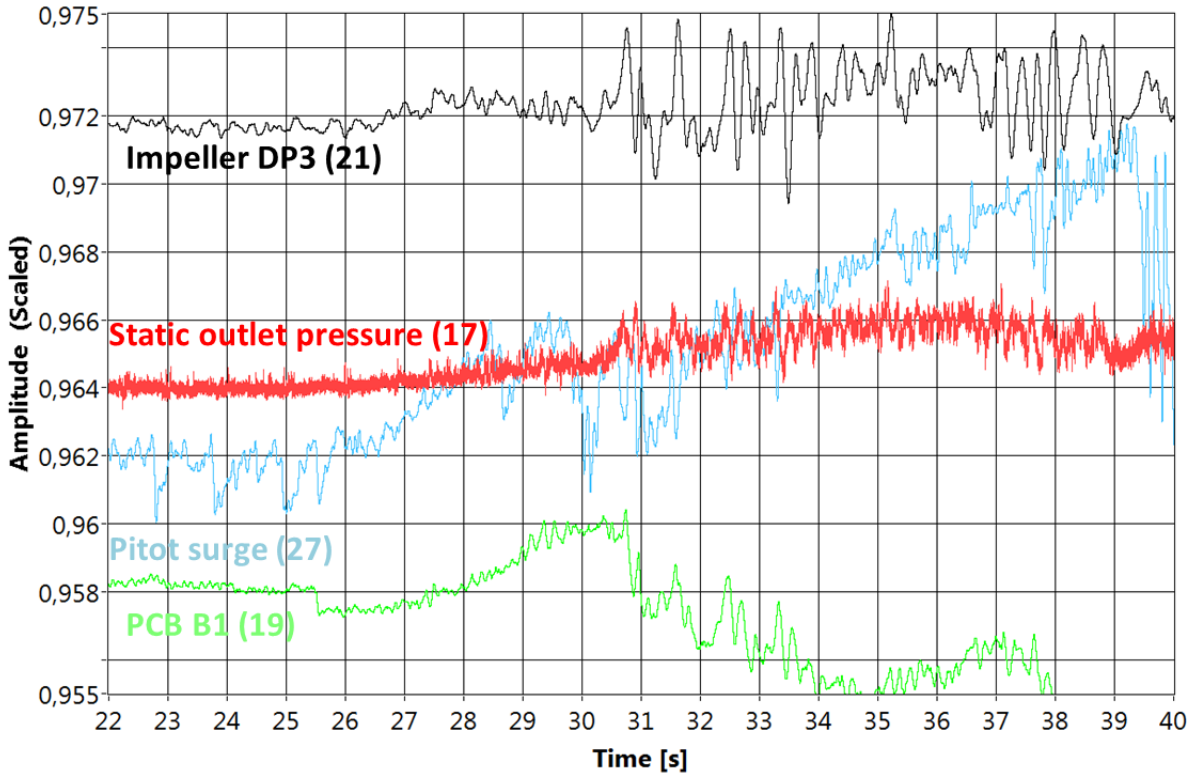

Figure A 12:

Appendix A.3 Visual Surge detection

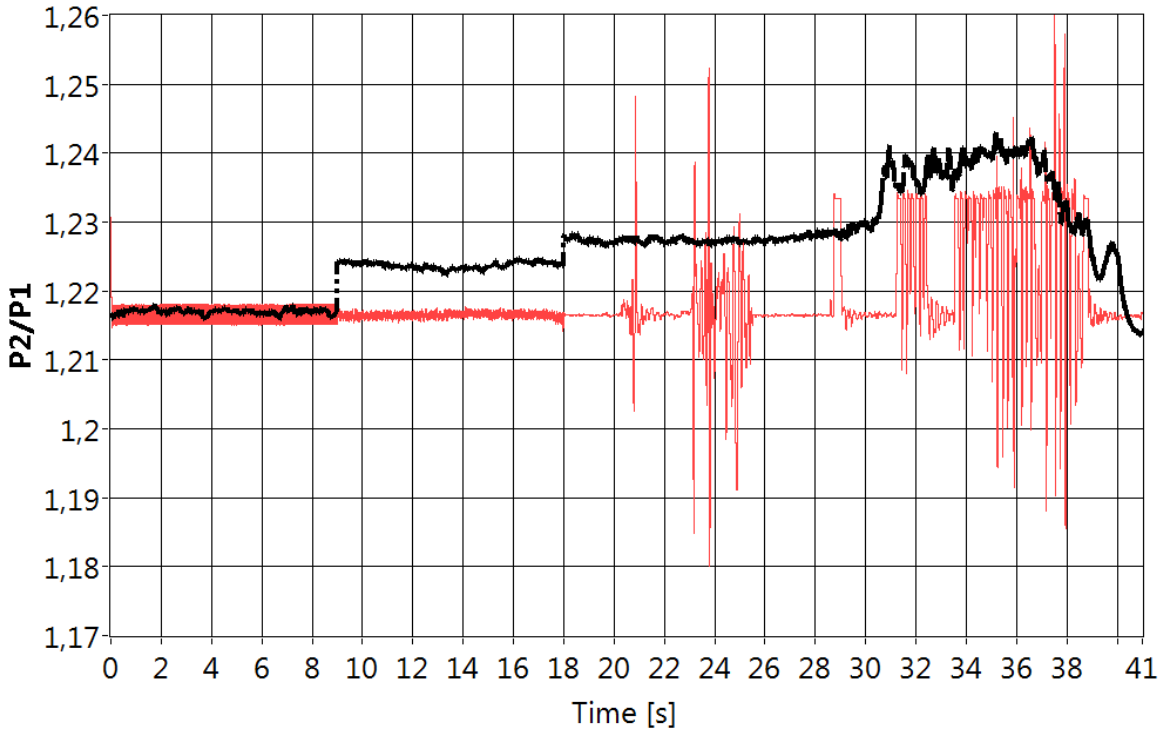

Figure A 13: Visual observation of wet gas surge with respect to pressure ratio

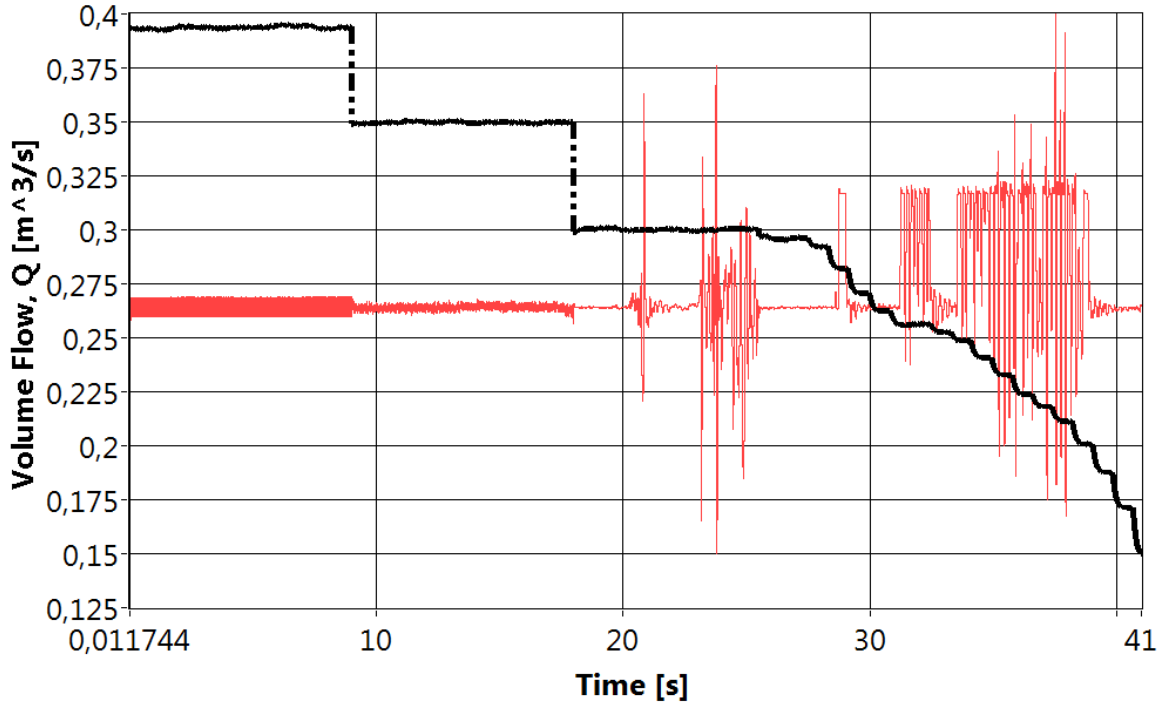

Figure A 14: Visual observation of wet gas surge with respect to volume flow

Appendix B: Technical drawings of the impeller rig

Appendix B includes technical drawings made with the CAD software Autodesk Inventor Professional describing the installation of pitot tubes inside the NTNU impeller rig. The impeller is unfortunately not included in the drawing because the impeller contains confidential geometries.

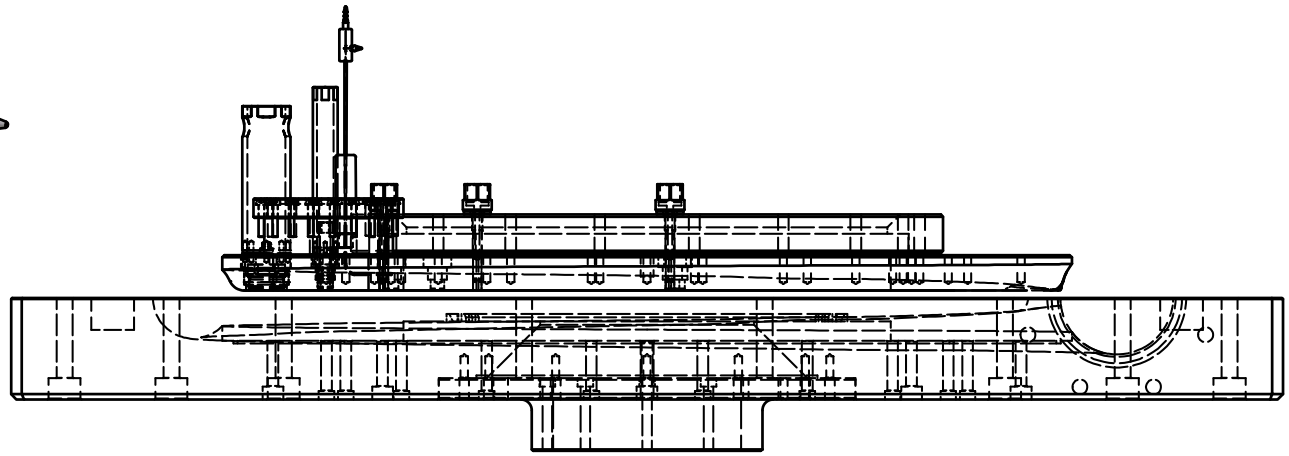

A (1 : 3)

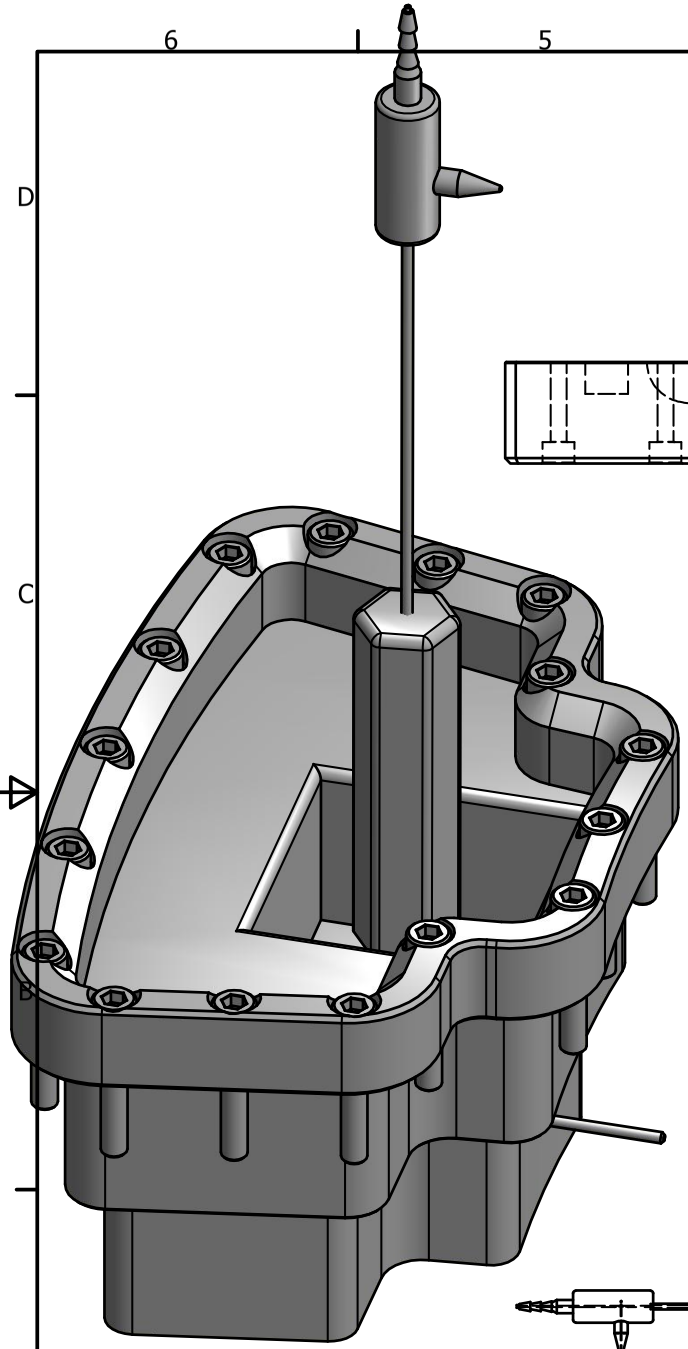

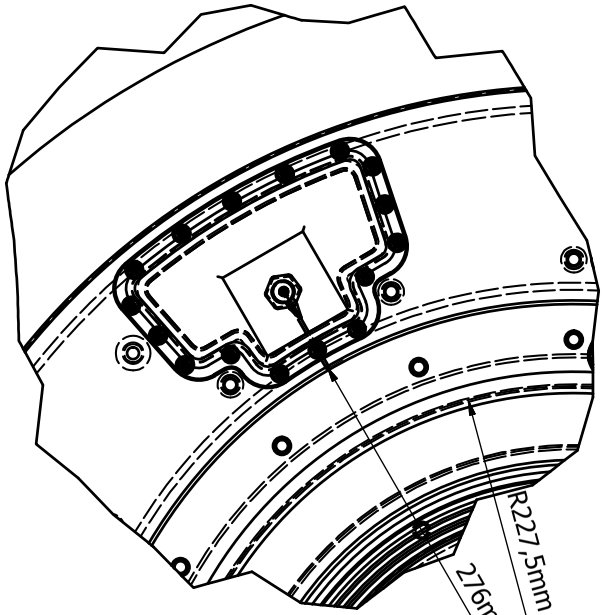

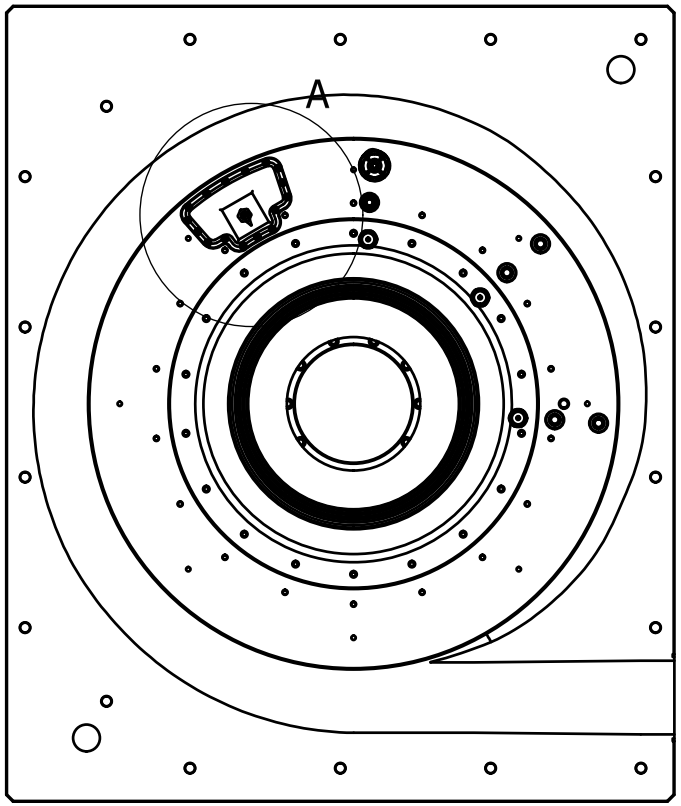

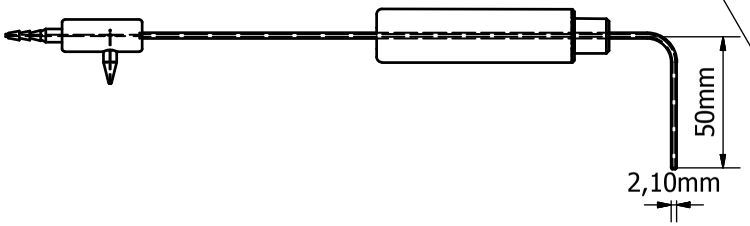

Designed by	Checked by	Approved by	Date		Date	
larsandr					29.03.2012	

lars28marsmhull		Edition	Sheet 1 / 1

A (1 : 2)

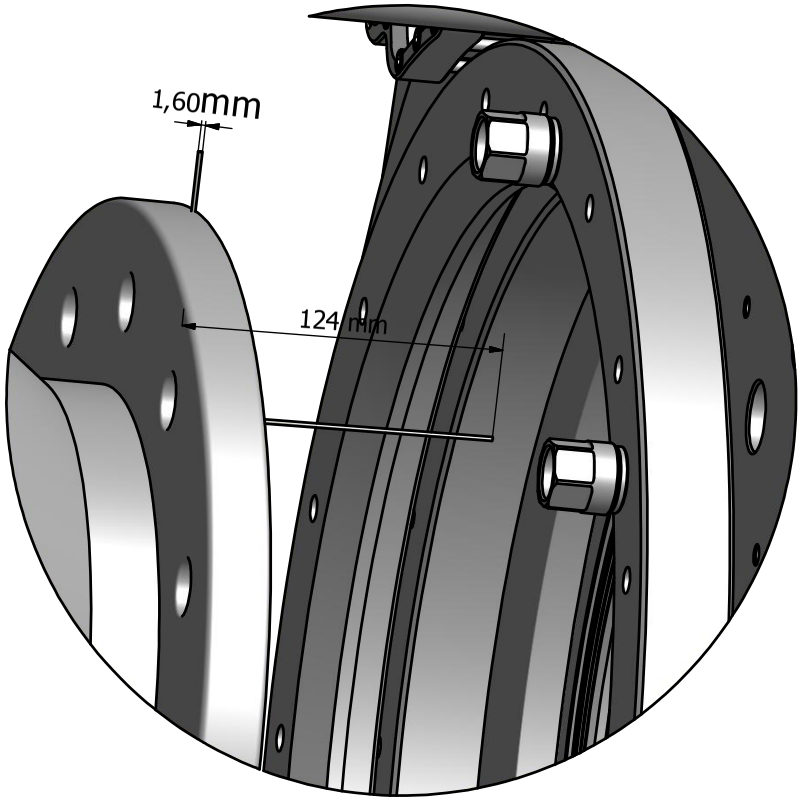

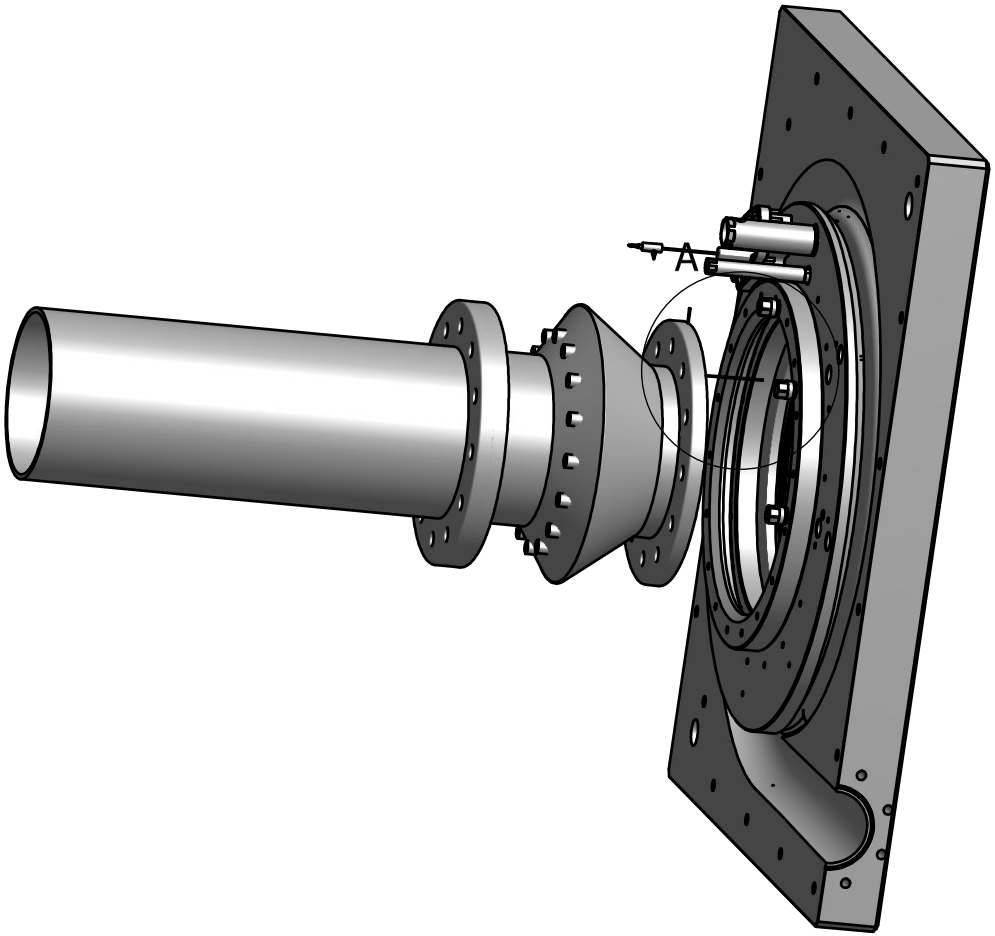

Designed by	Checked by	Approved by	Date		Date	
larsandr					30.05.2012	

		Edition	Sheet
			1 / 1

Appendix C: Instrumentation data sheets

Appendix C is intended to give the reader an overview of the different measuring channels that has been used for the execution of the tests. Data sheets of the main instrumentations from the channel list below are included in Appendix C.2

Table C-1: NTNU Impeller channel list

Channel	Description	Unit
0	5 Volts signal generator	bar
1	PCB B2	bar
5	P 3_1 dp volume flow	mbar
6	P 10_1 Pressure inlet p1	bar
7	P 11_1 Compressor dp	bar
8	T 5 1 Inlet Temperature T1	C
10	5 Volts signal generator	Nm
12	Turbin Flow meter	m3/s
13	P 3 3 Turbine pressure	bar
16	P 3 4 static inlet pressure	bar
17	P 3 5 static outlet pressure	bar
18	PCB 32822 A	bar
19	PCB 32845 B	bar
20	PCB 32844 C	bar
21	dp1 (Impeller)	bar
22	dp2 (Diffuser)	bar
23	dp3 (Volute)	bar
24	DP4 (Pitot diffuser pitot tube)	mbar
27	P12-2	bar

DIFFERENTIAL PRESSURE TRANSMITTER PRE-28

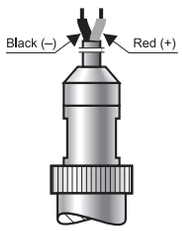

PK type
Electrical cable connection
Degree of protection **IP-67**
The cable electrical connection, contact with the atmosphere through the capillary inside the cable. The cable length 3m (other cable lengths available, if required)

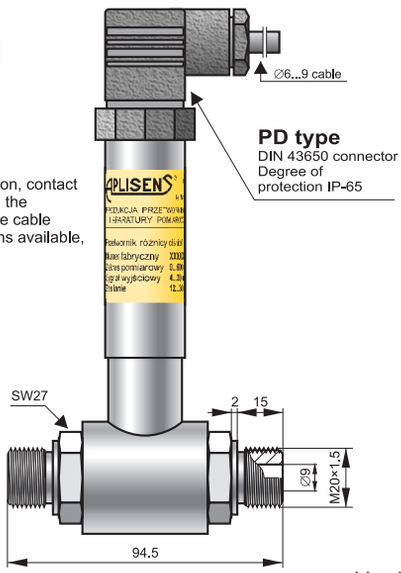

PD type
DIN 43650 connector
Degree of protection IP-65

Transmitter PRE-28
Process connection **P type**
Static pressure limit 40 bar

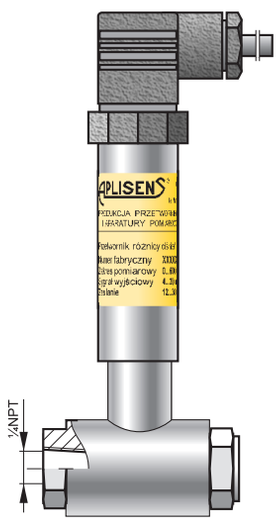

Transmitter **PRE-28**
Version with **PN type** process connection.
Static pressure limit 40 bar

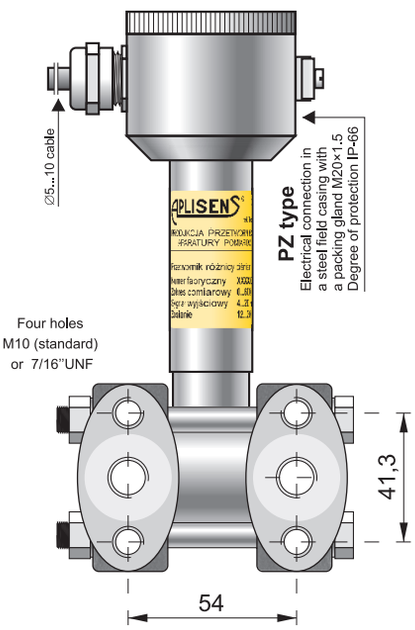

PZ type
Electrical connection in a steel field casing with a packing gland M20×1.5
Degree of protection IP-66

Transmitter PRE-28 – version with **type C** process connection to be mounted together with a valve manifold. Static pressure limit 250 or 320 bar

- ✓ **Overloads up to 420 bar total static pressure**
- ✓ **Accuracy 0.25%**
- ✓ **Any range from 0...16 mbar up to 0...25 bar**
- ✓ **ATEX Intrinsic safety (Gas and Dust)**
- ✓ **Marine certificate DNV**

Application

The PRE-28 transmitter is applicable to the measurement of dofferential pressure of gases, vapours and liquids.

Construction

The active element is a piezoresistance silicon sensor separated from the medium by separating diaphragm and a specially selected type of manometric fluid. The special desing of theactive sensing element ensures withstanding the pressure surges and overloads of up to 320bar. The electronics is placed in a casing with a degree of protection IP65, IP67, depending on the type of electrical connection applied.

Calibration

Potentiometers can be used to shift the zero position and the range by up to 10%, without altering the settings.

Installation

The transmitter with P type process connection is not heavy, so it can be installed directly onto impulse lines. For fitting in any desired position on a ∅25 pipe the Aplisens mounting bracket (Fi25 mounting bracket, page 65) is recommended.

The version with C type process connection can be fitted directly to a 3- or 5-valve manifold. The factory-mounted transmitters with VM type valve manifold (page 62) are recommended. A transmitter without a valve manifold can be fitted in any position on a 2" pipe or on a wall using the C-2" mounting bracket (page 65).

When the special process connections are required for the measurement of levels and pressures (e.g. at food and chemical industries), the transmitter is provided with an Aplisens diaphragm seal. The differential pressure transmitters with diaphragm seals are described in detail in the further part of the catalogue.

Technical data

Materials: Wetted parts:
- type P process conn. 316Lss
- type C process conn. 316ss
- Diaphragm: Hastelloy C 276
- Casing: 304ss
- Option: 316ss

Hysteresis, repeatability	0.05%
Thermal compensation range:	0÷ 70 C
Operating temperature range:	-25÷80 C
Medium temperature range:	-25÷120 C (direct measurement) Over 120C – measurement with the use of impulse line or diaphragm seals

CAUTION: the medium must not be allowed to freeze in the impulse line or close to the process connection of the transmitter.

Technical data

Any measuring range 0...16 mbar ÷ 0...25 bar

	Measuring Range			
	100 mbar	**1 bar**	**2 bar**	**25 bar**
Overpressure Limit Static Pressure Limit (repeated, without hysteresis)	250 bar (option 420 bar) (40 bar for P type process connection)			
Accuracy	0.4%	0.25%		
Long term stability	0.2% / year	0.1% / year		
Thermal error	Typically 0.3% / 10°C max 0.4% / 10°C	Typically 0.2% / 10°C max 0.3% / 10°C		
Zero shift error for static pressure*	0.1% / 10 bar			

* Zeroing the transmitter in conditions of static pressure can eliminate this error.

Output signal 4...20 mA, two wire transmission
0…10 V, three wire transmission

Power supply 10.5...36 V DC (EEx 12...28 V)
– two wire transmission
15…30 V DC – three wire transmission

Error due to supply voltage changes 0.005% (FSO) / V

Loadresistance (for current output) $R[\Omega] \leq \frac{U_{sup}[V] - 10.5\,V}{0.02\,A}$ 0.85

Loadresistance (for supply output) $R \geq 5\,k\Omega$

Electrical diagrams

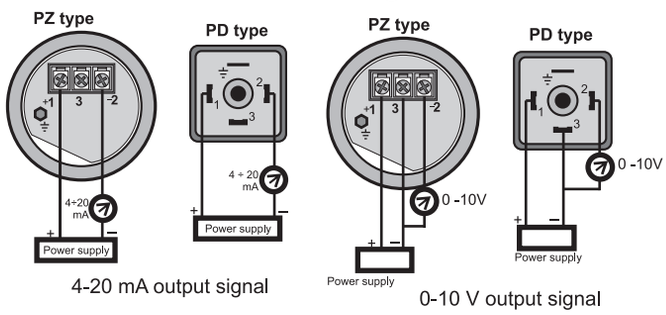

Ordering procedure

Model	Code	Description
PRE-28		Differential pressure transmitter.
Versions * *) more than one option is available	/EExia…… /TIen…… /MR……	Ex II 1/2G Ga/Gb Ex ia IIC T4/T5/T6, I M1 Ex ia I, II 1D Ex ia D20 T105C (only for transmitters with 4..20mA output) version for oxygen service (sensor filled with Fluorolube fluid). Marine Certificate DNV
Measuring range	/.....÷..... [required units]	Measuring range in relation to 4mA and 20mA (or 0 and 10V) output. Units: bar, MPa, kPa, etc.
⇒ Output signal	*(without marking)*..... /0...10V..... /(other).....	4...20mA (power supply 10,5÷36VDC) 0..10V DC (power supply 15÷30VDC) other output signal and power supply (e.g for NE or NN version)
⇒ Casing, Electrical connection,	/PD…… PZ…… PZ/316…… PK ..... (if other length of cable is required, please specify it /K=....[m])	Housing IP65 with DIN43650 connector PG-11 packing gland. 304SS housing, Ip66, packing gland M20x1,5. 316SS housing, Ip66, packing gland M20x1,5. Housing IP67 with thread M12x1 and connector 304SS housing, IP67, cable electrical connection, 3m of cable
⇒ Process connections	/C…… /P..... /PN..... /code of diaphragm seal.....	Thread 1/4NPT F on the cover flanges, diaphragms material Hastelloy C 276, cover flanges material SS316L. Allows mounting with a valve manifold. Thread M20x1,5 (male) with Ø9hole, diaphragms material Hastelloy C 276, wetted parts SS316L Thread 1/4"NPT (female), diaphragms material Hastelloy C 276, wetted parts SS316L Diaphragm seal (see chapter of diaphragm seals) mounted on Hi side of transmitter, Lo side 1/4NPT Female
⇒ Accessories	/C-2"..... /FI25..... /RedSpaw P…… /RedSpaw C…… /Red d/P ½''……	Mounting bracket for 2" pipe (to C process conn.), mat. zinced steel Mounting bracket for 2" pipe (to P process conn.), mat. stainless steel Connector to weld impulse pipes dia. 12 and 14 mm, material 15HM(SO) or SS 316(S) . Only process connection P type, Connector to weld impulse pipes dia. 12 and 14 mm, material 15HM. Only process connection C type. Adapter for differential pressure transmitters with C type process connection, output thread 1/2NPT F. Material 316 LSS
Other specification	/.....	Description of required parameters
The most typical specification is marked by "⇒" mark.		

Example: Differential pressure transmitter, version EExia, measuring range 0..160mbar, output signal 4..20mA, C type process connection, electrical process connection with DIN43650 connector

PRE-28/EExia/0÷160mbar/PD/C

Model Number	ICP® PRESSURE SENSOR SPECIFICATIONS	Revision: B
102A02		ECN #: 14825

Performance	ENGLISH	SI	
Measurement Range (for ± 5 V output)	100 psi	690 kPa	
Useful Overrange (for ± 10V output)	200 psi	1379 kPa	[1]
Sensitivity (±10 mV/psi)	50 mV/psi	7.3 mV/kPa	
Maximum Pressure	1 kpsi	6900 kPa	
Resolution	2 mpsi	0.014 kPa	
Resonant Frequency	≥250 kHz	≥ 250 kHz	
Rise Time	≤2 μ sec	≤2 μ sec	
Low Frequency Response (-5 %)	0.5 Hz	0.5 Hz	
Non-Linearity	≤1.0 % FS	≤1.0 % FS	[2]
Environmental			
Acceleration Sensitivity	≤0.002 psi/g	≤ 0.0014 kPa/(m/s²)	
Temperature Range (Operating)	-100 to +275 °F	-73 to +135 °C	
Temperature Coefficient of Sensitivity	≤0.03 %/°F	≤ 0.05 %/°C	
Maximum Flash Tempurature	3000 °F	5400 °C	
Maximum Shock	20000 g pk	196000 m/s² pk	
Electrical			
Output Polarity (Positive Pressure)	Positive	Positive	
Discharge Time Constant (at room temp)	≥1 sec	≥1 sec	
Excitation Voltage	20 to 30 VDC	20 to 30 VDC	
Constant Current Excitation	2 to 20 mA	2 to 20 mA	
Output Impedance	<100 ohms	<100 ohms	
Output Bias Voltage	8 to 14 VDC	8 to 14 VDC	
Electrical Isolation	100000000 ohms	100000000 ohms	
Physical			
Sensing Geometry	Compression	Compression	
Sensing Element	Quartz	Quartz	
Housing Material	Stainless Steel	Stainless Steel	
Diaphragm	Invar	Invar	
Sealing	Welded Hermetic	Welded Hermetic	
Electrical Connector	10-32 Coaxial Jack	10-32 Coaxial Jack	
Weight	0.39 oz	11.0 gm	

CE [3]

All specifications are at room temperature unless otherwise specified.
In the interest of constant product improvement, we reserve the right to change specifications without notice.

ICP® is a registered trademark of PCB Group, Inc.

OPTIONAL VERSIONS

Optional versions have identical specifications and accessories as listed for the standard model except where noted below. More than one option may be used.

H - Hermetic Seal

Sealing	Welded Hermetic	Welded Hermetic

M - Metric Mount
Supplied Accessory : Model 065A42 Floating clamp nut and thread seal, M10 x 1.0 thd. (1) replaces Model 065B01

N - Negative Output Polarity

S - Stainless Steel Diaphragm

Diaphragm	316L Stainless Steel	316L Stainless Steel

NOTES:

[1] For +10 volt output, minimum 24 VDC supply voltage required. Negative 10 volt output may be limited by output bias.
[2] Zero-based, least-squares, straight line method.
[3] See PCB Declaration of Conformance PS023 for details.

SUPPLIED ACCESSORIES:

Model 065B01 Floating clamp nut and thread seal 3/8-24 thd (1)

Entered: DBJ	Engineer: MEM	Sales: JMM	Approved: GKH	Spec Number:
Date: 4/9/02	Date: 4/9/02	Date: 4/9/02	Date: 4/9/02	6371

PCB PIEZOTRONICS
PRESSURE DIVISION
3425 Walden Avenue, Depew, NY 14043

Phone: 716-684-0001
Fax: 716-686-9129
E-Mail: pressure@pcb.com

APPLICATION		
NEXT ASS'Y	USED ON	VAR

REVISIONS				
REV	DESCRIPTION	ECN	DATE	APP'D
A	UPDATE DRAWING	15123	3/29/02	

8495

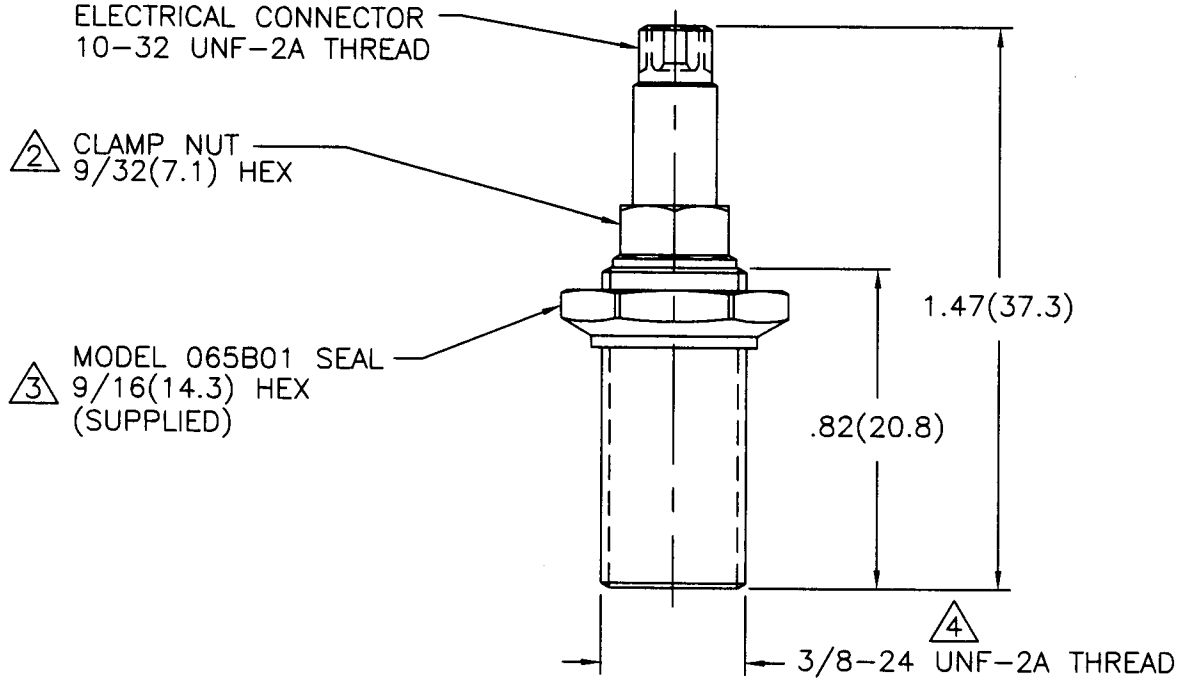

MOUNTING HOLE PREPARATION:

ø.332 THRU
TAP 3/8-24 UNF-2B
THRU

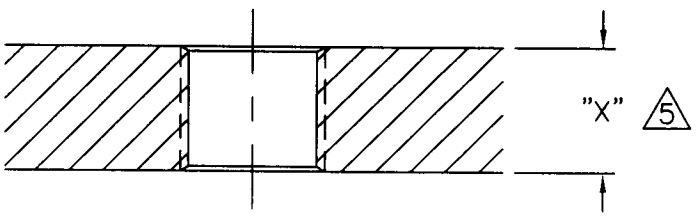

5 LENGTH TO SUIT USER REQUIREMENTS.

4 COAT THREADS OF SENSOR WITH TEFLON THREAD SEALANT IF REQUIRED. (FOR VACUUM TIGHT SEAL ONLY)

3 ADJUST MODEL 065B01 SEAL TO APPROXIMATE POSITION REQUIRED.

2 USE 9/32(7.1) NUT DRIVER TO TURN SENSOR INTO TAPPED HOLE. NORMAL LOCATION OF DIAPHRAGM FACE IS FLUSH WITH INSIDE SURFACE. RECESS .010(0.25) FOR ABLATIVE COATING IF DESIRED. WHILE HOLDING SENSOR WITH NUT DRIVER, TIGHTEN SEAL TO OBTAIN PRESSURE-TIGHT SEAL AND LOCK SENSOR IN PLACE. RECOMMENDED MOUNTING TORQUE 20-25 INCH POUNDS(226-282 NEWTON CENTIMETERS).

1.) THIS SENSOR IS A SEALED ASSEMBLY AND MUST BE RETURNED TO THE FACTORY SHOULD SERVICE BECOME NECESSARY.

UNLESS SPECIFIED TOLERANCES	
DIMENSIONS IN INCHES DECIMALS XX ±.01 XXX ±.005 ANGLES ±2 DEGREES	DIMENSIONS IN MILLIMETERS (IN PARENTHESIS) DECIMALS XX ±0.3 XXX ±0.13 ANGLES ±2 DEGREES
FILLETS AND RADII .003 - .005	FILLETS AND RADII (0.07 - 0.13)
DD011 REV. B 03/13/98	

DRAWN	DBJ	3/29/02	MFG	JMS	4/8/02
CHK'D	DM	4/4/02	ENGR	WSH	4/10/02
APP'D	WEM	4/8/02	DM	DPC	4/8/02

TITLE: INSTALLATION DRAWING
MODEL 101A & 102A02, A07, A09, A12
PRESSURE SENSORS

PCB PIEZOTRONICS
3425 WALDEN AVE. DEPEW, NY 14043
(716) 684-0001 EMAIL: SALES@PCB.COM

CODE IDENT. NO.	DWG. NO.
52681	8495
SCALE: 2X	SHEET 1 OF 1

GE
Sensing & Inspection Technologies

UNIK 5000

Pressure Sensing Platform

The UNIK 5000 is a high performance configurable solution to pressure measurement. The use of Druck silicon technology and analogue circuitry enables best in class performance for stability, low power and frequency response. The use of modular design and lean manufacturing techniques allow users to design the product required to their unique application requirements and for them to be delivered inside standard product lead times.

Features

- Ranges from 70 mbar (1.5 psi) to 700 bar (10,000 psi)
- Accuracy to ±0.04% Full Scale (FS) Best Straight Line (BSL)
- Stainless Steel construction
- Hazardous Area certifications (Pending)
- mV, mA, voltage and configurable voltage outputs.
- Multiple electrical connector options
- Multiple pressure connector options
- Operating temperature ranges to –55 to 125 °C
- Frequency response to 5 kHz
- High reliability
- High stability
- High over pressure capability

5000 Specifications

Measurement

Operating Pressure Ranges

Gauge ranges

Any zero based range between 70 mbar and 70 bar (1.5 to 1,000 psi) (values in psi are approximate)

Sealed Gauge Ranges

Any zero based range between 10 and 700 bar (145 to 10,000 psi)

Absolute Ranges

Any zero based range between 350 mbar and 700 bar (6 to 10,000 psi)

Differential Ranges

Wet/Dry

Uni-directional or bi-directional 70 mbar to 35 bar (1.5 to 500 psi)

Wet/Wet

Uni-directional or bi-directional 350 mbar to 35 bar (6 to 500 psi)

Line pressure: 70 bar max (1000 psi)

Barometric Ranges

Barometric ranges are available with a minimum span of 350 mbar (6 psi)

Non Zero Based Ranges

Non zero based ranges are available. Please contact GE Sensing to discuss your requirements

Over Pressure

- 10 × FS for ranges up to 150 mbar (2 psi)
- 6 × FS for ranges up to 700 mbar (10 psi)
- 2 × FS for barometric ranges
- 4 × FS for all other ranges (up to 200 bar for ranges ≤70 bar and up to 1200 bar for ranges >70 bar)

For differential versions the negative side must not exceed the positive side by more than:

- 6 × FS for ranges up to 150 mbar (2 psi)
- 4 × FS for ranges up to 700 mbar (10 psi)
- 2 × FS for all other ranges up to a maximum of 15 bar (200 psi)

Containment Pressure

Gauge, Sealed Gauge, Absolute and Differential (+ve port):

- 6 × FS for ranges up to 70 bar (1000 psi) (200 bar (2,900 psi) maximum)
- 6 × FS for ranges above 70 bar (1000 psi) (1200 bar (17,000 psi) maximum)

Differential (-ve port) must not exceed positive port by more than 4 × FS (15 bar (200 psi) maximum)

Supply and Outputs

Electronics Option	Description	Supply voltage (V)	Output
0	mV Passive	2.5 to 12	10 mV/V^
1	mV Linearised	7 to 12	10 mV/V^
2	mA	7 to 32	4-20 mA
3	0 to 5 V 4-wire	7 to 32	0 to 5 V
4	0 to 5 V 3-wire	7 to 32	0 to 5 V*
5	1 to 6 V 3-wire	7 to 32	1 to 6 V
6	0 to 10 V 4-wire	12 to 32	0 to 10 V
7	0.5 to 4.5 V Ratiometric	5.0 ± 0.5	0.5 to 4.5 V
8	Isolated/Configurable	7 to 36	See below

^ with a 10 volt supply mV output sensors give 100 mV over the full scale pressure.

- Output is ratiometric to the supply voltage
- Output reduces pro-rata below 350 mbar (5 psi)
- *0 to 5 V 3-wire output does not reach true zero voltage output at zero pressure. Minimum output is less than 50 mV

Isolated/Configurable (Option 8)

Any pressure signal output configurations will be available, subject to the following limitations:

- Minimum span: 2 V
- Maximum span: 20 V
- Output limits: ±10 V
- Maximum zero offset: ≤ span

Reverse output response to pressure is available.
The output will continue to respond to 110% FS. i.e. if a 0 to 10 V output is specified, the output will continue to increase proportionally to applied pressure until at least 11 V

Examples

Allowed	Not Allowed
-10 to 0 V	0 to 12 V (outside ±10 V limits)
0 to 5 V	6 to 10 V (offset too big)
-5 to +5 V	0 to 0.5 V (span too small)
-2 to 10 V	
1 to 6 V	
10 to 0 V	

Power-Up Time

- mV, Voltage and current versions: 10 ms
- Isolated/configurable version: 500 ms

Shunt Calibration

Shunt Calibration provides customer accessible connections which, when shorted together, cause a shift in output of 80% FS in order to simulate applied pressure. It is fitted to the mV and Isolated/Configurable versions as standard. It is not available with a DIN electrical connector (Option 7)

Mechanical Drawings

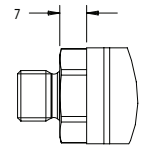

Male Pressure Connection [2]

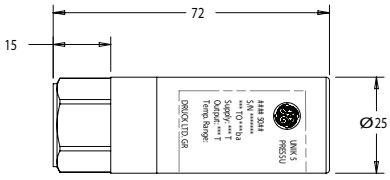

High Pressure Construction: >70 bar

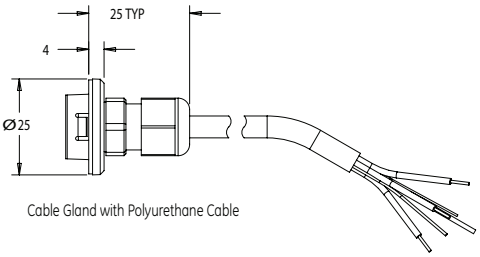

Cable Gland with Polyurethane Cable

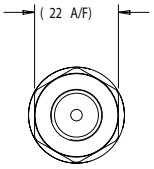

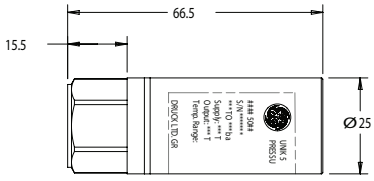

Medium Pressure Construction: ≤70 bar, ≥2 bar

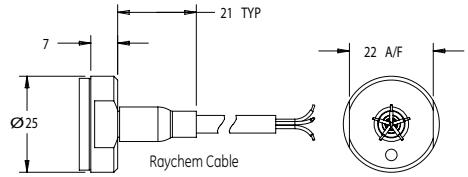

Raychem Cable

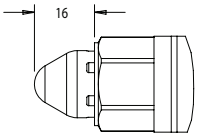

Depth Cone
Pressure Adaptor

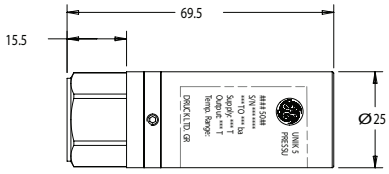

Low Pressure Construction: >2 bar

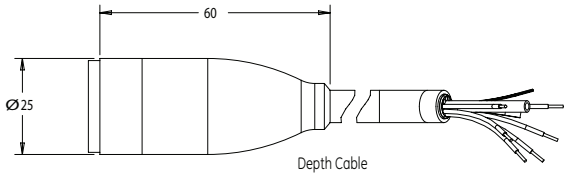

Depth Cable

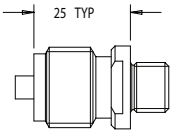

Optional Welded
Pressure Adaptor

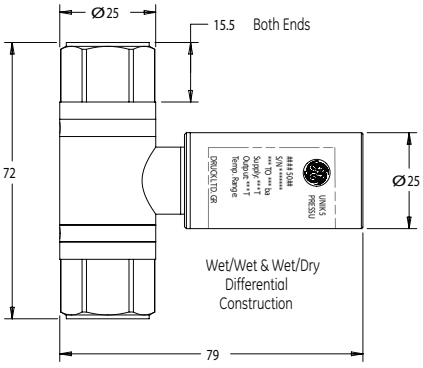

Wet/Wet & Wet/Dry
Differential
Construction

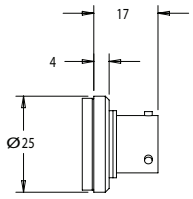

Bayonet Mil-C-26482 Non-demountable

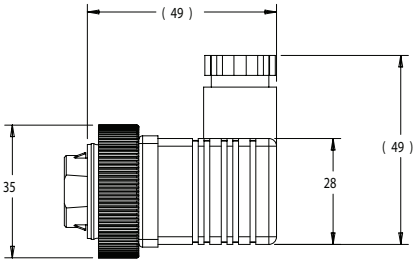

Din 43650 Demountable

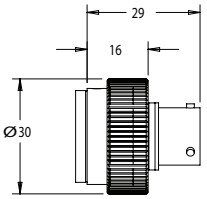

Bayonet Mil-C-26482
Demountable

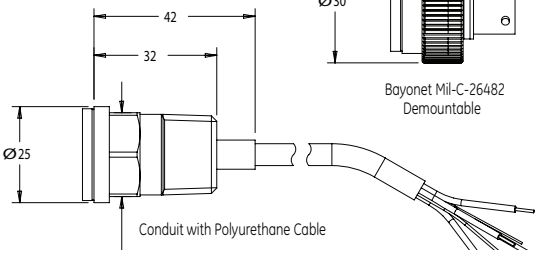

Conduit with Polyurethane Cable

Notes:

[1] Dimensions shown are for Standard Length Products with the following Electrical Output Options:
- mV Linearised
- 4 To 20 mA
- Standard Voltage Options

For mV Passive - Subtract 10mm
For Isolated Configurable Voltage - Add 15mm

[2] Refer to Page 3 for list of Pressure Connection Options (Orientation not critical)

LD300 Series

301 - 302 - 303

PRESSURE TRANSMITTERS

FOR PRESSURE, LEVEL AND FLOW APPLICATIONS

- ± 0.04% High Accuracy
- ± 0.2% of URL Stability Guarantee for 12 Years
- 120:1 Rangeability
- Non-volatile Flow Totalizer
- Tank Linearization
- 100 ms Total Response Time
- PID Control Capability
- Bi-directional Flow Measurement
- Advanced Diagnostics
- Largest Library of Function Block Execution Capacity
- Instantiable Function Blocks
- Supported by DD, EDDL and FDT/DTM
- Three Technology Options

smar

Temperature Limits	Ambient: -40 to 85 °C (-40 to 185 °F) Process: -40 to 100 °C (-40 to 212 °F) (Silicone Oil) 0 to 85 °C (32 to 185 °F) (Halocarbon and Fluorolube Oil) -20 to 85 °C (-4 to 185 °F) (Krytox Oil and Fomblim Oil) -25 to 85 °C (-13 to 185 °F) (Viton O'Ring) -40 to 150 °C (-40 to 302 °F) (LD301L) Storage: -40 to 100 °C (-40 to 212 °F) Digital Display: -20 to 80 °C (-4 to 176 °F) -40 to 85 °C (-40 to 185 °F) (without damage)
Turn-on Time	**HART®:** Performs within specifications in less than 5 seconds after power is applied to the transmitter. **FOUNDATION™ Fieldbus and PROFIBUS PA:** Performs within specifications in less than 10 seconds after power is applied to the transmitter.
Configuration	**HART®:** By digital communication (HART® protocol) using the configuration software CONF401, DDCON or HPC301 and HPC401 for Palms. It can also be configured using DD and FDT/DTM tools, and can be partially configured through local adjustment. **FOUNDATION™ Fieldbus and PROFIBUS PA:** Basic configuration may be done using the local adjustment magnetic tool if device is fitted with display. Complete configuration is possible using configuration tools.
Volumetric Displacement	Less than 0.15 cm^3 (0.01 in^3)
Overpressure and Static Pressure Limits	From 3.45 kPa abs. (0.5 psia)* to: 0.5 MPa (72.52 psi) for range 0 8 MPa (1150 psi) for range 1 16 MPa (2300 psi) for ranges 2, 3 & 4 32 MPa (4600 psi) for models H & A5 40 MPa (5800 psi) for model M5 52 MPa (7500 psi) for model M6 ** except the LD300A model* Flange Test Pressure: 60 MPa (8570 psi) For ANSI/DIN Level flanges (LD300L models): 150lb: 6 psia to 230 psi (-0.6 to 16 bar) at 38 °C (100.8 ºF) 300lb: 6 psia to 600 psi (-0.6 to 41 bar) at 38 °C (100.8 ºF) 600lb: 6 psia to 1200 psi (-0.6 to 83 bar) at 38 °C (100.8 ºF) PN10/16: -60 kPa to 1.4 MPa at 120 °C (248 °F) PN25/40: -60 kPa to 4 MPa at 120 °C (248 °F) The above pressures will not damage the transmitter, but a new calibration may be necessary.
Humidity Limits	0 to 100% RH
Damping Adjustment	User configurable from 0 to 128 seconds (via digital communication).

Performance Specifications

Reference Conditions	Span starting at zero, temperature of 25 °C (77 °F), atmospheric pressure, power supply of 24 Vdc, silicone oil fill fluid, isolating diaphragms in 316L SST and digital trim equal to lower and upper range values.
Accuracy	**For range 0, differential and gage models, diaphragms in SST 316L, fill fluid in Silicone or Halocarbon:** **0.1URL ≤ span ≤ URL:** ± 0.2% of span **0.05URL ≤ span ≤ 0.1 URL:** ± 0.1 [1 + 0.1 URL/span]% of span **For ranges 1, 2, 3 and 4:** **0.1 URL ≤ span ≤ URL:** ± 0.075% of span **0.025 URL ≤ span ≤ 0.1 URL:** ± 0.0375 [1+0.1 URL/span]% of span **0.0085 URL ≤ span ≤ 0.025 URL:** ± [0.0015+0.00465 URL/span]% of span **For ranges 5 and 6, absolute models; diaphragms in Tantalum or Monel; or fill fluid in Fluorolube:** **0.1 URL ≤ span ≤ URL:** ± 0.1% of span **0.025 URL ≤ span ≤ 0.1 URL:** ± 0.05 [1+0.1 URL/span]% of span **0.0085 URL ≤ span ≤ 0.025 URL:** ± [0.01+0.006 URL/span]% of span **For absolute models, range 1:** ± 0.2% of span Linearity, hysteresis and repeatability effects are included.
Stability	± 0.4% of URL for 12 months for range 0, at 20 °C temperature change and up to 100 kPa (1 bar) of static pressure ± 0.1% of URL for 24 months for ranges 2, 3, 4, 5 & 6 ± 0.2% of URL for 12 months for range 1 & L models ± 0.25% of URL for 5 years, at 20 °C temperature change and up to 7 MPa (1000 psi) of static pressure
Temperature Effect	± (0.1%URL + 0.3% span) per 20 °C for range 0 ± (0.02% URL+ 0.1% span) per 20 °C (36 °F) for ranges 2, 3, 4, 5 & 6 ± (0.05% URL+ 0.15% span) per 20 °C (36 °F) for range 1 For LD300L: 6 mmH_2O per 20 ºC for 4" and DN100 17 mmH_2O per 20 ºC for 3" and DN80 Consult for other flange dimensions and fill fluid.
Static Pressure Effect	**Zero error:** ± 0.1% URL per 7 MPa (1000 psi) for ranges 2, 3, 4 & 5 ± 0.1% URL per 3.5 MPa (500 psi) for L models ± 0.1% URL per 1.7 MPa (250 psi) for range 1 ± 0.2% URL per 0.5 MPa (5 bar) for range 0 The zero error is a systematic error that can be eliminated by calibrating at the operating static pressure. **Span error:** Correctable to ± 0.2% of reading per 7 MPa (1000 psi) for ranges 2, 3, 4 & 5 or 3.5 MPa (500 psi) for range 1 and L models. Correctable for ± 0.2% of reading per 0.5MPa (5 bar) for range 0.
Power Supply Effect	± 0.005% of calibrated span per volt
Mounting Position Effect	Zero shift of up to 250 Pa (1 inH2O) which can be calibrated out. No span effect.
Electro-Magnetic Interference Effect	Approved according to IEC 61000-6-2, IEC 61000-6-4 and IEC 61326:2002.

Dimensions are mm (in)

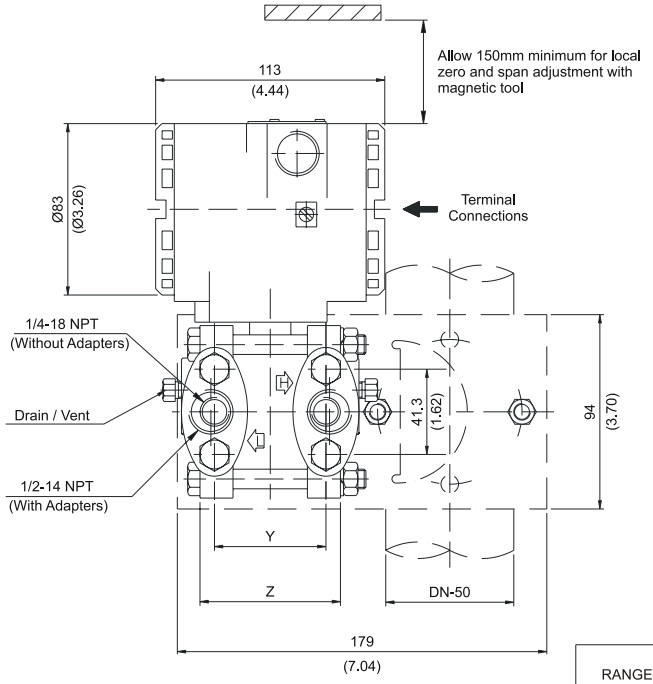

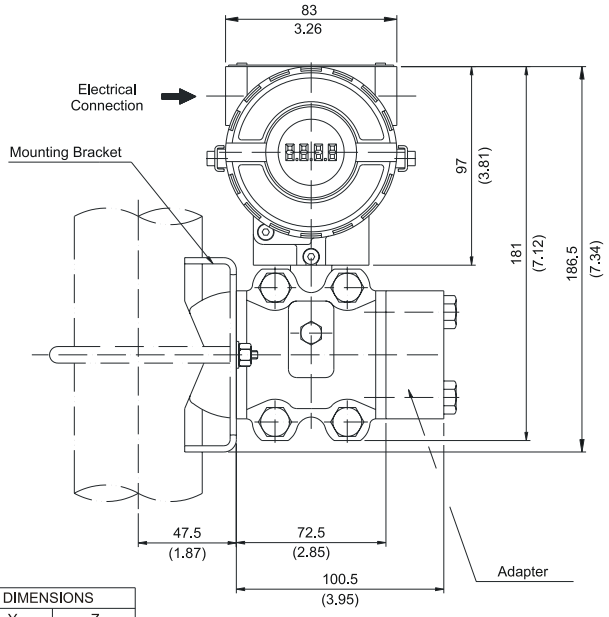

RANGE	DIMENSIONS			
	Y		Z	
	mm	in	mm	in
0, 1, 2, 3	54.0	2.13	68.6	2.70
4	56.0	2.20	70.6	2.78
5	58.3	2.30	72.9	2.87
6	58.7	2.31	73.3	2.89

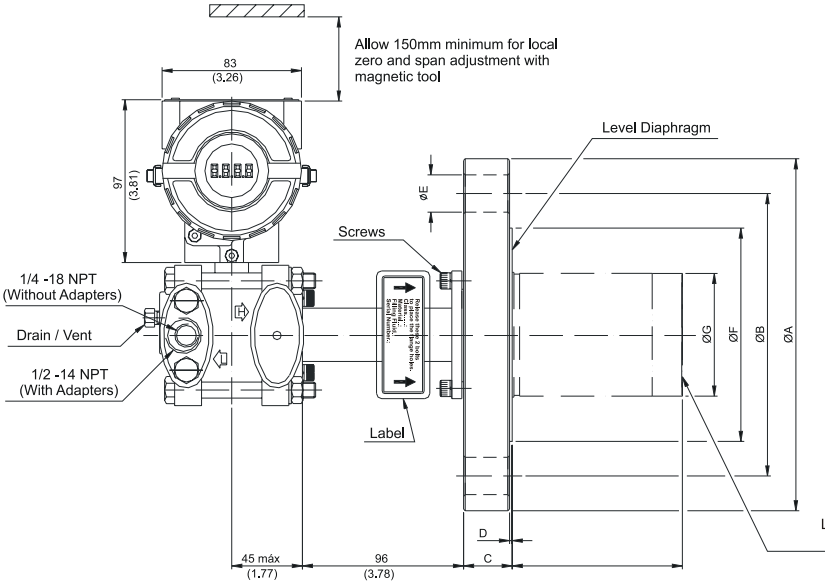

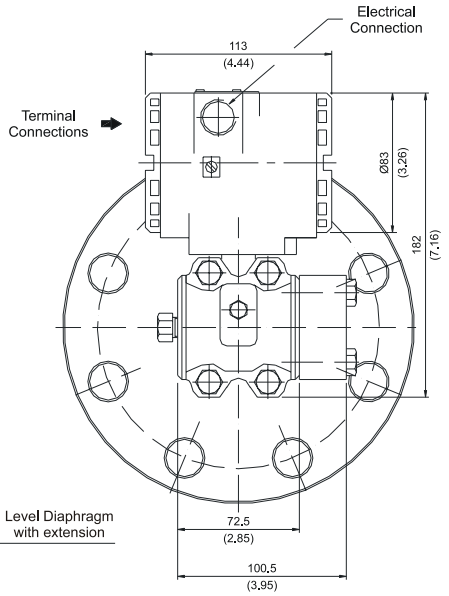

ANSI-B 16.5 DIMENSIONS									
DN	CLASS	A	B	C	D	E	F	G	# HOLES
2"	150	152.4	120.7	22	1.6	19.1	91.9	48	4
	300	165.1	127	22.8	1.6	19.1	91.9	48	8
	600	165.1	127	32.3	6.4	19.1	91.9	48	8
3"	150	190.5	152.4	24.4	1.6	19.1	127	73	4
	300	209.5	168.1	29	1.6	22.2	127	73	8
	600	209.5	168.1	38.7	6.4	22.2	127	73	8
4"	150	228.6	190.5	24.4	1.6	19.1	158	96	8
	300	254	200	32.2	1.6	22.3	158	96	8
	600	273	215.9	45	6.4	25.4	158	96	8
DIN2501/2526 FORM D DIMENSIONS									
DN	PN	A	B	C	D	E	F	G	# HOLES
50	10/40	165	125	20	3	18	102	48	4
80	10/40	200	160	24	3	18	138	73	8
100	10/16	220	180	20	3	18	158	96	8
	25/40	235	190	24	3	22	162	96	8

5 VDC OUTPUT IS® PRESSURE TRANSDUCER

ETM-375 (M) SERIES ETL-375 (M) SERIES

- 5 VDC Output
- Hybrid Microelectronic Regulator-Amplifier
- Flush Diaphragm
- All Welded Construction
- Secondary Containment On Absolute And Sealed Units
- Flight Qualified
- 3/8-24 UNJF or M10 X 1 Thread
- 4 Wire (ETM-375) 3 Wire (ETM-300-375)

ETM-375 series transducers are miniature, threaded flush diaphragm instruments. They utilize a flush metal diaphragm as a force collector. Force is transferred to a solid state piezoresistive sensing element via a thin intervening film of non-compressible silicone oil. This sensing sub-assembly is protected from mechanical damage by a solid screen which has been shown to have minimal influence of the frequency response of the sensor. For applications where a true flush diaphragm is needed, Kulite will supply these transducers without the screen. The ETL Series uses Kulite's Patented Leadless Technology.

Incorporation of a Kulite proprietary electronics module within the main body of this product allows for operation from an unregulated power supply ranging from 13 to 32 VDC. Standard output is a stable, low noise 0 to 5 VDC signal.

OPTIONAL CONNECTOR VERSION HERMETICALLY SEALED

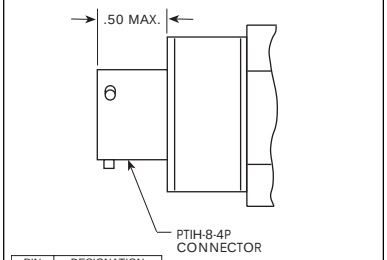

PIN	DESIGNATION
A	+ INPUT
B	– INPUT
C	+ OUTPUT
D	– OUTPUT

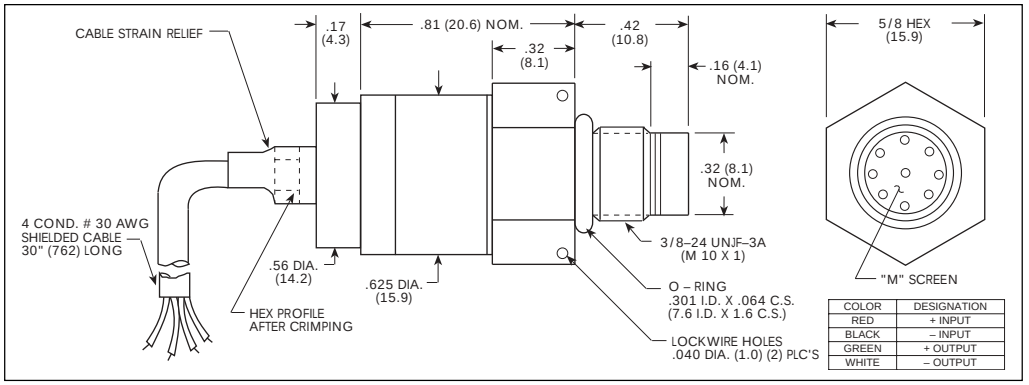

COLOR	DESIGNATION
RED	+ INPUT
BLACK	– INPUT
GREEN	+ OUTPUT
WHITE	– OUTPUT

INPUT Pressure Range	1.7 25	3.5 50	7 100	17 250	35 500	70 1000	170 2500	350 5000	700 10000	1400 BAR 20000 PSI
Operational Mode	Absolute, Gage, Sealed Gage									
Over Pressure	3.5 50	7 100	14 200	35 500	52 750	105 1500	210 3000	525 7500	1050 15000	2100 BAR 30000 PSI
Burst Pressure	3 Times Rated Pressure to a Max. of 35000 PSI (2400 BAR)									
Pressure Media	Any Liquid or Gas Compatible With 17-4PH or 316SS and Selected O-Ring									
Rated Electrical Excitation	13 - 32 VDC (Other Inputs Available on Special Order)									
Maximum Electrical Current	25 ma									
OUTPUT Output Impedance	200 Ohms (Typ.)									
Full Scale Output (FSO)	5 V ± 3%									
Bandwidth (–3dB)	DC to 5 KHz									
Residual Unbalance	0 to 100 mV (ETM-375)						200 mV ± 50 mV (ETM-300-375)			
Combined Non-Linearity, Hysteresis and Repeatability	± 0.1% FS BFSL (Typ.) (± 0.25% FS Max.) BFSL									
Hysteresis	± 0.1% FSO (Typ.)									
Repeatability	± 0.1% FSO (Typ.)									
Resolution	Infinitesimal									
Natural Frequency (KHz) (Typ.)	120	210	285	425	550	720	910	1120	1350	1600
Acceleration Sensitivity % FS/g Perpendicular Transverse	1.9×10^{-3} 1.9×10^{-5}	1.0×10^{-3} 1.0×10^{-5}	5.2×10^{-4} 5.2×10^{-7}	2.2×10^{-4} 2.2×10^{-7}	1.1×10^{-4} 1.1×10^{-7}	6.2×10^{-5} 6.2×10^{-8}	2.6×10^{-5} 2.6×10^{-8}	1.5×10^{-5} 1.5×10^{-8}	8.6×10^{-6} 8.6×10^{-9}	5.2×10^{-6} 5.2×10^{-9}
Insulation Resistance	100 Megohm Min. at 50 VDC									
ENVIRONMENTAL Operating Temperature Range	–65° F to +250° F (–55° C to +120° C)									
Compensated Temperature Range	0° F to +212° F (–18° C to +100° C) Other Ranges Quoted on Request									
Thermal Zero Shift	± 1% FSO/100° F (55° C) (Typ.)									
Thermal Sensitivity Shift	± 1% FSO/100° F (55° C) (Typ.)									
Linear Vibration	100g Peak, Sine up to 5000 Hz									
Altitude	Unaffected									
Humidity	100% Relative Humidity									
Mechanical Shock	100g 11 msec., 5000g 100µ sec.									
PHYSICAL Electrical Connection	4 Conductor 30 AWG Shielded Cable 30" (762) Long									
Weight	24.5 Grams (Max.) Excluding Cable									
Sensing Principle	Fully Active Four Arm Wheatstone Bridge Dielectrically Isolated Silicon on Silicon									
Mounting Torque	80 Inch-Pounds (Max.)									

Note: Custom pressure ranges, accuracies and mechanical configurations available.
Continuous development and refinement of our products may result in specification changes without notice - all dimensions nominal.

KULITE SEMICONDUCTOR PRODUCTS, INC. • One Willow Tree Road • Leonia, New Jersey 07605 • Tel: 201 461-0900 • Fax: 201 461-0990 • http://www.kulite.com

Tankføler med koblingshode

Type Tank MH

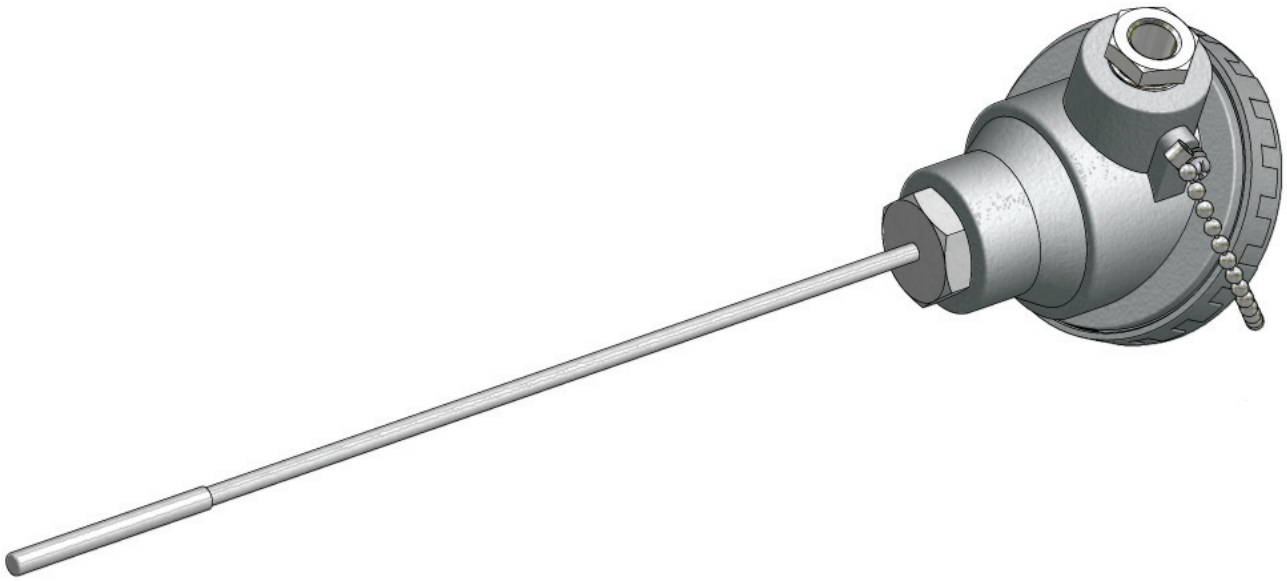

Tekniske spesifikasjoner

Type elementer	Pt 100 (IEC 751), klasse B, klasse A, 1/3 DIN
Mantel materiale	316SS
Koblingshode	Type KNE, IP67. Andre på forespørsel.
Prosessanslutning	På forespørsel

Teck Skotselv INSTRUMENTERING

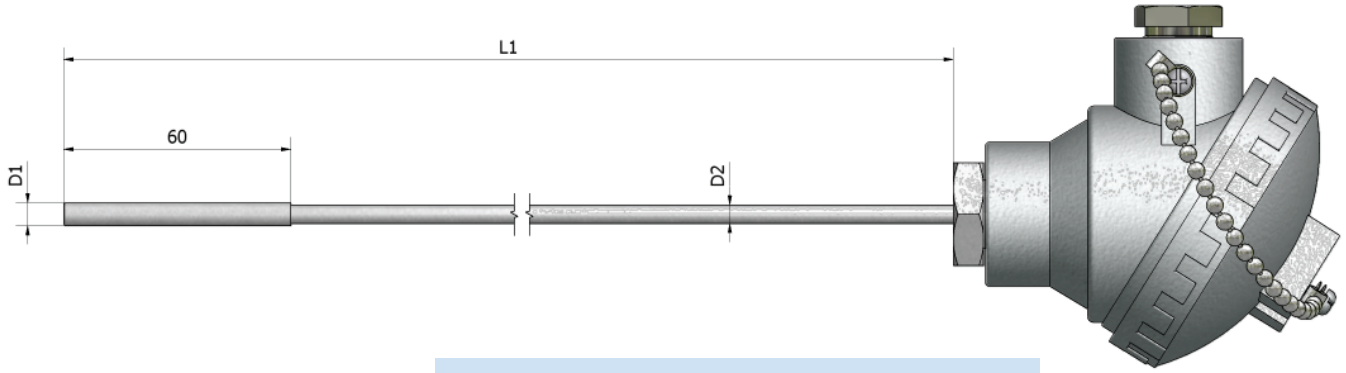

Bestillingskode

Tank MH Tankføler med koblingshode

Føler diameter - D	Mantel diameter - D2
6,0 6,0 mm	4,0/4,8 mm

Andre på forespørsel.

Antall ledere

2 2 ledere
3 3 ledere
4 4 ledere

Element

1 Enkelt element
2 Dobbelt element

Toleranse

A	Pt100 klasse A
B	Pt100 klasse B
1/3 DIN	Standard

Andre på forespørsel.

Føler lengde - L1

L1 Spesifiseres (mm)

Forskruvning

U	Uten
2N	1/2”NPT
2R	1/2”R

Andre på forespørsel.

Koblingshode		Kabelinngang	
KNE	Std. Aluminium	M20x1,5	
CS	Std. Syrefast	M20x1,5	**Standard**

Transmitter

U	Uten transmitter
5333 A	Standard
5333 B	Standard EEx
5331 A	Standard Galvanisk skille
5331 B	Standard Galvanisk skille EEx
5335 A	HART Galvanisk skille
5335 B	HART Galvanisk skille EEx
5350 A	Profibus PA/Foundation Field
5350 B	Profibus PA/Foundation Field EEx

06/07/1

(Eksempel på bestillingskode)

Tank MH - 6,0 - 3 - 1 - 1/3 - 100 - 2N - KNE - 5333A

Teck-Skotselv AS
E-mail: firmapost@skotselv.no
www.skotselv.no

Hovedkontor:
Verksveien 7
3330 Skotselv
Tlf: 32 25 09 70
Fax: 32 25 09 71

Bergen:
Postboks 38
5201 Os
Tlf: 56 57 61 10

Data sheet for

FLOW ELEMENT

NO	BY	DATE

SHEET: **1** OF **1**
SPEC#: REV: **01**
JOB # : **NTNU**
P.O. : **NTNU**
DATE : **14.04.2008** CHK:
BY : **LKS** APR:

Tag. No. : **FE-003-Tilbud** Eq./Line No. :
Service : Flowsheet :

Manuf. : **AUTEK** Model No. : **FEOR-010**

ELEMENT DATA	Element Type	:	**Orifice Plate-Standard**
	Press. Tap Loc. / Type	:	**Upstream / Corner**
	Element Material	:	**304 SS**
	Beta Ratio(d/D)	:	**0,4018**
	Element Bore	:	**100,4458 mm**
	Thickness	:	**0,0000 mm**
SIZING CRITERIA	Sizing Mode	:	**Exact Differential**
	Reference	:	**ISO 5167-2003**
PIPING DATA	Flange	:	**150# / RF**
	Pipe Size & SCH	:	
	Pipe I.D.	:	**250,0000 mm**
	Flange Material	:	**304 SS**
	Pipe Material	:	**316 SS**

COEFFICIENTS	Discharge Coeff.(C)	:	**0,603**	User Factor (Fuser)	: **1,000**
	Gas Expan. Coeff.(Y1)	:	**0,988**	Murdock Wet Gas Factor (Fx)	:
	Reynolds No.(Pipe)	:	**140508,82**	Velocity of Approach Factor (Ev)	: **1,013**
	Reynolds No.(Bore)	:	**349712,89**	Reynolds No.(Pipe - Normal)	: **736110**

PROCESS DATA		Base	Maximum Flow	Normal Flow		Property Method
Flow Rate	:		**0,50**		**kg/sec**	
Diff. Pressure	:		**45,98**		**millibar**	
Pressure Loss	:		**37,76**		**millibar**	
Static Pressure	:		**1,00**		**Bar**	
Base Pressure	:					
Temperature	:		**20,00**		**DEG C**	
Density	:		**1,19**		**kg/m3**	Redlich-Kwong
Spec. Gravity	:					
Z-Compressibility Factor	:		**0,999**			
Viscosity	:		**0,02**		**cP**	User Input
k-Factor (Cp/Cv)	:		**1,4016**			Redlich-Kwong Equation
Fluid Name / Fluid State	:	**Air**		**/**	**Gas**	
Liquid Density	:					
Gas Quality	:					

UNCERTAINTY DATA	Uncertainty in Flow Rate	:	
	in Discharge Coeff.	:	**±0,50%**
	in Expansion Factor	:	**±0,11%**
	in Primary Diameter	:	**±0,05%**
	in Pipe Diameter	:	**±0,30%**
	in Density	:	
	in Pressure	:	

Notes :

AUTEK
WWW.AUTEK.NO

KIMO®
CONSTRUCTEUR

Air velocity | Pressure | Humidity | Air flow | Temperature

TECHNICAL DATA SHEET

New

PITOT TUBES
type L

CE

KIMO offers a wide range of high-quality and accurate Pitot tubes, as per the AFNOR NFX 10-112 norm.
These Pitot tubes, when being connected to a differential column / or needle / or electronical manometer, can measure the dynamic pressure of a moving fluid in a duct, and then can deduct its air velocity in m/s and its airflow in m^3/h.
These Pitot tubes are used in HVAC field, vacuum cleaning and pneumatical transport. They are mainly dedicated to measure hot and particle-charged air, and also high air velocity.

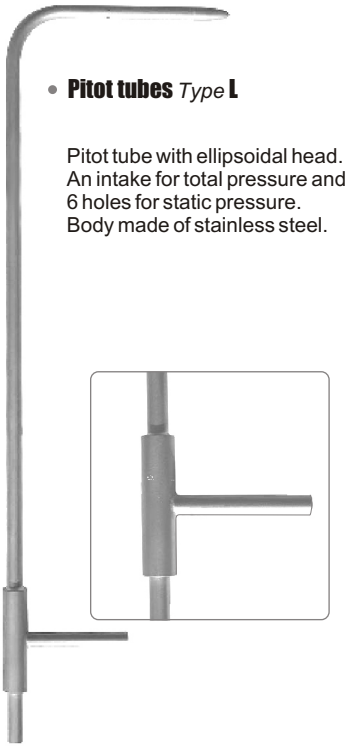

- **Pitot tubes** *Type* **L**

Pitot tube with ellipsoidal head.
An intake for total pressure and 6 holes for static pressure.
Body made of stainless steel.

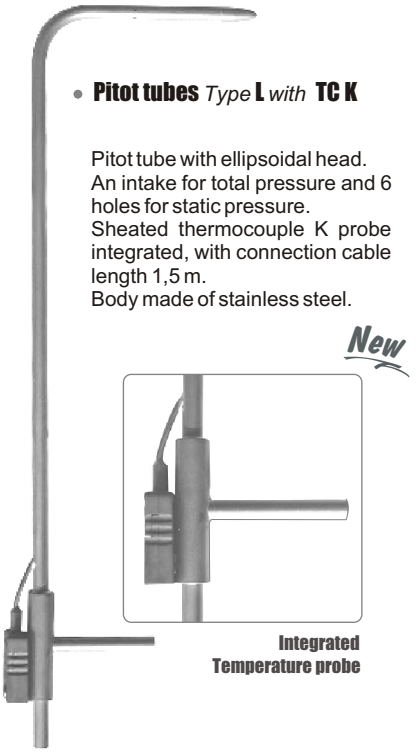

- **Pitot tubes** *Type* **L** *with* **TC K**

Pitot tube with ellipsoidal head.
An intake for total pressure and 6 holes for static pressure.
Sheated thermocouple K probe integrated, with connection cable length 1,5 m.
Body made of stainless steel.

New

Integrated Temperature probe

	Type **L**	*Type* **L** *with* **TC K**
Norm	AFNOR NFX10-112. Annex 4 dated 14.9.77. This norm meets the requirements of the International Norm ISO 3966.	
Model	NPL curved with ellipsoidal head	
Coefficient	1,0015	
Accuracy	More than 1 %, for a ± 10 ° alignment to the fluid flow.	
Quality	Hard stainless steel 4/4, as per AFNOR / Z2.CDN.17.12.	
Operating temperature	From 0 to 600 °C in standard and up to 1000 °C in option (except Ø 3 mm).	
⚠	The extent error of an air velocity or airflow measurement with a KIMO Pitot tube remains inferior to 2%, when being carried out as per the NFX10-112 norm.	
	It is recommended to carry out a calibration of the Pitot tube, in order to determine its exact coefficient.	

Introduction of the range

Pitot tubes *Type* **L**

	Ref.	Length
Ø 3 mm	TPL-03-100	100 mm
	TPL-03-200	200 mm
	TPL-03-300	300 mm
Ø 6 mm	TPL-06-300	300 mm
	TPL-06-500	500 mm
	TPL-06-800	800 mm
Ø 8 mm	TPL-08-1000	1000 mm
	TPL-08-1250	1250 mm
Ø 12 mm	TPL-12-1500	1500 mm
	TPL-12-2000	2000 mm
Ø 14 mm	TPL-14-2500	2500 mm
	TPL-14-3000	3000 mm

Pitot tubes *Type* **L** *with* **TC K**

	Ref.	Length
Ø 3 mm	TPL-03-100-T	100 mm
	TPL-03-200-T	200 mm
	TPL-03-300-T	300 mm
Ø 6 mm	TPL-06-300-T	300 mm
	TPL-06-500-T	500 mm
	TPL-06-800-T	800 mm
Ø 8 mm	TPL-08-1000-T	1000 mm
	TPL-08-1250-T	1250 mm
Ø 12 mm	TPL-12-1500-T	1500 mm
	TPL-12-2000-T	2000 mm
Ø 14 mm	TPL-14-2500-T	2500 mm
	TPL-14-3000-T	3000 mm

Description and dimensions

Pitot tubes *Type* **L**

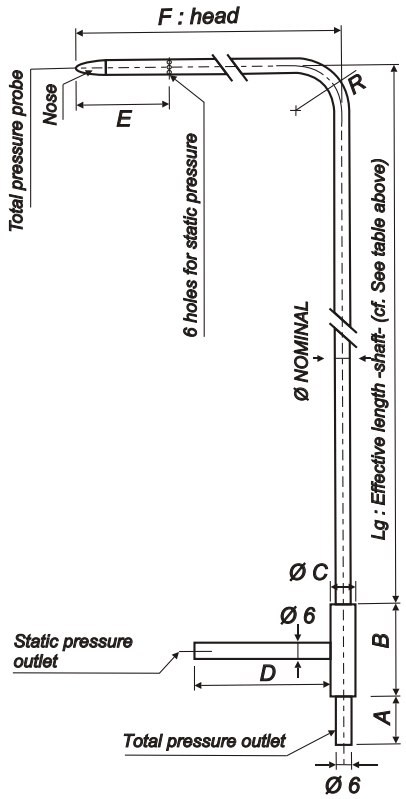

Pitot tubes *Type* **L** *with* **TC K**

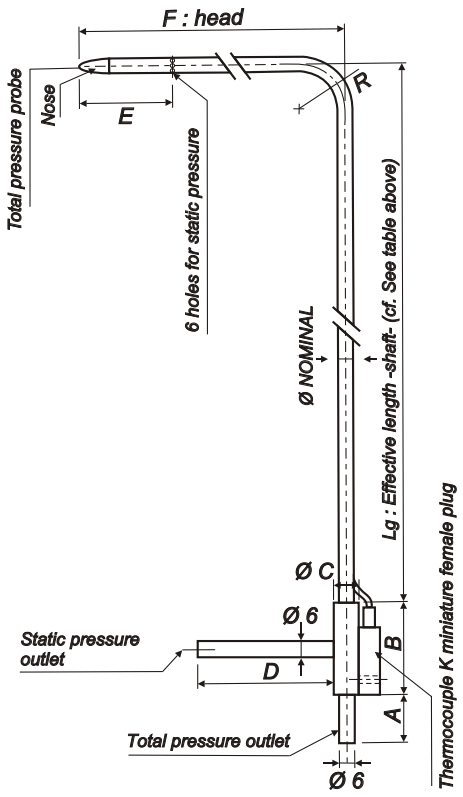

	A	B	Ø C	D	E	F	R
Pitot tubes Ø 3 mm	17	32	10	30	25	48	9
Pitot tubes Ø 6 mm	25	40	10	45	48	96	18
Pitot tubes Ø 8 mm	25	40	10	45	64	128	24
Pitot tubes Ø 12 mm	25	50	16	60	96	192	36
Pitot tubes Ø 14 mm	25	50	16	60	112	224	42

OPERATING

The Pitot tube must be introduced perpendicularly into the duct, in several points pre-determined (see table “location of measuring points”).

The head (ending with an ellipsoidal nose) must be maintained parallel and facing the flow.
The total pressure (+) catched by the nose, is connected to the + of the manometer
The static pressure (-) catched by the holes of the head, is connected to the - of the manometer.
The connection cable of the thermocouple K probe is connected to the thermocouple K inlet of the manometer (only on the Pitot type L with TC K).

Then, the instrument can display the dynamic pressure, also named “velocity pressure”.
The dynamic pressure corresponds to the difference between the total pressure and the static pressure : **Pd = Pt - Ps**

Pitot tubes type L with TC K : direct reading of the velocity with or without temperature balancing on the micromanometers of Class 200 and 300.

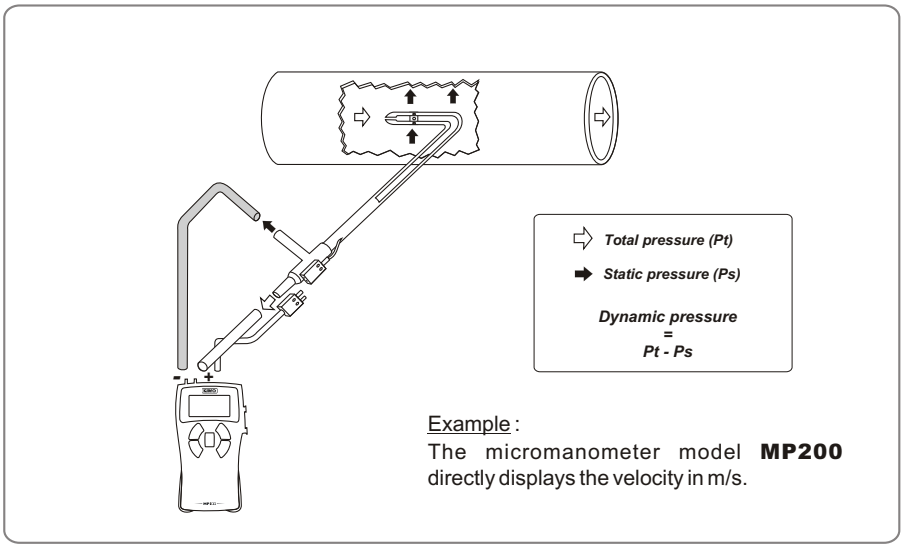

Example :
The micromanometer model **MP200** directly displays the velocity in m/s.

With the dynamic pressure in mm H_2O or in Pa, we can calculate the air velocity in m/s, with the simplified BERNOULLI formula :

$$\mathbf{V} \text{ in m/s at 20 °C : } 1{,}291\sqrt{\ \mathbf{Pd} \text{ in Pa}}$$

Or

$$\mathbf{V} \text{ in m/s : } \mathbf{4{,}05}\ \sqrt{\Delta\mathbf{P} \text{ in mmH2O}}$$

Formula to get the velocity, with temperature balancing of the airflow :

$$\mathbf{V} \text{ in m/s } = \mathbf{K} \times \sqrt{\frac{\mathbf{574{,}2}\ \theta + \mathbf{156842{,}77}}{Po}} \times \sqrt{\Delta\,\mathbf{P} \text{ in Pa}}$$

With :

Po = barometric pressure in Pa
θ = temperature in °C
K = coefficient of the Pitot tube

Location of measuring points

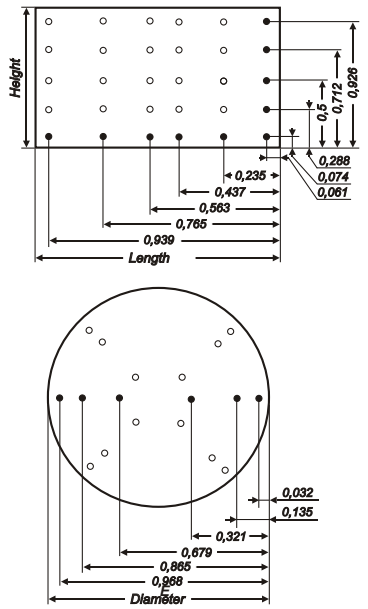

Simplified drawing of the NF.X10.112 norm, for measuring points, as per the method “Log. Tchebycheff”.

OPTION

- ***TIG welding :***
This option is recommended when using the Pitot tubes type L and S with TC K up to 1000°C, except for Pitot tubes Ø 3mm.

Data sheet for

FLOW ELEMENT

NO	BY	DATE

SHEET: **1** OF **1**
SPEC#: REV: **01**
JOB # : **NTNU**
P.O. : **NTNU**
DATE : **14.04.2008** CHK:
BY : **LKS** APR:

Tag. No. : **FE-003-Tilbud** Eq./Line No. :
Service : Flowsheet :

Manuf. : **AUTEK** Model No. : **FEOR-010**

ELEMENT DATA	Element Type	:	**Orifice Plate-Standard**
	Press. Tap Loc. / Type	:	**Upstream / Corner**
	Element Material	:	**304 SS**
	Beta Ratio(d/D)	:	**0,4018**
	Element Bore	:	**100,4458 mm**
	Thickness	:	**0,0000 mm**
SIZING CRITERIA	Sizing Mode	:	**Exact Differential**
	Reference	:	**ISO 5167-2003**
PIPING DATA	Flange	:	**150# / RF**
	Pipe Size & SCH	:	
	Pipe I.D.	:	**250,0000 mm**
	Flange Material	:	**304 SS**
	Pipe Material	:	**316 SS**

COEFFICIENTS	Discharge Coeff.(C)	:	**0,603**	User Factor (Fuser)	: **1,000**
	Gas Expan. Coeff.(Y1)	:	**0,988**	Murdock Wet Gas Factor (Fx)	:
	Reynolds No.(Pipe)	:	**140508,82**	Velocity of Approach Factor (Ev)	: **1,013**
	Reynolds No.(Bore)	:	**349712,89**	Reynolds No.(Pipe - Normal)	: **736110**

PROCESS DATA		Base	Maximum Flow	Normal Flow		Property Method
Flow Rate	:		**0,50**		**kg/sec**	
Diff. Pressure	:		**45,98**		**millibar**	
Pressure Loss	:		**37,76**		**millibar**	
Static Pressure	:		**1,00**		**Bar**	
Base Pressure	:					
Temperature	:		**20,00**		**DEG C**	
Density	:		**1,19**		**kg/m3**	Redlich-Kwong
Spec. Gravity	:					
Z-Compressibility Factor	:		**0,999**			
Viscosity	:		**0,02**		**cP**	User Input
k-Factor (Cp/Cv)	:		**1,4016**			Redlich-Kwong Equation
Fluid Name / Fluid State	:	**Air**		**/**	**Gas**	
Liquid Density	:					
Gas Quality	:					

UNCERTAINTY DATA	Uncertainty in Flow Rate	:	
	in Discharge Coeff.	:	**±0,50%**
	in Expansion Factor	:	**±0,11%**
	in Primary Diameter	:	**±0,05%**
	in Pipe Diameter	:	**±0,30%**
	in Density	:	
	in Pressure	:	

Notes :

AUTEK
WWW.AUTEK.NO

Appendix D: Risk assessment report

Risk Assessment Report

[Wet gas impeller test facility]

Prosjekttittel	
Prosjektleder	Lars Erik Bakken
Enhet	NTNU
HMS-koordinator	Erik Langørgen
Linjeleder	Olav Bolland
Plassering	
Romnummer	
Riggansvarlig	[Trond Grüner]
Risikovurdering utført av	Lars Andreas Øvrum Sørvik, Erik Mele, Dag Remi Reitan.

TABLE OF CONTENTS

1 INTRODUCTION

An open-loop facility is designed for impeller testing in a single-stage configuration with a direct axial inlet. The facility is adapted for different impeller and diffuser geometries as well as implementation of inlet configurations.

The test facility consists of a high-speed electric motor capable of 450 kW at 11,000 rpm, a bearing pedestal, and a compressor section. The latter includes an shrouded backswept impeller, an integrated diffuser, and a symmetrical circular volute section. All of the components is mounted on a single rigid frame. The rotational speed can be changed by controlling the frequency converter. A discharge throttle valve is used for volume flow regulation.

A single nozzle module has been mounted in the centre of the inlet pipe 0.6 m upstream of the impeller inlet. The nozzle is supplied with pressurized water at a maximum of 16 bar. The liquid flow rate is adjusted by the operating pressure of the pump and a needle valve for fine tuning. Compressor geometry and tube arrangement for the rig facility are presented in Table 1.

Table 1

Impeller		
Outlet diameter	D_2	455mm
Hub diameter	D_H	176-180mm
Shroud diameter	D_S	251,7mm
Outlet width	b_2	14mm
Number of blades	N	18
Exit blade angle	B_2	50˚
Diffuser		
Diffusion ratio	D_3/D_2	1,7
With	b_3	14mm

The experiments are conducted in the wet gas impeller test facility at the Norwegian University of Science and Technology (NTNU) in Trondheim, Norway[1].

2 ORGANISATION

Rolle	**NTNU**	**Sintef**
Lab Ansvarlig:	Morten Grønli	Harald Mæhlum
Linjeleder:	Olav Bolland	Mona J. Mølnvik
HMS ansvarlig: HMS koordinator HMS koordinator	Olav Bolland Erik Langørgen Bård Brandåstrø	Mona J. Mølnvik Harald Mæhlum
Romansvarlig:	Erik Langøren	
Prosjekt leder:	Lars Andreas Øvrum Sørvik, Erik Mele	
Ansvarlig riggoperatører:	Trond Grüner	

3 RISK MANAGEMENT IN THE PROJECT

Hovedaktiviteter risikostyring	Nødvendige tiltak, dokumentasjon	DATE
Prosjekt initiering	Prosjekt initiering mal	
Veiledningsmøte Guidance Meeting	Skjema for Veiledningsmøte med pre-risikovurdering	
Innledende risikovurdering Initial Assessment	Fareidentifikasjon – HAZID Skjema grovanalyse	
Vurdering av teknisk sikkerhet Evaluation of technical security	Prosess-HAZOP Tekniske dokumentasjoner	
Vurdering av operasjonell sikkerhet Evaluation of operational safety	Prosedyre-HAZOP Opplæringsplan for operatører	
Sluttvurdering, kvalitetssikring Final assessment, quality assurance	Uavhengig kontroll Utstedelse av apparaturkort Utstedelse av forsøk pågår kort	

4 DRAWINGS, PHOTOS, DESCRIPTIONS OF TEST SETUP

Attachments:
Process and Instrumentation Diagram (PID)
Shall contain all components in the experimental setup
Component List with specifications

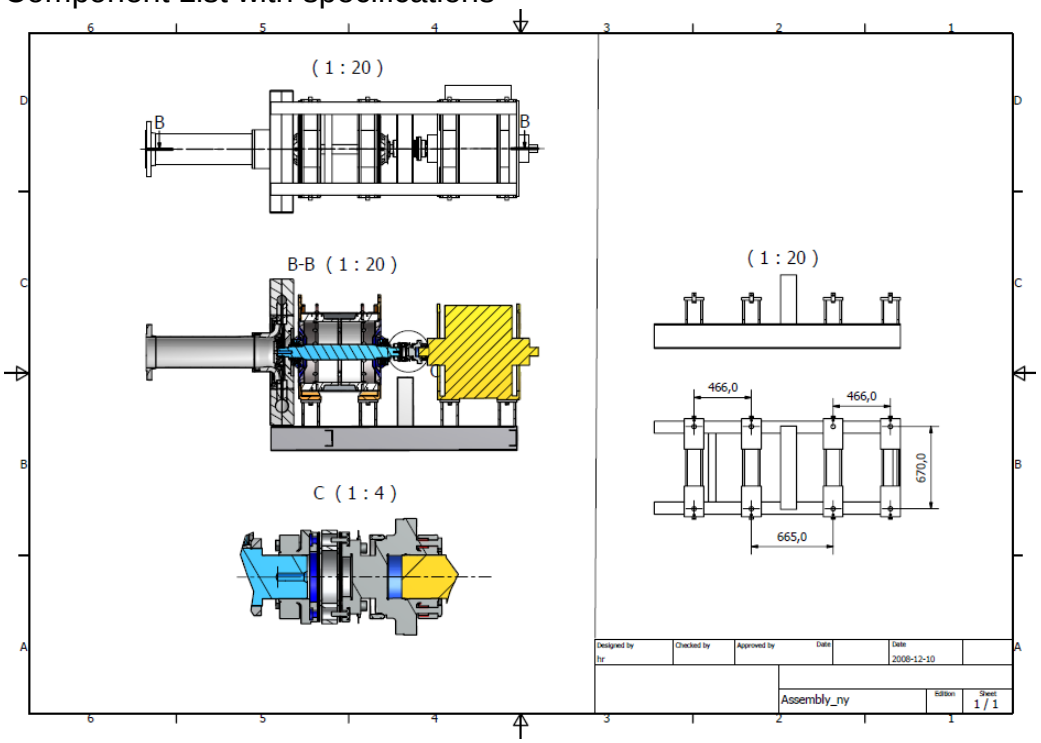

The compressor is driven by an electrical motor with maximum power of 450 kW at 11000 rpms. The Operator of the rig is present in the control room. The frequency converter which is used to change the rotational speed of the machine and the water pump can be controlled from here. Unfortunately, the manual throttling valve

downstream the compressor cannot be closed from the control room. Therefore, in order for attain transient conditions, the regulation of volume flow is done manually.

To ensure that the injection of water provides an equal distribution, 16 nozzles is distributed uniformly over the circumference of the tube.

The water pump is capable of flows up to 50kg/s at 16bar.

5 EVACUATION FROM THE EXPERIMENT AREA

Evacuate at signal from the alarm system or local gas alarms with its own local alert with sound and light outside the room in question, see 6.2
Evacuation from the rigging area takes place through the marked emergency exits to the meetingpoint, (corner of Old Chemistry Kjelhuset or parking 1a-b.)
Action on rig before evacuation:
(Shut off the air and water supply. Power off the electrical supply.)

6 WARNING

6.1 Before experiments

E-mail with information about the test run duration, (hour) and the involved to
HMS koordinator NTNU/SINTEF
Erik.langorgen@ntnu.no
Baard.brandaastro@ntnu.no
Project Managers on neighboring units alerted for clarification around the use of the exhaust system without fear or interference of any kind, see rig matrix.

All experiments should be planned and put into the activity calendar for the lab.
Experiment leader must get confirmation that the experiments are coordinated with other activity before start up.

6.2 Nonconformance

FIRE
Fire you are not able to put out with locally available fire extinguishers, activate, the nearest fire alarm and evacuate area. Be then available for fire brigade and building caretaker to detect fire place.
If possible, notifie:

NTNU	SINTEF
Labsjef Morten Grønli, tlf: 918 97 515	Labsjef Harald Mæhlum tlf 930 149 86
HMS: Erik Langørgen, tlf: 91897160	Forskningssjef Mona J Mølnvik tlf 930 08 868
Instituttleder: Olav Bolland: 91897209	

GASALARM
At a gas alarm, close gas bottles immediately and ventilated the area. If the level of gas concentration not decrease within a reasonable time, activate the fire alarm and

evacuate the lab. Designated personnel or fire department checks the leak to determine whether it is possible to seal the leak and ventilate the area in a responsible manner.
Alert Order in the above paragraph.

PERSONAL INJURY

- First aid kit in the fire / first aid stations
- Shout for help
- Start life-saving first aid•

CALL 113 if there is any doubt whether there is a serious injury

Other Nonconformance (AVVIK)

NTNU:

Reporting form for nonconformance at:
http://www.ntnu.no/hms/2007_Nettsider/HMSRV0401_avvik.doc

SINTEF:

Synergi

7 ASSESSMENT OF TECHNICAL SAFETY

7.1 HAZOP

See Chapter 14 "Guide to the report template".

Explosive zones

Zone 0	Always explosive area, for instance vessels with pressurized gas, or flamable liquid
Zone 1	Occasionally explosive zone, for instance fuel stations
Zone 2	Secondary emission discharge site, may be explosive due to accidents

Attachments:, skjema: Hazop_mal

Conclusion: The testrig is not classified as any of the descriptions above, it is not necessary to take EX precautions

7.2 Flammable, reactive and pressurized substances and gas

Contains the experiments Flammable, reactive and pressurized substances and gas

No	

Attachments: Hazop template

7.3 Pressurized equipment

Contain the set up pressurized equipment?

Yes	Equipment have to undergo pressure testes in accordance with the norms and be documented

Attachements:

7.4 Effects on the environment (emissions, noise, temperature, vibration, smell)

Yes	

Conclusion: The experimens will generate large amounts of noise and vibrations. Therefore, experiments at high speeds are scheduled after normal work hours. An eventual oil leakage will be minor and will be handled locally.

7.5 Radiation

See Chapter 14 "Guide to the report template".

No	

7.6 Usage and handling of chemicals.

See Chapter 14 "Guide to the report template".

No	

7.7 El safety (need to deviate from the current regulations and standards.)

Yes	Stay clear of perimeter during operational hours

8 ASSESSMENT OF OPERATIONAL SAFETY

Ensures that established procedures cover all identified risk factors that must be taken care of through procedures. Ensures that the operators and technical performance have sufficient expertise.

8.1 Prosedure HAZOP

See Chapter 14 "Guide to the report template".

The method is a procedure to identify causes and sources of danger to operational problems.
Attachments:: HAZOP_MAL_Prosedyre
Conclusion:

8.2 Operation and emergency shutdown procedure

See Chapter 14 "Guide to the report template".

The operating procedure is a checklist that must be filled out for each experiment.
Emergency procedure should attempt to set the experiment set up in a harmless state by unforeseen events.
Attachments: "Procedure for running experiments
Emergency shutdown procedure:

8.3 Training of operators

A Document showing training plan for operators
What are the requirements for the training of operators?
- *What it takes to be an independent operator*
- *Job Description for operators*

Attachments:*:* Training program for operators

8.4 Technical modifications

- Technical modifications made by the Operator
  o (for example: Replacement of components, equal to equal)
- • Technical modifications that must be made by Technical staff:
  o (for example, modification of pressure equipment).

Conclusion:

8.5 Personal protective equipment

- Mandatory use of eye protection in the rig zone
- Mandatory use of hearing protection.

Conclusion:.

8.5.1 General Safety

- The area around the staging attempts shielded.
- Gantry crane and truck driving should not take place close to the experiment.
- Gas cylinders shall be placed in an approved carrier with shut-off valve within easy reach.
- Monitoring, can experiment run unattended, how should monitoring be?

Conclusion:

Is Operator allowed to leave during the experiment?

8.6 Safety equipment

- Have portable gas detectors to be used during test execution?
- Warning signs, see the Regulations on Safety signs and signaling in the workplace

8.7 Special actions.

For example:

- Monitoring.
- Safety preparedness.
- Safe Job Analysis of modifications, (SJA)
- Working at heights
- Flammable / toxic gases or chemicals

9 QUANTIFYING OF RISK - RISK MATRIX

See Chapter 14 "Guide to the report template".

The risk matrix will provide visualization and an overview of activity risks so that management and users get the most complete picture of risk factors.

IDnr	Aktivitet-hendelse	Frekv-Sans	Kons	RV
xx	*Rotating shaft, locked room*	1	C1	C1
	Much noise, people without protective gear enter the rig site *Barriers and running experiments outside working hours*	1	B1	B1

Conclusion : *Participants will make a comprehensive assessment to determine whether the remaining risks of the activity / process is acceptable. Barriers and driving outside working hours e.g.*

10 CONCLUSJON

The rig is built in good laboratory practice (GLP).
What technical changes or changes in operating parameters will require new risk assessment?
(Other media, pressure, mechanical intervention)

Experiment unit card get a period of **XX months**
Experiment in progress card get a period of **XX months**

11 REGULATIONS AND GUIDELINES

Se http://www.arbeidstilsynet.no/regelverk/index.html

- Lov om tilsyn med elektriske anlegg og elektrisk utstyr (1929)
- Arbeidsmiljøloven
- Forskrift om systematisk helse-, miljø- og sikkerhetsarbeid (HMS Internkontrollforskrift)
- Forskrift om sikkerhet ved arbeid og drift av elektriske anlegg (FSE 2006)
- Forskrift om elektriske forsyningsanlegg (FEF 2006)
- Forskrift om utstyr og sikkerhetssystem til bruk i eksplosjonsfarlig område NEK 420
- Forskrift om håndtering av brannfarlig, reaksjonsfarlig og trykksatt stoff samt utstyr og anlegg som benyttes ved håndteringen
- Forskrift om Håndtering av eksplosjonsfarlig stoff
- Forskrift om bruk av arbeidsutstyr.
- Forskrift om Arbeidsplasser og arbeidslokaler
- Forskrift om Bruk av personlig verneutstyr på arbeidsplassen
- Forskrift om Helse og sikkerhet i eksplosjonsfarlige atmosfærer
- Forskrift om Høytrykksspyling
- Forskrift om Maskiner
- Forskrift om Sikkerhetsskilting og signalgivning på arbeidsplassen
- Forskrift om Stillaser, stiger og arbeid på tak m.m.
- Forskrift om Sveising, termisk skjæring, termisk sprøyting, kullbuemeisling, lodding og sliping (varmt arbeid)
- Forskrift om Tekniske innretninger
- Forskrift om Tungt og ensformig arbeid
- Forskrift om Vern mot eksponering for kjemikalier på arbeidsplassen (Kjemikalieforskriften)
- Forskrift om Vern mot kunstig optisk stråling på arbeidsplassen
- Forskrift om Vern mot mekaniske vibrasjoner
- Forskrift om Vern mot støy på arbeidsplassen

Veiledninger fra arbeidstilsynet
se: http://www.arbeidstilsynet.no/regelverk/veiledninger.html

12 DOCUMENTATION

- Tegninger, foto, beskrivelser av forsøksoppsetningen
- Hazop_mal
- Sertifikat for trykkpåkjent utstyr
- Håndtering avfall i NTNU
- Sikker bruk av LASERE, retningslinje
- HAZOP_MAL_Prosedyre
- Forsøksprosedyre
- Opplæringsplan for operatører
- Skjema for sikker jobb analyse, (SJA)
- Apparaturkortet
- Forsøk pågår kort

13 GUIDANCE TO RISK ASSESSMENT TEMPLATE

Kap 7 Assessment of technical safety.

Ensure that the design of the experiment set up is optimized in terms of technical safety.
Identifying risk factors related to the selected design, and possibly to initiate re-design to ensure that risk is eliminated as much as possible through technical security.
This should describe what the experimental setup actually are able to manage and acceptance for emission.

7.1 HAZOP

The experimental set up is divided into nodes (eg motor unit, pump unit, cooling unit.). By using guidewords to identify causes, consequences and safeguards, recommendations and conclusions are made according to if necessary safety is obtained. When actions are performed the HAZOP is completed.
(e.g. "No flow", cause: the pipe is deformed, consequence: pump runs hot, precaution: measurement of flow with a link to the emergency or if the consequence is not critical used manual monitoring and are written into the operational procedure.)

7.2 Flammable, reactive and pressurized substances and gas.

According to the Regulations for handling of flammable, reactive and pressurized substances and equipment and facilities used for this:

Flammable material: Solid, liquid or gaseous substance, preparation, and substance with occurrence or combination of these conditions, by its flash point, contact with other substances, pressure, temperature or other chemical properties represent a danger of fire.
Reactive substances: Solid, liquid, or gaseous substances, preparations and substances that occur in combinations of these conditions, which on contact with water, by its pressure, temperature or chemical conditions, represents a potentially dangerous reaction, explosion or release of hazardous gas, steam, dust or fog.
Pressurized : Other solid, liquid or gaseous substance or mixes havinig fire or hazardous material response, when under pressure, and thus may represent a risk of uncontrolled emissions

Further criteria for the classification of flammable, reactive and pressurized substances are set out in Annex 1 of the Guide to the Regulations "Flammable, reactive and pressurized substances"
http://www.dsb.no/Global/Publikasjoner/2009/Veiledning/Generell%20veiledning.pdf
http://www.dsb.no/Global/Publikasjoner/2010/Tema/Temaveiledning_bruk_av_farlig_stoff_Del_1.pdf

Experiment setup area should be reviewed with respect to the assessment of Ex zone
• Zone 0: Always explosive atmosphere, such as inside the tank with gas, flammable liquid.
• Zone 1: Primary zone, sometimes explosive atmosphere such as a complete drain

point
• Zone 2: secondary discharge could cause an explosive atmosphere by accident, such as flanges, valves and connection points

7.4 Effects on the environment

With pollution means: bringing solids, liquid or gas to air, water or ground, noise and vibrations, influence of temperature that may cause damage or inconvenience effect to the environment.
Regulations: http://www.lovdata.no/all/hl-19810313-006.html#6
NTNU guidance to handling of waste:http://www.ntnu.no/hms/retningslinjer/HMSR18B.pdf

7.5 Radiation

Definition of radiation

Ionizing radiation: Electromagnetic radiation (in radiation issues with wawelength <100 nm) or rapid atomic particles (e.g. alpha and beta particles) with the ability to stream ionized atoms or molecules.
Non ionizing radiation: Electromagnetic radiation (wavelength >100 nm), og ultrasound[1] with small or no capability to ionize.
Radiation sources: All ionizing and powerful non-ionizing radiation sources.
Ionizing radiation sources: Sources giving ionizing radiation e.g. all types of radiation sources, x-ray, and electron microscopes.
Powerful non ionizing radiation sources: Sources giving powerful non ionizing radiation which can harm health and/or environment, e.g. class 3B and 4. MR[2] systems, UVC[3] sources, powerful IR sources[4].
[1]Ultrasound is an acoustic radiation ("sound") over the audible frequency range (> 20 kHz). In radiation protection regulations are referred to ultrasound with electromagnetic non-ionizing radiation. [2]MR (e.g. NMR) - nuclear magnetic resonance method that is used to "depict" inner structures of different materials. [3]UVC is electromagnetic radiation in the wavelength range 100-280 nm. [4]IR is electromagnetic radiation in the wavelength range 700 nm - 1 mm.

For each laser there should be an information binder (HMSRV3404B) which shall include:
• General information
• Name of the instrument manager, deputy, and local radiation protection coordinator
• Key data on the apparatus
• Instrument-specific documentation
• References to (or copies of) data sheets, radiation protection regulations, etc.
• Assessments of risk factors
• Instructions for users
• Instructions for practical use, startup, operation, shutdown, safety precautions, logging, locking, or use of radiation sensor, etc.
• Emergency procedures
See NTNU for laser: http://www.ntnu.no/hms/retningslinjer/HMSR34B.pdf

7.6 Usage and handling of chemicals.

In the meaning chemicals, a element that can pose a danger to employee safety and health
See: http://www.lovdata.no/cgi-wift/ldles?doc=/sf/sf/sf-20010430-0443.html

Safety datasheet is to be kept in the HSE binder for the experiment set up and registered in the database for chemicals.

Kap 8 Assessment of operational procedures.

Ensures that established procedures meet all identified risk factors that must be taken care of through operational barriers and that the operators and technical performance have sufficient expertise.

8.1 Prosedure Hazop

Procedural HAZOP is a systematic review of the current procedure, using the fixed HAZOP methodology and defined guidewords. The procedure is broken into individual operations (nodes) and analyzed using guidewords to identify possible nonconformity, confusion or sources of inadequate performance and failure.

8.2 Procedure for running experiments and emergency shutdown.

Have to be prepared for all experiment setups.

The operating procedure has to describe stepwise preparation, startup, during and ending conditions of an experiment. The procedure should describe the assumptions and conditions for starting, operating parameters with the deviation allowed before aborting the experiment and the condition of the rig to be abandoned.

Emergency procedure describes how an emergency shutdown have to be done, (conducted by the uninitiated),

what happens when emergency shutdown, is activated. (electricity / gas supply) and

which events will activate the emergency shutdown (fire, leakage).

Kap 9 Quantifying of RISK

Quantifying of the residue hazards, Risk matrix

To illustrate the overall risk, compared to the risk assessment, each activity is plo tted with values for the probability and consequence into the matrix. Use task IDnr.

Example: If activity IDnr. 1 has been given a probability 3 and D for consequence the risk value become D3, red. This is done for all activities giving them risk values.

In the matrix are different degrees of risk highlighted in red, yellow or green. When an activity ends up on a red risk (= unacceptable risk), risk reducing action has to be taken

CONSEQUENSES	Svært alvorlig	E1	E2	E3	E4	E5
	Alvorlig	D1	D2	D3	D4	D5
	Moderat	C1	C2	C3	C4	C5
	Liten	B1	B2	B3	B4	B5
	Svært liten	A1	A2	A3	A4	A5
		Svært liten	Liten	Middels	Stor	Svært Stor
		PROBABILITY				

The principle of the acceptance criterion. Explanation of the colors used in the matrix

Farge		Beskrivelse
Rød		Unacceptable risk Action has to be taken to reduce risk
Gul		Assessment area. Actions has to be concidered
Grønn		Acceptable risk. Action can be taken based on other criteria

Attachment to Risk Assessment report

[Wet gas impeller test facility]

Prosjekttittel	
Prosjektleder	Lars Erik Bakken
Enhet	NTNU
HMS-koordinator	Erik Langørgen
Linjeleder	Olav Bolland
Plassering	
Romnummer	
Riggansvarlig	[Trond Grüner]
Risikovurdering utført av	Lars Andreas Øvrum Sørvik, Erik Mele

TABLE OF CONTENTS

- **ATTACHMENT A HAZOP MAL**

Project: Impeller rig **Node: 1 DRIVERSYSYTEM**							**Page** 1
Driver system: frekvensomformer, el.motor, lagerbukk og smøreenhet, (oljeaggregat)							
Ref #	**Guideword**	**Causes**	**Consequences**	**Safeguards**	**Rec#**	**Recommendations**	**Action**
1	No flow	Oljeaggregat går ikke Tom for olje	Varmgang, lagerhavari -"- oljepumpehavari	Varsellampe "alarm" Registrering av flow Temperaturmåling "shut down" ved overtemp. PLS overvåkning el.motor starter ikke Manuell resetfunksjon Nivåmåling oljetank	Systemuttestin g med manuell overvåkning, min to personer	Oljenivåsignal tas inn i styreprogram	Varsellampe styres av pls. Registrering av flow i pls. Pls styrer start av impellermotor. Forsvinner oljestrømmen under drift eller overtemp, må pls resettes Nivåmåling i pls. Styrer start av oljeagregat
2	Reverse flow	Koblingsfeil Slangebytte	Lekkasje Oljepumpehavari Motor vil ikke starte -"-	Ulike slangefittings	systemtestin g	Lekkasjesøk inngår i driftsprosedyre	OK (tgg)

Project: Impeller rig Node: 1 DRIVERSYSYTEM						Page 1	
Driver system: frekvensomformer, el.motor, lagerbukk og smøreenhet, (oljeaggregat)							
Ref #	**Guideword**	**Causes**	**Consequences**	**Safeguards**	**Rec#**	**Recommendations**	**Action**
3	More flow	Feil trykkinnstilling	Lekkasje	Manometerovervåking		Trykkontroll inngår i driftsprosedyre Trykkmåling tas inn i systemovervåking	Trykkontroll inngår i driftsprosedyre (manometer)lav nivå olje er i systemovervåkning
4	Less flow	Tett filter	Varmgang i lager	trykkbryter		Trykkbryter signal legges inn i systemovervåkning Kontroll av filter tas inn i driftsprosedyre	Trykkmåling i filter. Ivaretas av pls.
5	More level	overfylling	oljesøl	nivåglass			Påpasselighet ved fylling
6	Less level	For lite olje	Varmgang	Temperaturkontroll Signal fra temperaturkontroll ligger i systemovervåkning Nivåbryter i oljetank		Signal tas inn i systemovervåking	Nivåmåling ok. Pls styrer drift av smøreagregatet og impellermotoren.
7	More pressure	Se ref 3					

Project: Impeller rig Node: 1 DRIVERSYSYTEM						Page 1	
Driver system: frekvensomformer, el.motor, lagerbukk og smøreenhet, (oljeaggregat)							
Ref #	**Guideword**	**Causes**	**Consequences**	**Safeguards**	**Rec#**	**Recommendations**	**Action**
8	Less pressure	Se ref 4					
9	More temperature	Manglende smøring Manglende kjøling For høy last	Se Ref:1, 4, 6, 8 Varmgang motor Varmgang frekvensomformer Varmgang motor Varmgang frekvensomforme	6 stk temperaturfølere koblet til systemovervåking Temperaturovervåkning i frekvensomformer Lastbegrensing i frekvensomformer Lastbegrensing i frekvensomformer		Varsellys på ved testrigg og i kontrollrom Frekvensomformer plasseres med tilgang på kjøleluft	Pls styrer tempmåling. Først lysalarm, deretter shutdown Tempmåling i omformer ok. Ferdig programmert i softwaren.

Project: Impeller rig Node: 1 DRIVERSYSYTEM						Page 1	
Driver system: frekvensomformer, el.motor, lagerbukk og smøreenhet, (oljeaggregat)							
Ref #	**Guideword**	**Causes**	**Consequences**	**Safeguards**	**Rec#**	**Recommendations**	**Action**
			r Mekanisk overlast				
10	Less temperature	NA					
11	More viscosity	Feil oljetype	Ref: 4			Oljetype ivaretas i driftsprosedyre	OK (tgg)
12	Less viscosity	Feil oljetype	Ref: 3			Oljetype ivaretas i driftsprosedyre	OK (tgg)
13	Composition Change	NA					
14	Contamination	Støv inn i frekvensomforme r Støv inn i motor	Kortslutning varmgang kortslutning varmgang	Filterduk Industritype motor		Jevnlig støvsuging	Inn i driftsprosedyre
15	Relief, (trykkavlastning)			Overtrykksventil i aggregat			ok
16	Instrumentation	Uheldig rask Turtallsøkning		Frekvensomformer og el.motor er tilpasset hverandre		”Ramp time” på frekvensomforme r.	ok

Project: Impeller rig Node: 1 DRIVERSYSYTEM						Page 1	
Driver system: frekvensomformer, el.motor, lagerbukk og smøreenhet, (oljeaggregat)							
Ref #	**Guideword**	**Causes**	**Consequences**	**Safeguards**	**Rec#**	**Recommendations**	**Action**
17	Sampling	NA					
18	Corrosion/erosion	NA					
19	Service failure	Strømutfall PC utfall Olje tilførsel Mekanisk havari	Motorstopp Fullt turtall på motor Ref:3 og 4 driftsstopp	Utstyret tåler dette Nødstoppbrytere blir plassert hensiktsmessig Beskyttelses deksel rundt roterende deler Uvedkommende skal ikke oppholde seg ved testrigg under drift		Deksel reduserer utkast av komponenter Beskrives i driftsprosedyre	Nødstopp styrer kontaktor og rele. Må resettes for hver gang strømmen har vært borte.
20	Abnormal operation,	Strømutfall PC utfall Nødavstegning Feilsøking	Ingen Ref:19 Ingen Ingen			Benytt SJA	Utføres med GLP

Project: Impeller rig Node: 1 DRIVERSYSYTEM							Page 1
Driver system: frekvensomformer, el.motor, lagerbukk og smøreenhet, (oljeaggregat)							
Ref #	**Guideword**	**Causes**	**Consequences**	**Safeguards**	**Rec#**	**Recommendations**	**Action**
21	Maintenance	Demontasje Montasje	ingen	Lab rutiner for dette. Vedlikeholdspeosedyre		Benytt SJA	Utføres med GLP
	Ignition		Ingen HC i forbindelse med rigg	Lab rutiner for koordinering av forsøkskjøring			OK
	Spare equipment	NA					
	Safety	Høy lyd	hørselsskade	Hørselsvern Skilting Støysoner Tidsregulert forsøkskjøring Labrutiner for koordinering av forsøkskjøring		Beskrives i driftsprosedyre	OK

Project: Impeller rigg Node: 2							Page
Kompressorsystem							
Ref #	**Guideword**	**Causes**	**Consequences**	**Safeguards**	**Rec#**	**Recommendations**	**Action**
1	No flow	Motor går ikke Ventil stengt nnløp blokkert	ingen For høy temperatur Se pkt: ”ventil stengt”	Temperatur måler inn i systemovervåkning Kontroll tas inn i driftsprosedyre Gitter i front av innløp		Temperatur grenser settes i systemovervåking Alarmlampe ved for høy temperatur Egen oppstartsprosedyre lages	OK Lampe, stopp ved høy høy nivå
2	Reverse flow	Betjeningsfeil Programeringsfeil koblingsfeil	ingen	Turtallskontroll i frekvensomformer		Dreieretning kontrolleres i oppstartsprosedyre	OK
3	More flow	Turtall ut over driftsparameter	Ødelagt impeller	Turtallssperre i frekvensomformer		Kun ett program og fil for driftsoppsett	Ett oppsett lagret på server
4	Less flow	Ref:1					
5	More level	NA					
6	Less level	NA					

Project: Impeller rigg Node: 2							Page
Kompressorsystem							
Ref #	**Guideword**	**Causes**	**Consequences**	**Safeguards**	**Rec#**	**Recommendations**	**Action**
7	More pressure	Blokkert utløp, stengt ventil	Ref:1	Trykkføler med HH alarm til systemovervåkning		Behov vurderes i årsaksdiagram	Utløpstrykk måles i pls. Overtrykk medfører aut. nedstengning
8	Less pressure	Ref:1					
9	More temperature	Ref:1	Varm overflatetemperatur på komponenter Fare for brannskader på personell			Isolering eller skjerming av varme komponenter	OK
10	Less temperature	NA					
11	More viscosity	NA					
12	Less viscosity	NA					
13	Composition	NA					

Project: Impeller rigg Node: 2							Page
Kompressorsystem							
Ref #	**Guideword**	**Causes**	**Consequences**	**Safeguards**	**Rec#**	**Recommendations**	**Action**
	Change						
14	Contamination	NA					
|15	Relief	NA					
16	Instrumentation	Uheldig plassering av temperaturmåler Feilmontasje	Feil måling av utløpstemperatur Feil mengde måling Feil målinger	Plassering av temperatur transmitter Følg leverandørens spesifikasjoner Korrekt montasje av kabler		Kontroller leverandørens anbefalinger Beskrives i driftsprosedyrer Kontrolleres og kalibreres før drift	Benytter ASME standard, OK
17	Sampling	NA					
18	Corrosion/erosion	NA					
19	Service failure	Bortfall av måleinstrumenter Kabelbrudd Mekanisk havari	Bortfall av feilmeldinger og nedstengningsfunksjoner Økonomisk og tidsplan	Manuell overvåkning og nødstopp Solid		Nullpunkt legges til verdi over null	Programmert i pls. Alarm og shutdown.

Project: Impeller rigg Node: 2							Page
Kompressorsystem							
Ref #	**Guideword**	**Causes**	**Consequences**	**Safeguards**	**Rec#**	**Recommendations**	**Action**
			overskridelser Trond blir ikke Dr Grüner	kompressorhus, lav sannsynlighet for personskade			
20	Abnormal operation	Nødstopp Ref:1 og node 1	ingen				Nødstopp kutter all strøm til motor.
21	Maintenance	Inspeksjon av kompressor	feilmontasje	Styrepinner Utføres av kvalifisert personell Støy fra frekvensomformer indikerer at strøm er slått på		Inspeksjon dokumenteres i prosedyre Hovedsikring låses ut SJA på vedlikehold	Ivaretatt vedlikeholdsprosedyre
22	Ignition	NA					
23	Spare equipment	NA					
24	Safety	Ref: 21 og node 1		Nødstopp bryter, solid kompressorhus Prosedyrer			2 separate nødstoppbrytere

Project: Impeller rigg Node: 2							Page
Kompressorsystem							
Ref #	**Guideword**	**Causes**	**Consequences**	**Safeguards**	**Rec#**	**Recommendations**	**Action**
				Verneutstyr Skilting og varsling			

- **ATTACHMENT B PRØVESERTIFIKAT FOR LOKAL TRYKKTESTING**

Trykktesten skal utføres I følge NS-EN 13445 del 5 (Inspeksjon og prøving).
Se også prosedyre for trykktesting gjeldende for VATL lab

Trykkpåkjent utstyr: …….

Benyttes i rigg: …….

Design trykk for utstyr: ……..bara

Maksimum tillatt trykk: ……..bara
(i.e. burst pressure om kjent)

Maksimum driftstrykk i denne rigg: ……..bara

Prøvetrykket skal fastlegges i følge standarden og med hensyn til maksimum tillatt trykk.

Prøvetrykk: ……..bara (……. x maksimum driftstrykk)
I følge standard

Test medium: _____

Temperatur: _____°C

Start: Tid: _____

Trykk: _____bara

Slutt: Tid: _____

Trykk: _____bara

Eventuelle repetisjoner fra atm. trykk til maksimum prøvetrykk:…….

Test trykket, dato for testing og maksimum tillatt driftstrykk skal markers på (skilt eller innslått)

_____ _____
Sted og dato Signatur

- **ATTACHMENT F HAZOP TEMPLATE PROCEDURE**

Project: **Node: 1**						**Page**	
Ref #	**Guideword**	**Causes**	**Consequences**	**Safeguards**	**Recommendations**	**Action**	**Date Sign**
	Not clear procedure	Procedure is to ambitious, or confusingly					
	Step in the wrong place	The procedure can lead to actions done in the wrong pattern or sequence					
	Wrong actions	Procedure improperly specified					
	Incorrect information	Information provided in advance of the specified action is wrong					
	Step missing	Missing step, or step requires too much of operator					
	Step unsucessful	Step has a high probability of failure					
	Influence and effects from other	Procedure's performance can be affected by other sources					

- # ATTACHMENT G PROCEDURE FOR RUNNING EXPERIMENTS

Experiment, name, number:	**Date/ Sign**
Project Leader:	
Experiment Leader:	
Operator, Duties:	

	Conditions for the experiment:	**Completed**
	Experiments should be run in normal working hours, 08:00-16:00 during winter time and 08.00-15.00 during summer time. Experiments outside normal working hours shall be approved.	
	One person must always be present while running experiments, and should be approved as an experimental leader.	
	An early warning is given according to the lab rules, and accepted by authorized personnel.	
	Be sure that everyone taking part of the experiment is wearing the necessary protecting equipment and is aware of the shut down procedure and escape routes.	
	Preparations	**Carried out**
	Post the “Experiment in progress” sign.	
	Start up procedure	
	During the experiment	
	Control of temperature, pressure e.g.	
	End of experiment	
	Shut down procedure	
	Remove all obstructions/barriers/signs around the experiment.	
	Tidy up and return all tools and equipment.	
	Tidy and cleanup work areas.	
	Return equipment and systems back to their normal operation settings (fire alarm)	
	To reflect on before the next experiment and experience useful for others	
	Was the experiment completed as planned and on scheduled in professional terms?	
	Was the competence which was needed for security and completion of the experiment available to you?	
	Do you have any information/ knowledge from the experiment that you should document and share with fellow colleagues?	

- **ATTACHMENT H TRAINING OF OPERATORS**

Experiment, name, number:	**Date/ Sign**
Project Leader:	
Experiment Leader:	
Operator	

	Knowledge to EPT LAB in general	
	Lab - Access -routines and roules -working hour	
	Knowledge about the evacuation procedures.	
	Activity calendar for the Lab	
	Knowledge to the experiments	
	Procedures for the experiments	
	Emergency shutdown.	
	Nearest fire and first aid station.	

Operatør

Dato

Signert

HMS responsible

Dato

Signert

14 ATTACHMENT I FORM FOR SAFE JOB ANALYSIS

SJA tittel:		
Dato:		Sted:
Kryss av for utfylt sjekkliste:		

Deltakere:		
SJA-ansvarlig:		

Arbeidsbeskrivelse: (Hva og hvordan?)
Risiko forbundet med arbeidet:
Beskyttelse/sikring: (tiltaksplan, se neste side)
Konklusjon/kommentar:

Anbefaling/godkjenning:	**Dato/Signatur:**	**Anbefaling/godkjenning:**	**Dato/Signatur:**
SJA-ansvarlig:		Områdeansvarlig:	
Ansvarlig for utføring:		Annen (stilling):	

HMS aspekt	Ja	Nei	Ikke aktuelt	Kommentar / tiltak	Ansv.
Dokumentasjon, erfaring, kompetanse					
Kjent arbeidsoperasjon?					
Kjennskap til erfaringer/uønskede hendelser fra tilsvarende operasjoner?					
Nødvendig personell?					
Kommunikasjon og koordinering					
Mulig konflikt med andre operasjoner?					
Håndtering av en evnt. hendelse (alarm, evakuering)?					
Behov for ekstra vakt?					
Arbeidsstedet					
Uvante arbeidsstillinger?					
Arbeid i tanker, kummer el.lignende?					
Arbeid i grøfter eller sjakter?					
Rent og ryddig?					
Verneutstyr ut over det personlige?					
Vær, vind, sikt, belysning, ventilasjon?					
Bruk av stillaser/lift/seler/stropper?					
Arbeid i høyden?					
Ioniserende stråling?					
Rømningsveier OK?					
Kjemiske farer					
Bruk av helseskadelige/giftige/etsende kjemikalier?					
Bruk av brannfarlige eller eksplosjonsfarlige kjemikalier?					
Må kjemikaliene godkjennes?					
Biologisk materiale?					
Støv/asbest?					
Mekaniske farer					
Stabilitet/styrke/spenning?					
Klem/kutt/slag?					
Støy/trykk/temperatur?					
Behandling av avfall?					
Behov for spesialverktøy?					
Elektriske farer					
Strøm/spenning/over 1000V?					
Støt/krypstrøm?					
Tap av strømtilførsel?					
Området					
Behov for befaring?					
Merking/skilting/avsperring?					
Miljømessige konsekvenser?					
Sentrale fysiske sikkerhetssystemer					
Arbeid på sikkerhetssystemer?					
Frakobling av sikkerhetssystemer?					
Annet					

15 ATTACHMENT J APPARATURKORT UNITCARD

Apparatur/unit

Dette kortet SKAL henges godt synlig på apparaturen!*This card MUST be posted on a visible place on the unit!*

Faglig Ansvarlig (Scientific Responsible)	**Telefon mobil/privat** (Phone no. mobile/private)
Apparaturansvarlig (Unit Responsible)	**Telefon mobil/privat** (Phone no. mobile/private)
Sikkerhetsrisikoer (Safety hazards)	
Sikkerhetsregler Safety rules)	
Nødstopp prosedyre Emergency shutdown)	

Her finner du (Here you will find):

Prosedyrer (Procedures)
Bruksanvisning (Users manual)

Nærmeste (nearest)

Brannslukningsapparat (fire extinguisher)	
Førstehjelpsskap (first aid cabinet)	

NTNU
Institutt for energi og prosessteknikk

Dato

Signert

SINTEF Energi
Avdeling energiprosesser

Dato

Signert

16 ATTACHMENT K FORSØK PÅGÅR KORT

Forsøk pågår!
Experiment in progress!

Dette kort skal settes opp før forsøk kan påbegynnes This card has to be posted before an experiment can start

Ansvarlig / Responsible	**Telefon jobb/mobil/hjemme**
Operatører/Operators	**Forsøksperiode/Experiment time(start – slutt)**
Prosjektleder	**Prosjekt**
Kort beskrivelse av forsøket og relaterte farer **Short description of the experiment and related hazards**	

NTNU
Institutt for energi og prosessteknikk

Dato

Signert

SINTEF Energi
Avdeling energiprosesser

Dato

Signert

1. Grüner, T.G.a.L.E.B., *Aerodynamic instability investigation of a centrifugal compressor exposed to wet gas.* 2010.

EPT HMS-håndbok	4.5.8 Apparaturkort	utarbeidet av	Nummer	dato
		E. Langørgen	HMSEPT-458	10/28/2009
		Godkjent av	side	erstatter
			1 av1	

Apparaturkort

UTSTYRSENHET/INSTRUMENT
(Unit/Instrument)

Impeller-rigg

Apparaturansvarlig (navn/tlf jobb/hjemme) varsles hvis noe er galt
(Instrument responsible – alert if anything goes wrong)
Trond G Grüner 99011717 / 735 92797

Linjeleder eller stedlig representant
(Research manager or local representative)
Morten Grønli

Godkjente (opplærte) operatører
Trond G. Grüner
Lars E. Bakken

Sikkerhetsrisikoer
(Safety hazards)
Støy ved drift.
I

Sikkerhetsregler
(Safety rules/precautions)
Området er avgrenset. Ingen adgang for uvedkommende.
Bruk av verneutstyr i hht forsøk pågår skilt. (støy, meget høy støy)

Slik slås utstyret av i et krisetilfelle
(Emergency turn-off-procedure)
Nødstopp i impeller rom benyttes.

Her finner du :
(Here you will find:)
- First aid suitcase, HMS skap ved heis I 1. Etg.
- Fire extinguisher Slangepost ved slusa.

NTNU
ENERGI OG PROSESSTEKNIKK
Dato:4/11-09 M. Grønli

Signert:.....
(Dette kortet skrives ut/kopieres på lysegrønt papir, "Colorit lime green" 140/160 g)

Impeller rigg

PÅBUDT VERNEUTSTYR I SONE

PERSONAL PROTECTIVE EQUIPMENT MANDATORY IN ZONE

	Trykk start på skapdør Slå over hovedbryter til impellerrig Q1	
4	Velg flowmåler, blendeplate eller turbinmåler (1: 0,3-1,2 kg/s xxxs) Labview	
5	Motor kjøres trinnvis opp til 3000 rpm. Drift under 3000 rpm unngås.	
#	**Drift**	*Utført*
1	Periodevis kontroll av utløpstemperatur og trykk	
2	Periodevis kontroll av oljetrykk	
	Periodevis kontroll av oljelekkasje	
	Periodevis kontroll av vikling og lagertemperatur	
	Pumpefilter skal jevnlig undersøkes	
	Manuell kontroll av temperatur på blokka	
	Periodevis kontroll av utluft	
	Vær obs på unormal støy og vibrasjon	
	Unngå ugunstige turtall, (kvin og vibrasjon)	

#	**Ved injeksjon av vann**	*Utført*
	Sjekk om tilstrekkelig med vann på tank	
1	Kontroller vannlinje, Åpne ventiler,	
	Start pumpe – kontroll av innløpstrykk*	
	Juster mengde rolig opp til ønsket vannmengde	
	Slå av pumpe, steng ventil etter at frekvens er 0 Hz	
	Steng ventiler….	
	Etter vanninjeksjon kjøres impeller i min 10 min uten vann	

#	**Nedstegning**	*Utført*
	Utløpsventil åpnes fullt	
	Motor stanses ved kontrollert nedkjøring	
	Slå av oljesmøring	
	Slå av frekvensomformer	

Nødstopp
Nødstopp benyttes ved behov for akutt stopp eller mistanke om uheldig drifttilstand som kan medføre skade på personell og/eller utstyr. Ved PC-utfall benyttes nødstopp. Reset aktiveres før igangkjøring.

Appendix E: Gantt chart

Appendix E provides an overview of the planned activities during the master thesis.

ID	Task Mode	Task Name	Duration	Start	Finish
1		Order pitot probes	20 days	Mon 16.0	Fri 10.02.1
2		Litterature survey with the respect to the use of pitot measurements to detect the flow pattern and	74 days	Mon 16.01.12	Thu 26.04.12
3		Planning the installation of pitot sensors for measuring theflow pattern in the diffuser wall and tube	9 days	Mon 13.02.12	Thu 23.02.12
4		Litterature survey theory	11 days	Tue 21.02	Tue 06.03
5		Litterature survey of pitot sensors	10,5 days	Wed 07.03.12	Wed 21.03.12
6		Installation of sensors on NTNU's impeller rig.	11 days	Thu 15.03.12	Mon 02.04.12
7		Validate the stream at the impeller dis	11 days	Mon 02.0	Tue 17.04
8		Identification of wet gas surge at impe	12 days	Thu 12.04	Fri 27.04.1
9		Establishing a representative model fo	14 days	Tue 24.04	Fri 11.05.1
10		Establish model, validate, compare to cfd	8 days	Thu 10.05.12	Mon 21.05.12
11		Report writing	71 days	Mon 05.0	Mon 11.0
12		Theory chapter	18 days	Mon 05.0	Wed 28.0
13		Method chapter	22 days	Thu 29.03	Fri 27.04.1
14		Results chapter	17 days	Mon 30.0	Tue 22.05
15		Discussion/conclusion chapter	4 days	Wed 23.05.12	Mon 28.05.12
16		Buffer	10 days	Tue 29.05	Mon 11.0

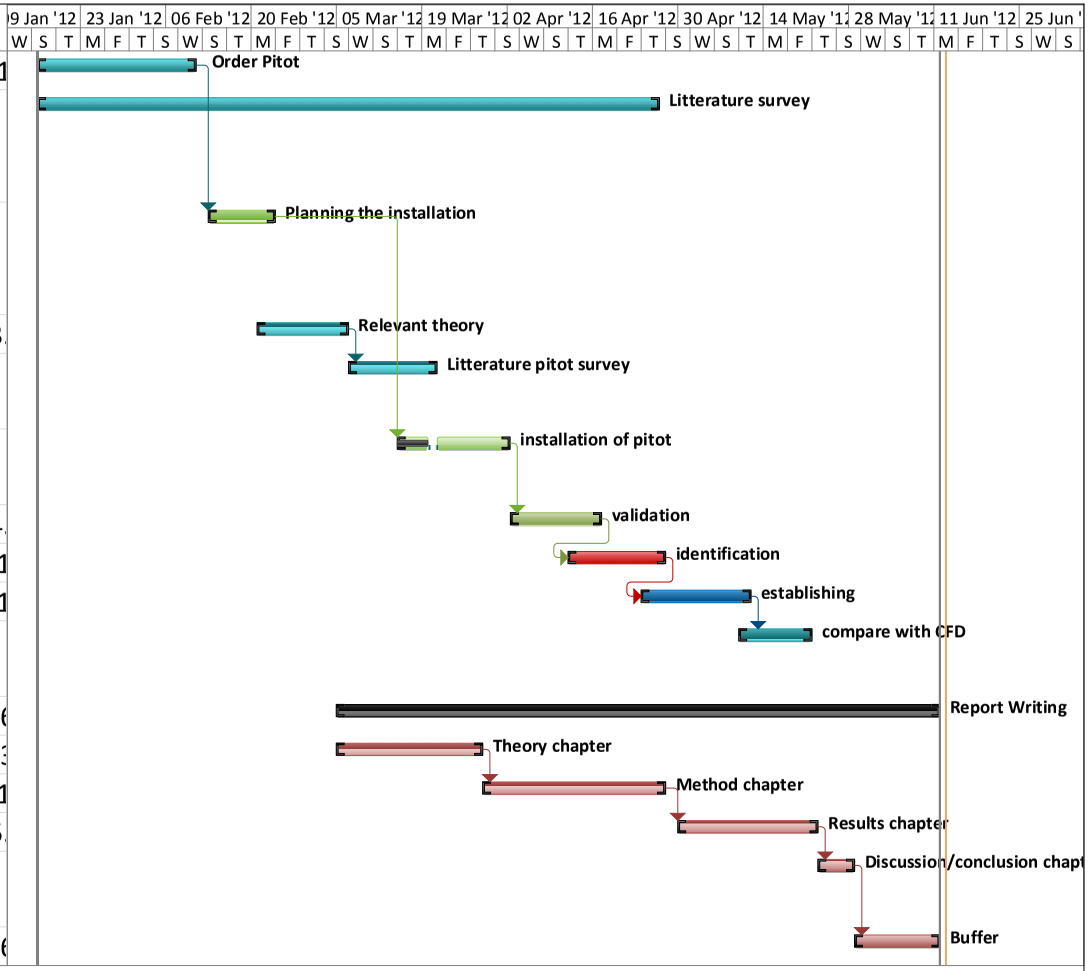

Project: Gant master thesis
Date: Wed 13.06.12

Task	Project Summary	Inactive Milestone	Manual Summary Rollup	Deadline			
Split	External Tasks	Inactive Summary	Manual Summary	Progress			
Milestone	External Milestone	Manual Task	Start-only				
Summary	Inactive Task	Duration-only	Finish-only				